VOLUME 35 AUGUST 1957 NUMBER 8

Canadian Journal of Physics

Editor: H. E. DUCKWORTH

Associate Editors:

L. G. ELLIOTT, *Atomic Energy of Canada, Ltd., Chalk River*
J. S. FOSTER, *McGill University*
G. HERZBERG, *National Research Council of Canada*
L. LEPRINCE-RINGUET, *Ecole Polytechnique, Paris*
B. W. SARGENT, *Queen's University*
G. M. VOLKOFF, *University of British Columbia*
W. H. WATSON, *University of Toronto*
G. A. WOONTON, *McGill University*

Published by THE NATIONAL RESEARCH COUNCIL
OTTAWA CANADA

CANADIAN JOURNAL OF PHYSICS

(*Formerly Section A, Canadian Journal of Research*)

Under the authority of the Chairman of the Committee of the Privy Council on Scientific and Industrial Research, the National Research Council issues THE CANADIAN JOURNAL OF PHYSICS and five other journals devoted to the publication, in English or French, of the results of original scientific research. Matters of general policy concerning these journals are the responsibility of a joint Editorial Board consisting of: members representing the National Research Council of Canada; the Editors of the Journals; and members representing the Royal Society of Canada and four other scientific societies.

EDITORIAL BOARD

Representatives of the National Research Council

R. B. Miller, *University of Alberta*
H. G. Thode, *McMaster University*
D. L. Thomson, *McGill University*
W. H. Watson (Chairman), *University of Toronto*

Editors of the Journals

D. L. Bailey, *University of Toronto*
T. W. M. Cameron, *Macdonald College*
H. E. Duckworth, *McMaster University*
K. A. C. Elliott, *Montreal Neurological Institute*
Léo Marion, *National Research Council*
R. G. E. Murray, *University of Western Ontario*

Representatives of Societies

D. L. Bailey, *University of Toronto*
Royal Society of Canada
T. W. M. Cameron, *Macdonald College*
Royal Society of Canada
H. E. Duckworth, *McMaster University*
Royal Society of Canada
Canadian Association of Physicists
K. A. C. Elliott, *Montreal Neurological Institute*
Canadian Physiological Society
R. G. E. Murray, *University of Western Ontario*
Canadian Society of Microbiologists
H. G. Thode, *McMaster University*
Chemical Institute of Canada
T. Thorvaldson, *University of Saskatchewan*
Royal Society of Canada

Ex officio

Léo Marion (Editor-in-Chief), *National Research Council*
F. T. Rosser, Vice-President (Administration and Awards), *National Research Council*

Manuscripts for publication should be submitted to Dr. H. E. Duckworth, Editor, Canadian Journal of Physics, Hamilton College, McMaster University, Hamilton, Ontario.

(For instructions on preparation of copy, see **Notes to Contributors** (inside back cover).)

Proof, correspondence concerning proof, and orders for reprints should be sent to the Manager, Editorial Office (Research Journals), Division of Administration and Awards, National Research Council, Ottawa 2, Canada.

Subscriptions, renewals, requests for single or back numbers, and all remittances should be sent to Division of Administration and Awards, National Research Council, Ottawa 2, Canada. Remittances should be made payable to the Receiver General of Canada, credit National Research Council.

The journals published, frequency of publication, and prices are:

Canadian Journal of Biochemistry and Physiology	Monthly	$3.00 a year
Canadian Journal of Botany	Bimonthly	$4.00 a year
Canadian Journal of Chemistry	Monthly	$5.00 a year
Canadian Journal of Microbiology	Bimonthly	$3.00 a year
Canadian Journal of Physics	Monthly	$4.00 a year
Canadian Journal of Zoology	Bimonthly	$3.00 a year

The price of single numbers of all journals is 75 cents.

CORRECTION

Canadian Journal of Physics, Vol. 35.

p. 342. In the section $(jj'\,5/2-5/2|2\,0)$ for $j = 17/2$, $j' = j$, .20327975 should read $-.20327975$.
In the section $(jj'\,7/2-7/2|2\,0)$ for $j = 15/2$, $j' = j+1$, .25141195 should read .25141495.

p. 343. In the section $m = 7/2$ for $j = 13/2$, $j' = j$, $-.06153845$ should read $+.06153845$.

p. 345. In the section $m = 9/2$, the numbers printed in the $j = 7/2$ column should be moved to the $j = 9/2$ column.

Canadian Journal of Physics

Issued by THE NATIONAL RESEARCH COUNCIL OF CANADA

VOLUME 35 AUGUST 1957 NUMBER 8

A NEW TECHNIQUE FOR THE STUDY OF SCATTER PROPAGATION IN THE TROPOSPHERE[1]

J. H. CHAPMAN, W. J. HEIKKILA, AND J. E. HOGARTH

ABSTRACT

The power spectrum of the fluctuations in received signal strength on a near-optical U.H.F. circuit has been measured. The sidebands associated with these fluctuations can overlap the information-carrying sidebands of a communication system. When this happens, these sidebands must be taken into account in determining the signal-to-noise ratio of the system. In other words, the fluctuations then have the characteristics of noise, and therefore they are called propagation noise in the present paper. Experiments at a carrier frequency of 500 Mc. have shown that the propagation noise power density usually varies with sideband frequency f (measured from the carrier) as $1/f^2$, for f in the range 0.1 to 10 c.p.s. Departures from this law have been observed in the regions near 0.1 c.p.s. and 10 c.p.s. The measurement of the power spectrum directly offers several advantages over the conventional signal strength recording method, and these are discussed herein.

I. INTRODUCTION

During the last few years, radio waves at U.H.F. have been used considerably in broadcasting and communication systems. As a result, wave propagation at U.H.F. through the troposphere has been subject to intensive studies (Proceedings of the Institute of Radio Engineers 1955). These studies have shown the feasibility of long-range beyond-the-horizon communication at frequencies very much higher than the maximum frequencies usable for ionospheric propagation. This long-range propagation has been called 'scatter propagation' in the belief that it is due to scattering from irregularities in the refractive index structure of the troposphere. However, general agreement on the exact mechanism has not yet been achieved.

The irregularities which are associated with this long-distance scatter propagation affect propagation over short line-of-sight paths also. In some ways the short paths are more suitable for studies of scattering of radio waves by atmospheric inhomogeneities than are the long paths. For example, the use of short paths and moderately narrow beam antennas involves scattering volumes near the surface of the earth where atmospheric studies are most easily made. In addition, the atmospheric conditions are more likely to be uniform over the shorter path. An experimental method that is especially applicable to the short-path experiments is presented in this paper.

[1]Manuscript received in original form November 13, 1956, and, as revised, May 3, 1957.
Contribution from Defence Research Telecommunications Establishment, Defence Research Board, Ottawa. Research conducted under Defence Research Board Project D48-38-03-24.

II. FACTORS AFFECTING U.H.F. PROPAGATION

There are five factors which have appreciable effect upon U.H.F. signals propagated through the troposphere: diffraction occurs around obstacles in the path (Bullington 1947, 1955; Crysdale *al et.* 1956); reflections occur at ground or water surfaces (Kerr 1951); refraction takes place because of the vertical gradient of refractive index that normally exists in the lower atmosphere (Kerr 1951); scattering or reflection may take place from large-scale structure in the troposphere, such as clouds or elevated layers (Northover 1955; Starkey 1956); finally, scattering may be caused also by small-scale turbulent structure in the troposphere (Sutton 1953; Booker and Gordon 1950; Gordon 1955; Villars and Weisskopf 1954, 1955; Fannin 1956; Muchmore and Wheelon 1955).

Other phenomena, such as reflections from ionospheric layers, meteor trails, and aurora, which influence radio wave propagation at lower frequencies, can be neglected in the U.H.F. region. Absorption can be neglected also, except at the highest microwave frequencies. Some miscellaneous effects, such as reflections from aircraft, usually can be identified and accounted for.

Qualitatively, at least, these factors can be divided into two classes: first, those which produce slow changes in signal strength and, second, those which produce rapid changes. A slow change is one whose effect on a radio system can be described in terms of signal strength alone. A rapid change, on the other hand, is one in which the rate of change of signal strength as well as the instantaneous signal amplitude must be taken into account. This is done by considering the sidebands associated with the fluctuations. If these sidebands overlap the sidebands that carry the information, then the fluctuation in signal strength is termed a rapid one.

It can be seen that this classification of change in signal strength as fast or slow depends on the particular system being considered. Modern equipment makes it possible to use sidebands removed only a few cycles per second from the carrier. Thus, for the sake of being definite, fluctuations of the order of 1 c.p.s. or lower might be considered as slow, and those above 1 c.p.s. as fast. At any rate, information on the behavior of these sidebands can be used to determine whether noise due to propagation or to equipment limits the minimum frequency shift usable.

When the fluctuations in signal strength are fast (for a particular system), the information signals of lowest frequency must compete with the fluctuations. Clearly then, the variations take on the characteristics of noise; hence the fluctuations are called propagation noise in this paper. In line with this outlook, experimental methods common to noise studies have been used. The power spectrum of the fluctuations has been determined experimentally by means of band-pass filters. This technique is well known in noise studies, for example, as used by van der Ziel (1954). It has proved to be quite applicable to the present problem, and it offers several advantages over the conventional signal strength analysis. These will be discussed at the end of this paper.

Consideration of the above-mentioned factors in radio wave propagation

leads to the conclusion that the first three produce slow changes in signal strength, while in general the other two produce fast changes. Since there are experimental difficulties in the use of band-pass filters at the frequencies involved in slow signal changes, the method here presented is best suited to the last two factors. In short, the direct determination of the power spectrum of propagation noise should permit detailed study of those features of the radio signal received over a short path which are due to scattering from atmospheric irregularities.

III. EXPERIMENTAL RESULTS ON PROPAGATION NOISE

Experiments on propagation noise have been carried out in the Ottawa valley by the Radio Physics Laboratory since January, 1955. Three experimental paths have been used. The transmitters were located at White Lake, Meath, and Foymount, at distances of 31, 60, and 70 miles respectively from the receiver site at R.P.L. Path profiles on a four-thirds earth basis are shown in Fig. 1. Other paths were used for short tests. The equipment used is indicated in the block diagram, Fig. 2. In principle, the equipment is very simple, but it was found, as discussed below, that the equipment had to be of very high quality. Standard communications equipment, operating at 500 Mc.,

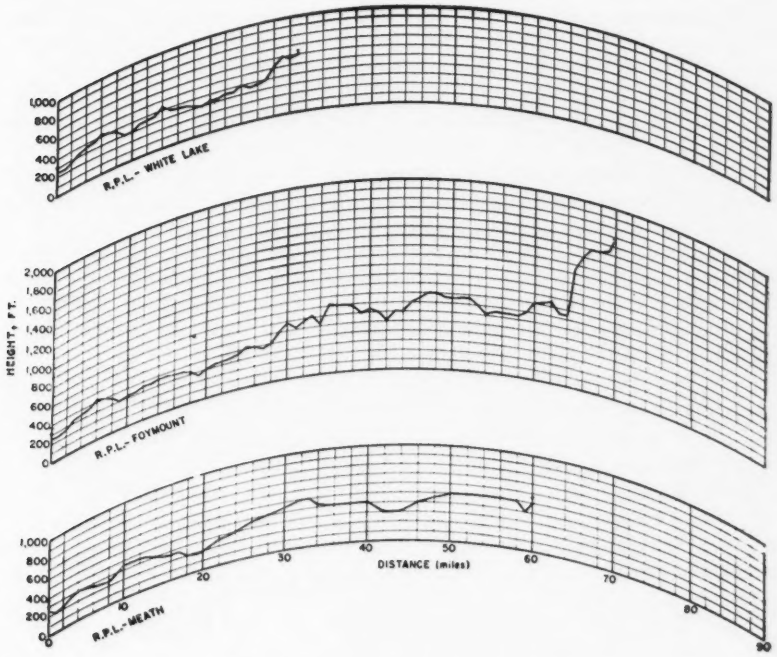

FIG. 1. Path profiles for the three paths used for most of the experiments, based on a four-thirds earth radius to allow for normal refraction.

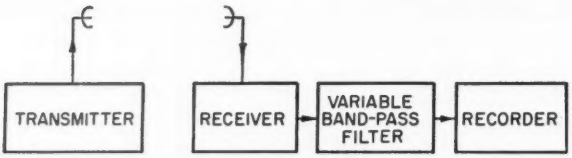

FIG. 2. Block diagram of the equipment used in the experiments on propagation noise. For continuous recordings several band-pass filters were used in parallel.

was modified in order to obtain the lower noise levels needed. In the experiments to date, 5-ft. parabolic antennas were used, with gains of about 15 db. relative to isotropic radiators. These were mounted on 50-ft. towers, although other heights up to 120 ft. were used for short tests.

The audio signal was taken from the second detector of the receiver. This was analyzed by the use of Krohn-Hite model 330-A band-pass filters which have upper and lower cutoff frequencies independently variable between 0.02 c.p.s. and 2000 c.p.s., and have a minimum usable bandwidth of one octave. For continuous recordings, several filters in parallel were used, but short determinations of power spectrum often were made using one filter with various pass bands in turn. The outputs from the filters were recorded directly using Edin pen recorders, run at slow chart speeds. By the use of well-known statistical relations for Gaussian noise (Rice 1945), the r.m.s. value of each filter output was determined from the records. The receiving and recording equipments were calibrated either by using the front end noise, taking advantage of the known noise figure, or by the use of a crystal diode modulator.

Most of the measurements made indicated that the noise at the output of the second detector has a power spectrum given approximately by

$$w(f) = k^2/f^2 + w_R. \tag{1}$$

Here $w(f)$ is the power density, or power per unit bandwidth, and w_R is the receiver noise power density, the latter being independent of frequency. Also, k is independent of f; the dimensions of k are discussed below. Fig. 3 gives one experimental result. For the results shown in Fig. 3 each separate measurement was made in turn with one filter, the pass band always being one octave wide. To emphasize the fact that a filter of finite bandwidth was used, each measurement is depicted by a horizontal line rather than by a point, where the length of the line indicates the bandwidth of the filter. Two determinations of the power spectrum were made, about 3 hours apart, with each determination taking about 30 minutes; the results are shown separately on the graph. The agreement between the two runs demonstrates the stationary character of the fluctuations during this time. In addition to the experimental results, Fig. 3 shows a curve representing equation (1) with $k^2/w_R = 380$. The constant value of $w(f)$ at very high frequencies,

$$w(f) = w_R, \qquad f^2 \gg k^2/w_R, \tag{2}$$

means simply that receiver noise predominates. At lower frequencies, where

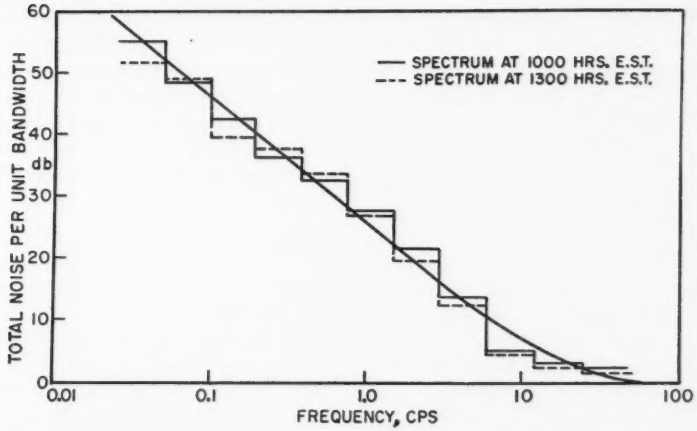

FIG. 3. Propagation noise power spectrum on a 70 mile path, Feb. 16, 1955. The short horizontal lines indicate the average power density in the filter pass bands, in decibels above the receiver noise power density. The smooth curve represents the power spectrum given by equation (1) with $k^2 = 380 w_R$.

receiver noise can be neglected in relation to propagation noise, an inverse square relation holds,

$$w(f) = k^2/f^2 = w_0 f_c^2/f^2, \qquad f^2 \ll k^2/w_R. \tag{3}$$

Here k^2 has been written as $w_0 f_c^2$ to bring out the dimensions explicitly. Continuous records showed that the exponent of f in equation (3) was not always exactly equal to 2. This is evident from the sample continuous recordings in Fig. 4. Three filters, separated in frequency by factors of five,

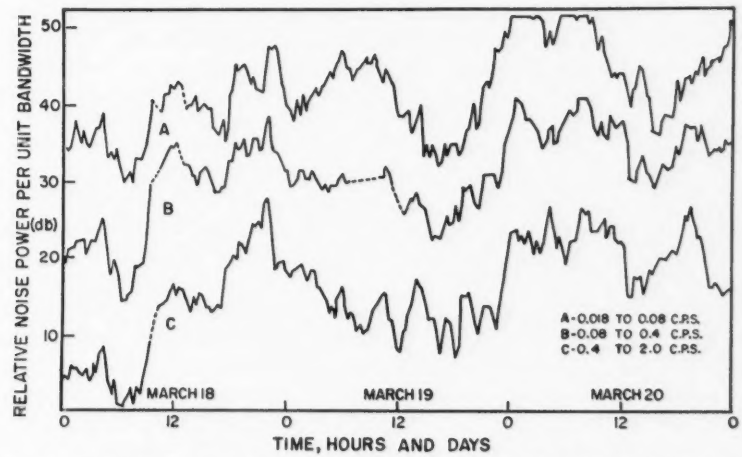

FIG. 4. A continuous record of propagation noise on a 30 mile path. The three curves represent the noise power densities at the outputs of three band-pass filters as indicated, in decibels above receiver noise.

were used here simultaneously. Therefore, on the logarithmic plot, if the inverse square law were to hold the three curves should be separated by 14 db. It is apparent that the inverse square law is fairly well obeyed at the higher frequencies, but is not so valid at the low frequencies. At the low frequencies, a slightly smaller exponent is indicated. Other results have indicated a stronger dependence than inverse square above 1 c.p.s. Nevertheless, the inverse square law is a very good representation of results in the region immediately above 0.1 c.p.s.

IV. DISCUSSION

Over a short path the received signal is quite strong, and the fluctuations are a small part of the total signal. On a 30 mile path, for example, the r.m.s. value of the fluctuating part was only a few per cent, at most, of the mean signal. Therefore, some means of suppressing the steady component must be used if the fluctuations are to be studied on the short path. Differential d-c. recorders have been used by others but it is perhaps easier experimentally to work with filters instead. In either case, equipment noise levels, in particular transmitter hum and receiver front end noise, determine the minimum propagation noise levels that can be studied. It was found that a dynamic range of at least 80 db. was needed for the study of propagation noise on the present paths.

The experimental observation that the power spectrum of propagation noise follows an inverse square law for a wide range of frequencies has a direct bearing on the choice of equipment. Suppose that a signal strength recording is made with a fast differential recorder, for the purpose of studying fast fading. The recorder sensitivity is determined by the low frequencies, since they occur with the larger amplitudes as shown by the present results. Since the higher frequency components occur with diminishing amplitudes, they will not be apparent on the recording, owing to its finite resolution. Such a recording thus acts as a filter, which discriminates against the high frequencies because of their small amplitude. The use of band-pass filters, as in the present experiments, permits the use of higher gain for the higher frequencies. The dynamic range of the recording instrument need not then limit the range of variation of the variables of interest.

It should be noted also that, as compared with conventional methods, the use of narrow band-pass filters reduces the amount of computation needed in the analysis of the results. The determination of either the power spectrum or the autocorrelation function from a signal strength recording is a tedious task.

The experimental result here presented indicates a predominance of low-frequency components in the spectrum of propagation noise. However, for physical reasons, it is obvious that the inverse square law cannot hold down to $f = 0$ or up to $f = \infty$. This is demonstrated clearly by considering the fading rate of the signal. The fading rate may be defined as the number of crossings of the mean signal level, which is given by Rice (1945) as

$$n(0) = \left[\int_0^\infty f^2 w(f) df \Big/ \int_0^\infty w(f) df \right]^{\frac{1}{2}}. \tag{4}$$

The lower integral diverges at the lower limit and the upper integral diverges at the upper limit. Physically, the divergence at the lower limit implies an infinite amount of power in the sidebands. This can be corrected by adding a constant term to the denominator, i.e. by assuming the power spectrum

$$w(f) = w_0 f_c^2/(f_c^2+f^2) \tag{5a}$$

or

$$w(f) = w_0/(1+f^2/f_c^2), \tag{5b}$$

where f_c is some characteristic frequency for the system. In this form, w_0 represents a constant power density at frequencies well below $f = f_c$. This power spectrum implies an exponential autocorrelation function.

The difficulty at the upper limit remains. It is related to the cusp at the origin in the exponential autocorrelation function. This has been discussed by others, e.g. Rice (1945) and Muchmore and Wheelon (1955). Physically, it implies a completely discontinuous process and, in practice, parasitic effects always enter the problem to introduce a high-frequency cutoff. Mathematically, this may be taken care of by a stronger dependence on frequency, e.g. by a power spectrum of the form

$$w(f) = \frac{w_0 f_c^2}{f_c^2+f^2} - \frac{w_0 f_c^2}{F_c^2+f^2}. \tag{6}$$

or, equivalently,

$$w(f) = w_0 \Big/ \left(1 + \frac{f^2}{f_c^2} + \frac{f^4}{f_c^2 F_c^2}\right) \qquad \text{for } F_c^2 \gg f_c^2. \tag{7}$$

This form of the power spectrum is equivalent to the rounded exponential autocorrelation function as proposed by Muchmore and Wheelon (1955). Incidentally, the fading rate then is a geometric mean between the two characteristic frequencies.

It might be added here that if deficiencies in the experimental equipment, e.g. the finite resolution of a signal strength record, introduce the upper cutoff frequency F_c, then the observed fading rate is partly determined by the equipment, and it is not a parameter of the received signal alone.

In conclusion, it can be said that the simple inverse square law describes most of the present results, obtained on a variety of paths and weather conditions. Nevertheless some of the experiments have indicated upper and lower cutoff frequencies F_c and f_c, F_c being of the order of 1 to 10 c.p.s. and f_c being of the order of 0.01 to 0.1 c.p.s., with the 500 Mc. carrier frequency. While the form of the power spectrum seems to be independent of such things as path length and weather conditions, it seems obvious that the three suggested parameters w_0, f_c, and F_c cannot be. These will be discussed in the future.

REFERENCES

Booker, H. G. and Gordon, W. E. 1950. Proc. I.R.E. **38**, 401.
Bullington, K. 1947. Proc. I.R.E. **35**, 1122.
——— 1955. Proc. I.R.E. **43**, 1175.
Crysdale, J. H., Day, J. W. B., Cook, W. S., Psutka, M. E., and Robillard, P. E. 1956. Radio Physics Laboratory, Ottawa, Project Report 34-0-3.

FANNIN, B. M. 1956. Ph.D. Thesis, University of Texas, Austin, Texas.
GORDON, W. E. 1955. Proc. I.R.E. **43**, 23.
KERR, D. E. 1951. Propagation of short radio waves, M.I.T. Radiation Laboratory Series, Vol. 13 (McGraw-Hill Book Company, Inc., New York and London).
MUCHMORE, R. B. and WHEELON, A. D. 1955. Proc. I.R.E. **43**, 1381, 1437, 1450.
NORTHOVER, F. H. 1955. Can. J. Phys. **33**, 241, 316, 347.
Proceedings of the Institute of Radio Engineers. 1955. Scatter Propagation Issue (Vol. 43, No. 10, October).
RICE, S. O. 1945. Bell System Tech. J. **24**, 55.
STARKEY, B. J. 1956. Technical Note RAD. 638, Royal Aircraft Establishment, Farnborough, England.
SUTTON, O. G. 1953. Micrometeorology (McGraw-Hill Book Company, Inc., New York).
VAN DER ZIEL, A. 1954. Rev. Sci. Instr. **25**, 899.
VILLARS, F. and WEISSKOPF, V. F. 1954. Phys. Rev. **94**, 232.
——— 1955. Proc. I.R.E. **43**, 1232.

ROTATIONAL TEMPERATURES MEASURED IN AURORAE AT CHURCHILL, MANITOBA[1]

R. MONTALBETTI[2]

ABSTRACT

A series of auroral spectra showing the 0–0 N_2^+ band have been obtained at Churchill, Manitoba. Rotational temperatures ranging from 230° K. to 480° K. have been deduced. These are in agreement with measurements made at Saskatoon, Saskatchewan, and indicate that there is no latitude effect. A vertical temperature gradient of some 6° K./km. is suggested by the observations.

INTRODUCTION

One of the methods used to determine temperatures in the upper atmosphere at auroral heights is to measure the intensity distribution of the rotational fine structure of the N_2^+ first negative system of the aurora. The validity of this method has been discussed and demonstrated for the case of electron excitation of the band by Vallance Jones and Harrison (1955) and by Shepherd and Hunten (1955). Their results for Saskatoon indicate temperatures ranging from approximately 170° K. to 450° K., depending on the type and height of the aurorae. The results of Shepherd and Hunten, in particular, point to a vertical temperature gradient of some 6° K./km. in agreement with the measurements made by rocket flights (The Rocket Panel 1952). Petrie (1953), also at Saskatoon, but during a period of greater auroral activity, measured temperatures ranging from 450° K. to 700° K. These were likely derived from spectra obtained near the summit of visible aurorae. On the other hand, Vegard (1951), on the basis of a large number of measurements, concluded that a constant temperature of 230°±20° K. is characteristic of all types and heights of aurorae. Furthermore, this result was obtained both at Oslo and at Tromsö, latitudes 60° N. and 69.7° N. respectively.

Vegard (1956) has suggested that the higher temperatures measured at Saskatoon were a result of proton excitation of the N_2^+ band. This possibility is based on the Solar Ray Bundle theory (Vegard 1956) which predicts that the proton flux should be greater in low latitude and high altitude aurorae. Recent observations (Montalbetti and Vallance Jones 1957) confirm that a proton flux tends to be associated with the southern extent of an auroral display.

Since Churchill is situated at the center of the auroral zone, it seemed desirable to make temperature measurements at this station and to compare them with the results obtained at Saskatoon. The intensity of any aurora which occurred at Saskatoon during the interval that exposures were being made was noted, since this provided an indication of the position of the proton flux.

[1]Manuscript received May 15, 1957.
Contribution from Radio Physics Laboratory, Defence Research Board, Ottawa, Ontario.
[2]Present address: Physics Department, University of Saskatchewan, Saskatoon, Saskatchewan.

EXPERIMENTAL

A high-dispersion spectrograph consisting essentially of an 8×8 in. grating and a camera having a relative aperture of $f/0.8$ was used. A step entrance slit was employed so that certain spectral features could be used to determine the "characteristic curve" of the emulsion. The aurora was imaged on the slit by means of a 14-in. focal length quartz lens and a movable mirror. The 0–0 band of N_2^+ was photographed in the third order with a dispersion of about 18 Å/mm.

During the months of August to November, 1954, and November, 1956, a number of satisfactory plates were obtained. No attempt was made to differentiate between forms of aurorae which occurred during any one exposure interval, but it was observed that most of the displays were either strong or weak. In practically all cases satisfactory plate densities resulted from exposure times of 1 to 4 hours, the length of the exposure depending on the intensity of the visible aurorae.

A microphotometer tracing of the 0–0 band of N_2^+ obtained on the night of September 30, 1956, is reproduced in Fig. 1. It is clear that the band is

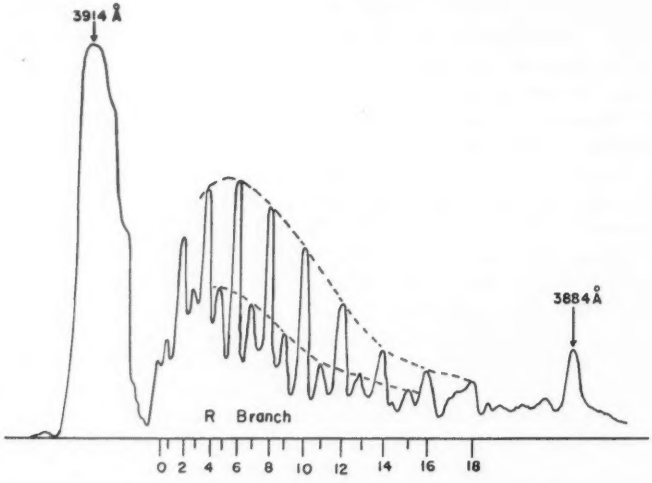

FIG. 1. Microphotometer tracing of 0–0 N_2^+ first negative band.

sufficiently resolved to determine the intensity distribution of the rotational fine structure, if lines characterized by rotational quantum numbers greater than six are considered. Near the band head the overlapping of the individual lines prevents accurate determination of their relative intensities. Two independent methods were used to measure the relative intensities of the individual lines. One was to take advantage of the 2:1 intensity ratio between alternate lines, as was done by Vallance Jones and Harrison (1955); and the other was to utilize the spectrum obtained by the stepped slit. For purposes

of calibration, the 3884 Å band may be considered as a continuum, and hence a microphotometer tracing taken along the length of the image of the stepped slit gives the relation between plate density and relative intensity. Fig. 2 is an example of the calibration curve obtained by the two methods for the plate shown in Fig. 1.

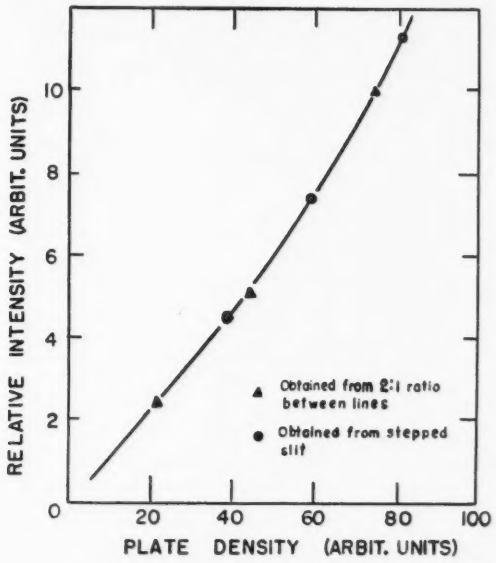

FIG. 2. Characteristic curve of emulsion of plate shown in Fig. 1.

The temperature was determined by two well-known methods:

Method 1.—The rotational quantum number K_m' which corresponds to the maximum intensity of the R branch is determined. This quantity is related to the absolute temperature T_m by the following equation:

$$T_m = 3.00\, K_m'(2K_m'+1).$$

Method 2.—Since the relative intensity $I_{K'}$ of the components of the R branch varies with the rotational quantum number K' according to the relation

$$\log_{10}(I_{K'}/K') = \text{constant} - 1.30K'(K'+1)/T,$$

a plot of $\log_{10}(I_{K'}/K')$ vs. $K'(K'+1)$ yields a straight line. The slope of this line is related to the absolute temperature by

$$T = 1.30/\text{slope}.$$

Fig. 3 shows the plots of $\log_{10}(I_{K'}/K')$ against $K'(K'+1)$ for each plate that was sufficiently well exposed. In almost every case a straight line resulted. In two instances curved lines were obtained which could be represented essentially by two straight lines. The temperatures calculated from the initial and

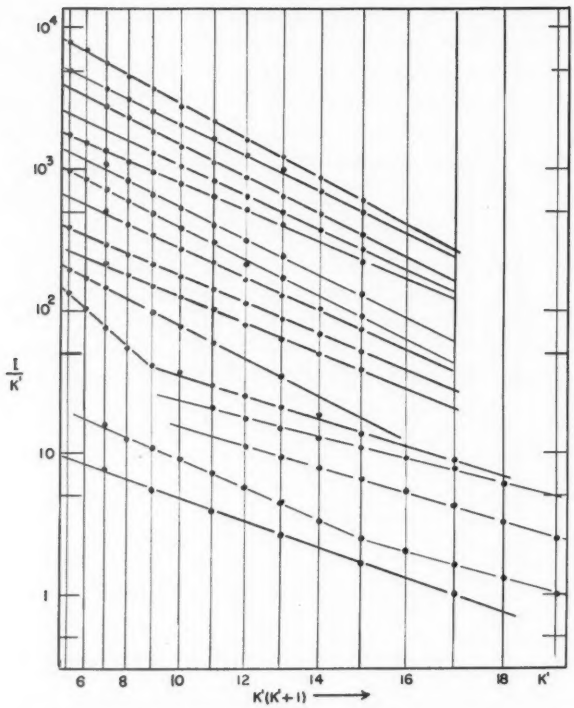

FIG. 3. Plots of $\log(I_{K'}/K')$ against $K'(K'+1)$ for auroral plates described in Table I.

final slopes correspond to rather conservative upper and lower limits for the temperature range as shown by Vallance Jones and Harrison (1955). It is worth noting that the exposure time for these two plates was of the order of 8 hours, whereas for all the other plates the exposure time ranged from 1 to 4 hours. A number of plates were not sufficiently well exposed to measure temperatures by the slope method but it was still possible to determine the position of the maximum of the intensity distribution, and hence the temperature, from them.

RESULTS AND DISCUSSION

Table I lists the temperatures calculated by both methods. T_m and T(slope) correspond to the temperatures deduced by method 1 and method 2 respectively. The temperatures listed at the bottom of the table were calculated by method 1 only, since these plates were not sufficiently well exposed to make possible accurate intensity measurements of the individual rotational lines. These temperatures are probably reliable, since there is good agreement between the two methods as seen from the upper portion of the table, and in view of the fact that in only a very few cases were straight line plots not obtained.

TABLE I

Date		Aurorae at Churchill		Temperature, ° K.		Saskatoon aurorae	Curve No. in Fig. 3
		Forms	Intensity	T(slope)	T_m		
1954							
Aug.	16	RA, RB	2–3	245	235		1
	19	RA, PS, R, B	3	285	275	None	2
	25			270	270	None	3
	29	R, RA, B	3	285	260		4
Sept.	1	PS, RA, B	2	330	315		5
	15	HA, PS, B	2–3	250	220		6
	18	Faint arcs	1	350	320	1	16
	30	HA	1	265	265	2	7
	30	Auroral clouds	1	290	220	2	8
Oct.	2	Auroral clouds	1	320	315	2	9
	17	PS, faint arcs	1	330	315	2	10
	18	Clouds, arcs	1	300	315	1	11
1956							
Oct.	1	RB, DS, HA	1–2	340–660	360		12
Nov.	13	RB, HA, R, DS	1–2	440	410	2	13
	15	RB, RA, R, HB	1–2	480	430	1	14
	16	RB, DS, HA, R	1–2	310–490	315	None	15
1954							
Sept.	21	Auroral clouds	1		315	1	
	14	Faint arcs	1		315	1	
	18	RA, PS, B	2–3		230	1	
Oct.	2	PS, C, B	3		230	2	
	2	R, RA	1		315	2	
	20	Faint arcs	1		315	0–1	
	23	RA, R, B	2–3		230	2	

Mean temperature of weak aurorae (Intensity 0–2) = 335±52° K.
Mean temperature of strong aurorae (Intensity >2) = 250±23° K.

Observations of the occurrence of the Hα emissions at Saskatoon and Churchill (latitude 52.1° and 58.8° N. respectively) indicated that the proton flux tends to be associated with the southern extent of an auroral display (Montalbetti and Vallance Jones 1957). Similar observations have been reported by Vegard (1952). Thus the occurrence of aurorae over Saskatoon was taken as evidence that the proton flux was south of Churchill. In the second last column of Table I, the intensity of the aurora which occurred over Saskatoon during the time that an exposure was being made at Churchill is listed. If proton excitation of the N_2^+ band is important, it is likely that higher temperatures would be measured at Churchill during times of weak or no aurora over the southern station. Examination of Table I shows that no correlation exists between the temperature measured at Churchill and the intensity of aurora over Saskatoon. Furthermore, these temperatures range from approximately 230° K. to 480° K., in agreement with the results obtained by the Saskatoon group. These results suggest that either the excitation of the N_2^+ band by protons is unimportant or the protons excite the nitrogen molecules in such a manner as not to affect the thermal equilibrium.

The intensity of the aurora at Churchill which occurred during the exposure interval is listed in the third column of Table I. Averaging the temperature variation for weak aurora and for strong aurora shows that the temperature is some 85° K. greater for the weak auroral displays. According to Störmer

(1955) the average difference of height between the two types of displays is approximately 15 km. Thus a vertical temperature gradient of 6° K./km. is noted in agreement with other observations (The Rocket Panel 1952; Shepherd and Hunten 1955).

As mentioned in the previous section, the exposure times for the two cases when curved lines were obtained was of the order of 8 hours. It is thus likely that the exposure was of sufficient duration to obtain spectra of very weak aurorae superposed on the spectra of stronger aurorae. The upper temperature limit deduced from such spectra very likely corresponds to very weak high altitude aurorae.

ACKNOWLEDGMENTS

The author is indebted to Dr. B. W. Currie for advice and encouragement and to Drs. A. Vallance Jones and D. M. Hunten for valuable discussions.

REFERENCES

MONTALBETTI, R. and VALLANCE JONES, A. 1957. J. Atm. and Terrest. Phys. (In press).
PETRIE, W. 1953. J. Atm. and Terrest. Phys. **4**, 5.
ROCKET PANEL, THE. 1952. Phys. Rev. **88**, 1027.
SHEPHERD, G. G. and HUNTEN, D. M. 1955. J. Atm. and Terrest. Phys. **6**, 336.
VALLANCE JONES, A. and HARRISON, A. W. 1955. J. Atm. and Terrest. Phys. **6**, 336.
VEGARD, L. 1951. The aurorae (L. Harang) (Chapman & Hall, Ltd., London), p. 83.
——— 1952. Nature, **170**, 536.
——— 1956. Geofys. Publikasjoner, **19**, No. 9.
STÖRMER, C. 1955. The polar aurora (Clarendon Press, Oxford).

HIGH RESOLUTION RAMAN SPECTROSCOPY OF GASES

X. ROTATIONAL SPECTRUM OF BUTATRIENE ($H_2C{=}C{=}C{=}CH_2$)[1]

B. P. STOICHEFF

ABSTRACT

The rotational Raman spectrum of butatriene ($H_2C{=}C{=}C{=}CH_2$) at a pressure of 2 cm. Hg was photographed with a 21 ft. grating spectrograph. An analysis of this spectrum (based on the symmetric top approximation) yields the rotational constant $\frac{1}{2}(B_0+C_0) = 0.1314_1 \pm 0.0001$ cm^{-1}. If the two outer C=C bonds in butatriene are assumed to have the same length as the C=C bonds in allene, namely 1.309 Å, it is found that the central C=C bond has a length of 1.284 ± 0.006 Å, a value which is shorter than that of the C=C bonds in ethylene and in allene.

A. INTRODUCTION

The length of carbon–carbon single bonds is known to depend primarily on adjacent bond types (for a summary see Herzberg and Stoicheff 1955). Recently a dependence of bond length on environment has also been found for carbon–carbon double bonds, and the present paper reports further results to support such a dependence.

Evidence for a carbon–carbon double bond considerably shorter than that in ethylene was found in ketene from its microwave spectrum (Johnson and Strandberg 1952) and in allene from its infrared and Raman spectra (Overend and Thompson 1953; Stoicheff 1955). The lengths in ketene[2] and allene are respectively 1.313 ± 0.003 Å and 1.309 ± 0.001 Å as compared with 1.344 Å for ethylene.[3] This difference of approximately 0.03 Å in bond length is apparently due to the fact that in allene and ketene, the C=C bonds are adjacent to two single bonds and one double bond while in ethylene the C=C bond is adjacent to four single bonds. In butatriene ($H_2C{=}C{=}C{=}CH_2$), the central C=C bond is adjacent to two double bonds, and the present analysis of the rotational Raman spectrum of butatriene shows that this bond is even shorter than that in allene and ketene.

B. EXPERIMENTAL

The apparatus described in paper I (Stoicheff 1954) with some modifications was used to photograph the rotational Raman spectrum; four lamps replaced the original two, and a cylindrical lens was placed in front of the photographic plate of the spectrograph. The sample of butatriene was prepared by Merck and Co., Montreal. A mass spectrometer analysis showed that at least 95%

[1]Manuscript received May 6, 1957.
Contribution from the Division of Pure Physics, National Research Council, Ottawa, Canada.
Issued as N.R.C. No. 4404.

[2]Johnson and Strandberg (1952) obtained the value 2.475 ± 0.003 Å for the sum of the C=C and C=O distances in ketene. If one assumes that r_0(C=O) = 1.162 Å as found for the CO_2 molecule (Herzberg and Herzberg 1953), then r_0(C=C) = 1.313 ± 0.003 Å in ketene.

[3]The value r_0(C=C) = 1.344 Å in ethylene was calculated from the Raman value of B_0 (Romanko, Feldman, Stansbury, and McKellar 1954) using r_0(C—H) = 1.071 Å and ∠HCH = 120° as obtained from the infrared spectra of C_2H_4 and C_2D_4 (Gallaway and Barker 1942).

was of mass 52; the remainder was mainly of mass 54 and was probably butadiene.

A difficulty was encountered when filling the Raman tube with butatriene to a pressure of 15–30 cm. Hg commonly used in these researches: at gas pressures higher than 2 cm. Hg, the Rayleigh light became extremely intense within a few minutes of introducing the gas into the tube. This phenomenon was due to the rapid polymerization of the butatriene or of the impurities. The difficulty was overcome by working with pressures of 1–2 cm. Hg, by renewing the sample every hour, and by keeping the Raman tube and $NaNO_2$ filter solution surrounding the tube at a temperature of about 5° C. Fortunately, butatriene with its three double bonds has an extremely intense rotational Raman spectrum and it was possible to photograph the spectrum even at this low pressure in reasonable exposure times.

Several photographs of the rotational Raman spectrum were obtained in the second order of the 21 ft. grating, two with the cylindrical lens placed in front of the photographic plate and two without this lens. The exposure times of the former were 1 and 2 hours and of the latter 12 and 20 hours. Fig. 1 shows the Raman spectrum on the Stokes side of the exciting line, photographed in 1 hour. The rotational lines have a spacing of about 0.52 cm^{-1} and are fairly well resolved. However, the spectrum falls within 35 cm^{-1} of the exciting line, a region which is masked by grating ghosts, and therefore many of the rotational lines are superimposed on an intense background and some are blended with the grating ghosts. Second- and third-order iron lines excited in an iron hollow cathode (Stanley and Dieke 1955) were used as wavelength standards.

Two plates were evaluated, one photographed in 1 hour with the cylindrical lens, and the other in 20 hours without this lens. The wavenumber displacements agreed to within ± 0.02 cm^{-1} and the average values are listed in Table I.

TABLE I

OBSERVED WAVENUMBER SHIFTS OF THE ROTATIONAL RAMAN LINES OF BUTATRIENE ($H_2C_4H_2$)

J	$\lvert\Delta\nu\rvert$,[a] cm^{-1}	J	$\lvert\Delta\nu\rvert$,[a] cm^{-1}	J	$\lvert\Delta\nu\rvert$,[a] cm^{-1}
20	11.28_6	35	—*	50	27.07_3
21	11.83_1	36	19.69_5*	51	27.58_5
22	12.34_5*	37	20.24_5*	52	28.10_5*
23	12.86_7	38	20.75_1	53	—*
24	13.40_8	39	21.28_7	54	—*
25	13.90_1*			55	29.70_9
26	14.44_5	40	21.80_9	56	30.19_6
27	14.98_4	41	22.33_7	57	30.70_9
28	15.51_3	42	22.84_7	58	31.27_4
29	16.02_4	43	23.35_5*	59	31.79_0
		44	23.89_2		
30	16.52_6*	45	24.44_9	60	32.28_6
31	17.09_3	46	24.96_6	61	32.82_3
32	17.60_9	47	25.47_5	62	33.38_3
33	18.16_1*	48	26.02_3	63	33.90_2
34	18.70_9*	49	26.52_9		

[a]All values are averages of the Stokes and anti-Stokes lines measured on two plates.
*Lines blended with grating ghosts.

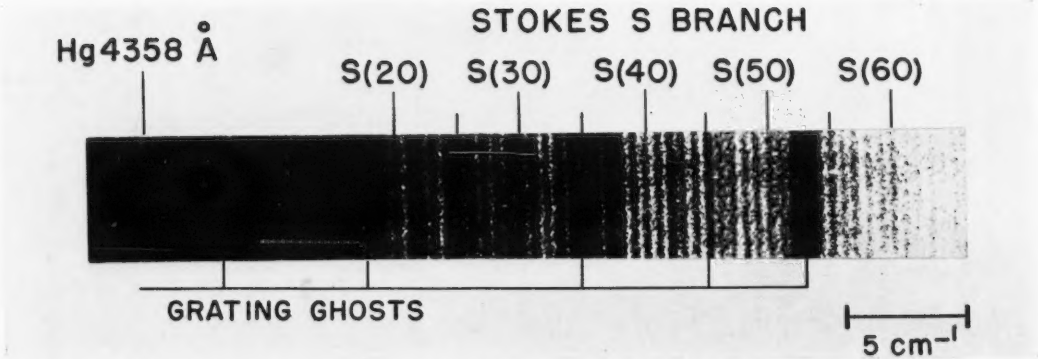

FIG. 1. Pure rotational Raman spectrum (Stokes branch) of the slightly asymmetric top molecule butatriene ($H_2C_4H_2$).

C. ROTATIONAL ANALYSIS

The simple appearance of the rotational spectrum, with its relatively sharp lines and narrow regular spacing, suggests that the rotational lines correspond to transitions of the type $\Delta K = 0$, $\Delta J = 2$; that is, the observed spectrum resembles that of a symmetric top. This, of course, is to be expected once it is assumed that the four carbon atoms in butatriene are collinear. In this case of a slightly asymmetric prolate top, the selection rule $\Delta K = 0$ holds approximately and the most intense lines are due to transitions $\Delta J = 2$. Therefore, the displacements of the Raman lines can be expressed to a good approximation by the equation

$$|\Delta\nu| = 4B_0(J+3/2) - 8D_J(J+3/2)^3,$$

where $B_0 = \frac{1}{2}(B_0+C_0)$. The observed line spacing ($\approx 4B_0$) was used to determine the rotational numbering and the rotational constants were evaluated in the usual way by plotting a graph (Fig. 2) of $|\Delta\nu|/(J+3/2)$ against $(J+3/2)^2$. The values obtained are

$$\tfrac{1}{2}(B_0+C_0) = 0.1314_1 \pm 0.0001 \text{ cm}^{-1} \text{ and } D_J \approx 1\times10^{-8} \text{ cm}^{-1}.$$

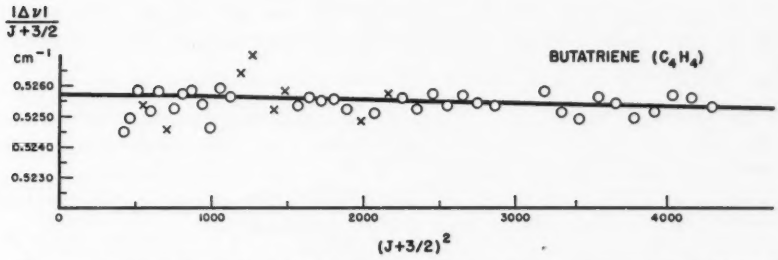

FIG. 2. $|\Delta\nu|/(J+3/2)$ graph for the ground state of butatriene (× represents lines blended with grating ghosts).

The rotational constant is related to the moments of inertia of the molecule by the equation $\frac{1}{2}(B_0+C_0) = \frac{1}{2}\times27.9890\times10^{-40}[(1/I_b)+(1/I_c)]$ and leads to the value $[(1/I_b)+(1/I_c)] = 9.390_1\times10^{37}$ g^{-1} cm^{-2}.

D. MOLECULAR STRUCTURE

Although the symmetry of the butatriene molecule has not yet been determined experimentally, there is little doubt that the molecule is planar and belongs to the point group V_h. Its structure and four structural parameters are represented in Fig. 3. The moment of inertia about the axis b–b is

$$I_b = 2[m_C(r_1^2+r_2^2)+2m_H r_3^2]$$

and that about an axis through the center and perpendicular to the plane of the molecule is

$$I_c = 2[m_C(r_1^2+r_2^2)+2m_H(r_3^2+h^2)].$$

When it is assumed that the C—H distance is $1.07\pm.01$ Å and the HCH

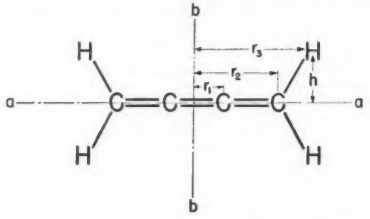

FIG. 3. Structure and structural parameters of butatriene.

angle is $117\pm1.5°$ (the values found in allene by Stoicheff 1955), the above value of $[(1/I_b)+(1/I_c)]$ leads to a relation for the $\rangle C{=}C{=}$ and $=C=C=$ distances, namely, $r_0(=C=C=) = 3.3324-1.565r_0(\rangle C{=}C{=})$. If the three carbon–carbon bonds are assumed to be of equal length one finds a value of 1.299 Å. But since the central bond ($=C=C=$) and the outer bonds ($\rangle C{=}C{=}$) have different adjacent bond types it seems preferable to assume that the bond lengths differ. In this case the similarity of the environment of the outer carbon–carbon bonds to that in allene suggests that the length of 1.309 ± 0.003 Å found for the $\rangle C{=}C{=}$ bonds in allene be assumed for these bonds. This leads to a value of 1.284 ± 0.006 Å for the length of the central carbon–carbon double bond in butatriene, a value considerably shorter than in allene or ketene.

The known lengths of carbon–carbon double bonds, obtained from spectroscopic investigations, can be summarized as follows:

$\rangle C{=}C\langle$	$\rangle C{=}C{=}$	$=C=C=$
1.344 Å	1.309 Å	1.284 Å

All three values quoted here refer to r_0 values, that is, they include zero point vibration and hence might differ from the equilibrium internuclear distances by as much as 0.005 Å. Of the three values, that for $\rangle C{=}C{=}$ is probably the most accurately known, and as mentioned earlier (Section A) nearly equal values were found in allene and ketene. The present value for $\rangle C{=}C\langle$ is not without objection even though the values of B_0 and A_0 for ethylene used in this calculation are thought to be the most accurate available. A more reliable value can probably be obtained by a study of the pure rotational Raman spectra of C_2H_4 and C_2D_4 under the conditions of high resolution used in the present research.

A short length for the $=C=C=$ bond has also been obtained from electron diffraction experiments with carbon suboxide ($O=C=C=C=O$). Mackle and Sutton (1951) found a value of 1.28 ± 0.03 Å and more recently Bastiansen (1951) has found 1.279 Å. Yet in spite of the good agreement this value cannot

be considered as definitive since there is still some doubt as to the linearity of the C_3O_2 molecule.

In the present paper, admittedly, several assumptions were necessary in order to obtain a value for the central carbon–carbon bond length in butatriene, and it would be desirable to determine the structural parameters independently of any assumptions. If the B_0 value for the isotopic molecule $D_2C_4D_2$ were known, it could lead to the independent evaluation of the central and outer carbon–carbon bond lengths. However, the limited accuracy with which these rotational constants can presently be obtained would not lead to a significant result.

I am grateful to Dr. F. P. Lossing for the mass spectrometer analysis of the sample of butatriene, and to Dr. G. Herzberg for helpful discussions.

REFERENCES

BASTIANSEN, O. 1956. Private communication.
GALLAWAY, W. S. and BARKER, E. F. 1942. J. Chem. Phys. **10**, 88.
HERZBERG, G. and HERZBERG, L. 1953. J. Opt. Soc. Amer. **43**, 1037.
HERZBERG, G. and STOICHEFF, B. P. 1955. Nature, **175**, 79.
JOHNSON, H. R. and STRANDBERG, M. W. P. 1952. J. Chem. Phys. **20**, 687.
MACKLE, H. and SUTTON, L. E. 1951. Trans. Faraday Soc. **47**, 937.
OVEREND, J. and THOMPSON, H. W. 1953. J. Opt. Soc. Amer. **43**, 1065.
ROMANKO, J., FELDMAN, T., STANSBURY, E. J., and MCKELLAR, A. 1954. Can. J. Phys. **32**, 735.
STANLEY, R. W. and DIEKE, G. H. 1955. J. Opt. Soc. Amer. **45**, 280.
STOICHEFF, B. P. 1954. Can. J. Phys. **32**, 330.
——— 1955. Can. J. Phys. **33**, 811.

ULTRAVIOLET ABSORPTION SPECTRA OF HCN AND DCN

I. THE α—X AND β—X SYSTEMS[1]

G. HERZBERG AND K. K. INNES[2]

ABSTRACT

The ultraviolet absorption spectra of HCN and DCN have been investigated below 2000 Å. Four band systems have been found of which two, α—X and β—X, are described and analyzed in the present paper. At the long wavelength end the α—X system in both HCN and DCN consists of simple progressions of sharp bands whose fine structure has been measured. At shorter wavelengths diffuseness (predissociation) sets in gradually but at somewhat different energies in HCN and DCN. Both the vibrational and rotational analyses lead independently and unambiguously to the conclusion that in the upper state, α, unlike in the ground state, the molecule is non-linear. The geometrical parameters obtained from the rotational fine structure are $r_0(\mathrm{CH}) = 1.14_0$ Å, $r_0(\mathrm{CN}) = 1.297$ Å, and $\angle$ H—C—N = 125.0°. Two vibrational frequencies in the α state are established: for HCN, $\nu_1 = 1506$, $\nu_2 = 949$; for DCN, $\nu_1 = 1506$, $\nu_2 = 735$ cm^{-1}. The CH stretching frequency has not been found.

The β—X system has been clearly observed only for DCN. In HCN it is apparently so strongly predissociated that its presence among the diffuse α—X bands is difficult to establish. In the β state, as in the α state, the molecule is bent. The somewhat fragmentary rotational analysis leads to $r_0(\mathrm{CN}) = 1.33_4$ Å and $\angle$ D—C—N = 114.5° when $r_0(\mathrm{CD}) = 1.14_0$ Å is assumed. Only one vibrational frequency, $\nu_2 = 731$ cm^{-1}, has been established in the β state of DCN. The vibrational quantum number v_2 is uncertain since no isotope effect is available to establish the position of the 0-0 band.

In the rotational analysis, particularly of the α—X system, the effects of the asymmetry of the molecule in the upper state are clearly demonstrated by the doubling of the levels with $K = 1$ and $K = 2$ and the large contributions of the asymmetry to the terms in $J^2(J+1)^2$. From the sign of the K-type doubling for $K = 1$ it follows unambiguously that both the α and the β state belong to the species A'', i.e. the electronic eigenfunctions are antisymmetric with respect to the plane of the molecule. It appears probable that both transitions α—X and β—X correspond to forbidden transitions ($^1\Delta$—$^1\Sigma^+$ and $^1\Sigma^-$—$^1\Sigma^+$) of the linear case. The non-linear structure of the excited states is briefly discussed in terms of electron configurations.

A number of interesting features of the predissociation in the α state are pointed out. It is shown that the dissociation products are in all probability H+CN($^2\Pi$).

A. INTRODUCTION

Hydrogen cyanide exhibits no absorption throughout the visible and near ultraviolet regions down to 2000 Å. Price (1934) and Price and Walsh (1945) were the first to investigate the absorption in the vacuum ultraviolet and found extremely strong diffuse absorption bands below 1120 Å and somewhat weaker sharp absorption bands in the region 1550 to 1350 Å. Hilgendorff (1935) reported the observation of another absorption band system at longer wavelengths (2000–1700 Å) which is very much weaker than Price's band systems and requires an absorbing path of about 10 cm-atm. In several respects this HCN absorption appears analogous to the near ultraviolet C_2H_2 bands while the HCN bands near 1500 Å appear analogous to the C_2H_2 bands in the same region.

[1]Manuscript received April 24, 1957.
Contribution from the Division of Pure Physics, National Research Council, Ottawa, Ontario.
Issued as N.R.C. No. 4400.

[2]National Research Laboratories Postdoctorate Fellow, 1951–53; now with the Department of Chemistry, Vanderbilt University, Nashville, Tennessee.

The fine structure of the near ultraviolet C_2H_2 bands has recently been analyzed in detail by Ingold and King (1952, 1953) and by Innes (1954). The analysis showed unambiguously that in the upper state the C_2H_2 molecule has a non-linear C_{2h} structure and the dimensions of the molecule in this state were determined from the spectrum. In view of the similarity of the electronic structure of HCN and C_2H_2 and in view of the fact that so few rotational structures of electronic spectra of polyatomic molecules have been analyzed, it appeared worth while to attempt a more detailed investigation of the HCN and DCN bands including, where possible, an analysis of the rotational structure. In the present paper, we report on the results of the study of the first weaker absorption region (2000–1600 Å) where two band systems have been found (designated α—X and β—X). A later paper will deal with the second, much stronger absorption region at 1500 Å and below. The principal result of these investigations is that the HCN molecule is non-linear in at least three excited electronic states.

B. EXPERIMENTAL

All HCN and DCN spectra were taken in the fourth order of the 3 meter vacuum grating spectrograph described by Brix and Herzberg (1954). The dispersion was 0.65 Å/mm. and the resolving power actually obtained was 150,000. The spectra were measured against iron lines of second order. The accuracy of non-blended lines is estimated to be ± 0.05 cm^{-1}.

Two absorption tubes were used, one 50 cm., the other 100 cm. long. They were filled with HCN or DCN to pressures ranging from 0.01 to 240 mm. Unlike the case of C_2H_2, because of the low vapor pressure of HCN, it was not possible to obtain spectra at low temperature.

For the earlier exposures with the first absorption tube, the continuous background for the absorption spectra was a Lyman flash discharge tube viewed end-on as described by Brix and Herzberg (1954). Some of the later exposures above 1500 Å with the second absorption tube were taken with the superior continuum of a Xe discharge as described by Wilkinson and Tanaka (1955).

The discharge tube was separated from the absorption tube by a spherical LiF lens whose focal length was so chosen that light of the desired wavelength range was focused on the grating. An LiF prism with one cylindrical face (Curry and Herzberg 1934) was placed between the absorption tube and the spectrograph and focused the desired spectral region on the slit of the spectrograph.

C. OBSERVED SPECTRA

In the region from 2000 to 1600 Å, there are several fairly long progressions of simple bands both in HCN and in DCN. Fig. 1 shows sections of the spectrum for both isotopic molecules. At the long wavelength end the bands are quite sharp, each having two heads and a well-developed fine structure. This is shown by the two enlargements in Fig. 2 of an HCN and a DCN band. As one goes to shorter wavelengths, first the individual lines become

more and more diffuse, then only two diffuse heads are recognizable, and finally even these merge into one broad diffuse peak. The diffuseness sets in earlier and is more pronounced for HCN than for DCN. For this reason, more sharp progressions are found for DCN than for HCN. In particular, as will be shown below, three of these progressions extending from 1700 to 1550 Å form a separate band system which we shall call the β—X system to distinguish it from the main system which we designate α—X. No bands of the β—X system have been identified with certainty in HCN. The strong band system below 1550 Å to be described in a subsequent paper will be referred to as γ—X.

In Tables I and II the wave numbers and assignments of the heads of all the observed bands of HCN and DCN, respectively, are given for the region 2000 to 1550 Å. In the case of sharp bands, both R and Q heads are listed; for the diffuse bands, only one head or, if the head is no longer pronounced, the position of the intensity maximum is given. These latter wave numbers are clearly much less accurate than those of the sharp band heads. The intensities given in the second last column are rough estimates.

D. VIBRATIONAL ANALYSIS

As shown by Fig. 1 and Table I two fairly long progressions are immediately obvious in the α—X band system of HCN. The spacing in both progressions is about 940 cm^{-1} and decreases regularly toward shorter wavelengths. In addition, five weaker progressions with similar spacings can readily be distinguished. Similar progressions are found in DCN.

One of the strong progressions of HCN extends on the long-wave side to 52278 cm^{-1}, while the other extends to 53767 cm^{-1}. We conclude therefore that the second progression is one in which, in addition to the vibration excited in the first, another vibration is excited by a fixed amount. The separation 940 cm^{-1} of successive bands in either progression corresponds in all probability to a vibration ν_2' of the upper state similar to the bending vibration ν_2'' (=712 cm^{-1}) of the ground state. We assume that in the first progression no other vibration is excited, that is, it might be described as $(0v_2'0) \leftarrow (000)$. In the second progression the additional vibration has the frequency 1496 cm^{-1}, which is presumably the analogue of ν_1'' (=2095.5 cm^{-1}) of the lower state. Thus the second progression may be described as $(1v_2'0) \leftarrow (000)$. Members of the progressions $(2v_2'0) \leftarrow (000)$, $(3v_2'0) \leftarrow (000)$, and possibly $(4v_2'0) \leftarrow (000)$ may be assigned among the diffuse bands in the shortward part of the band system (see Table I).

According to the Franck–Condon principle the presence of a long progression in the bending vibration ν_2' with a maximum of intensity far removed from the first band can be accounted for only on the assumption that the equilibrium angle of the molecule in the excited electronic state is different from that in the ground state, i.e., that the molecule is bent in the excited state. If the molecule were linear in the excited state, the first band in a progression of the bending vibration should be by far the strongest, which is contrary to observation if the identification of the 940 cm^{-1} interval with the bending vibration ν_2' is correct.

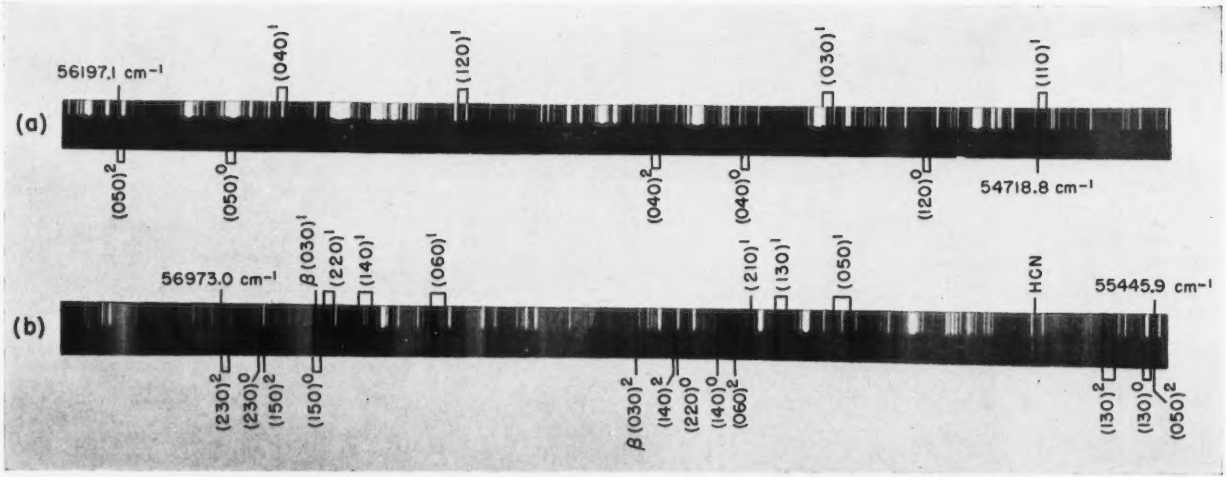

FIG. 1. Sections of the α—X absorption band systems of (*a*) HCN and (*b*) DCN. The main bands with lower state (00^00) are indicated above the spectrograms, the "hot" bands with lower states (01^10) below the spectrograms.

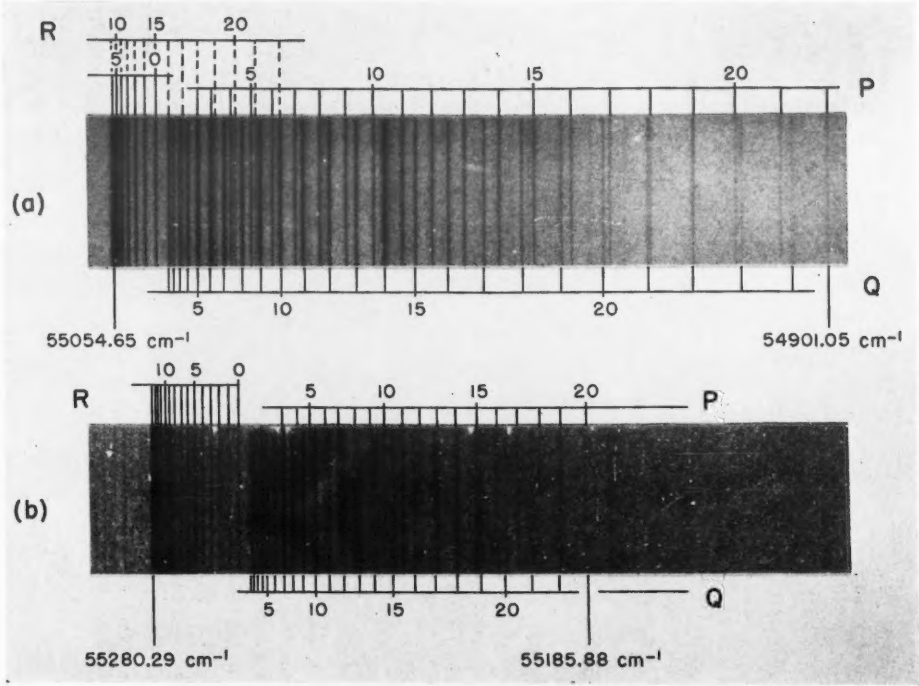

FIG. 2. Fine structure of $\alpha - X$ bands. (*a*) The $(030)^1 \leftarrow (00^00)$ band of HCN. (*b*) The $(040)^1 \leftarrow (00^00)$ band of DCN. The lines of the *P* and *R* branches are indicated above the spectrograms and those of the *Q* branches below.

TABLE I

BAND HEADS AND BAND ORIGINS IN THE α—X SYSTEM OF HCN

Assignment			ν_{vac} (cm^{-1}) observed					Assignment			ν_{vac} (cm^{-1}) observed				
Upper state $(v_1v_2v_3)^K$	—	Lower state $(v_1v_2^lv_3)$	R head	Q head	Band origin	I	ν_{calc}	Upper state $(v_1v_2v_3)^K$	—	Lower state $(v_1v_2^lv_3)$	R head	Q head	Band origin	I	ν_{calc}
α (0 0 0)^0	—	X (0 1^1 0)	51554.4	51539.5	51544.88	1		α (1 3 0)^0	—	X (0 1^1 0)?	55787.$_3$	55759.$_8$		50 d	
α (0 0 0)^2	—	X (0 1^1 0)	51638.1	51625.7	51628.08	1		α (0 4 0)^1	—	X (0 0^0 0)	55932.5	55920.8	55920.39	1000	55920.30
α (0 1 0)^1	—	X (0 2^0 0)	51818.1			0.5		α (0 5 0)^0	—	X (0 1^1 0)	56014.8	56004.9	56005.65	150	
α (0 1 0)^2	—	X (0 2^2 0)	51984.8	51961.9		0.5		α (0 5 0)^2	—	X (0 1^1 0)	56197.1	56184.9	56187.34	200 d	
α (0 0 0)^1	—	X (0 0^0 0)	52289.4	52277.7	52278.00	5	52277.70	α (1 3 0)^1	—	X (0 0^0 0)	56530.9	56519.5		1000 d	56519.83
α (0 1 0)^0	—	X (0 1^1 0)	52492.7	52482.8	52483.13	6		α (0 5 0)^1	—	X (0 0^0 0)	56782.9	56770.3	56770.34	3000	56770.60
α (0 1 0)^2	—	X (0 1^1 0)	52585.6	52574.5	52575.68	6		?α (0 6 0)^0	—	X (0 1^1 0)	56795.1			150	
α (0 2 0)^1	—	X (0 2^0 0)	52740.8	52729.9	52729.54	1	52729.62	α (0 6 0)^2	—	X (0 1^1 0)	57056.$_4$			150 d	
α (0 2 0)^2	—	X (0 2^2 0)	52927.7	52917.4	52917.93	1		α (1 4 0)^1	—	X (0 0^0 0)	57405.$_7$			2500 dd	57391.12
α (1 0 0)^0	—	X (0 1^1 0)	53047.$_7$			0.5[a]		α (0 6 0)^1	—	X (0 0^0 0)	57605.4	57591.6		4000 d	57590.52
α (0 1 0)^1	—	X (0 0^0 0)	53229.7	53217.9	53218.30	25	53218.32	?α (2 3 0)^1	—	X (0 0^0 0)	57995.$_0$			400 d	57976.92
α (1 1 0)^1	—	X (0 2^0 0)	53306.6			2	53296.53	α (1 5 0)^1	—	X (0 0^0 0)	58262.$_0$			5000 dd	58235.15
α (0 2 0)^0	—	X (0 1^1 0)	53412.0	53401.9	53402.39	15		α (0 7 0)^1	—	X (0 0^0 0)	58413.$_2$	58398.$_7$		4000 d	58376.94
α (0 2 0)^2	—	X (0 1^1 0)	53516.4	53506.0	53506.44	18		?α (2 4 0)^1	—	X (0 0^0 0)		58854.$_8$		1000 dd	58841.94
α (0 3 0)^1	—	X (0 2^0 0)	53642.5	53630.9	53631.34	2	53631.32	α (1 6 0)^1	—	X (0 0^0 0)		59090.$_8$		7000 dd	59048.80
α (1 0 0)^1	—	X (0 0^0 0)	53780.8	53765.1	53766.78	7	53773.60	α (0 8 0)^1	—	X (0 0^0 0)	59220.$_1$	59204.$_7$		3000 d	59126.74
α (0 3 0)^2	—	X (0 2^2 0)	53855.5	53848.3	53846.06	2		α (2 5 0)^1	—	X (0 0^0 0)		59697		2000 dd	59679.70
α (1 1 0)^0	—	X (0 1^1 0)	53982.0	53972.5	53972.90	9		α (1 7 0)^1	—	X (0 0^0 0)		59871		6000 dd	59828.95
α (0 2 0)^1	—	X (0 0^0 0)	54152.7	54140.2	54140.84	120	54141.04	α (3 4 0)^1	—	X (0 0^0 0)		60190		1000 dd	60272.76
α (0 3 0)^0	—	X (0 1^1 0)	54309.9	54299.1	54300.37	30		α (2 6 0)^1	—	X (0 0^0 0)		60490		3000 dd	60487.08
α (0 3 0)^2	—	X (0 1^1 0)	54429.0	54418.1	54419.26	35		α (1 8 0)^1	—	X (0 0^0 0)		60626		5000 dd	60572.48
α (0 4 0)^1	—	X (0 2^0 0)	54520.4	54507.9	54508.96	6	54508.88	α (3 5 0)^1	—	X (0 0^0 0)		60982		1500 dd	61104.25
α (1 1 0)^1	—	X (0 0^0 0)	54718.8	54707.4	54707.91	55	54707.95	α (2 7 0)^1 }	—	X (0 0^0 0)		61327		4000 dd	{ 61260.96
α (0 4 0)^2	—	X (0 2^2 0)	54769.$_0$			7		α (1 9 0)^1 }							{ 61276.27
α (1 2 0)^0	—	X (0 1^1 0)	54896.2	54887.3	54887.17	30		α (3 6 0)^1	—	X (0 0^0 0)		61773		2000 dd	61905.36
α (1 2 0)^2	—	X (0 1^1 0)	54996.2			30[b]		α (2 8 0)^1	—	X (0 0^0 0)		62051		3000 dd	61998.22
α (0 3 0)^1	—	X (0 0^0 0)	55054.9	55042.8	55042.79	350	55042.74	α (4 5 0)^1	—	X (0 0^0 0)		62391		500 dd	62508.80
α (0 4 0)^0	—	X (0 1^1 0)	55180.6	55170.8	55171.12	50		α (3 7 0)^1	—	X (0 0^0 0)		62535		2000 dd	62672.97
α (2 0 0)^1	—	X (0 0^0 0)	55252.0	55229.1?		10	55249.50	α (2 9 0)^1	—	X (0 0^0 0)		62800		2000 dd	62695.74
α (0 4 0)^2	—	X (0 1^1 0)	55323.1	55310.8	55313.57	150		α (4 6 0)^1	—	X (0 0^0 0)		63187		1500 dd	63303.64
α (0 5 0)^2 }	—	X (0 2^2 0) }	55435.4	55423.3		20 d		α (2 10 0)^1	—	X (0 0^0 0)		63501		3000 dd	63350.40
α (1 3 0)^2 }	—	X (0 2^2 0) }													
α (1 2 0)^1	—	X (0 0^0 0)	55635.8	55623.6	55624.44	350	55624.40								

Note.—d means diffuse with some fine structure.
dd means very diffuse.

[a] Overlapped by (0 1 0)^1 — (0 0^0 0).
[b] Overlapped by (0 3 0)^1 — (0 0^0 0).

TABLE II. BAND HEADS AND BAND ORIGINS IN THE α—X AND β—X SYSTEMS OF DCN

Assignment			ν_{vac} (cm^{-1}) observed					Assignment			ν_{vac} (cm^{-1}) observed				
Upper state $(v_1v_2v_3)^K$	—	Lower state $(v_1v_2^lv_3)$	R head	Q head	Band origin	I	ν_{calc}	Upper state $(v_1v_2v_3)^K$	—	Lower state $(v_1v_2^lv_3)$	R head	Q head	Band origin	I	ν_{calc}
α (0 1 0)^1	—	X (0 0^0 0)	53156.4			0.5	53135.24	β (0 4 0)^1	—	X (0 2^0 0)	56402.1	56389.3		8	56389.50
α (0 2 0)^0	—	X (0 1^1 0)	53284.9			0.5		α (1 5 0)^2	—	X (0 2^2 0)	56430.9	56409.0		7	
α (0 2 0)^2	—	X (0 1^1 0)	53344.5	53330.0		1		α (2 3 0)^3	—	X (0 2^2 0)	56477.3	56455.8		7	
			53599.2					α (0 6 0)^1	—	X (0 0^0 0)	56623.2	56600.8	56600.97	200	56600.92
α (0 2 0)^1	—	X (0 0^0 0)	53875.8	53855.5	53855.90	3	53855.64	α (0 3 1)^1	—	X (0 0^0 0) ?	56647.2	56635.4 ?		15	
α (0 3 0)^0	—	X (0 1^1 0)	53991.9	53978.6		3		α (1 4 0)^1	—	X (0 0^0 0)	56744.6	56725.3	56725.56	300	56725.26
α (1 1 0)^0	—	X (0 1^1 0)	54049.7	54038.0		3		α (2 2 0)^1	—	X (0 0^0 0)	56802.5	56788.0		100	56787.48
α (0 3 0)^2	—	X (0 1^1 0)	54057.4	54042.5		6		β (0 3 0)^1	—	X (0 0^0 0)	56816.0			150	56803.53
α (1 1 0)^2	—	X (0 1^1 0)	54102.2 L					α (1 5 0)^0	—	X (0 1^1 0)	56819.8	56808.1		200	
			54220.5	54212.6		2		α (1 5 0)^2	—	X (0 1^1 0)	56902.0			300	
?α (1 2 0)^2	—	X (0 2^2 0)	54275.0 L			2		α (2 3 0)^0	—	X (0 1^1 0)	56910.3			200	
α (1 2 0)^2	—	X (0 2^2 0)	54331.9	54320.4		2		α (2 3 0)^2	—	X (0 1^1 0)	56973.0	56961.2		200	
α (0 3 0)^1	—	X (0 0^0 0)	54584.4	54563.9	54564.05	10	54564.14	β (0 4 0)^2	—	X (0 1^1 0)	57002.3	56990.8		80	
α (1 1 0)^1	—	X (0 0^0 0)	54638.1	54619.8		3	54620.50	α (2 4 0)^1	—	X (0 2^0 0)	57053.8	57038.5		30	57037.82
α (0 4 0)^0	—	X (0 1^1 0)	54684.7	54671.7	54671.65	6		β (0 5 0)^1	—	X (0 2^0 0)	57113.1	57097.4		40	57101.35
α (0 4 0)^2	—	X (0 1^1 0)	54758.2	54743.3	54743.83	10		α (0 7 0)^1	—	X (0 0^0 0)	57266.4	57243.6	57243.95	400	57244.46
α (1 2 0)^0	—	X (0 1^1 0)	54762.4	54750.4	54750.44	6		α (1 5 0)^1	—	X (0 0^0 0)	57418.8	57399.1		800	57398.42
α (1 2 0)^2	—	X (0 1^1 0)	54820.6	54807.7	54807.90	10		α (2 3 0)^1	—	X (0 0^0 0)	57501.0	57484.6		600	57484.50
β (0 1 0)^2	—	X (0 1^1 0)	54838.6	54828.8		2		β (0 4 0)^1	—	X (0 0^0 0)	57533.2	57519.2	57519.55	200	57519.58
			54923.4	54914.9		2		α (2 4 0)^0	—	X (0 1^1 0)	57591.9	57581.0		250	
α (0 4 0)^1	—	X (0 0^0 0)	55280.5	55258.8	55259.06	30	55259.02	β (0 5 0)^0 }	—	X (0 1^1 0)	57662.2	57650.2		200	
α (1 2 0)^1	—	X (0 0^0 0)	55351.9	55335.0		25	55334.56	α (2 4 0)^2 }							
α (0 5 0)^0	—	X (0 1^1 0)	55360.7	55348.0		15		α (3 2 0)^2	—	X (0 1^1 0)	57690.5			50	
α (0 5 0)^2	—	X (0 1^1 0)	55445.9	55430.8		30		β (0 5 0)^2	—	X (0 1^1 0)	57715.3	57704.2		200	
α (1 3 0)^0	—	X (0 1^1 0)	55463.2	55451.2	55451.55	20		α (0 8 0)^1	—	X (0 0^0 0)	57891.1	57868.0		300	57867.42
α (1 3 0)^2	—	X (0 1^1 0)	55527.6	55514.5[a]		30		β (0 6 0)^2	—	X (0 2^2 0)	57931.5	57920.0		100	
β (0 2 0)^2	—	X (0 1^1 0)	55562.7 ?			10		α (1 6 0)^1	—	X (0 0^0 0)	58075.5	58053.9		1000 d	58054.48
β (0 3 0)^1	—	X (0 2^2 0)	55671.8	55663.6		5	55665.45				58124.9[b]?	58100.2 ?			
β (0 3 0)^1	—	X (0 2^0 0)	55685.2	55677.0		5	55673.45	α (2 4 0)^1	—	X (0 0^0 0)	58185.4	58168.3	58168.16	800 s	58167.90
α (1 4 0)^2	—	X (0 2^2 0)	55738.1	55722.7		10		α (3 2 0)^1	—	X (0 0^0 0)	58224.8			150	58214.40
α (2 2 0)^2	—	X (0 2^2 0)	55784.0	55762.$_5$?		15		β (0 5 0)^1	—	X (0 0^0 0)	58244.6	58231.4		500	58231.43
α (0 5 0)^1	—	X (0 0^0 0)	55960.5	55939.2	55938.69	80	55938.52	α (2 5 0)^0	—	X (0 1^1 0)	58256.8			150	
α (1 3 0)^1	—	X (0 0^0 0)	56054.7	56035.9		100	56036.72				58332.5			100	
α (2 1 0)^1	—	X (0 0^0 0)	56095.0	56080.5 ?		20	56077.02	α (2 5 0)^2	—	X (0 1^1 0)	58338.2	58327.8		200	
α (0 6 0)^2	—	X (0 1^0 0)	56120.$_5$			25		β (0 6 0)^0	—	X (0 1^1 0)	58364.7			60	
α (1 4 0)^0	—	X (0 1^1 0)	56149.7	56138.0	56138.22	40		?α (3 3 0)^2	—	X (0 1^1 0)	58392.3			150	
α (2 2 0)^0	—	X (0 1^1 0)	56214.7	56197.9		20		β (0 6 0)^2	—	X (0 1^1 0)	58424.1	58412.3		200	
α (1 4 0)^2	—	X (0 1^1 0)	56221.4	56209.1		50		α (0 9 0)^1	—	X (0 0^0 0)	58572.0	58486.4		100 d	58468.04
β (0 3 0)^2	—	X (0 1^1 0)	56283.9	56269.8		20		β (0 7 0)^2	—	X (0 2^2 0)	58640.0			100	
α (2 3 0)^1	—	X (0 2^0 0)	56369.6	56353.8		7	56354.42	α (1 7 0)^1	—	X (0 0^0 0)	58714.$_3$	58691.$_7$		500 d	58691.68
								α (2 5 0)^1	—	X (0 0^0 0)	58854.6	58836.5		1600 s	58835.92

Note.—L, line-like feature which is probably band head.
d, s mean diffuse and sharp, respectively.

[a]Large zero gap indicating $K = 2$.
[b]There seems to be both a sharp and a diffuse head near here.

TABLE II. BAND HEADS AND BAND ORIGINS IN THE α—X AND β—X SYSTEMS OF DCN (*concluded*)

Assignment			ν_{vac} (cm^{-1}) observed				
Upper state $(v_1v_2v_3)^K$	—	Lower state $(v_1v_2^lv_3)$	*R* head	*Q* head	Band origin	*I*	ν_{calc}
α (3 3 0)^1	—	X (0 0^0 0)	58921.8	58907.1		300	58907.48
β (0 6 0)^1	—	X (0 0^0 0)	58952.0	58939.1		500	58939.08
α (2 6 0)^2	—	X (0 1^1 0)	59000.$_0$	59000.$_0$		200 d	
α (3 4 0)^0	—	X (0 1^1 0)	59009.$_5$			150	
β (0 7 0)^0	—	X (0 1^1 0)	59068.0			150	
α (3 4 0)^2	—	X (0 1^1 0)	59072.5$_5$	59063.7 ?		200	
?β (1 4 0)^1	—	X (0 0^0 0)	59088.3			150	
β (0 7 0)^2	—	X (0 1^1 0)	59129.2	59118.8		400	
β (0 8 0)^3	—	X (0 2^2 0)	59344.0			100	
α (1 8 0)^1	—	X (0 0^0 0)	59336.$_2$	59313.$_1$		400 d	59308.30
			59293.0 L			50	
α (2 6 0)^1	—	X (0 0^0 0)	59507.1	59487.5		3000 d	59486.84
α (3 4 0)^1	—	X (0 0^0 0)	59600.6	59585.9		1200	59586.94
			59617.1	59605.4		200	
β (0 7 0)^1	—	X (0 0^0 0)	59653.5	59642.2	59642.21	1000	59642.53
			59657.4			500	
			59670.4			200	
			59728.0			150	
α (3 5 0)^2	—	X (0 1^1 0)	59750.0	59738.9		300	
β (0 8 0)^0	—	X (0 1^1 0)	59766.7			150 d	
α (3 6 0)^1	—	X (0 2^0 0)	59786.9			200 d	59767.92
β (0 8 0)^2	—	X (0 1^1 0)	59829.6	59819.$_4$		400 d	
α (1 9 0)^1	—	X (0 0^0 0)	59919			300[a] d	59902.58
β (0 9 0)^3	—	X (0 2^2 0)	60044.1	60036.4 ?		100 d	
α (2 7 0)^1	—	X (0 0^0 0)	60142.2	60119.6		3500 d	60118.90
α (3 5 0)^1	—	X (0 0^0 0)	60266.9	60250.0		2500	60251.02
α (4 3 0)^1	—	X (0 0^0 0)	60313.0	60302.0		400	60305.66
β (0 8 0)^1	—	X (0 0^0 0)	60352.2	60341.6		500	60341.78
			60356.6	60349.1		300	
			60382.7			100	
α (3 6 0)^2	—	X (0 1^1 0)	60410.3	60399.$_7$		400 d	
β (0 9 0)^0	—	X (0 1^1 0)	60460.7	60451.3		250	
			60472.8 L			200 d	
β (0 9 0)^2	—	X (0 1^1 0)	60526.5	60517.0		500	
β (0 10 0)^1	—	X (0 2^0 0)	60608.8			80	60597.60
α (2 8 0)^1	—	X (0 0^0 0)	60767.$_8$	60740.8	[b]	2000 d	60730.38
α (3 6 0)^1	—	X (0 0^0 0)	60916.$_3$	60897.8		4000 d	60898.00
?α (5 2 0)^1	—	X (0 0^0 0)		60977.3		400	60990.24
α (4 4 0)^1	—	X (0 0^0 0)	60999.2	60986.2		1500	60982.38
			61043.3			300	

[a] There seems to be both a sharp and a diffuse head near here.

Assignment			ν_{vac} (cm^{-1}) observed				
Upper state $(v_1v_2v_3)^K$	—	Lower state $(v_1v_2^lv_3)$	*R* head	*Q* head	Band origin	*I*	ν_{calc}
β (0 9 0)^1	—	X (0 0^0 0)	61050.4	61036.9		2000	61036.83
			61058.6			100	
			61130.8			150	
β (0 10 0)^0	—	X (0 1^1 0)	61150.5			200	
			61159.7			150	
β (0 10 0)^2	—	X (0 1^1 0)	61218.4	61209.4		500	
β (0 11 0)^1	—	X (0 2^0 0)	61295.6			50	61284.25
α (2 9 0)^1	—	X (0 0^0 0)	61369.0	61344.0		500 d	61319.52
β (0 11 0)^2	—	X (0 2^2 0)	61432.9			100	
α (3 7 0)^1	—	X (0 0^0 0)	61550.$_0$	61530.$_4$		3000 dd	61526.12
α (4 5 0)^1	—	X (0 0^0 0)	61654.1	61638.9		2000	61643.72
α (5 3 0)^1	—	X (0 0^0 0)	61685.0			1500	61679.04
β (0 10 0)^1	—	X (0 0^0 0)	61740.5	61727.7		2500	61727.68
β (0 11 0)^0	—	X (0 1^1 0)	61836.5			200	
α (5 4 0)^2	—	X (0 1^1 0)	61844.3			300	
β (0 11 0)^2	—	X (0 1^1 0)	61907.2	61897.6		400 d	
α (3 8 0)^1	—	X (0 0^0 0)	62146.$_1$	62122.$_8$ L		2500 dd	62133.66
α (4 6 0)^1	—	X (0 0^0 0)	62305.$_6$	62290.$_8$		3000 d	62287.96
α (5 4 0)^1	—	X (0 0^0 0)	62371.2	62357.$_2$		2000 d	62351.22
β (0 11 0)^1	—	X (0 0^0 0)	62427.4	62413.8		3500 d	62414.33
α (5 5 0)^0	—	X (0 1^1 0)	62476.8			100 d	
β (0 12 0)^0	—	X (0 1^1 0)	62522.8	62508.6		350 d	
α (5 5 0)^2	—	X (0 1^1 0)	62533.5			50 ?	
			62540.0			50 ?	
β (0 12 0)^2	—	X (0 1^1 0)	62592.8	62583.6		400 d	
α (3 9 0)^1	—	X (0 0^0 0)	62763	62734		250 dd	62718.86
			62808.3			100 d	
α (4 7 0)^1	—	X (0 0^0 0)	62917.$_8$			2000 dd	62913.34
			63002.7			400 d	
α (5 5 0)^1	—	X (0 0^0 0)	63045.2	63038.9		1000 d	
β (0 12 0)^1	—	X (0 0^0 0)	63110.8	63097.1		4000 d	63096.78
			63140.7	63134.4		100 d	
			63162.1			50 d	
β (0 13 0)^0	—	X (0 1^1 0)	63199.6	63186.1		250 d	
β (0 13 0)^2	—	X (0 1^1 0)	63272.8	63262.4		400 d	
β (0 13 0)^1	—	X (0 0^0 0)	63787.7	63775.1		4000 d	63775.03
β (0 14 0)^2	—	X (0 1^1 0)	63952.0			400 d	
β (0 14 0)^1	—	X (0 0^0 0)	64460.7	64448.0		3000 d	64449.08
β (0 15 0)^2	—	X (0 1^1 0)	64624.4			500 d	
β (0 15 0)^1	—	X (0 0^0 0)	65133.4	65116.$_9$		2000 d	65118.93

[b] Q branch is line-like in addition to a diffuse branch probably due to overlapping band.

Further independent and conclusive evidence for the non-linear configuration of HCN in the α state comes from a study of the weaker progressions just as in the case of C_2H_2. Two of these weaker progressions of HCN have fairly constant separations (735–750 cm^{-1} and 645–605 cm^{-1}, respectively) from the main progression $(0v_2'0) \leftarrow (000)$. It is impossible to assume the presence of two further vibrations of this magnitude in the upper state. One of these weaker progressions might have been accounted for as the "hot" progression of a molecule linear in both upper and lower state if it had the correct separation from the main progression, which is 712 cm^{-1} and which should be constant. Since the observed weak progressions do not fulfill these conditions, a different explanation must be sought.

Both the occurrence of two rather than one weak progression, whose separations from the main progression lie on either side of the bending frequency of the ground state, and the slight variability of the separations with v_2' can be immediately accounted for if the assumption is made that the molecule is non-linear in the upper state. Under this assumption, HCN would be a nearly-symmetric top in the upper state with one very small moment of inertia, and one would have a very coarse rotational structure corresponding to the small moment of inertia. Fig. 3 gives a schematic energy level diagram

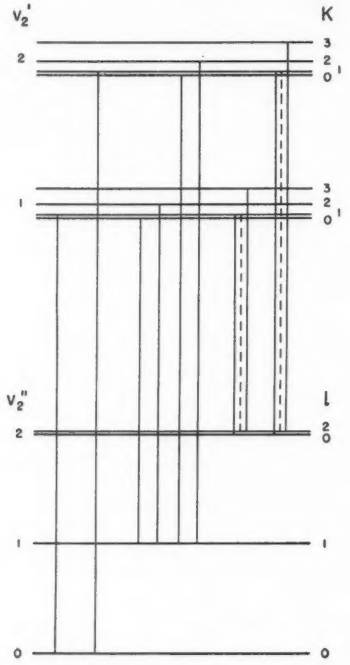

FIG. 3. Vibrational levels and coarse rotational structure in the upper and lower states of the α—X bands of HCN.

showing two successive vibrational levels of the upper state with the coarse rotational structure, as well as the three lowest vibrational levels of the ground state. The main bands must correspond to transitions from $v_2 = 0$, $l = 0$ of the ground state to the $K = 1$ levels of the upper state since they are perpendicular bands (see Section E). The bands of the two weaker progressions under discussion are interpreted as transitions from the first excited vibrational level $v_2'' = 1$, $l = 1$ to upper levels with $K = 0$ and $K = 2$; that is, these bands are also perpendicular bands with $K - l = \pm 1$. In this way the fact is understood that the interval $\nu_2'' = 712\ \text{cm}^{-1}$ is not observed as a band separation anywhere in the spectrum. Rather, two separations, one larger and one smaller than $712\ \text{cm}^{-1}$, are found and these separations vary with v_2' because of the variation of the rotational constant A' with v_2' (see below).

In addition to the two weak progressions just discussed, which may be designated $(0v_2'0)^2$—(01^10) and $(0v_2'0)^0$—(01^10), there is a weak progression $(1v_2'0)^0$—(01^10) corresponding to the second main progression $(1v_2'0)^1$—(00^00). Only one member of the progression $(1v_2'0)^2$—(01^10) has been found for HCN. Finally, two still weaker progressions are observed which can be readily interpreted as arising from the second excited vibrational level $v_2'' = 2$ of the ground state. As shown by Fig. 3, according to the selection rule $K - l = \pm 1$, three such progressions may be expected: $(0v_2'0)^1$—(02^00), $(0v_2'0)^1$—(02^20), and $(0v_2'0)^3$—(02^20). The two observed progressions fit the first and last of these. The first progression has the same upper states as the main progression $(0v_2'0)^1$—(00^00), and the wave number differences of corresponding bands should be constant (unlike the other "hot" progressions) and equal to the wave number of the $2\nu_2^0$ infrared band, which is $1411.42\ \text{cm}^{-1}$. The observed differences of the ultraviolet bands are 1411.60, 1411.39, and $1411.42\ \text{cm}^{-1}$, which agree very satisfactorily with the infrared value.

The assignments of all observed HCN bands are included in Table I. The origins (Q heads) of the main bands $(\alpha(v_1'v_2'0)^1 \leftarrow X(00^00))$ of HCN can be well represented by the formula

$$\nu = 52277.7_0 + 1505.9v_1' - 10.0v_1'^2 + 948.53v_2' - 7.39v_2'^2 - 0.52v_2'^3 - 6.27v_1'v_2'. \tag{1}$$

The wave numbers calculated from this formula are given in the last column of Table I. Except for the band $\alpha(100)^1$—$X(00^00)$ the agreement with the observed wave numbers for all the sharp bands is well within $\pm 0.8\ \text{cm}^{-1}$. For the diffuse bands, particularly those for which Q and R heads merge and only one peak was measured, the agreement is much poorer. This includes all bands with $v_1' = 2$ and 3 and therefore the value of the coefficient of the term in $v_1'^2$ is quite uncertain. Attempts to improve the agreement were not successful possibly on account of the overlapping β—X system which otherwise was not definitely recognized in HCN (see below). The rather large deviation between calculation and observation for the $\alpha(100)^1$—$X(000)$ band is far outside the experimental error. It must be ascribed either to a vibrational perturbation or to a wrong assignment: possibly the band belongs to the β—X system of HCN.

In the upper state of the main bands there is a small amount of rotational energy due to the term $(A_v'-B_v')K^2$ (see Section E) since $K = 1$. This amount has been included in formula (1), that is, the formula holds for the $K = 1$, $J = 0$ rotational levels of the upper state. The weaker ("hot") progressions with $v_2'' = 1, 2$ in the lower state and $K = 0, 1, 2, 3$ in the upper state (see Fig. 3) can be obtained from formula (1) by subtracting

$$G_0''(0v_2'0)-(A_v'-B_v')(K^2-1),$$

where $G_0''(01'0) = 711.7$, $G_0''(02^00) = 1411.42$, and $G_0''(02^20) = 1425.9_4$ cm^{-1} (see Douglas and Sharma 1953). Since $A_v'-B_v'$ will be determined from the observed differences of corresponding main bands and "hot" bands (see Tables IX and X), calculated wave numbers of the "hot" bands are not given in Table I except for the bands with $K = 1$ and $l = 0$ for which $K^2-1 = 0$ and thus $A_v'-B_v'$ drops out.

In DCN the analogues of the two main progressions of HCN start only at appreciably shorter wavelengths in agreement with expectation on account of the narrower Franck–Condon region. It turns out by extrapolation to lower v_2' values and ascertaining which extrapolated DCN band corresponds to the 000–000 HCN band that the first measured DCN band has $v_2' = 2$. In addition to the progressions $(0v_2'0)^1 \leftarrow (00^00)$ and $(1v_2'0)^1 \leftarrow (00^00)$, further fairly strong progressions are observed at shorter wavelengths, three of which are readily identified as $(2v_2'0)^1 \leftarrow (00^00)$, $(3v_2'0)^1 \leftarrow (00^00)$, and $(4v_2'0)^1 \leftarrow (00^00)$. These progressions are much more clearly developed in DCN than in HCN since, as mentioned before, the diffuseness of the bands sets in only at shorter wavelengths in DCN. Therefore, it is possible to have a somewhat more complete vibrational formula than for HCN. This formula is (again for the $K = 1$, $J = 0$ rotational levels of the upper state)

$$\nu = 52404.7_0+1505.8v_1'-14.2v_1'^2+735.0_4v_2'-4.20_5v_2'^2 -0.29v_2'^3-6.94v_1'v_2'+0.6v_1'^2v_2'. \tag{2}$$

The assignments of the DCN bands and the wave numbers calculated from (2) are included in Table II. The wave numbers of the "hot" bands (the weak progressions) are again obtained from (2) by subtracting $G_0''(0v_2'0) -(A_v'-B_v')(K^2-1)$ where now $G_0''(01^10) = 569.13$, $G_0''(02^00) = 1130.08$ (see Checkland and Thompson 1955), and $G_0''(02^20) = 1138.08$ cm^{-1} (see Allen, Tidwell, and Plyler 1956).

There is one additional fairly strong and very long progression in DCN which at first was thought to be the progression $(0v_2'1) \leftarrow (00^00)$ of the α—X system, that is, to correspond to the excitation of one quantum of the C—D stretching vibration. However, such an interpretation would have led to quite anomalous cubic and quartic anharmonic constants because the second difference in this progression is less than half that in the other progressions and, moreover, is constant, unlike the behavior in the other progressions for which the cubic term in (2) is quite noticeable. This interpretation was therefore abandoned in favor of the assumption that this progression is due to another electronic transition β—X (see Section E). A weaker but very distinct

progression accompanies the main β—X progression and is readily interpreted as the "hot" progression $(0v_2'0)^2$—(01^10) of the β—X system. A still weaker and somewhat fragmentary progression is $\beta(0v_2'0)^0$—$X(01^10)$.

The main β—X progression can be represented by the formula

$$\nu = 54630.1_8+730.7_5v_2'-2.10v_2'^2 \tag{3}$$

while the "hot" progressions are obtained again by subtracting $569.13-(A_v'-B_v')(K^2-1)$. The v_2' numbering in (3) is quite uncertain since the β—X system was observed only for DCN. The reason that no definite evidence for the β—X system has been found in HCN must be sought in the fact that diffuseness in the α—X system sets in earlier than in DCN. This makes it more difficult to ascertain the presence of the weaker bands of the β—X system. In addition, the β—X bands of HCN are very probably much more diffuse than those of DCN thus increasing the difficulty of detection.

Neither for the β—X system nor for the α—X system can the zero order frequencies ω_i of the upper state be determined since not all the anharmonic constants are known and, for the β—X system, even the absolute numbering is unknown. A rigorous discussion of the isotope effect is therefore not possible. But the differences of the $\omega_i^{0'}$ values (the coefficients of v_i') in the α—X systems of HCN and DCN are of the expected order. The wave number difference of the $\alpha(000)$—$X(000)$ bands of HCN and DCN is 123.3 cm^{-1} and must equal the difference of the differences of the zero-point energies in the upper and lower states. The difference of the zero-point energies of HCN and DCN in the lower state (using the data of Douglas and Sharma 1953) is 595.4 cm^{-1}. Therefore it follows that the corresponding difference in the upper state must be 472.1 cm^{-1}. Of this difference, according to (1) and (2) about 105 cm^{-1} is accounted for as due to ν_1' and ν_2' leaving 367 cm^{-1} for ν_3'. Thus the difference between ν_3'(HCN) and ν_3'(DCN) must be about 730 cm^{-1}. This value is of about the same magnitude as in the ground state, which is what might have been expected. Thus the assignments of the $\alpha(000)$—$X(000)$ bands in HCN and DCN are confirmed.

E. ROTATIONAL ANALYSIS

The fine structures of 28 bands of HCN and 16 bands of DCN have been measured and analyzed. The wave numbers of the lines are given in Tables III, IV, and V. All bands have strong Q branches in addition to P and R branches.

The bands of the main progressions $(0v_2'0)^1$—(00^00), $(1v_2'0)^1$—(00^00), etc. of both the α—X and β—X systems are similar in every respect to Π—Σ bands of a linear molecule as shown by the examples in Fig. 2. The numbering of the lines in many of the bands is obtained by inspection since the first lines of each of the branches, $R(0)$, $Q(1)$, and $P(2)$, are well resolved. The numbering so obtained is confirmed unambiguously by the agreement of the combination differences $R(J-1)-P(J+1) = \Delta_2F''(J)$ with those obtained from the infrared bands as measured by Douglas and Sharma (1953). This agreement is shown for the case of DCN in Table VI.

TABLE III. WAVE NUMBERS OF THE LINES IN THE α—X BANDS OF HCN (ν_{vac}, cm^{-1})

	$(000)^1$—(00^00) $\nu_0 = 52278.00$ cm^{-1}			$(010)^1$—(00^00) $\nu_0 = 53218.30$ cm^{-1}			$(020)^1$—(00^00) $\nu_0 = 54140.84$ cm^{-1}		
J	$P(J)$	$Q(J)$	$R(J)$	$P(J)$	$Q(J)$	$R(J)$	$P(J)$	$Q(J)$	$R(J)$
0			52280.56			53221.02			54143.37
1		52277.65	282.85		53217.90	223.28		54140.15*	145.80
2	52271.80*	276.67	284.75	53211.92*	217.00	225.20	54134.37*	139.52	147.78
3	267.90	275.47	286.40	208.48	215.74	226.78	130.99	138.25	149.24*
4	264.16	273.92	287.30*	204.54	214.04	228.04	127.03	136.44	150.63*
5	259.61*	271.80*	288.41*	200.28	211.92*	228.76*	122.75	134.37*	151.57*
6	255.55*	268.94	289.44*	195.62	209.38	229.74*	118.28	131.86	152.10*
7	250.16*	266.43	289.44*	190.12*	206.34	229.74*	113.28	128.76	152.71*
8	245.20	263.08	289.44*	185.10*	203.00	229.74*	107.98	125.33*	152.71*
9	239.35	259.61*	288.41*	179.50*	199.12	229.74*	102.38	121.31*	152.10*
10	233.33	255.55*	288.41*	173.52*	194.82	228.76*	096.46	117.02	151.57*
11	226.71	251.13 250.16*	287.30*	167.46	190.12*	227.52	090.16	112.22	150.63*
12	220.04	245.20		160.74	185.10*	226.10	083.54	107.02	149.24*
13	213.01	239.35		153.72	179.50*	224.36	076.60	101.32	147.30
14		233.33		146.40	173.52*	222.24		095.22	145.28
15		226.71		138.66	166.90	219.76	061.76	088.71	142.88
16		220.04		130.66	160.02	*	053.75	081.73	140.15*
17		213.01			152.78		045.46	074.40	136.99
18		205.54			145.06		036.81		133.53
19		197.82			136.98		027.85	057.94	129.69
20		190.29			128.32		018.52	049.12	125.33*
21					119.14		008.72	039.84	121.31*
22					109.80		53998.62*	030.20	
23							988.38	020.13	
24								009.57	
25								53998.62*	

	$(030)^1$—(00^00) $\nu_0 = 55042.79$ cm^{-1}			$(040)^1$—(00^00) $\nu_0 = 55920.39$ cm^{-1}			$(050)^1$—(00^00) $\nu_0 = 56770.34$ cm^{-1}		
J	$P(J)$	$Q(J)$	$R(J)$	$P(J)$	$Q(J)$	$R(J)$	$P(J)$	$Q(J)$	$R(J)$
0			55045.27*			55923.15*			56773.12*
1		55042.40*	047.65*		55919.83	925.28		56770.28	775.28*
2	55036.48	041.44	049.65*	55914.26*	919.01	927.39*	56763.52*	768.92	777.28*
3	032.89	040.15	051.31*	910.59*	917.66*	929.05*	760.60*	767.44	779.06*
4	028.99	038.36	052.65*	906.59	915.93	930.33*	757.28*	765.64	780.20*
5	024.71	036.12*	054.20*	902.40	913.31	931.36*	752.22	763.52*	781.50*
6	020.11	033.51	054.20*	897.86	910.74	932.49*	747.74	760.60*	781.50*
7	015.17	030.50	054.65*	892.82	907.73	932.49*	742.72	757.28*	782.94*
8	009.92	026.63	054.65*	887.58	904.04	932.49*	737.60	753.98	782.94*
9	004.32	022.67	054.65*	882.01	899.95	932.49*	732.04	749.60	782.94*
10	54998.41	018.31*	053.68*	876.10	895.44	931.36*	726.20	744.98	781.50*
11	992.12	013.56	052.65*	869.92	890.43	930.33*	720.00	739.78	780.20*
12	985.73	007.84	051.31*	863.38	884.98	929.05*	713.34	734.16	779.06*
13	978.76	002.12	049.65*	856.52	879.07	927.39*	706.76*	728.14	777.28*
14	971.51	54996.05	047.65*	849.34	872.72	925.41	699.18*	721.72	775.28*
15	963.95	989.40	045.27*	841.82	865.93	923.15*	691.82*	714.52	773.12*
16	956.00	982.27	042.40*	833.95*	858.64	920.79	683.86	706.76	770.28*
17	947.73	974.68	039.41	825.86	850.89	917.66*	675.70	699.18	767.44*
18	939.12	966.66	036.12*	817.29	842.74	914.26*	667.02	690.60	
19	929.87	958.13	032.22	808.34	833.95*	910.59*		681.38	
20	920.91	949.19	028.11	799.33	824.64	905.38		672.46	
21	911.24	939.72	023.65	789.81	814.91			662.62	
22	901.20	930.20	018.80		804.62			652.14	
23		920.29			793.96			640.48	
24		908.74							
25		897.50							

*Blended lines.

TABLE III (*continued*)

WAVE NUMBERS OF THE LINES IN THE α—X BANDS OF HCN (ν_{vac}, cm^{-1}) (*continued*)

	$(100)^1$—(00^00) $\nu_0 = 53766.78$ cm^{-1}			$(110)^1$—(00^00) $\nu_0 = 54707.91$ cm^{-1}			$(120)^1$—(00^00) $\nu_0 = 55624.44$ cm^{-1}		
J	$P(J)$	$Q(J)$	$R(J)$	$P(J)$	$Q(J)$	$R(J)$	$P(J)$	$Q(J)$	$R(J)$
0			53769.69			54710.53			55626.40*
1	53763.33*		772.30		54707.44	712.69			629.66*
2	760.29	53765.20	774.35	54701.60*	706.55*	714.63*	55617.74	55623.04	630.82*
3	757.47	763.33*	775.72	697.96	705.14	716.15	614.88*	621.80	632.54*
4	753.46	761.49	778.19	693.94	703.27*	717.35	610.48	619.92	633.84*
5	749.22	758.79	779.52*	689.58	702.30 700.48	718.15*	606.20	617.74*	634.76*
6	745.20	755.62	780.39*	684.78	698.84	718.63*	601.50	614.88*	635.56*
7	741.07	751.81	780.77*	679.64	695.59*	718.63*	596.44	611.80	635.56*
8	735.94	747.57	780.77*	674.21	691.95*	718.63*	591.04	608.16	635.56*
9	730.48	742.86	780.39*	668.36	687.82	718.15*	585.26	604.12	634.76*
10	724.62	737.47	779.52*	662.17	683.30	716.57*	579.20	599.48	633.84*
11	718.19*	731.89	777.10	655.74	678.34	714.99*	572.66	594.50	632.54*
12	711.13*	725.23		648.52	672.99	714.63* 712.09*	565.88	589.00	630.82*
13		718.19*		641.04	667.09	712.09* 708.65	558.66	583.08	628.76*
14		711.13*		634.81 632.64	660.80	709.41	551.16	576.72	626.40*
15				626.35 622.97	653.99	706.55*	543.24	569.80	623.64*
16				617.81*	646.80	703.27*	534.94	562.44	620.62
17				609.06	639.10	699.67	526.22	554.66	617.04
18				599.98	630.96	695.59*	517.24	546.40	613.22
19				590.44	622.36	691.95*	507.78	537.64	
20				580.38	613.34	686.73		528.52	
21				570.45*	603.76	681.61		518.80	
22				559.96	593.77	676.15		508.84	
23				548.97*	583.37	670.11		498.10	
24				537.52	572.43				
25				526.08*	561.09				
26					548.97*				
27					536.53				
28					524.12				

	$(000)^0$—(01^10) $\nu_0 = 51544.88$ cm^{-1}			$(010)^0$—(01^10) $\nu_0 = 52483.13$ cm^{-1}			$(020)^0$—(01^10) $\nu_0 = 53402.39$ cm^{-1}		
J	$P(J)$	$Q(J)$	$R(J)$	$P(J)$	$Q(J)$	$R(J)$	$P(J)$	$Q(J)$	$R(J)$
0									
1			51549.64		52482.80	52487.56		53401.94*	53406.86
2	51538.37	51544.18	551.25		481.96	489.56		401.28	408.66
3		542.57	552.89		480.93	490.98	53392.36	400.18	410.18
4		541.30	554.44*	52469.27	479.39	491.94*	388.58*	398.56	411.28
5		539.74	554.44*	464.30	477.41	492.74*	383.16	396.62	412.02*
6		536.72		459.38	475.05	492.74*	378.60	394.52	412.02*
7		534.00		453.98	472.29	492.74*	373.22	391.66	412.02*
8		530.96		448.15	469.27		367.68	388.58*	
9		527.61		442.14	465.91		361.58*	385.16	
10		523.79			462.05			381.28	
11		519.62			457.80			376.94	
12		515.03			453.17			372.22	
13		509.97			448.15			367.16	
14		504.31						361.58*	
15		498.68							

TABLE III (*continued*)

WAVE NUMBERS OF THE LINES IN THE α—X BANDS OF HCN (ν_{vac}, cm^{-1}) (*continued*)

	$(030)^0$—(01^10) ν_0 = 54300.37 cm^{-1}			$(040)^0$—(01^10) ν_0 = 55171.12 cm^{-1}			$(050)^0$—(01^10) ν_0 = 56005.65 cm^{-1}		
J	$P(J)$	$Q(J)$	$R(J)$	$P(J)$	$Q(J)$	$R(J)$	$P(J)$	$Q(J)$	$R(J)$
0									
1	54296.57*	54299.10*	54304.28*	55168.05	55170.77	55176.09*		56004.88*	56010.88*
2	293.09	298.06	305.40*	164.61	169.91	177.69*		004.88*	012.38*
3	289.14	296.57*	305.40*	161.03	168.89	178.99*	55995.88	003.38	013.66*
4	284.57	293.92	309.58	157.19*	167.29	180.03*	991.40	001.70	014.84*
5	278.83*	294.99	309.94*	152.25	165.47	180.69*	986.50	55999.66	014.84*
6	277.03	292.33	309.94*	147.29	163.05	180.69*	981.62	997.40	014.84*
7	271.25	289.56	309.58	141.93*	160.27	180.03*	976.14	994.46	013.66*
8	265.33	286.35	308.83	136.15*	157.19*	178.99*	970.28	991.40	013.66*
9	259.10*	282.76	307.74	130.03	153.95	178.99*	963.62	987.72	012.38*
10	252.42	278.83*	306.19	123.35	150.33	177.69*	957.26	983.46	010.88*
11	245.37	274.53	304.28*	116.93		176.09*	949.98	979.36	008.76
12	237.86	269.78	301.86	110.19	141.93*		942.58	974.32	006.42
13	229.91	264.66	299.10*	102.87	136.15*			969.02	
14	221.68	259.10*	295.83					963.62	
15	213.57	253.10	292.33					957.26	
16	203.84	246.70	288.06					951.04	
17	194.23	239.88	283.56					943.90	
18	184.13	232.60						936.59	
19	173.82	224.94							
20	162.71	216.74							
21		208.30							
22		199.24							
23		189.67							
24		179.70							
25		169.33							

	$(110)^0$—(01^10) ν_0 = 53972.90 cm^{-1}			$(120)^0$—(01^10) ν_0 = 54887.17 cm^{-1}			$(000)^2$—(01^10) ν_0 = 51628.08 cm^{-1}		
J	$P(J)$	$Q(J)$	$R(J)$	$P(J)$	$Q(J)$	$R(J)$	$P(J)$	$Q(J)$	$R(J)$
0									
1		53972.54	53977.61*	54884.15	54886.65	54891.67			51633.00
2	53966.49	971.70	979.47*	880.77	885.77	893.67*		51627.06	634.78
3	962.81	970.46	980.74*	876.89	884.63	894.89*		625.74	636.13
4	958.48*	968.93	981.55*	872.59*	883.19	895.73*	51613.92	624.22	637.15
5	953.93	966.92	982.01*	868.13	881.17	896.15*		622.44	638.11*
6	948.89	964.50	982.01*	863.03	878.63	896.15*		620.12	638.11*
7	943.33	961.61	981.55*	857.55	875.81	895.73*		617.58	638.11*
8	937.47	958.48*	980.74*	851.57	872.59*	894.89*			
9	931.09	954.76	979.47*	845.21	868.91	893.67*			
10	924.21	950.59	977.61*	838.47	864.75	892.07			
11	917.35	945.98	973.38	831.31*	860.27	889.83			
12	909.40	941.87		823.67	855.37				
13		936.13		815.55	850.03				
14		930.39		807.09	844.23				
15		924.21*		798.01	837.97				
16		917.35*		788.69	831.31*				
17		910.47		778.93	824.15				
18		902.71		768.53	816.61				
19		894.93			808.57				
20					800.17				
21					791.19				
22					781.73				

TABLE III (*continued*)

WAVE NUMBERS OF THE LINES IN THE α—X BANDS OF HCN (ν_{vac}, cm^{-1}) (*continued*)

	$(010)^2$—(01^10) $\nu_0 = 52575.68$ cm^{-1}			$(020)^2$—(01^10) $\nu_0 = 53506.44$ cm^{-1}			$(030)^2$—(01^10) $\nu_0 = 54419.26$ cm^{-1}		
J	$P(J)$	$Q(J)$	$R(J)$	$P(J)$	$Q(J)$	$R(J)$	$P(J)$	$Q(J)$	$R(J)$
0									
1			52580.51*			53511.26*			54424.01*
2		52574.48	582.30*		53505.22	513.04		54418.09	425.80*
3		573.34	583.67*		504.08	514.44*	54409.22	416.81*	427.12*
4	52561.52*	571.89	584.64*	53492.20*	502.60	515.38*	404.82*	415.26	428.09*
5	556.98	569.97	585.59*		500.68	516.02*	400.43	413.34*	428.95*
6	552.18	567.61	585.59*	483.12 482.62	498.54 498.12	516.38* 516.02*	395.57	411.14 410.80	428.95* 428.66*
7	546.45	564.87	584.64*	477.62 476.98*	495.76 495.28	516.02* 515.38*	390.56 390.10	408.50 408.02	428.95* 428.66*
8	541.31*	561.52*	585.59* 584.64*	472.18* 471.68	492.78 492.20*	516.02* 515.38*	384.99 384.25	405.37 404.82*	428.66* 428.09*
9	534.11	558.79 557.87	584.64* 583.67	465.64 464.70*	489.36 488.60	514.44* 513.78*	378.70 378.14	401.91 401.17	427.12* 426.77
10	528.13	554.98 553.93	583.03 582.30	458.94	484.82 483.94	513.78* 512.22*	372.18 371.45	398.00 397.03	425.80* 425.09
11	521.69	550.75 549.55	581.45 580.51	452.34	481.52 480.00	512.22* 511.26*	364.97 364.57	393.48 392.32	
12	515.00 514.02	546.45 544.80	579.46 578.53	445.60	476.98* 475.60	511.26* 509.36	358.09 356.86		
13	507.57 506.76	541.31* 539.68			472.18* 470.40				
14	500.01 498.43	536.26 534.11*			466.76 464.70				
15		530.85 528.13*							
16		524.79 521.69							

	$(040)^2$—(01^10) $\nu_0 = 55313.57$ cm^{-1}			$(050)^2$—(01^10) $\nu_0 = 56187.34$ cm^{-1}		
J	$P(J)$	$Q(J)$	$R(J)$	$P(J)$	$Q(J)$	$R(J)$
0						
1			55318.67			56192.18
2			319.55			194.34
3	55302.39*	55310.77	321.41		56184.88	195.82
4	298.89*	309.19	323.05*	56173.22	183.74	197.14*
5	295.25*	307.63	323.05*	169.74	181.52	197.14*
6		305.19	323.05*	163.82	179.24	197.14*
7		302.39*	323.05*		176.00	197.14*
8		299.69 298.89*	323.05* 321.41*		173.22	
9		296.19 295.25*	321.41* 320.45		169.74	
10		292.31 291.23	319.55 317.83		166.28	
11			315.81 314.05		161.32	
12						
13						
14						
15						
16						
17						

TABLE III (*concluded*)

WAVE NUMBERS OF THE LINES IN THE α—X BANDS OF HCN (ν_{vac}, cm^{-1}) (*concluded*)

	$(020)^1$—(02^00) $\nu_0 = 52729.54$ cm^{-1}			$(030)^1$—(02^00) $\nu_0 = 53631.34$ cm^{-1}			$(040)^1$—(02^00) $\nu_0 = 54508.96$ cm^{-1}		
J	$P(J)$	$Q(J)$	$R(J)$	$P(J)$	$Q(J)$	$R(J)$	$P(J)$	$Q(J)$	$R(J)$
0			52731.76			53633.83			54511.50
1		52728.94	734.47*		53630.91	636.16			513.68
2	52722.73*	727.99	736.48*	53624.42*	629.87	638.38*	54502.97	54507.87*	515.92
3	719.46	726.76	738.03*	621.53*	628.60	639.90*	499.17*	506.20	517.75
4	715.63	725.00	739.28*	617.36	626.66	641.19*	494.81	504.11	518.90
5	711.33	722.73*	740.08*	612.94	624.42*	642.63*	490.24	501.73	520.34*
6	706.91	720.20	740.77*	608.45	621.53*	642.63*	485.87	499.17*	520.34*
7	701.66	717.04	740.77*	603.60	618.57	642.63*	481.26	495.87	520.34*
8	695.78	713.39	740.77*	597.94	614.60	642.63*	475.80	492.25	520.34*
9	690.28	709.39	740.08*	592.19	610.68	642.63*	470.28	487.73	520.34*
10	684.48	704.81	739.28*	586.15	606.23	641.19*	464.18	483.17	
11	677.94	699.96	738.03*	580.01	601.08	639.90*	457.53	478.09	
12	671.21	694.46	736.48*	572.98	595.34	638.38*	450.59	472.36	
13		688.75	734.47*	566.06	589.52	637.06	443.98	466.56	
14		682.42	732.67	558.43	583.02	634.73	436.08	459.80	
15		675.54	729.85	550.84	576.38	632.16		452.65	
16		668.52	726.76		569.20				
17		660.90			561.15				
18					553.32				

	$(020)^2$—(02^20) $\nu_0 = 52917.93$ cm^{-1}			$(030)^2$—(02^20) $\nu_0 = 53846.06$ cm^{-1}		
J	$P(J)$	$Q(J)$	$R(J)$	$P(J)$	$Q(J)$	$R(J)$
0						
1						
2			52924.50			53852.37
3		52915.27	925.70		53843.94	853.75
4	52903.54*	913.99	926.73	53831.52	842.09	854.73
5		912.07	927.61*		840.02	855.48*
6		909.55			837.42	
7		906.87		817.08	834.81	
8		903.54*			831.52	
9		900.14			827.98	
10		896.09			823.80	
11		891.73			819.55	
12					814.71	
13					809.30†	
14					804.39†	
15					798.35†	
16					791.72 790.74	
17					785.12 784.23	

†Unresolved doublet.

TABLE IV. Wave numbers of the lines in the α—X bands of DCN (ν_{vac}, cm^{-1})

	$(020)^1$—(00^00) $\nu_0 = 53855.90$ cm^{-1}			$(030)^1$—(00^00) $\nu_0 = 54564.05$ cm^{-1}			$(040)^1$—(00^00) $\nu_0 = 55259.06$ cm^{-1}		
J	$P(J)$	$Q(J)$	$R(J)$	$P(J)$	$Q(J)$	$R(J)$	$P(J)$	$Q(J)$	$R(J)$
0			53858.12			54566.64			55261.54
1		53855.16*	860.26		54563.90	568.84		55258.85	263.60
2	53850.62*	855.16*	862.27		563.46	570.82		258.26	265.49
3	848.06	854.30	864.15		562.78	572.78	55251.75*	257.48	267.51
4	845.32	853.34	865.94	54553.90	561.90	574.64	248.53	256.48	269.40
5	842.48	852.10	867.80	551.08	561.46 559.24	576.40	245.85	255.18	270.97
6	839.29*	850.62*	868.97	548.06	558.36	578.16	242.81	253.63	272.54
7	836.16*	848.89	870.44	544.98	556.72	579.88 577.76*	239.54	251.75*	273.89
8	832.81*	846.89	871.70	541.82	554.76	579.40	236.26	249.71	275.54
9	829.32*	844.61	872.61	538.84 536.90*		580.60	232.81	247.28	276.47
10	825.58*	841.96	873.46	533.54	549.90	581.60	229.74	244.71	277.44
11	821.87	839.29*	874.29	529.86	547.02	582.52	225.74	241.76	278.28
12	817.85	836.16*	874.86	526.16	544.00	583.30	221.95	238.48	279.03
13	814.10	832.81*		522.14	540.62	583.98	217.89	235.17	279.60
14	809.72	829.32*		518.06	536.90*		213.84*	231.62	280.29*
15	805.40	825.58*		513.78	533.08		209.57	227.63	
16	800.85	821.19		509.28*	528.84	584.36	205.28	223.30	
17	795.56	816.91		504.70	524.40		200.69	218.73	
18		812.28		500.06	519.62		196.01	213.84*	
19		807.59		495.02	514.62		191.44*	208.77	
20		802.22		490.02	509.28		185.88	203.42	
21		796.47		484.56	503.72			197.57	
22		791.13		479.48	497.74			191.44*	
23				473.28	491.72				
24				467.22	485.20	577.76*			
25					478.56	575.72			
26					471.42	573.66			
27					463.72	571.90			
28						569.60			
29						567.36			

	$(050)^1$—(00^00) $\nu_0 = 55938.69$ cm^{-1}			$(060)^1$—(00^00) $\nu_0 = 56600.97$ cm^{-1}			$(070)^1$—(00^00) $\nu_0 = 57243.95$ cm^{-1}		
J	$P(J)$	$Q(J)$	$R(J)$	$P(J)$	$Q(J)$	$R(J)$	$P(J)$	$Q(J)$	$R(J)$
0			55941.28			56603.39			57246.36
1		55938.72	943.34		56600.73	605.47		57243.78	248.51
2		937.98	945.18	56596.03	600.12	607.65		243.08	250.56
3	55931.14*	937.10	947.16	593.30*	599.33	609.62		242.19	252.48
4	928.32	936.06	948.92	590.97*	598.30	611.41	57233.72*	241.13	254.30
5	925.40	934.82	950.56	587.77	596.87	613.23	231.04*	239.69	256.02
6	922.38	932.98	952.34	584.79	595.17	614.71	228.14*	237.96	257.54
7	918.94	931.14*	953.66	581.62	593.30*	616.16	224.94*	236.09	258.99
8	915.96	929.04	954.96	578.42	590.97*	617.49	221.53*	233.72*	260.36
9	912.68	926.98	956.12	574.91	588.56	618.65	217.88*	231.04*	261.49
10	909.12	924.02	957.10	571.71*	585.79	619.69	214.40	228.14*	262.50
11	905.42	921.02	957.98	567.75*	582.67	620.60	210.79	224.94*	263.40
12	901.90*	917.70	958.78	564.13	579.34	621.32	207.03	221.53*	264.26
13	897.74	914.18	959.40	560.19	575.72	622.14*	203.08	217.88*	
14	893.70	910.54	960.40*	556.21	571.71*	623.23*	199.01	213.68	
15	889.46	906.32	960.40*	552.02	567.75*	623.23*	194.77*	209.44	
16	885.00	901.90*		548.55	563.09	623.23*	190.66	204.75	
17	880.60	897.20		543.27	558.44	623.23*	186.20	199.89	
18		892.22		538.70	553.26		181.64	194.77*	
19		886.94		533.86			176.87*	189.01	
20		881.44			542.08		171.91	183.07	
21		875.92			536.07		166.75	176.87*	
22		869.68					161.60	170.49	
23		863.52					156.43*	163.50	
24		856.24						156.43*	
25		849.10							

*Blended lines.

TABLE IV (*continued*)

WAVE NUMBERS OF THE LINES IN THE α—X BANDS OF DCN (ν_{vac}, cm^{-1}) (*continued*)

	$(140)^1$—(00^00) $\nu_0 = 56725.56$ cm^{-1}			$(240)^1$—(00^00) $\nu_0 = 58168.16$ cm^{-1}			$(040)^0$—(01^10) $\nu_0 = 54671.65$ cm^{-1}		
J	$P(J)$	$Q(J)$	$R(J)$	$P(J)$	$Q(J)$	$R(J)$	$P(J)$	$Q(J)$	$R(J)$
0			56727.88			58170.42			54674.25
1		56725.32	730.03		58167.96	172.44		54671.45	676.11
2		724.68	731.99	58162.86	167.28	174.42	54666.62	671.04	677.69
3		723.87	733.80	160.06*	166.32	176.16	663.76	670.50	679.35
4		722.76	735.50	157.62*	165.24	177.74	660.84*	669.72	680.75
5		721.37	737.20	154.46	163.78	179.38	657.43	668.81	681.85
6	56708.96	719.74	738.52	151.26	162.04	180.60*	653.93	667.64	683.00
7	705.66	717.80	739.83	147.88	160.06*	181.70*	650.42*	666.24	683.72
8	702.27	715.54	740.96	144.38	157.62*	182.66*	646.45	664.64	
9	698.81	713.06	741.92	140.68	155.02	183.56*	642.36	662.85	
10	695.02	710.24	742.72	137.06*	152.02	184.18*	637.78	660.84*	
11	691.26	707.17	743.39	132.76*	148.78	185.00*	633.18	658.58	
12	687.33*	703.83	744.01	128.54	145.18	185.00*	628.60	656.14	
13	682.81*	700.20	744.46*	124.30	141.50	185.00*		653.40	
14	678.71	696.21		119.68	137.06*	185.00*		650.42*	
15		691.99		114.92	132.76*	185.00*		647.27	
16		687.33*		110.12	127.90	184.18*		643.72	
17		682.81*		104.88	122.96	183.56*		640.09	
18		677.64		58099.62	117.72	182.66*		635.95	
19				093.96	112.38	181.70*			
20				088.34	106.40	180.60*			
21				082.56		178.44			
22						176.92			
23						175.34			
24						173.40			
25						171.48			
26						169.32			

	$(120)^0$—(01^10) $\nu_0 = 54750.44$ cm^{-1}			$(130)^0$—(01^10) $\nu_0 = 55451.55$ cm^{-1}			$(140)^0$—(01^10) $\nu_0 = 56138.22$ cm^{-1}		
J	$P(J)$	$Q(J)$	$R(J)$	$P(J)$	$Q(J)$	$R(J)$	$P(J)$	$Q(J)$	$R(J)$
0									
1		54750.03*	54754.41		55451.28	55455.85		56138.06	56142.45
2	54745.30	750.03*	756.24	55446.40	450.99	457.69	56133.14	137.62	144.36
3	741.96	749.15	757.67*	443.72*	450.30	459.18	130.37*	136.97	145.76*
4	739.46	748.27	759.26	440.42	449.37	460.53	127.15	136.08	146.98*
5	736.02*	747.22	760.37	437.04*	448.35	461.52	123.84*	134.99	148.09*
6	732.54	745.97	760.94	433.56	447.06	462.32	120.53*	133.76	148.72*
7	728.63	744.42	761.47	429.81	445.64	463.24*	116.48	132.23	150.18*
8	724.66	742.71	761.92*	425.59	443.72*		112.49	130.37*	150.18*
9	720.35	740.72		421.44	441.62		108.14	128.46	150.18*
10		738.44		416.43	439.64		103.70	126.23	150.18*
11		736.02*			437.04*		099.12	123.84*	148.72*
12		733.25			434.59		094.38	121.10	148.09*
13		730.29			431.23		088.62*	118.06	146.98*
14		727.13			428.00		083.07*	114.69	145.76*
15		724.04 723.08			424.49		076.75*	111.17	
16		719.72			420.54		070.80*	107.28	
17		715.69			416.43			103.07	
18					412.01			098.65	
19					407.14			093.77	
20					401.83			088.62*	
21								083.07*	
22								076.75*	
23								070.80*	
24								063.79	
25								056.53	

TABLE IV (*concluded*)

WAVE NUMBERS OF THE LINES IN THE α—X BANDS OF DCN (ν_{vac}, cm^{-1}) (*concluded*)

	$(040)^2$—(01^10) $\nu_0 = 54743.83$ cm^{-1}			$(120)^2$—(01^10) $\nu_0 = 54807.90$ cm^{-1}		
J	$P(J)$	$Q(J)$	$R(J)$	$P(J)$	$Q(J)$	$R(J)$
0						
1			54747.22†			54812.04*
2		54742.71	749.15†		54807.16	813.81
3		741.96	750.85	54799.81*	806.50	815.32
4		741.10	753.08	796.89	805.61	817.04
5		740.72†	754.41†	793.30	804.57	817.94
6		739.46†	756.24†	790.12*	803.38	818.82*
7		738.44	757.67†	786.41*	801.99 801.56	819.77*
8		736.50 736.02		782.74* 782.10	800.42 799.81*	820.18* 819.77*
9		734.59 733.25†		778.70 778.17	798.41 797.73	820.18* 819.77*
10		732.54† 731.65		774.32 773.47	796.32 795.40	
11		730.29† 729.66		769.85 768.98	794.25 792.89	
12		727.93 726.33		765.01 763.49	791.88 790.12*	
13		725.26 723.08		759.79 757.67	789.22 787.23	
14		722.25 719.72†			786.41* 784.05	
15		718.94 716.58			782.74* 780.54	
16					779.89 776.76	
17					775.98 772.78	
18					771.71 768.53	
19					767.44 764.25	
20					762.86 759.26	

†Blended with a line of the stronger $(120)^0$ band.

TABLE V

WAVE NUMBERS OF THE LINES IN TWO β—X BANDS OF DCN (ν_{vac}, cm^{-1})

	$(040)^1$—(00^00) $\nu_0 = 57519.55$ cm^{-1}			$(070)^1$—(00^00) $\nu_0 = 59642.21$ cm^{-1}		
J	$P(J)$	$Q(J)$	$R(J)$	$P(J)$	$Q(J)$	$R(J)$
0			57521.52			
1		57519.22	523.98		59642.10	59646.30
2	57514.22	518.66	525.50	59638.16	641.43	648.31
3	511.50	517.84	527.22	634.54	640.28	649.71
4	508.72*	516.48	528.64	631.28	639.04	650.90
5	505.52	514.96	529.90	627.56*	637.37	651.88
6	502.10	513.22	530.78	624.34*	635.41	652.53
7		510.96	531.74	620.70*	633.03	653.09*
8		508.72*	532.58	616.33	630.51	653.09*
9		505.96	533.02	611.92	627.56*	653.09*
10		502.92		607.28	624.34*	
11				602.39	620.70*	
12					616.82	
13					612.64	
14					608.12	
15					603.26	

TABLE VI

COMBINATION DIFFERENCES $\Delta_2F''(J) = R(J-1)-P(J+1)$ FOR THE GROUND STATE OF DCN

	From the α—X bands									From the infrared[a] (mean)
J	$(020)^1$ —(00^00)	$(030)^1$ —(00^00)	$(040)^1$ —(00^00)	$(050)^1$ —(00^00)	$(060)^1$ —(00^00)	$(070)^1$ —(00^00)	$(140)^1$ —(00^00)	$(240)^1$ —(00^00)	Mean	
1	(7.50)				7.36			7.56	7.46	7.26
2	12.20		(11.85)	(12.20)	(12.17)			(12.38)	12.20	12.08
3	16.95	16.92	16.96	16.86	(16.68)	(16.83)		(16.80)	16.92	16.92
4	21.67	21.70	21.66	21.76	21.85	(21.44)		21.70	21.72	21.74
5	(26.65)	26.58	26.59	26.54	26.62		26.54	26.48	26.56	26.59
6	(31.64)	31.42	31.43	31.62	31.61		31.54	31.50	31.52	31.41
7	(36.16)	36.34	36.28	36.38	36.29	(35.98)	36.25	(36.22)	36.31	36.24
8	(41.12)	41.04 (40.86)	41.08	40.98	41.25	(41.09)	41.02	(41.02)	41.07	41.04
9	(46.12)	45.86	45.80	45.84	(45.78)	45.97	45.94	(45.60)	45.88	45.90
10	50.74	50.74	50.73	50.70	(50.90)	50.68	50.66	(50.80)	50.71	50.75
11	55.61	55.44	55.49	(55.20)	55.56	55.45	(55.39)	(55.64)	55.51	55.53
12	60.19	60.38	60.39	60.24	60.41	60.30	(60.58)	(60.70)	60.32	60.36
13	65.14	65.24	(65.19)	65.08	65.11	65.23	65.30	(65.32)	65.18	65.22
14		70.20	70.03	69.94	(70.12)			(70.08)	70.06	70.00
15			(75.01)	(75.40)	(74.68)			(74.88)	(74.99)	74.83
16				(79.80)	(79.96)			(80.12)	(79.96)	79.64
17					(84.53)			(84.56)	(84.54)	84.44
18					(89.37)			(89.60)	(89.48)	89.28
19								(94.32)	(94.32)	94.12
20								(99.14)	(99.14)	98.92

[a]From Douglas and Sharma (1953).
( ) Values in parentheses are based on blended lines and are not included in the average.

Further confirmation of the numbering is provided by the occurrence of a number of perturbations in both the HCN and DCN bands. They occur at corresponding J' values in the P and R branches of a given band at different J' values in the Q branch confirming that it is the upper state which is of II type. In many instances at the peak of the perturbations extra lines appear and these are included in Tables III and IV.

Just as in the case of C_2H_2 (Ingold and King 1953; Innes 1954) the combination differences for the upper state of the HCN and DCN bands, $R(J)-Q(J)$ and $Q(J+1)-P(J+1)$, show a very considerable combination defect, far larger than can be accounted for by l-type or Λ-type doubling. Again the cause of this splitting must be sought in the non-linearity of the molecule in the upper states α and β, which has already been shown to follow from the vibrational structure of the band systems. If the molecule is non-linear, it is nearly a symmetric top with one very small moment of inertia I_A about the a-axis (see Fig. 4) and two nearly equal moments of inertia I_B and I_C about the b and c axes. The energy levels are given approximately by

$$F(J, K) = \bar{B}J(J+1)+(A-\bar{B})K^2 \tag{4}$$

where

$$\bar{B} = \tfrac{1}{2}(B+C) = \frac{h}{16\pi^2 c}\left(\frac{1}{I_B}+\frac{1}{I_C}\right), \qquad A = \frac{h}{8\pi^2 c I_A}. \tag{5}$$

In this approximation the levels with $K \neq 0$ are doubly degenerate. Since

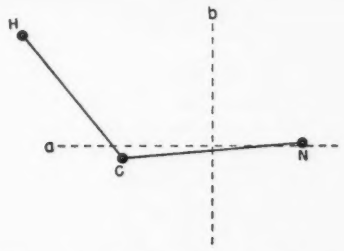

FIG. 4. Structure and principal axes of HCN. The c axis is perpendicular to the plane of the molecule.

actually the molecule is an asymmetric top, i.e., $B \neq C$, this degeneracy is split, the splitting being large for low (non-zero) K values but negligibly small for high K values. According to Wang (1929) and Lawrance and Strandberg (1951) the splitting for $K = 1$ is given by

$$F_d(J, 1) - F_c(J, 1) = \tfrac{1}{2}(B-C)J(J+1) \tag{6}$$

where F_d and F_c refer to the upper and lower of the two components into which a level of given J and K is split. It is this K type splitting that causes a large combination defect between the Q branch on the one hand and the P and R branches on the other, similar to the l-type and Λ-type doubling in linear (and diatomic) molecules with $l = 1$ or $\Lambda = 1$. Here the levels of one series (F_c for a totally symmetric electronic state) are "positive" for even J and "negative" for odd J while those of the other series have opposite parities. In the (00^{0}0) $^1\Sigma^+$ ground state of HCN, which has only one series of rotational levels, the even levels are positive, the odd negative. Because of the selection rule that positive combine only with negative levels, the transitions with $\Delta J = 0$ (Q branch) go to one series of sublevels of the upper state with $K = 1$ (F_d if the upper state is totally symmetric) while those with $\Delta J = \pm 1$ (P and R branch) go to the other.

In both the α—X and β—X systems the sign of the combination defect indicates that the upper levels of the Q lines form the lower series of sublevels, F_c. This observation shows unambiguously that the upper electronic states α and β are *not* totally symmetric (A') but have the species A'' (are antisymmetric with respect to the plane of the molecule). In a triatomic non-linear XYZ molecule all *vibrational* levels are, of course, totally symmetric and thus the A'' character of the upper states cannot be due to vibration.

An A'' upper state implies that the transition moment of the transition is perpendicular to the figure axis of the nearly symmetric top, a conclusion that is in agreement with the observation that for all observed bands $K'-l'' = \pm 1$ corresponding to the selection rule $\Delta K = \pm 1$ of perpendicular bands of symmetric top molecules (see also Section D). Unlike C_2H_2 no transitions violating these rules have been observed for HCN or DCN.

If (6) is introduced into (4) and if a symmetric splitting is assumed, one obtains for the rotational levels of a slightly asymmetric top with $K = 1$

$$F_c(J, 1) = (A-B)+\tfrac{1}{4}(B+3C)J(J+1),$$
$$F_d(J, 1) = (A-B)+\tfrac{1}{4}(3B+C)J(J+1). \tag{7}$$

These formulae represent the rotational levels in the present case with very good accuracy since both HCN and DCN, even when they are strongly bent, are nearly symmetric tops. According to the accompanying paper by Polo (1957) the deviations of the energy levels from (7) on account of the asymmetry of the rotator can be represented by quadratic and higher terms in $J(J+1)$ in addition to very small correction terms of order ϵ^2, ϵ^3 in the constant and linear terms in (7) where

$$\epsilon = (B-C)/4(A-\bar{B}). \tag{8}$$

Since in the present case ϵ is less than 10^{-3} the corrections to the constant and linear terms can be safely neglected. The quadratic term in $J(J+1)$ is for $K = 1$, again neglecting higher powers of ϵ,

$$-\delta^{(1)}J^2(J+1)^2 = -\tfrac{1}{8}(A-\bar{B})\epsilon^2J^2(J+1)^2. \tag{9}$$

This term can be combined with the centrifugal stretching term $-D_JJ^2(J+1)^2$. If, in addition, we introduce the centrifugal stretching terms $-D_KK^4$ and $-D_{JK}K^2J(J+1)$, we obtain in place of (7)

$$F_c(J, 1) = (A-\bar{B}-D_K)+\tilde{B}_cJ(J+1)-\tilde{D}^{(1)}J^2(J+1)^2,$$
$$F_d(J, 1) = (A-\bar{B}-D_K)+\tilde{B}_dJ(J+1)-\tilde{D}^{(1)}J^2(J+1)^2. \tag{10}$$

where

$$\tilde{B}_c = \tfrac{1}{4}(B+3C)-D_{JK}, \quad \tilde{B}_d = \tfrac{1}{4}(3B+C)-D_{JK}, \quad \tilde{D}^{(1)} = D_J+\delta^{(1)}. \tag{11}$$

In (10), terms cubic in $J(J+1)$ and still higher terms, all given by Polo, would have to be added if it is to be applied to high J values, in the present case for $J > 25$. The cubic term

$$\tfrac{1}{64}(A-\bar{B})\epsilon^3J^3(J+1)^3$$

has opposite sign for the F_c and F_d levels while for the quadratic terms the asymmetry correction is the same for F_c and F_d.[3]

On the basis of (10) the values of $\tilde{B}_c$ and $\tilde{B}_d$ in the upper states of the Π—Σ type HCN and DCN bands can now be evaluated by standard methods from the observed lines (see Herzberg 1945). The combination sums $R(J-1)+P(J)$ and the Q branch were used to obtain $\tilde{B}_d'-B''$ and $\tilde{B}_c'-B''$ respectively as well as $\tilde{D}^{(1)}-D''$. Since B_0'' and D_0'' are accurately known from the infrared ($B_0'' = 1.47823$, $D_0'' = 2.85\times10^{-6}$ cm^{-1} for HCN and $B_0'' = 1.20776$, $D_0'' = 2.1\times10^{-6}$ cm^{-1} for DCN; see Douglas and Sharma 1953), the values of $\tilde{B}_c'$, $\tilde{B}_d'$, $\tilde{D}^{(1)}$ obtained in this way are more accurate than those which one would have obtained from the combination differences Δ_2F' (without the use of B'', D''). The final $\tilde{B}_c'$, $\tilde{B}_d'$, and $\tilde{D}^{(1)}$ values for the various vibrational levels of HCN and DCN are listed in Tables VII and VIII. The $\tilde{D}^{(1)}$ values are given separately for the F_c and F_d levels since in a

[3]The difference in the *apparent* quadratic term found by Herzberg and Ramsay (1955) for HCO is due to the effect of the cubic terms.

TABLE VII

EFFECTIVE ROTATIONAL CONSTANTS $\tilde{B}$ AND $\tilde{D}$ OF THE VIBRATIONAL LEVELS OF THE α STATE OF HCN

Level $(v_1v_2v_3)^K$	$\tilde{B}_c$	$\tilde{B}_d$	$\bar{B}$	$\tilde{D}_c^{(K)}$	$\tilde{D}_d^{(K)}$	$\delta_c^{(K)}$	$\delta_d^{(K)}$	D_J^c	D_J^d	Remarks
	cm^{-1}			10^{-6} cm^{-1}						
(0 0 0)^0			1.2872	10		9.49		0.5		
(0 0 0)^1	1.2723	1.3128	1.2926	34.6	26.6	2.37		32.2	24.2	
(0 0 0)^2			1.2921	(2.7)		+1.58	−7.91			
(0 1 0)^0			1.2870	10		11.32		−1.3		
(0 1 0)^1	1.2649	1.3111	1.2880	5.2	7.4	2.83		2.4	4.6	
(0 1 0)^2			1.2860	6.6	−9.2	+1.89	−9.43	4.7	0.2	
(0 2 0)^0			1.2886	26		12.23		14		
(0 2 0)^1	1.2621	1.3135	1.2878	7.4	8.0	3.06		4.3	4.9	
(0 2 0)^2			1.2876	6.2	−7.1	+2.04	−10.19	4.2	3.1	
(0 2 0)^3			1.2870	(7.3)		−1.53				
(0 3 0)^0			1.2833	13		13.59		−0.5		Pert. $J = 4$
(0 3 0)^1	1.2565	1.3144	1.2855	5.7	7.4	3.37		2.3	4.0	
(0 3 0)^2			1.2847	(4)		+2.25	−11.25			
(0 3 0)^3			1.2846	(7.3)		−1.69				
(0 4 0)^0			1.286$_1$	(10)		13.02		−3		Pert. $J > 9$
(0 4 0)^1	1.2523	1.315$_4$	1.2839	6.9	6.6	3.26		3.6	3.3	
(0 4 0)^2			1.2834	(4)		+2.17	−10.85			Pert. $J > 10$
(0 5 0)^0			1.2788	(11)		10.26				
(0 5 0)^1	1.2475	1.3150	1.2813	8.5	(6.9)	2.56		5.9		
(0 5 0)^2			1.2869	(4)		+1.71	−8.55			
(1 0 0)^1	1.2126	1.355$_0$	1.2838	8.9	(10)					Pert. $J > 7$ in *PR*
(1 1 0)^0			1.2777	(15)		11.94				
(1 1 0)^1	1.2543	1.301$_6$	1.2780	5.9	9.9	2.98		2.9	6.9	Pert. $J = 13$ in *PR*
(1 2 0)^0			1.2758	15		13.75		1.2		
(1 2 0)^1	1.2515	1.3048	1.2782	7.2	12.9	3.44		3.8	9.5	

Note.—D values in parentheses are assumed.

few cases differences were found which are entirely outside the limits of error of the determinations.

The bands of the "hot" progressions $(0v_2'0) \leftarrow (01^10)$, $(1v_2'0) \leftarrow (01^10)$, consist of two subbands, one with $K = 0$, the other with $K = 2$ in the upper state. In agreement with this interpretation, the fine structure of the subbands with $K = 0$ is of the Σ—Π type and that of the subbands with $K = 2$ is of the Δ—Π type.

The Σ—Π subbands like the Π—Σ main bands consist of simple P, Q, and R branches. Here again there is a combination defect, but it is much smaller than for the main bands Π—Σ and agrees within the accuracy of the measurements with the l-type doubling found for the (01^10) level of the ground state in the infrared (Douglas and Sharma 1953). Those Δ—Π subbands that are well resolved show a double P, a double Q, and a double R branch, as is to be expected since the upper state has K-type splitting and the lower state l-type doubling.

The bands arising from the second vibrational level (020) of the ground state consist in general of three subbands $(v_1'v_2'0)^1$—(02^00), $(v_1'v_2'0)^3$—(02^20),

TABLE VIII

EFFECTIVE ROTATIONAL CONSTANTS $\tilde{B}$ AND $\tilde{D}$ OF THE VIBRATIONAL LEVELS OF THE α AND β STATES OF DCN

Level $(v_1v_2v_3)^K$	$\tilde{B}_c$	$\tilde{B}_d$	$\bar{B}$	$\tilde{D}_c^{(K)}$ $\tilde{D}_d^{(K)}$	$\delta_c^{(K)}$ $\delta_d^{(K)}$	D_J^c D_J^d	Remarks
	cm^{-1}			10^{-6} cm^{-1}			
α (0 2 0)^1	1.0826	1.1409	1.1117	8.7 (8.7)	6.9_9	1.7 (1.7)	
α (0 3 0)^1	1.0801	1.142_3	1.111_2	8.1 8.1	7.3_6	0.7 0.7	Pert. $PRJ>8$, $Q(5)$
α (0 4 0)^0			1.1135	28	$32._3$	-4	
α (0 4 0)^1	1.0782	1.1471	1.1126	9.3 11.1	8.0_8	1.2 3.0	Pert. $Q(13)$
α (0 4 0)^2			1.109_6	47 19	$5._4$ $-26._9$	42 46	Pert.
α (0 5 0)^1	1.0742	1.1475	1.1108	8.6 (8.6)	7.6_8	0.9	
α (0 6 0)^1	1.0701	1.1504	1.1102	8.2 22			
α (0 7 0)^1	1.0654	1.1475	1.1064	8.0 8.0			
α (1 2 0)^0			1.1027	$25._5$			
α (1 2 0)^2			1.1041	12			
α (1 3 0)^0			1.1033	32			
α (1 4 0)^0			1.1033	32	$31._2$	0.8	
α (1 4 0)^1	1.0696	1.1373	1.1034	$7._7$ $7._9$	7.8_0	-0.1 0.1	
α (2 4 0)^1	1.0631	1.129_5	1.096_3	8.7 13	7.5_4	$1._2$ $5._5$	
β (0 4 0)^1	1.0565	1.109_9	1.083_2		6.6_0		
β (0 7 0)^1	1.045_3	1.09_{62}	1.070_7		5.2_9		

Note.—D values in parentheses are assumed.

and $(v_1'v_2'0)^1$—(02^20) which are respectively of the types II—Σ, Φ—Δ, and II—Δ. The structure of the first type is identical with that of the main bands. That of the second is similar, since the doubling of the branches expected in this type has not been resolved (see below). No II—Δ subbands were sufficiently strong or sufficiently free of overlapping for their structures to be analyzed.

Further confirmation of the subband types comes from the number of missing lines near the band origin. In all cases in which there is sufficient freedom from overlapping the first lines of the branches are in agreement with expectation (see Tables III and IV). In particular, while in the main bands of II—Σ type $R(0)$ is present, it is missing in bands of types Σ—II, Δ—II, and Φ—Δ. In the last named in addition $R(1)$, $Q(1)$, and $Q(2)$ are missing. This leads to a very characteristic gap between the first line of the Q branch and the first line of the R branch (see Fig. 1).

The rotational levels of a nearly symmetric top with $K = 0, 2, 3$ unlike those with $K = 1$ (see (10) above) can be represented by

$$F(J, K) = (A-\tilde{B})K^2-D_KK^4+\tilde{B}^{(K)}J(J+1)-\tilde{D}^{(K)}J^2(J+1)^2 \tag{12}$$

where

$$\tilde{B}^{(K)} = \tilde{B}-D_{JK}K^2, \qquad \tilde{D}^{(K)} = D_J+\delta^{(K)}. \tag{13}$$

While for $K = 1$ the coefficient of $J(J+1)$, i.e. $\tilde{B}$, is changed markedly compared to the symmetric top and differently for the F_c and F_d levels (eq. (10)), here changes occur only in the quadratic and higher terms and only

they differ for the F_c and F_d levels of $K = 2, 3 \cdots$. According to Polo (1957), the quantities $\delta^{(K)}$ are again determined by the asymmetry parameter ϵ. For $K = 0$, 2, and 3 one has

$$\delta^{(0)} = \tfrac{1}{2}(A-\bar{B})\epsilon^2,$$

$$\delta_c^{(2)} = +\tfrac{1}{12}(A-\bar{B})\epsilon^2, \qquad \delta_d^{(2)} = -\tfrac{5}{12}(A-\bar{B})\epsilon^2, \tag{14}$$

$$\delta^{(3)} = -\tfrac{1}{16}(A-\bar{B})\epsilon^2.$$

Small corrections to the coefficients of the principal terms of (12) are also of the order $(A-\bar{B})\epsilon^2$; but these can be neglected entirely compared to $(A-\bar{B})$ and $\tilde{B}^{(K)}$.

The constants $\tilde{B}^{(K)}$ and $\tilde{D}^{(K)}$ for $K = 0, 2, 3$ could again have been evaluated in the standard way from the observed branches. However, actually a somewhat different procedure was followed since most of the bands with $K = 0, 2, 3$ are weak and often lines of the P and R branches are not available for corresponding J values. Therefore the appropriate quantities $F_c''(J)$ or $F_d''(J)$ known from the infrared were added to the wave numbers of the lines; the resulting term values of the upper state were averaged for each J and, for $K = 2$, separately for the c and d sublevels. These average term values were then fitted to an equation of the form (12) to yield $\tilde{B}^{(K)}$ and $\tilde{D}^{(K)}$ values. The resulting values are included in Tables VII and VIII. The J-independent term in (12) is included in ν_0 as given in Tables I to V.

By comparing (11) with (13) it is immediately seen that the average of $\tilde{B}_c$ and $\tilde{B}_d$ for $K = 1$ would agree with $\tilde{B}$ for $K = 0, 2, 3$ of the same vibrational level if D_{JK} were negligible. Conversely the observed agreement between $\frac{1}{2}(\tilde{B}_c+\tilde{B}_d)_{K=1}$ and $\tilde{B}_{K=0,2,3}$ within the accuracy of the determinations (which is lower for $K = 0$, 2, 3 than for $K = 1$) shows that D_{JK} is negligible compared to $\tilde{B}$ and cannot be determined from differences of the $\tilde{B}$ values. Within the inaccuracy introduced by this neglect, we obtain directly from $\tilde{B}_c$ and $\tilde{B}_d$ for $K = 1$ the values of the rotational constants B and C. Their values are collected in Tables XI and XII.

In columns 7 and 8 of Tables VII and VIII the asymmetric top corrections $\delta^{(K)}$ are included as calculated according to (9) and (14) from the final A, B, C values of Tables XI and XII. Throughout, the $\delta^{(K)}$ values for DCN are larger than the corresponding values for HCN since the deviation from the symmetric top is greater. In spite of the rather low accuracy of the observed $\tilde{D}^{(K)}$ values they do show, as expected, the same trend as the $\delta^{(K)}$ values. In particular the relatively high $\tilde{D}^{(0)}$ values correspond to high $\delta^{(0)}$ values (see, e.g., the $(000)^0$, $(010)^0$, $(030)^0$ levels of HCN and the $(040)^0$ and $(140)^0$ levels of DCN; note that according to (9) and (14) $\delta^{(0)} = 4\delta^{(1)}$). There are, however, a few cases (e.g., the $(000)^1$ and $(020)^0$ levels of HCN) in which $\tilde{D}^{(K)}$ is much larger than $\delta^{(K)}$ presumably owing to perturbations. The differences $\tilde{D}^{(K)}-\delta^{(K)}$ give the centrifugal stretching constants D_J, which are listed in the last two columns of Tables VII and VIII. The scatter of these values is considerable but, apart from the few values that are clearly perturbed, it is seen that D_J is smaller for DCN than for HCN, again as expected.

Since $\delta^{(1)}$ is the same for the F_c and F_d levels to an accuracy of better than $\pm 0.01 \times 10^{-6}$ cm^{-1} the difference between the observed $\tilde{D}_c^{(1)}$ and $\tilde{D}_d^{(1)}$ must arise from a difference in the D_J values of the F_c and F_d levels. As shown by Polo (1957) the formulae given by Kivelson and Wilson (1952) for centrifugal stretching in asymmetric top molecules do indeed give different effective D_J for F_c and F_d, but it is not easy to predict the magnitude of this effect.

For $K = 2$ there is a difference between $\delta_c^{(2)}$ and $\delta_d^{(2)}$ which is indeed the reason for the K-type doubling for $K = 2$. Its magnitude is

$$(\delta_c^{(2)} - \delta_d^{(2)}) J^2(J+1)^2 = \tfrac{1}{2}(A - \bar{B})\epsilon^2 J^2(J+1)^2. \tag{15}$$

The observed line splitting in the best-resolved Δ—Π subbands after subtraction of the splitting due to the Π state fits quite well with that predicted from the $\delta^{(2)}$ values (see Tables VII and VIII). In agreement with the negative sign of $\delta_d^{(2)}$ the sign of $\tilde{D}_d^{(2)}$ is found negative in the few well-resolved cases ($(010)^2$ and $(020)^2$ of HCN and $(040)^2$ of DCN).

In the evaluation of $\tilde{B}$ and $\tilde{D}$, we obtain at the same time the origins ν_0 of the subbands (see Tables I–V), which in turn can now be used for an evaluation of the rotational constants A. According to eq. (12) the separation of the origins of the subbands Δ—Π and Σ—Π of a given vibrational transition (see Fig. 3), that is, the separation of the levels $K = 2$ and $K = 0$, is $4(A - \bar{B}) - 16D_K$. The separation of the levels $K = 1$ and $K = 0$, which is $A - \bar{B} - D_K$ according to (12), can be obtained as the separation of the Π—Π and Σ—Π subbands. While Π—Π subbands have not been observed, their positions can be obtained by subtracting in the case of HCN, $\Delta G'' = 711.7_0$ cm^{-1}, in the case of DCN, $\Delta G'' = 569.13$ cm^{-1}, from the corresponding Π—Σ main bands. Similarly the separation of the levels $K = 2$ and $K = 1$, which is $3(A - \bar{B}) - 15D_K$ according to (12), can be obtained as the separation of the Δ—Π and Π—Π subbands. Designating by $\nu_0(\Sigma)$, $\nu_0(\Pi)$, and $\nu_0(\Delta)$ the origins of the Σ—Π, Π—Π, and Δ—Π subbands respectively, we have according to the above discussion

$$\begin{aligned} \tfrac{1}{3}[\nu_0(\Delta) - \nu_0(\Pi)] &= A - \bar{B} - 5D_K, \\ \tfrac{1}{4}[\nu_0(\Delta) - \nu_0(\Sigma)] &= A - \bar{B} - 4D_K, \\ [\nu_0(\Pi) - \nu_0(\Sigma)] &= A - \bar{B} - D_K. \end{aligned} \tag{16}$$

In Tables IX and X the observed values of $\frac{1}{4}[\nu_0(\Delta) - \nu_0(\Sigma)]$ and $\nu_0(\Pi) - \nu_0(\Sigma)$ are listed for the various levels of HCN and DCN. In addition, in Table X for DCN the values $\frac{1}{3}[\nu_0(\Delta) - \nu_0(\Pi)]$ are given since in several cases they appear preferable to $\nu_0(\Pi) - \nu_0(\Sigma)$. For all the α levels of HCN and DCN one finds

$$\tfrac{1}{3}[\nu_0(\Delta) - \nu_0(\Pi)] < \tfrac{1}{4}[\nu_0(\Delta) - \nu_0(\Sigma)] < \nu_0(\Pi) - \nu_0(\Sigma)$$

as expected from (16) if the centrifugal stretching constant D_K is positive and appreciable. The resulting values of $A - \bar{B}$ and D_K are given in the last two columns of Tables IX and X. It is seen that for HCN, D_K increases rapidly with v_2; for DCN, this increase is much less pronounced. This difference in behavior is similar to that of D_J (see above). For the β levels the effect of D_K cannot clearly be established. It was therefore assumed to be zero.

TABLE IX

ROTATIONAL CONSTANTS $A-\bar{B}$ AND D_K AS DETERMINED FROM SUBBAND ORIGINS FOR THE VIBRATIONAL LEVELS OF THE α STATE OF HCN

Level $(v_1v_2v_3)$	$\frac{1}{4}[\nu_0(\Delta)-\nu_0(\Sigma)]$	$\nu_0(\Pi)-\nu_0(\Sigma)$	$A-\bar{B}$	D_K
	cm^{-1}		cm^{-1}	
$\alpha(0\,0\,0)$	20.80	21.41	21.61_3	0.20_3
$\alpha(0\,1\,0)$	23.14	23.47	23.58	0.11
$\alpha(0\,2\,0)$	26.01	26.75	26.99_7	0.24_7
$\alpha(0\,3\,0)$	29.72	30.72	31.05_3	0.33_3
$\alpha(0\,4\,0)$	35.61	37.57	38.22_3	0.65_3
$\alpha(0\,5\,0)$	45.42	52.99	55.51_3	2.52_3
$\alpha(1\,1\,0)$		23.31	23.42	(0.11)
$\alpha(1\,2\,0)$		25.57	25.82	(0.25)

TABLE X

ROTATIONAL CONSTANTS $A-\bar{B}$ AND D_K AS DETERMINED FROM SUBBAND ORIGINS OR Q HEADS FOR THE VIBRATIONAL LEVELS OF THE α AND β STATES OF DCN

Level $(v_1v_2v_3)$	$\frac{1}{4}[\nu_0(\Delta)-\nu_0(\Sigma)]$	$\frac{1}{3}[\nu_0(\Delta)-\nu_0(\Pi)]$	$\nu_0(\Pi)-\nu_0(\Sigma)$	$A-\bar{B}$	D_K
	cm^{-1}			cm^{-1}	
$\alpha(0\,2\,0)$	(14.9)	(14.41)	$(16.3_7)^a$	$15._2$	[0.11]
$\alpha(0\,3\,0)$	(15.9_8)	(15.86)	16.3_2	16.4_3	0.11_4
$\alpha(0\,4\,0)$	18.04_5	(17.97)	18.28	18.35_8	0.078
$\alpha(0\,5\,0)$	(20.7_0)	(20.41)	(21.5_6)	21.8_5	0.28_7
$\alpha(1\,1\,0)$			(12.7)	$12._9$	[0.2]
$\alpha(1\,2\,0)$	14.36_5	(14.01)	(15.4_3)	15.3	[0.20]
$\alpha(1\,3\,0)$	(15.74)	(15.91)	(15.2_2)	$16._0$	[0.20]
$\alpha(1\,4\,0)$	(17.72)	(17.56)	18.21	18.37_3	0.16_3
$\alpha(1\,5\,0)$	(20.55)	(20.1)	(21.8_7)	$22.2_7{}^b$	0.40^b
$\alpha(2\,3\,0)$	(15.6_8)	(15.24)	(17.0)	$17.0_4{}^c$	0.34^c
$\alpha(2\,4\,0)$	(17.3_0)	(17.06)	(18.0_3)	18.2_7	0.24
$\alpha(2\,5\,0)$	(20.35)	(20.14)	(21.0)	21.2	0.22
$\alpha(3\,4\,0)$		(15.64)		$16._5$	[0.30]
$\alpha(3\,5\,0)$		(19.34)		$20._2$	[0.30]
$\alpha(3\,6\,0)$		(23.67)		$24._6$	[0.30]
$\beta(0\,4\,0)$		(13.4_6)		13.5	
$\beta(0\,5\,0)$	(13.5)	(13.9_8)	$(12._1)$	13.7	
$\beta(0\,6\,0)$	(14.8_5)	(14.1_1)	$(17._1)$	14.7	
$\beta(0\,7\,0)$	(15.3_0)	(15.2_4)	$(15._5)$	15.3	
$\beta(0\,8\,0)$	(15.7_2)	(15.6_4)	$(16._0)$	15.8	
$\beta(0\,9\,0)$	(16.4_3)	(16.4_1)	$(16._5)$	16.4	
$\beta(0\,10\,0)$	(16.9_8)	(16.9_4)	$(17._1)$	17.0	
$\beta(0\,11\,0)$	(17.6_8)	(17.6_4)	$(17._8)$	17.7	
$\beta(0\,12\,0)$	(18.7_5)	(18.5_4)	(19.4)	18.6	
$\beta(0\,13\,0)$	(19.0_8)	(18.8_1)	(19.9)	18.9	
$\beta(0\,14\,0)$		(20.6_1)		20.6	
$\beta(0\,15\,0)$		(20.0_4)		20.0	

Note.—( ) Values based on Q heads rather than band origins.
[ ] Assumed D values.
[a] This value is based on the R head of the $(020)^0$—(01^10) band.
[b] $\frac{1}{3}[\nu_0(\phi)-\nu_0(\Pi)] = 18.49_8$ has been included in these average values.
[c] $\frac{1}{3}[\nu_0(\phi)-\nu_0(\Pi)] = 13.66$ has been used rather than the less accurate $\nu_0(\Pi)-\nu_0(\Sigma)$ value.

It should be emphasized again that the asymmetry corrections to the terms $(A-\bar{B})K^2-D_KK^4$ in (12) as shown by the formulae of Polo (1957) are entirely negligible in the present case.

The $A-\bar{B}$ values of Tables IX and X when combined with the B and C values of Tables XI and XII lead to the A values given in the second column of the latter tables.

The rotational constants A, B, C vary with v_i in a fairly normal manner, similar to that found for C_2H_2 and C_2D_2. In Fig. 5(*a*) and (*b*) this variation, as a function of v_2', is represented graphically for the α states of HCN and

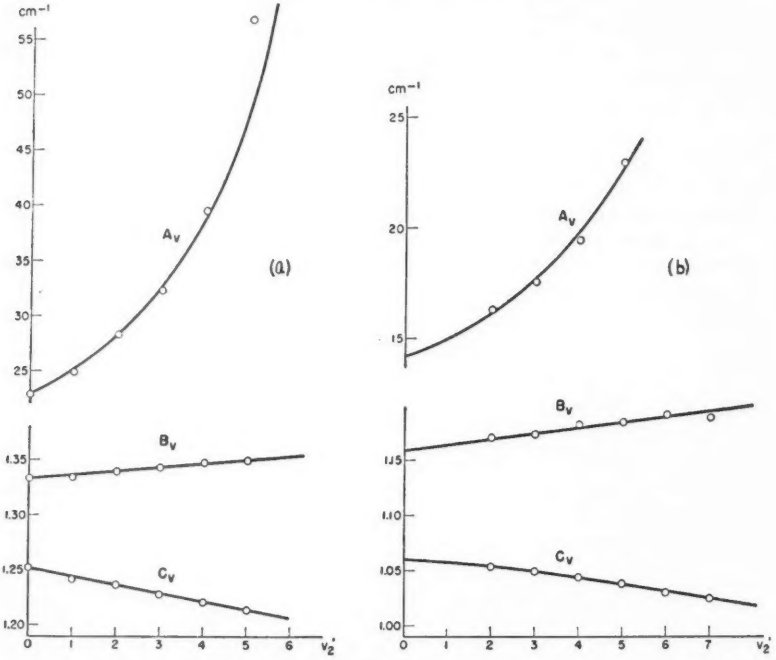

FIG. 5. Dependence of the rotational constants A_v, B_v, C_v on v_2' in the α state of (*a*) HCN and (*b*) DCN. Note the difference in scale in the upper and lower parts of the diagrams.

DCN respectively. While C decreases with increasing v_2', A and B increase. The (non-linear) increase of A is very marked (note the difference in scale for A as compared to B and C): A_{050} of HCN is 2.5 times as large as A_{000}. It may be noted that a similar behavior of the rotational constants is found in the ground states of H_2O and D_2O where also A and B increase with increasing v_2 (bending vibration) and where in particular the increase of A with v_2 is very marked. This strong increase of A with the bending vibration is clearly connected with the gradual approach to a situation similar to that of a linear molecule. In contrast, all three rotational constants show a normal

TABLE XI

ROTATIONAL CONSTANTS, MOMENTS OF INERTIA, AND INERTIAL DEFECTS IN THE α STATE OF HCN

Level ($v_1v_2v_3$)	A	B	C	I_A	I_B	I_C	Δ
	cm^{-1}			10^{-40} g. cm.^{2}			10^{-40} g. cm.^{2}
(000)	22.90_6	1.3330	1.2520	1.221_9	20.997	22.355	0.137
	[22.76]	$[1.332_0]$	$[1.250_7]$	$[1.229_7]$	[21.013]	[22.379]	[0.136]
(010)	24.86_8	1.3342	1.2418	1.125_5	20.978	22.539	0.435
(020)	28.28_5	1.3392	1.2364	0.989_5	20.900	22.638	0.748
(030)	32.33_8	1.3434	1.2276	0.865_5	20.834	22.800	1.100
(040)	39.50_7	1.3470	1.2208	0.708_5	20.779	22.927	1.440
(050)	56.79_4	1.3488	1.2138	0.492_8	20.751	23.059	1.815
(100)		1.4262	1.1414	—	—	—	—
(110)	24.69_8	1.3252	1.2306	1.133_2	21.121	22.744	0.490
(120)	27.09_8	1.3314	1.2248	1.032_9	21.022	22.852	0.797

Note.—Values in square brackets correspond to eq. (17).

TABLE XII

ROTATIONAL CONSTANTS, MOMENTS OF INERTIA, AND INERTIAL DEFECTS IN THE α AND β STATES OF DCN

Level ($v_1v_2v_3$)	A	B	C	I_A	I_B	I_C	Δ
	cm^{-1}			10^{-40} g. cm.^{2}			10^{-40}g. cm.^{2}
α(000)	[14.2]	$[1.158_4]$	$[1.060_1]$	$[1.97_1]$	[24.162]	[26.402]	[0.269]
α(020)	16.3	1.1700	1.0534	1.71_7	23.921	26.569	0.931
α(030)	17.5_4	1.1734	1.0490	1.59_6	23.853	26.682	1.233
α(040)	19.47_1	1.1816	1.0438	1.437_5	23.688	26.816	1.690
α(050)	22.9_8	1.1842	1.0376	1.219	23.636	26.976	2.121
α(060)		1.1906	1.0300		23.509	27.175	
α(070)		1.1886	1.0244		23.549	27.324	
α(110)	$14._0$			2.00			
α(120)	$16._5$	1.1034		1.69_6			
α(130)	17.1	1.1033		1.63_6			
α(140)	19.47_6	1.1712	1.0358	1.437_1	23.899	27.023	1.687
α(150)	23.3_7			1.197			
α(230)	18.1_4			1.542			
α 240)	19.3_7	1.1627	1.0299	1.445	24.072	27.176	1.659
α(250)	22.3			1.25_5			
β(000)	[12.0]	$[1.156_6]$	$[1.043_0]$	$[2.33_2]$	$[24.19_9]$	$[26.83_5]$	$[0.30_3]$
β(040)	14.6	1.1366	1.0298	1.91_7	24.625	27.179	0.637
β(050)	14.8			1.89_1			
β(060)	15.8			1.77_1			
β(070)	16.4	1.1216	1.0198	1.70_6	24.953	27.444	0.784
β(080)	16.9			1.65_6			
β(090)	17.5			1.59_9			
β(0100)	18.1			1.54_6			
β(0110)	18.8			1.48_8			
β(0120)	19.7			1.42_0			
β(0130)	20.0			1.39_9			

Note.—Values in square brackets are extrapolated according to eqs. (18) and (19).

decrease with increasing v_1, although for A(DCN) this decrease is within the rather large experimental error and for A(HCN) it is complicated by a term in v_1v_2.

For the β state (DCN) the increase of A with v_2 is linear while B and C both decrease. It must be remembered that the vibrational numbering is not established and that all rotational constants are less accurate than for the α state.

The following equations for the constants were found:

(17) HCN α state
$$\begin{cases} A_{v_1v_2v_3} = 22.76+1.7_3v_2+0.5v_2^2, \\ B_{v_1v_2v_3} = 1.332_0-0.0090v_1+0.0036v_2, \\ C_{v_1v_2v_3} = 1.250_7-0.0117v_1-0.0075v_2; \end{cases}$$

(18) DCN α state
$$\begin{cases} A_{v_1v_2v_3} = 14.2+0.45v_2+0.25v_2^2, \\ B_{v_1v_2v_3} = 1.158_4-0.0095v_1+0.0054v_2, \\ C_{v_1v_2v_3} = 1.060_1-0.0070v_1-0.0025v_2-0.0004v_2^2; \end{cases}$$

(19) DCN β state
$$\begin{cases} A_{v_1v_2v_3} = 12.0+0.62v_2, \\ B_{v_1v_2v_3} = 1.156_6-0.0050v_2, \\ C_{v_1v_2v_3} = 1.043_0-0.0033v_2. \end{cases}$$

The constant terms in these expressions are the A_0, B_0, C_0 values. Since α_3 for the α state and α_1 and α_3 for the β state cannot be determined, it is not possible to obtain the equilibrium values A_e, B_e, C_e.

From the rotational constants A, B, C of Tables XI and XII the effective moments of inertia are obtained according to

$$I_A = \frac{h}{8\pi^2cA} = \frac{27.9889\times10^{-40}}{A}\ \text{g. cm.}^2 \tag{20}$$

and similar relations for I_B and I_C. These values are included in Tables XI and XII. The last column gives the *inertial defect*

$$\Delta = I_C-I_A-I_B. \tag{21}$$

As is well known, in the equilibrium position this defect is zero for any planar molecule, but it deviates increasingly from zero with increasing vibration. This is borne out by the data of Tables XI and XII. The value of Δ for the (000) level of the α state of HCN as well as of DCN is by far the smallest, as would be expected. In this way the vibrational numbering is confirmed.

Since equilibrium moments of inertia cannot be determined, it is not possible to obtain unambiguous equilibrium internuclear distances and angles. However, effective values for the lowest vibrational level of the α state can be obtained. Since with the two isotopic molecules there are four independent moments of inertia while there are only three geometrical parameters it is possible to get two (or more) sets of parameters whose agreement or disagreement gives an indication of the effect of zero-point vibration on these parameters.

The moment of inertia I_C of a non-linear triatomic molecule XYZ is readily seen to be given by

$$I_C = m_Xr_{XY}^2+m_Zr_{YZ}^2-\frac{1}{M}(m_X^2r_{XY}^2+m_Z^2r_{YZ}^2+2m_Xm_Zr_{XY}r_{YZ}\cos\theta) \tag{22}$$

where m_X, m_Y, m_Z are the masses of the three atoms, $M = m_X+m_Y+m_Z$, r_{XY} and r_{YZ} the two internuclear distances, and θ the $X—Y—Z$ angle. If this equation is applied to HCN and DCN, it is possible to eliminate simultaneously $r_{XY} \equiv r_{CH}$ and θ and one obtains

$$r_{CN}^2 = \frac{(M/m_H)I_C-(M^*/m_D)I_C^*}{m_C m_N[(1/m_H)-(1/m_D)]} \tag{23}$$

where M and I_C refer to HCN and M^* and I_C^* to DCN.

Using the I_C values for the $\alpha(000)$ levels as obtained from equations (17) and (18) (i.e., not the directly observed values but the smoothed values) one finds

$$r_{CN} = 1.296_6 \text{ Å}. \tag{24}$$

Using this value for r_{CN} we can determine r_{CH} (r_{CD}) and θ separately for HCN and DCN from the observed I values.

From Hirschfelder's (1940) equations one finds

$$I_A I_B = \frac{1}{M} m_X m_Y m_Z r_{XY}^2 r_{YZ}^2 \sin^2\theta\,. \tag{25}$$

Substituting the final I_A and I_B values for the $\alpha(000)$ state of HCN and DCN as well as the r_{CN} value determined above and combining with eq. (22) we obtain

$$\begin{aligned} &\text{for HCN:} \quad r_{CH} = 1.143 \text{ Å}, \quad \theta = 124°24', \\ &\text{for DCN:} \quad r_{CD} = 1.134 \text{ Å}, \quad \theta = 125°35'. \end{aligned}$$

The values for HCN and DCN agree in a fairly satisfactory way. The differences are of the order expected on account of the effect of zero-point vibration. It must also be remembered that the moments of inertia for DCN are extrapolated values (see Fig. 5) and therefore not as reliable as those of HCN. The following geometrical data for the α state may therefore be adopted:

$$r_{CH} = 1.140\pm0.005 \text{ Å}, \quad r_{CN} = 1.297\pm0.00\,2 \text{ Å}, \quad \theta = 125.0°\pm0.2°. \tag{26}$$

If the effect of zero-point vibration is neglected, that is if the inertial defect is assumed to be zero, $I_A I_B$ in (25) can be replaced by $I_B I_C - I_B^2$ and thus the geometrical parameters can be evaluated without recourse to I_A. In this way we find

$$\begin{aligned} &\text{for HCN:} \quad r_{CH} = 1.165 \text{ Å}, \quad \theta = 121° 28', \\ &\text{for DCN:} \quad r_{CD} = 1.161 \text{ Å}, \quad \theta = 122° 5'. \end{aligned}$$

These values deviate somewhat more from the previous set than the difference between HCN and DCN found in either case. If one were to calculate the moments of inertia back from this second set of parameters one would find exact agreement for I_B and I_C while I_A would come out incorrectly by the whole amount of the inertial defect, i.e. by 11% and 14% respectively for HCN and DCN. The first set on the other hand gives I_A, I_B, I_C values which deviate from the input values in no case by more than 1.2%. This set is therefore a much better compromise between the conflicting values arising from the effect of zero-point vibration.

In the ground state of HCN $r_e(\mathrm{CH}) = 1.0657$, $r_e(\mathrm{CN}) = 1.1530$ Å, and $\theta = 180°$. Thus, on excitation a considerable increase of $r(\mathrm{CN})$ takes place in addition to the large change of the angle. While the latter accounts according to the Franck–Condon principle for the length of the main progression $(0v_2'0)$—(000), the former accounts for the strong excitation of ν_1 by one quantum. The change of $r(\mathrm{CH})$ seems large enough for ν_3 to be excited in the upper state as well. The fact that its excitation has not been found may be related to the particular form of the normal vibrations in the α state, viz. the fact that the H atom in ν_2 and ν_3 does not move respectively perpendicular and parallel to the CH bond, or possibly to predissociation (see Section F).

For the β state reliable geometrical parameters cannot be obtained since it has only been observed for DCN and since the vibrational numbering is uncertain. Assuming the numbering to be correct, i.e. using the extrapolated rotational constants for the $\beta(000)$ state, we give the parameters for two assumptions about the CH distance (*a*) $r_0(\mathrm{CH}) = 1.140$ Å as in the α state and (*b*) $r_0(\mathrm{CH}) = 1.064$ Å as in the ground state:

$$(a) \quad r_0(\mathrm{CN}) = 1.334 \text{ Å}, \quad \theta = 114° 29',$$
$$(b) \quad r_0(\mathrm{CN}) = 1.370 \text{ Å}, \quad \theta = 108° 25'.$$

Unless one were to assume that the CH distance is much greater than 1.14 Å, it follows that in the β state $r(\mathrm{CN})$ is distinctly larger, θ distinctly smaller than in the α state.

F. PREDISSOCIATION

As mentioned in Section C, the bands of the α—X system become more and more diffuse toward shorter wavelengths. This diffuseness is undoubtedly due to predissociation in the upper state. Very little is known as yet about the details of predissociation in polyatomic molecules. It is therefore of some interest to study the predissociation in a case such as the present one where the nature of the rotational, vibrational, and electronic states involved is known with certainty.

In the main progression $(0v_2'0)^1$—(00^00) of HCN a very slight lack of sharpness of the lines is barely perceptible for $v_2' = 4$. For $v_2' = 5$ the lines are distinctly diffuse, but still well separated from one another. For higher v_2' the lines become more and more diffuse merging more and more into one another. Up to $v_2' = 8$ the R and Q heads are still distinct but beginning with $v_2' = 9$ the bands are completely diffuse and show no longer distinct heads. We may set the predissociation limit in this progression at 55900 cm^{-1}. However, if a more sensitive criterion were used, such as the breaking off of emission bands, the limit might possibly be found to be much lower.

In the $(1v_2'0)^1$—(00^00) progression, the diffuseness sets in somewhat sooner, namely at $v_2' = 2$, corresponding to an energy of 55600 cm^{-1} and the bands become entirely diffuse at $v_2' = 5$, that is much sooner than for the $(0v_2'0)^1$—(000) progression. In other words, the excitation of one quantum of the

vibration ν_1' greatly accelerates the predissociation. This appears not unreasonable since ν_1' is a stretching vibration while ν_2' is a bending vibration (see below).

Another striking difference in diffuseness occurs between the two "hot" progressions. This is clearly shown by Fig. 1*a*, which shows the $(050)^0$—(01^10) band to be only very slightly diffuse while the $(050)^2$—(01^10) band is completely diffuse. Similarly, the $(040)^0$—(01^10) band is entirely sharp while the $(040)^2$—(01^10) band shows already a slight diffuseness. The diffuseness of the main band $(040)^1$—(00^00) is intermediate between the last two. Thus, there is a considerable increase of predissociation probability with increasing K in each vibrational level for which predissociation is possible.

For DCN the predissociation limit is shifted very appreciably to higher energies. In the $(0v_2'0)^1$ progression diffuseness is barely noticeable for the $(070)^1$—(000) band and becomes distinct only for the $(080)^1$—(000) band. The predissociation limit may be set at 57200 cm^{-1} while for HCN it was at 55900 cm^{-1}. In the $(1v_2'0)^1$—(000) progression diffuseness sets in at about the same energy but increases much more rapidly: in the $(160)^1$—(000) band the rotational lines are no longer separated.

Part of the difference between the predissociation limits of HCN and DCN can be accounted for as due to the difference in zero-point energy of the ground state, which is 568 cm^{-1}. The beginning of diffuseness in DCN must necessarily appear shifted by this amount to higher frequencies compared to HCN. The remaining difference can be explained if a fairly narrow potential barrier is assumed between the discrete and the dissociated state, a barrier that can be penetrated more easily, i.e. at a lower energy, by H than by D. For diatomic hydrides such an effect has been observed for example for AlH (Olsson 1938; Herzberg and Mundie 1940).

An understanding of the effect of the vibration ν_1 on the predissociation appears possible by the use of considerations of Franck, Sponer, and Teller (1932). These authors have emphasized that the complicated Lissajous motion of a polyatomic molecule will affect the predissociation phenomenon. They concluded that there should be a strong dependence of the predissociation probability on the particular vibrational motion in the upper vibrational level which is reached by light absorption from the ground state. This dependence is strikingly illustrated by HCN. The bending vibration ν_2' is clearly one that does not lead directly to the pass at which a transition to the dissociated state (H+CN or HC+N) could occur, and only after a considerable time will the Lissajous motion lead the image point to the pass. Therefore, in accordance with the considerations of Franck, Sponer, and Teller, diffuseness sets in very gradually in the $(0v_2'0)$—(000) progression. With the excitation of one quantum of ν_1' the situation is changed: predissociation sets in earlier (at a lower v_2' and a lower energy) since apparently the CN vibration in the upper state changes the Lissajous motion in such a way that the pass is reached much sooner. It would be expected that the CH vibration ν_3 leads to the pass even more readily and therefore predissociation is even more accelerated than for ν_1. This consideration may account for the

non-observation of ν_3' in the spectrum since the corresponding bands may be so diffuse that they are not readily observed.

An explanation of the strong dependence of the predissociation on the rotational quantum number K requires a more detailed study of the form of the eigenfunctions involved and the resulting selection rules. A similar and even more striking dependence on the quantum number l was found (subsequent to the observations here described) by Herzberg and Ramsay (1955) for HCO where in the (linear) excited state only the levels with $l = 0$ are sharp, those with $l = 1$ are entirely diffuse, and those with $l > 1$ are so strongly broadened that they are no longer observable.

From the heat of formation of HCN (−31.2 kcal.) given by Rossini (1948), the dissociation energies of H_2 and N_2 (Douglas 1952), and the heat of sublimation of carbon (Gaydon 1953), one finds for the atomic heat of formation of HCN the value 304.0 kcal. This yields, with the values of $D(\mathrm{CH}) = 80.0_6$ kcal. and $D(\mathrm{CN}) = 191$ kcal.,

$$D(\mathrm{HC{-}N}) = 223.9 \text{ kcal. and } D(\mathrm{H{-}CN}) = 113 \text{ kcal.}^4$$

The first of these is much higher than the energy of the first diffuse band of the α—X system of HCN (159.8 kcal.). Therefore, the products of predissociation cannot be HC+N in spite of the fact that excitation of the C—N stretching vibration of the upper state favors predissociation. On the other hand, D(H—CN) is well below the predissociation limit and therefore the products at the limit must be H+CN.

The energy difference between the predissociation limit and D(H—CN) is large enough so that the CN radical formed in the predissociation may be excited to the $^2\Pi$ state which is 26.42 kcal. above the $^2\Sigma^+$ ground state. The observed strength of the predissociation indicates that the radiationless transition is an allowed one and since the α state is in all probability a singlet state like the ground state it follows that the state causing the predissociation is also a singlet state. On the other hand only one singlet state, presumably the ground state, arises from $H(^2S)+CN(^2\Sigma^+)$ and therefore the state causing the predissociation must arise from $H(^2S)+CN(^2\Pi)$; in other words the dissociation products in the predissociation process are $H(^2S)+CN(^2\Pi)$. This still leaves near the limit 20 kcal. of excess energy which may be distributed as kinetic or vibrational (or rotational) energy among the dissociation products. Thus it is quite possible that there is a fairly narrow potential hill of appreciable height such as is required for the explanation of the change of the limit in going from HCN to DCN.

For the bent configuration, $H(^2S)+CN(^2\Pi)$ gives rise to two singlet states $^1A'$ and $^1A''$. Since the observed predissociation is a strong one affecting equally all rotational levels it is likely to be a homogeneous predissociation, that is, since the α state is $^1A''$ the state causing the predissociation is the $^1A''$ state arising from $H(^2S)+CN(^2\Pi)$. A $^1A''$—$^1A'$ predissociation would be forbidden for zero rotation.

[4]This value is independent of the value assumed for the heat of sublimation of carbon.

G. DISCUSSION AND CONCLUSION

In the preceding sections two excited electronic states of HCN and DCN, designated α and β, have been studied. It has been shown unambiguously that unlike the ground state the molecule is non-linear in both excited states. In a subsequent paper it will be shown that in the upper state of the γ—X system which extends from 1550 Å to shorter wavelengths the molecule is also non-linear. The non-linearity in excited states of molecules which are linear in their ground states was first suspected by Mulliken (1941) in the case of CS_2 but first definitely established in the case of C_2H_2 by Ingold and King (1952, 1953) and confirmed by Innes (1954).

Ingold and King (1953) have discussed the reasons for the bent structure of C_2H_2 in its first excited state and have concluded that it is due to the fact that by a change in σ-bond hybridization from sp (linear) to sp^2 (120° bond angle) the energy is lowered in states in which an electron is excited from the bonding π orbital (filled in the ground state) to what in the linear case would be an antibonding π orbital. The same reasons apply to HCN, which has the same number of electrons as C_2H_2. It is therefore not surprising to find that in the first excited state HCN is in fact non-linear.

Independently Walsh (1953) had predicted that both HCN and C_2H_2 should be non-linear in their first excited states. However, his detailed predictions with regard to HCN have to be somewhat modified in the light of the observed spectra here under discussion.

In the ground state HCN has the electron configuration $\ldots \sigma^2\pi^4\ {}^1\Sigma^+$. The lowest excited states are obtained by taking an electron from the π or σ orbital to an antibonding π^* orbital. This gives rise to four excited states of linear HCN or six states of non-linear HCN as follows (in the order of increasing energy):

linear		non-linear					
$\sigma^2\pi^3\pi^*$	$^1\Delta$	a'^2	a''^2	a'	a'		$^1A'$
		a'^2	a''	a'^2	a'		$^1A''$
$\sigma^2\pi^3\pi^*$	$^1\Sigma^-$	a'^2	a''^2	a'		a''	$^1A''$
$\sigma^2\pi^3\pi^*$	$^1\Sigma^+$	a'^2	a''	a'^2		a''	$^1A'$
$\sigma\ \pi^4\pi^*$	$^1\Pi$	a'	a''^2	a'^2	a'		$^1A'$
		a'	a''^2	a'^2		a''	$^1A''$

The orbitals in the non-linear case are those used by Walsh. We have indicated by underlining in which states the molecule is linear and in which non-linear. The question is whether the observed excited singlet states (which are presumably the lowest excited singlet states) can be correlated with these predicted states.

The lowest predicted $^1A''$ state is the second excited state at the right of the above list. It appears natural to identify the α state with this predicted state. The observed type of the α state is thus accounted for and the low

intensity of the α—X transition can be ascribed to the fact that for linear HCN it would be a forbidden transition ($^1\Delta$—$^1\Sigma^+$).

Walsh has identified the γ state with $^1\Sigma^+$ of the above list, i.e., he assumed the molecule to be linear in this state. However, the structure of the γ—X system shows conclusively (as will be elaborated in paper II) that the molecule is non-linear in the γ state, which moreover is of type $^1A'$. Since the γ state lies much higher than the α state it cannot be identified with the first state of the above list but must in all probability correspond to the $^1A'$ state arising from $^1\Pi$ of linear HCN. This state is predicted to be non-linear and to have roughly the right excitation energy (it is the exact analogue of the $a^1\Pi$ state of N_2).

According to its energy one would be tempted to identify the observed $\beta\,^1A''$ state with the third predicted state at the right of the above list. However, according to Walsh this state is predicted to be linear while the observed β state is definitely non-linear. It is difficult to believe that the β state could correspond to the last state of the list (derived from $^1\Pi$ of linear HCN) since it would be expected to be above the γ state while actually β is close to α.

Walsh's predictions are based on certain assumptions about the variation of orbital energy with angle (see Fig. 1 of Walsh's paper). In order to shift the equilibrium in the $^1\Sigma^-$ state from the linear to the non-linear configuration some modification of Walsh's curves will be required. It may also be that the discrepancy found is just a consequence of the drastic simplifications inherent in Walsh's treatment.

A much more elaborate treatment of the electronic structure of HCN has recently been given by Iguchi (1955) using both the molecular orbital method with configuration interaction and the Heitler–London method including ionic-homopolar resonance. However, the calculations have been restricted to a linear framework and to configurations involving π electrons only. The first two excited singlet states are calculated to be $^1\Sigma^-$ at 5.60 ev. and $^1\Delta$ at 10.08 ev. Presumably these correspond to the first two states in the list above. The correlation with the observed states is clearly not very good. Calculations on the effect of bending on the energies of the predicted states would be important.

In addition to HCN and C_2H_2 there are three other molecules for which a change from linear to non-linear configuration has been established. In HCO, with one more electron than HCN, it is, as expected from Walsh's considerations, the ground state in which the molecule is non-linear. Upon exciting the most loosely bound electron from the a' to the a'' component of the π orbital a linear configuration is predicted and has indeed been observed (Herzberg and Ramsay 1955). Similarly in NH_2, it has been shown by Ramsay (1956) that, while the molecule is non-linear in the ground state, it is linear in the upper state of the α bands. In CS_2, as mentioned before, Mulliken had already predicted a non-linear configuration in the first excited state. This configuration has now been established in detail by recent work of Kleman in this laboratory.

The numerous perturbations that have been observed in the α—X system both in HCN and in DCN are probably produced by the otherwise unidentified

but expected A' state arising from $^1\Delta$. While it seemed possible that they might have been caused by the β state no agreement of levels was found that could account for the perturbations on this basis.

The potential energy of the HCN molecule in the α state as a function of the angle of bend ϕ assuming the molecule to be fixed to a plane is represented schematically in Fig. 6. There are two equivalent minima separated by a

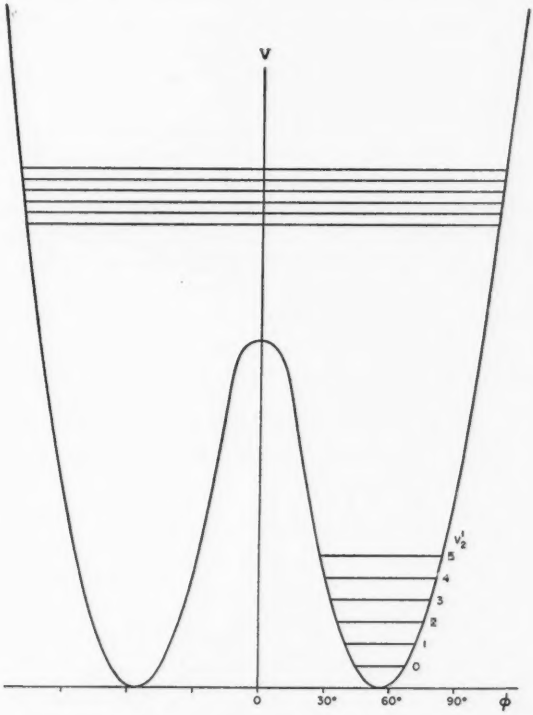

FIG. 6. Potential function for the bending vibration of a non-linear triatomic molecule. The abscissa is the angle of bend. It is assumed that the motion is restricted to one plane.

maximum for $\phi = 0$, i.e. corresponding to the linear configuration. The vibrational levels near the minima would be expected to follow a regular course. Again far above the maximum they would follow such a regular course but with half the spacing. Here the levels are essentially those of a linear molecule, alternate levels having even and odd l values while near the minima all K values occur for each value of v_2. In the region near the maximum the levels would follow a rather irregular course. The observed $(0v_20)$—(000) progression of the α—X system is perfectly regular for both HCN and DCN. Since in addition, at least for HCN, it includes the (000)—(000) band it must correspond to the region in the neighborhood of the potential minima. On the other

hand the Franck–Condon principle would lead one to expect the maximum of intensity in the $(0v_20)$—(000) progression to correspond to the region of the potential maximum since in the lower state the molecule is linear, that is, the spacings should be quite irregular. This apparent lack of agreement between observation and expectation can be readily explained if account is taken of the fact that according to the preceding discussion the α—X system corresponds in the linear case to a forbidden transition ($^1\Delta$—$^1\Sigma^+$), that is, the Franck-Condon intensities have to be multiplied by a factor which is 0 for $\phi = 0$ and rises rapidly with increasing ϕ. Similar considerations apply to the β—X system, which very probably also corresponds to a forbidden transition ($^1\Sigma^-$—$^1\Sigma^+$) in the linear case.

An alternative explanation of the above apparent discrepancy might be sought in the fact that predissociation which broadens the higher vibrational levels is so strong near the potential maximum that there remains only a continuous absorption whose intensity is difficult to compare with that of the discrete bands. However, the effect of the forbidden character of the absorption in the linear case must arise unless the interpretation of the electronic structure discussed above should turn out to be incorrect.

In the case of the near ultraviolet bands of C_2H_2 analyzed by Ingold and King (1953) and Innes (1954) the situation is very similar. The upper state A_u with a non-linear equilibrium configuration in all probability corresponds to a $^1\Sigma^-$ state for a linear configuration which cannot combine with the ground state. Again the vibrational levels are perfectly regular and the region of the potential maximum is not reached. However, the shortward end of the spectrum has not been well investigated.

ACKNOWLEDGMENTS

We are greatly indebted to Dr. P. G. Wilkinson (University of Chicago) for supplying us with a Xe discharge tube which served as a continuous background in part of the work, to Mr. J. Shoosmith for his help in obtaining the spectrograms, and to Dr. A. E. Douglas for advice and discussion at various stages of the work. Miss Lila L. Howe prepared the illustrations and checked the numerous tables. Mrs. K. Innes and Miss Howe gave very efficient help in the extensive calculations. We are most grateful to both of them for their untiring efforts. Finally we wish to thank Dr. S. R. Polo for many discussions of his work on the asymmetric top and its application to the present paper as well as for a critical reading of the manuscript.

REFERENCES

ALLEN, H. C., Jr., TIDWELL, E. D., and PLYLER, E. K. 1956. J. Chem. Phys. **25**, 302.
BRIX, P. and HERZBERG, G. 1954. Can. J. Phys. **32**, 110.
CHECKLAND, P. B. and THOMPSON, H. W. 1955. Trans. Faraday Soc. **51**, 1.
CURRY, J. and HERZBERG, G. 1934. Ann. Physik, **19**, 800.
DOUGLAS, A. E. 1952. Can. J. Phys. **30**, 302.
DOUGLAS, A. E. and SHARMA, D. 1953. J. Chem. Phys. **21**, 448.
FRANCK, J., SPONER, H., and TELLER, E. 1932. Z. physik. Chem. B, **18**, 88.
GAYDON, A. G. 1953. Dissociation energies and spectra of diatomic molecules, 2nd ed. (Chapman and Hall, London).
HERZBERG, G. 1945. Molecular spectra and molecular structure, Vol. II, Infrared and Raman spectra of polyatomic molecules (D. Van Nostrand Co., Inc., New York).

HERZBERG, G. and MUNDIE, L. G. 1940. J. Chem. Phys. **8**, 263.
HERZBERG, G. and RAMSAY, D. A. 1955. Proc. Roy. Soc. A, **233**, 34.
HILGENDORFF, H. J. 1935. Z. Physik, **95**, 781.
HIRSCHFELDER, J. O. 1940. J. Chem. Phys. **8**, 431.
IGUCHI, K. 1955. J. Chem. Phys. **23**, 1983.
INGOLD, C. K. and KING, G. W. 1952. Nature, **169**, 1101.
——— 1953. J. Chem. Soc. 2702.
INNES, K. K. 1954. J. Chem. Phys. **22**, 863.
KIVELSON, D. and WILSON, E. B., JR. 1952. J. Chem. Phys. **20**, 1575.
LAWRANCE, R. B. and STRANDBERG, M. W. P. 1951. Phys. Rev. **83**, 363.
MULLIKEN, R. S. 1941. Phys. Rev. **60**, 506.
OLSSON, E. 1938. Diss. Stockholm.
POLO, S. R. 1957. Can. J. Phys. **35**, 880.
PRICE, W. C. 1934. Phys. Rev. **46**, 529.
PRICE, W. C. and WALSH, A. D. 1945. Trans. Faraday Soc. **41**, 381.
RAMSAY, D. A. 1956. J. Chem. Phys. **25**, 188.
ROSSINI, F. D. 1948. Selected values of chemical thermodynamic properties (National Bureau of Standards, Washington, D.C.).
WALSH, A. D. 1953. J. Chem. Soc. 2288.
WANG, S. C. 1929. Phys. Rev. **34**, 243.
WILKINSON, P. G. and TANAKA, Y. 1955. J. Opt. Soc. Amer. **45**, 344.

ENERGY LEVELS OF SLIGHTLY ASYMMETRIC TOP MOLECULES[1]

S. R. Polo

ABSTRACT

For the rotational analysis of the band spectra of slightly asymmetric tops it is convenient to have explicit expressions for the rotational energies in terms of the rotational quantum numbers. In the tables available at present the coefficients of the power series in the asymmetry parameter are only tabulated numerically for each individual rotational level. In the present work more general expressions are derived, giving the explicit dependence on J, K, and the asymmetry parameter ϵ (including terms up to ϵ^5). First-order corrections for centrifugal distortion in terms of J, K, and ϵ have also been included.

INTRODUCTION

In the rotational analysis of the band spectra of asymmetric top molecules the energies of a (usually) large number of rotational levels can be determined. In order to deduce the values of the rotational constants it is convenient to have expressions giving the explicit dependence of the energies on the rotational quantum numbers. While for a general asymmetric top this is not possible, in the case of a near-symmetric top the energies can be expressed very conveniently as power series in J and K whose coefficients are functions of the rotational constants. The main terms in the series are those in $J(J+1)$ and K^2, while the coefficients of all the other terms are of the order of some power, ϵ, ϵ^2, etc., of an asymmetry parameter ϵ, and vanish in the limiting case of a symmetric top. Fitting the data to power series presents no essential difficulties, provided the convergence is fast. The rotational constants can be determined from the series coefficients. This procedure has been found very convenient in the analysis of the ultraviolet absorption bands of HCN and DCN (Herzberg and Innes 1957). In the upper state both molecules have a bent configuration and are slightly asymmetric, near-prolate tops.

There are tables available for the calculation of the energy levels of slightly asymmetric tops (King, Hainer, and Cross 1943), (Lotspeich, Kraitchman, and Solimene 1955), (Schwendeman 1957), which give the energies as a power series in a certain asymmetry parameter. However, the series coefficients are only tabulated numerically for each energy level, and are thus inadequate for our purpose. In the present work more general expressions are derived, giving the explicit dependence of the energies on ϵ, J, and K. Since the effects of the non-rigidity of the molecule are also important, expressions for the first-order centrifugal distortion corrections in terms of J, K, and ϵ have also been included.

THE RIGID ROTOR

The rotational Hamiltonian, in the case of a near-prolate top, can be written most conveniently in the form[2]

[1]Manuscript received May 1, 1957.
Contribution from the Division of Pure Physics, National Research Council, Ottawa, Ont. Issued as N.R.C. No. 4407.

[2]If the momenta are measured in units of $\hbar$ and the rotational constants are defined as $A = h/8\pi^2 cI_A$, etc., the energy levels are expressed in cm^{-1}.

$$(1)\quad \mathbf{H}_r = A\mathbf{P}_A^2+B\mathbf{P}_B^2+C\mathbf{P}_C^2$$
$$= \tfrac{1}{2}(B+C)\mathbf{P}^2+[A-\tfrac{1}{2}(B+C)]\left\{\mathbf{P}_A^2+\frac{B-C}{2A-B-C}(\mathbf{P}_B^2-\mathbf{P}_C^2)\right\}.$$

In a representation that diagonalizes $\mathbf{P}^2$ ($=\mathbf{P}_A^2+\mathbf{P}_B^2+\mathbf{P}_C^2$) and $\mathbf{P}_A$, the non-vanishing matrix elements of the angular momentum operators in Eq. (1) are

$$(2)\quad \begin{aligned}(J,K|\mathbf{P}^2|J,K) &= J(J+1),\\ (J,K|\mathbf{P}_A|J,K) &= K,\\ (J,K|\mathbf{P}_B^2-\mathbf{P}_C^2|J,K\pm2) &= \tfrac{1}{2}\{[J(J+1)-K(K\pm1)][J(J+1)-(K\pm1)(K\pm2)]\}^{\frac{1}{2}}.\end{aligned}$$

Since the Hamiltonian is diagonal in J, and $\mathbf{P}^2$ is independent of K, the determination of the eigenvalues of $\mathbf{H}_r$ can be reduced to finding those of

$$(3)\quad \mathbf{E}(\epsilon) = \mathbf{P}_A^2+2\epsilon(\mathbf{P}_B^2-\mathbf{P}_C^2)$$

where the asymmetry parameter, ϵ, has been chosen[3] as

$$(4)\quad \epsilon = \frac{B-C}{2(2A-B-C)}.$$

It may be noticed that ϵ is not identical with the parameter b introduced by Wang (1929). They are related by

$$(5)\quad \epsilon = -\tfrac{1}{2}b.$$

The eigenvalues of $\mathbf{E}(\epsilon)$ can be obtained by standard methods of perturbation theory (Condon and Shortley 1935), treating the term in ϵ in Eq. (3) as a small perturbation. The results given below have also been checked by an alternative derivation using the continuous fraction method (King, Hainer, and Cross 1943).

Each rotational level is specified by the values of J, K_a (prolate K value), and K_c (oblate K value). In the near-prolate case $K_a = K$, while K_c can be either $J-K+1$ (lower) or $J-K$ (upper).

The rotational energies are given as a power series in the form

$$(6)\quad F(J_{K,K_c}) = \tfrac{1}{2}(B+C)J(J+1)+[A-\tfrac{1}{2}(B+C)]K^2$$
$$+[A-\tfrac{1}{2}(B+C)]\left\{K^2\sum_{n=2}^{\infty}c_{0n}\epsilon^n + J(J+1)\sum_{n=1}^{\infty}c_{1n}\epsilon^n + J^2(J+1)^2\sum_{n=2}^{\infty}c_{2n}\epsilon^n+\dots\right\}.$$

The series expansion has been followed up to and including the fifth power of ϵ. To this approximation, for $K > 5$ the two energy levels associated with a given K are degenerate, and a simple general expression for the coefficients

[3]There are several reasons that perhaps justify the introduction of another asymmetry parameter. Since $A \geqslant B \geqslant C$, the parameter ϵ is always positive, while b is always negative. The symbol ϵ seems preferable to b, as this is also used to denote rotational constants. The inclusion of the factor $\frac{1}{2}$ in the parameter simplifies the numerical coefficients in the power series expansions for the energies. The use of the parameter $\delta = (B-C)/(A-C)$ of King, Hainer, and Cross (1943) has more serious disadvantages. The secular determinant is an even function of ϵ (or b), but not of δ. The result is that the energy expressions for even K are even functions of ϵ, while for odd K a change of ϵ by $-\epsilon$ only interchanges the expressions for the two levels with the same K. These simple properties do not obtain in the case of δ, and the energy expressions always contain odd powers of δ.

c_{mn} can be given. For $K \leqslant 5$, the energies also depend on K_c and expressions for each value of the pair K, K_c are given. For odd K, only the levels with $K_c = J-K+1$ need be given. Those with $K_c = J-K$ can be obtained from them by replacing ϵ by $-\epsilon$.

The coefficients c_{mn} of Eq. (6) are presented in Tables I and II. The headings of the rows and columns indicate directly the factors $J^m(J+1)^m$ or K^2, and ϵ^n, that multiply the coefficient c_{mn}. For even K, the energy is an even function of ϵ; for odd K, there are both even and odd powers, but the lowest odd power in the series is ϵ^K.

TABLE I

COEFFICIENTS IN THE EXPRESSION FOR THE ENERGY LEVELS
$K > 5$, $K_c = J-K$ or $J-K+1$

	ϵ^2	ϵ^4
K^2	$-\frac{3}{2}$	$-\frac{51}{32}$
$J(J+1)$	$+1$	$+\frac{9}{8}$
$J^2(J+1)^2$	$+\frac{1}{2(K^2-1)}$	$+\frac{11K^2-38}{16(K^2-1)(K^2-4)}$
$J^3(J+1)^3$	0	$-\frac{3}{8(K^2-1)(K^2-4)}$
$J^4(J+1)^4$	0	$+\frac{5K^2+7}{32(K^2-1)^3(K^2-4)}$

All expressions and tables are given for a near-prolate top ($A > B \simeq C$). Those valid for a near-oblate top ($A \simeq B > C$) are obtained by interchanging A and C throughout. It should be remembered that in the near-oblate case K stands for K_c, while $J-K$ or $J-K+1$ stands for K_a, and ϵ for $(A-B)/2(A+B-2C)$.

As may be seen from the tables, the contribution to the energy by the terms containing high powers of $J(J+1)$ becomes more significant for low K values. This contribution is most important for the level $K = 0$ and the level of the same species $K = 2$, $K_c = J-2$, but much less for the level $K = 2$, $K_c = J-1$. The energies for these three levels are given including up to terms in ϵ^7, although it should be remembered that when high order terms become significant, the convergence of the series expansion is usually poor.

The general expression (6) takes a simpler form when the relative importance of the different terms in ϵ is properly assessed, and only the most significant ones retained. For sufficiently small ϵ, it is usually enough to retain only the terms in $J^m(J+1)^m\epsilon^m$, that is, only the first terms in the summations of Eq. (6).[4] Thus, for example, the energies for the levels $J_{1,J}$ (lowest of the pair with $K = 1$) can be written as

[4]This is equivalent to the (unmodified) Mathieu function approximation of Golden (1948).

TABLE II

COEFFICIENTS IN THE EXPRESSION FOR THE ENERGY LEVELS

	$K=0,\ K_c=J$			$K=2,\ K_c=J-1$			$K=2,\ K_c=J-2$			$K=4,\ K_c=J-3$		$K=4,\ K_c=J-4$	
	ϵ^2	ϵ^4	ϵ^6	ϵ^2	ϵ^4	ϵ^6	ϵ^2	ϵ^4	ϵ^6	ϵ^2	ϵ^4	ϵ^2	ϵ^4
K^2				$-\frac{3}{2}$	$-\frac{51}{32}$	$-\frac{213}{64}$	$-\frac{3}{2}$	$-\frac{51}{32}$	$-\frac{213}{64}$	$-\frac{3}{2}$	$-\frac{51}{32}$	$-\frac{3}{2}$	$-\frac{51}{32}$
$J(J+1)$	$+1$	$+\frac{9}{8}$	$+\frac{39}{16}$	$+\frac{3}{2}$	$+\frac{13}{8}$	$+\frac{1757}{512}$	$+\frac{1}{2}$	$+\frac{5}{8}$	$+\frac{739}{512}$	$+1$	$+\frac{19}{16}$	$+1$	$+\frac{17}{16}$
$J^2(J+1)^2$	$-\frac{1}{2}$	$-\frac{19}{32}$	$-\frac{85}{64}$	$-\frac{1}{12}$	$-\frac{9}{128}$	$-\frac{1849}{15360}$	$+\frac{5}{12}$	$+\frac{55}{128}$	$+\frac{13361}{15360}$	$+\frac{1}{30}$	$+\frac{1}{960}$	$+\frac{1}{30}$	$+\frac{91}{960}$
$J^3(J+1)^3$	0	$-\frac{3}{32}$	$+\frac{67}{192}$	0	$-\frac{7}{1152}$	$-\frac{7357}{368640}$	0	$+\frac{121}{1152}$	$+\frac{161677}{368640}$	0	$+\frac{19}{2880}$	0	$-\frac{31}{2880}$
$J^4(J+1)^4$	0	$+\frac{7}{128}$	$-\frac{445}{2304}$	0	$+\frac{5}{13824}$	$+\frac{511}{737280}$	0	$-\frac{763}{13824}$	$-\frac{152551}{737280}$	0	$-\frac{317}{864000}$	0	$+\frac{433}{864000}$
$J^5(J+1)^5$	0	0	$+\frac{17}{576}$	0	0	$+\frac{121}{1474560}$	0	0	$-\frac{127763}{4423680}$				
$J^6(J+1)^6$	0	0	$-\frac{29}{2304}$	0	0	$-\frac{289}{79626240}$	0	0	$+\frac{1002401}{79626240}$				

	$K=1,\ K_c=J$					$K=3,\ K_c=J-2$				$K=5,\ K_c=J-4$		
	ϵ	ϵ^2	ϵ^3	ϵ^4	ϵ^5	ϵ^2	ϵ^3	ϵ^4	ϵ^5	ϵ^2	ϵ^4	ϵ^5
K^2	0	$-\frac{3}{2}$	0	$-\frac{51}{32}$	0	$-\frac{3}{2}$	0	$-\frac{51}{32}$	0	$-\frac{3}{2}$	$-\frac{51}{32}$	0
$J(J+1)$	-1	$+1$	$+\frac{3}{16}$	$+\frac{9}{8}$	$+\frac{113}{256}$	$+1$	$-\frac{3}{16}$	$+\frac{9}{8}$	$-\frac{27}{64}$	$+1$	$+\frac{9}{8}$	$-\frac{5}{256}$
$J^2(J+1)^2$	0	$-\frac{1}{8}$	$-\frac{1}{8}$	$-\frac{35}{192}$	$-\frac{19}{64}$	$+\frac{1}{16}$	$+\frac{1}{8}$	$+\frac{61}{640}$	$+\frac{9}{32}$	$+\frac{1}{48}$	$+\frac{79}{2688}$	$+\frac{1}{64}$
$J^3(J+1)^3$	0	0	$+\frac{1}{64}$	$+\frac{1}{96}$	$+\frac{161}{4608}$	0	$-\frac{1}{64}$	$-\frac{3}{320}$	$-\frac{129}{4096}$	0	$-\frac{1}{1344}$	$-\frac{127}{36864}$
$J^4(J+1)^4$	0	0	0	$-\frac{1}{1536}$	$+\frac{5}{2304}$	0	0	$+\frac{13}{20480}$	$-\frac{5}{2048}$	0	$+\frac{11}{774144}$	$+\frac{5}{18432}$
$J^5(J+1)^5$	0	0	0	0	$-\frac{11}{36864}$	0	0	0	$+\frac{5}{16384}$	0	0	$-\frac{1}{147456}$

$$(7)\quad F(J_{1,J}) = [A-\tfrac{1}{2}(B+C)]+\{\tfrac{1}{2}(B+C)+[A-\tfrac{1}{2}(B+C)]\epsilon\}J(J+1)$$
$$+[A-\tfrac{1}{2}(B+C)]\left(-\frac{1}{8}\epsilon^2\right)J^2(J+1)^2+[A-\tfrac{1}{2}(B+C)]\left(\frac{1}{64}\epsilon^3\right)J^3(J+1)^3+\text{ etc.}$$

This expression is of the same form as that for symmetric top molecules, and the coefficients can be determined by the same methods. The energies for the $J_{1,J-1}$ levels are obtained from Eq. (7) by changing ϵ into $-\epsilon$. The most significant change occurs in the coefficient of $J(J+1)$, and causes the large K-type splitting characteristic of the $K = 1$ levels in asymmetric tops.

THE NON-RIGID ROTOR

The first-order centrifugal distortion corrections in terms of the rotational quantum numbers are given below. The results are based on the treatment by Kivelson and Wilson (1952). The distortion constants are those used by Nielsen (1951). In the limiting case of a symmetric top, the constants R_5, R_6, and δ_J vanish, and the usual expression in D_J, D_K, and D_{JK} is obtained.

$$(8)\quad F(J_{0,J}) = F(J_{0,J})_{\text{rigid}}+[-4R_6+8R_5\epsilon]J(J+1)$$
$$+[-D_J-(4R_5+2\delta_J)\epsilon]J^2(J+1)^2+[\delta_J\epsilon]J^3(J+1)^3$$

$$(9)\quad F(J_{1,J}) = F(J_{1,J})_{\text{rigid}}+[-D_K+10R_6-30R_5\epsilon]$$
$$+[-D_{JK}-4R_6-\underline{2R_5}+(\underline{3R_6}+20R_5+3\delta_J)\epsilon]J(J+1)$$
$$+\left[-D_J+\underline{\delta_J}-\left(\underline{2R_6}+\frac{5}{2}R_5+2\delta_J\right)\epsilon\right]J^2(J+1)^2+[\tfrac{1}{4}(\underline{R_6}+\delta_J)\epsilon]J^3(J+1)^3$$

For $K = 1$, $K_c = J-1$, the sign of the underlined terms should be reversed.

$$(10)\quad F(J_{2,J-1}) = F(J_{2,J-1})_{\text{rigid}}+[-16D_K+40R_6-240R_5\epsilon]$$
$$+[-4D_{JK}-2R_6+(60R_5+12\delta_J)\epsilon]J(J+1)$$
$$+\left[-D_J-R_6-\left(\frac{10}{3}R_5+3\delta_J\right)\epsilon\right]J^2(J+1)^2+\left[\frac{1}{6}\delta_J\epsilon\right]J^3(J+1)^3$$

$$(11)\quad F(J_{2,J-2}) = F(J_{2,J-2})_{\text{rigid}}+[-16D_K+40R_6-240R_5\epsilon]$$
$$+[-4D_{JK}-6R_6+(52R_5+12\delta_J)\epsilon]J(J+1)$$
$$+\left[-D_J+R_6+\left(\frac{2}{3}R_5-\delta_J\right)\epsilon\right]J^2(J+1)^2+\left[-\frac{5}{6}\delta_J\epsilon\right]J^3(J+1)^3$$

$$(12)\quad F(J_{3,J-2}) = F(J_{3,J-2})_{\text{rigid}}+[-81D_K+90R_6-990R_5\epsilon]$$
$$+[-9D_{JK}-4R_6+(-\underline{3R_6}+116R_5+27\delta_J)\epsilon]J(J+1)$$
$$+\left[-D_J+\left(\underline{4R_6}-\frac{7}{4}R_5-2\delta_J\right)\epsilon\right]J^2(J+1)^2+\left[\left(-\frac{1}{4}\underline{R_6}-\frac{1}{8}\delta_J\right)\epsilon\right]J^3(J+1)^3$$

For $K = 3$, $K_c = J-3$, the sign of the underlined terms should be reversed.

For $K > 3$, $K_c = J-K+1$ or $J-K$,

$$F(J_{K,K_c}) = F(J_{K,K_c})_{\text{rigid}}+[-K^4D_K+10K^2R_6-10K^2(K^2+2)R_5\epsilon]$$
$$+[-K^2D_{JK}-4R_6+(4(3K^2+2)R_5+3K^2\delta_J)\epsilon]J(J+1)$$
$$+\left[-D_J-\left(2\frac{K^2-2}{K^2-1}R_5+2\delta_J\right)\epsilon\right]J^2(J+1)^2+\left[-\frac{1}{K^2-1}\delta_J\epsilon\right]J^3(J+1)^3 \tag{13}$$

The above distortion constants are related to the τ's used by Kivelson and Wilson (1952) as follows:

$$\begin{aligned}
D_J &= -\frac{\hbar^4}{32}(3\tau_{xxxx}+3\tau_{yyyy}+2\tau_{xxyy}+4\tau_{xyxy}) \\
D_K &= D_J-\frac{\hbar^4}{4}(\tau_{zzzz}-\tau_{zzxx}-\tau_{yyzz}-2\tau_{xzxz}-2\tau_{yzyz}) \\
D_{JK} &= -D_J-D_K-\frac{\hbar^4}{4}\tau_{zzzz} \qquad (14) \\
R_6 &= \frac{\hbar^4}{64}(\tau_{xxxx}+\tau_{yyyy}-2\tau_{xxyy}-4\tau_{xyxy}) \\
R_5 &= -\frac{\hbar^4}{32}(\tau_{xxxx}-\tau_{yyyy}-2\tau_{xxzz}-4\tau_{xzxz}+2\tau_{yyzz}+4\tau_{yzyz}) \\
\delta_J &= -\frac{\hbar^4}{16}(\tau_{xxxx}-\tau_{yyyy})
\end{aligned}$$

In obtaining Eqs. (8) to (13) the identification of the axes has been $a \rightarrow z$, $b \rightarrow x$, $c \rightarrow y$.

ACKNOWLEDGMENTS

The author would like to thank Drs. G. Herzberg and B. P. Stoicheff, who read the manuscript and made helpful suggestions.

REFERENCES

CONDON, E. U. and SHORTLEY, G. H. 1935. The theory of atomic spectra (Cambridge University Press), p. 30.
GOLDEN, S. 1948. J. Chem. Phys. **16**, 78.
HERZBERG, G. and INNES, K. K. 1957. Can. J. Phys. **57**, 842.
KING, G. W., HAINER, R. M., and CROSS, P. C. 1943. J. Chem. Phys. **11**, 27 (Appendix III).
KIVELSON, D. and WILSON, E. B. 1952. J. Chem. Phys. **20**, 1575.
LOTSPEICH, J. F., KRAITCHMAN, J., and SOLIMENE, N. 1955. *Reproduced in* Microwave spectroscopy, *by* C. H. Townes and A. L. Schawlow (McGraw-Hill Book Co., Inc., New York), p. 522.
NIELSEN, H. H. 1951. Revs. Mod. Phys. **23**, 90.
SCHWENDEMAN, R. 1957. Unpublished work, Chemistry Department, Harvard University (Private communication).
WANG, S. C. 1929. Phys. Rev. **34**, 243.

DISCUSSION OF THE ELECTRICAL PROPERTIES OF COMPOUNDS WITH THE NICKEL ARSENIDE STRUCTURE[1]

W. B. PEARSON

ABSTRACT

A valence scheme has been proposed for alloys such as CrSe, MnTe, and FeS, with the nickel arsenide structure, which indicates why they may be semiconductors, while chalcogenides of Co and Ni and antimonides and bismuthides of Cr, Mn, Fe, Co, and Ni with a similar structure are metallic. The valence scheme is thus consistent with the known electrical properties (and also magnetic properties) of these phases. It then predicts that FeSe and CrS may well be semiconductors and indicates that all other compounds of Cr, Mn, Fe, Co, and Ni with the NiAs structure should be metallic.

I. INTRODUCTION

Although it is now possible to classify and predict semiconductivity in compounds which do not contain transition metal elements (cf. Mooser and Pearson 1956, 1957), this is not generally possible in compounds containing the transition metals, because of a lack of experimental data on the electrical properties of these compounds under precisely specified conditions of structure and composition on which to base an initial analysis. This is particularly so in compounds with the chalcogenides (S, Se, and Te), although in the case of the oxides and mixed oxides much theoretical and practical work has been done towards an understanding of the conduction mechanisms.

The difficulty which arises in the transition metal chalcogenide compounds is a lack of *a priori* knowledge of the valence state of the transition metal. That is to say, we do not know whether the *d* electrons are involved in the bonding (formation of the valence band) and, if they are not directly involved, whether they exist in discrete states or form a *d* band. It is, however, well known from the semiconductivity of compounds such as chalcopyrite ($CuFeS_2$, cf. Austin *et al.* 1956) that the valence band (which must contain an even number of electron states*) can be quite independent of the *d* shell of the transition metal. A transition metal compound which is a semiconductor may therefore contain an odd number of "apparent" valence electrons (i.e., *d*, *s*, and *p* electrons).

In an attempt to develop a systematic picture of the electrical properties of compounds of the transition metals with the chalcogenides and other elements, we discuss in this paper the electrical properties of compounds with the nickel arsenide structure. We propose a valence state for the transition metal (Cr, Mn, Fe, Co, and Ni) in these compounds which is consistent with the known magnetic properties and which permits a qualitative discussion and explanation of the known occurrence of metallic conductivity and semi-

[1]Manuscript received May 21, 1957.
Contribution from the Division of Pure Physics, National Research Council Laboratories, Ottawa, Canada.
Issued as N.R.C. No. 4414.
*See Appendix.

conductivity, and hence allows prediction of the electrical properties of the compounds which have not yet been examined.

II. THE NICKEL ARSENIDE STRUCTURE AND ELECTRICAL PROPERTIES OF COMPOUNDS WITH THIS STRUCTURE

The NiAs structure can be regarded as built up from a close-packed hexagonal structure of As atoms in the octahedral holes of which lie the Ni atoms (the holes are precisely octahedral if the axial ratio has the value 1.63). When phases with this structure occur on the As-rich side of the stoichiometric composition, vacancies occur in the transition metal sites, and when phases occur on the As-poor side, extra transition metal atoms are admitted in the trigonal-bipyramidal holes where the coordination is five. In the stoichiometric compound where all of the octahedral holes are filled the transition metal atoms lie in lines along the *c* axis so that the As atoms are also six-coordinated, being located at the center of a right-trigonal prism.

At present we know of three compounds with the NiAs type of structure which appear to exhibit intrinsic semiconducting properties. MnTe has a high resistivity (~1 to 5 ohm-cm.), a negative temperature coefficient of resistance in the paramagnetic range above about 325° K., and a large thermoelectric power (Squire 1939; Uchida *et al.* 1956; see also Palmer 1954). FeS has a fairly high resistivity (up to ~1 ohm-cm.) and a negative temperature coefficient of resistance (Kamigaichi *et al.* 1956), and we have also been informed that CrSe appears to behave as a semiconductor having a negative temperature coefficient of resistance and a resistivity of ~1/40 ohm-cm. (F. Hulliger, private communication). These characteristics have since been confirmed in our laboratory on a sample with a resistivity of 0.05 ohm-cm. The magnetic moments of the transition metals in these substances have frequently been taken as indicating predominantly ionic properties but the large thermoelectric power (~550 μv./° C. at 100° C.) of MnTe found by Uchida *et al.* leaves no doubt that the conductivity is electronic (cf. Joffé 1956, quoting Justi 1948 and Meisner 1955).

With one possible exception, all of the other compounds with the nickel arsenide structure whose electrical properties have been examined appear to be metallic conductors.

III. THE VALENCE STATE OF THE TRANSITION METAL

The valence states of, say, the Mn and Te atoms in MnTe must satisfy the requirement that the valence band contains an even number of electrons per unit cell, the magnetic requirement of five unpaired electrons on each Mn atom (*vide infra*), the requirement that the bonding is predominantly covalent, and also the particular coordination of the Mn and Te atoms in the unit cell.

If we postulate the following valence states for MnTe and similar compounds, not only are these requirements satisfied, but we are led straightway to a qualitative explanation of the electrical properties of compounds with the nickel arsenide structure.

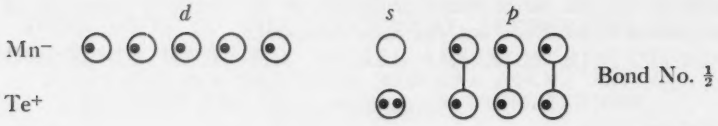

(1) First we may note that the resonating p^3 bonds (bond number $\frac{1}{2}$) satisfy the octahedral and trigonal-prismatic coordination of the Mn and Te atoms respectively and furthermore that a state which does not involve formal electron transfer but uses resonating linear p^2 bonds is excluded by the spatial distribution of Mn atoms about Te.

(2) These valence states lead to five unpaired electron spins on each Mn atom, which is consistent with a magnetic moment of about 6 μ_B found for the Mn atoms in MnTe by Serres (1947), although Uchida *et al.* (1956) found a rather lower number of 5.10 μ_B. These states predict four unpaired electrons for the Cr atom in CrSe, which agrees with Haraldsen and Mehmed's (1938) conclusion that CrSe contains Cr^{2+} ions (the magnetic moment observed for the Cr atoms in stoichiometric CrSe was actually 4.6 μ_B). The expectation of four unpaired spins for the Fe atom in FeS is probably not inconsistent with the observations of Haraldsen (1941) carried out over a rather small temperature range in the paramagnetic region (i.e. above 320° C.).

(3) These magnetic measurements do not distinguish between covalent and ionic bonding, provided that the former does not involve the *d* electrons. However, the thermoelectric measurements of Uchida *et al.* (1956), already referred to, leave little doubt that the bonding in MnTe is predominantly covalent.

(4) The electrons in the *d* shell of the transition metal are not concerned in the chemical bonding (i.e. they exist in discrete states, usually referred to as the shell model, cf. Zener and Heikes 1956) and hence semiconductivity may occur in compounds having either odd or even numbers of *d*, *s*, and *p* electrons.

(5) With this bond scheme the conditions for semiconducting bonds (Mooser and Pearson 1956) are fulfilled as alternate atoms bonded together have a complete "octet" and the bonds run continuously throughout the crystal lattice.

(6) The final condition for the semiconducting bond—that there should be no metal–metal bonds—is satisfied in MnTe in which the axial ratio is equal to 1.62, in FeS where $c/a = 1.70$, and in CrSe where $c/a = 1.63$. When the transition metal atoms along the *c* axis approach each other too closely they interact with the formation of intermetallic bonds. That is to say a *d* band is formed instead of the discrete *d* states which exist at larger values of c/a, when the transition metal atoms have a greater separation. Metallic conduction then occurs owing to the formation of the *d* band while it is also possible that the *s* orbitals of the transition metal atoms play a part if these overlap. The value of c/a is a good criterion of the probability of metal–metal

bonding as changes in this ratio come largely from changes of c rather than of a. Present experience shows that we can expect semiconductivity in compounds of Cr, Mn, Fe, Co, and Ni, with the nickel arsenide structure provided that c/a is not much smaller than the ideal ratio 1.63;* when it is much less, say 1.50, metallic conduction certainly occurs.

(7) A further requirement for there to be no metallic conductivity is that the composition should not extend towards the transition metal-rich side of the equiatomic ratio, for the presence of metal atoms in the bipyramidal holes leads to bonds between the transition metal atoms.

(8) This bond scheme should not compromise explanations of antiferromagnetism based on superexchange in these compounds if the electrons in s states of the chalcogenide atom are available for this purpose, while ferromagnetism could arise either through direct or indirect exchange mechanisms. Heikes (1955) has discussed conduction mechanisms in these compounds maintaining that a ferromagnetic alignment of the d shell spins leads to metallic conduction and an antiferromagnetic alignment should lead to semiconducting properties. Our bond scheme can, however, lead to semiconducting properties without the compound being in an antiferromagnetic state.

The conclusion outlined in 4 and 6 above, that electrons in the d shell of the transition metal remain independent of the bonding process, and do not lead to metallic conduction provided that the transition metal atoms do not approach each other too closely, is supported by the behavior of the intrinsic semiconductor chalcopyrite, $FeCuS_2$, already mentioned. There are many compounds with the chalcopyrite type of structure which do not contain transition metals and in which the chemical bonding is well understood, so it is known that in $CuFeS_2$, iron contributes three valence electrons and forms sp^3 bonds with the neighboring sulphur atoms. The valence band so formed is independent of the five unpaired electrons in the d shell of iron.

IV. DISCUSSION OF ELECTRICAL PROPERTIES

The suggested valence states for these compounds with the nickel arsenide structure indicate why MnTe (c/a = 1.62) and FeS (c/a = 1.70) have semiconducting properties, and why CrSe (c/a = 1.63) probably has. They suggest an explanation for the surprising difference between the antiferromagnetic semiconductor CrSe and the ferromagnetic, metallic CrTe (c/a = 1.54), for in the latter compound with the smaller axial ratio the chromium atoms are close enough for the formation of a d band (direct metal–metal bonds), while in the former the d electrons of the chromium atoms follow the shell model of discrete states. They indicate why CoSe (c/a = 1.46) and β-NiSe (c/a = 1.46) are metallic conductors while FeS is a semiconductor. Furthermore, they indicate why none of the compounds of Cr, Mn, Fe, Co, or Ni with Sb or Bi are semiconductors, because in all

*Mr. G. Fischer has pointed out that the ratio should depend also on the size of the d shell which increases to a maximum with five unpaired electrons in manganese.

of these compounds the axial ratios lie below the value $c/a = 1.43$ and interaction takes place between the d shells of the transition metal atoms.*

Surveying compounds with the NiAs structure whose electrical properties do not yet appear to have been measured, we see that CrS ($c/a = 1.66$) and FeSe ($c/a = 1.63_8$) should exhibit semiconducting properties. Compounds of vanadium and titanium (TiS, VS, TiSe, VSe, TiTe, VP, β-TiAs) and NbS also have axial ratios greater than $c/a = 1.63$; however, in the case of these substances (and possibly also in the case of chromium compounds) it is by no means certain, because of the fewer valence electrons which they contain, that the valence states will be similar to that proposed for MnTe above. The bonds formed by the transition metals may involve d orbitals and therefore an investigation of their electrical and magnetic properties will be awaited with some interest.

It is also interesting to note that the majority of the NiAs phases which are metallic conductors and the metallic phases with the hexagonal tungsten carbide structure have c/a values that agree fairly well with the calculated c/a values taken as a function of r_B/r_A (Schönberg 1954), where r_A is the radius of the transition metal atom, r_B the radius of the non-metal or metalloid atom, and c/a_{calc} is given by

$$4r_A/\sqrt{3r_B(r_B+2r_A)}.$$

However, in the compounds which are known or predicted semiconductors and in the chalcogenides of Ti, V, and Nb, the observed and calculated c/a values do not agree, indicating a difference in the chemical bonding of these substances and of the remaining nickel arsenide-type phases. This difference is presumably the absence of any direct intermetallic bonding in the compounds having $c/a \geqslant 1.6$, which we have discussed.

APPENDIX

The filled valence band of an intrinsic semiconductor is equivalent to a filled Brillouin zone. As there have been some diverse statements in the literature generally on the selection of Brillouin zones for intermediate compounds and in particular on a zone for the NiAs structure (Makarov 1943), and furthermore as the influence of a variable axial ratio is of some interest in compounds which are intrinsic semiconductors, we append the following remarks on the problem, which was resolved in discussion with Dr. R. G. Chambers, Mr. G. Fischer, and others, to whom I am grateful.

Each successive Brillouin zone of a crystal structure must contain an integral even number of electronic states, and the volume occupied in k-space by the nth zone must exactly cover all of the faces of the $(n-1)$th zone, as three zones may only be coincident at a point or along a line in k-space and not over a plane. It therefore follows that the integral number of states in a

*We have heard that a sintered CrSb sample has been prepared which showed a negative temperature coefficient of resistance. Fused samples which we have prepared were metallic. Furthermore, Haraldsen *et al.* (1949) reported the phase to be homogeneous only on the metal-rich side of the stoichiometric composition ($CrSb_{0.96}$ to $CrSb_{0.99}$). We would not, therefore, expect it to be a semiconductor.

given Brillouin zone is independent of the unit cell volume and of the ratios of the lengths of the unit cell edges, although the relative axial ratios may be important in determining the size of the energy gap (if one exists) between the nth and $(n-1)$th zones.

REFERENCES

AUSTIN, I. G., GOODMAN, C. H. L., and PENGELLY, A. E. 1956. J. Electrochem. Soc. **103**' 609.

HARALDSEN, H. 1941. Z. anorg. u. allgem. Chem. **246**, 169, 195.

HARALDSEN, H. and MEHMED, F. 1938. Z. anorg. u. allgem. Chem. **239**, 369.

HARALDSEN, H., ROSENQVIST, T., and GRØNVOLD, F. 1949. Arch. Math. Naturvidenskab. **50**, No. 4, 95.

HEIKES, R. R. 1955. Phys. Rev. **99**, 1232.

JOFFÉ, A. F. 1956. Semiconductors for thermocouples (Izdatel'stvo Akademii Nauk S.S.S.R., Moscow, Leningrad).

JUSTI, E. 1948. Leitfähigkeit und Leitungsmechanismus fester Stoffe (Vandenhoeck and Ruprecht, Göttingen), p. 88.

KAMIGAICHI, T., HIHARA, T., TAZAKI, H., and HIRAHARA, E. 1956. J. Phys. Soc. Japan, **11**, 606.

MAKAROV, E. S. 1943. Doklady Akad. Nauk S.S.S.R. **40**, 191.

MOOSER, E. and PEARSON, W. B. 1956. J. Electronics, **1**, 629.

——— 1957. J. Chem. Phys. **26**, 893.

PALMER, W. 1954. J. Appl. Phys. **25**, 125.

SCHÖNBERG, N. 1954. Acta Met. **2**, 427.

SERRES, A. 1947. J. phys. radium, **8**, 146.

SQUIRE, C. F. 1939. Phys. Rev. **56**, 960.

UCHIDA, E., KONDOH, H., and FUKUOKA, N. 1956. J. Phys. Soc. Japan, **11**, 27.

ZENER, C. and HEIKES, R. R. 1956. Private communication: Scientific paper 8-0628-P9 Westinghouse Research Laboratories.

LOW TEMPERATURE RESISTIVITY OF TRANSITION ELEMENTS: VANADIUM, NIOBIUM, AND HAFNIUM[1]

G. K. WHITE AND S. B. WOODS

ABSTRACT

Measurements of the thermal conductivity from 2° to 90° K. and electrical conductivity from 2° to 300° K. are reported for vanadium, niobium, and hafnium. Although the vanadium and hafnium are not as pure as we might wish, measurements on these metals and on niobium allow a tabulation of the "ideal" electrical resistivity due to thermal scattering for these elements from 300° K. down to about 20° K. Ice-point values of the "ideal" electrical resistivity are 18.3 μΩ-cm. for vanadium, 13.5 μΩ-cm. for niobium, and 29.4 μΩ-cm. for hafnium. Values for the "ideal" thermal resistivity of vanadium and niobium are deduced from the experimental results although for vanadium and more particularly for hafnium, higher purity specimens are required before a very reliable study of "ideal" thermal resistivity can be made. For the highly ductile pure niobium, the superconducting transition temperature, as determined from electrical resistance, appears to be close to 9.2° K.

INTRODUCTION

In a number of recent papers we have presented experimental data on the electrical and thermal resistivity of some transition elements at temperatures between 1° and 300° K. (White and Woods 1957*a*, *b*, *c*; and also see Kemp *et al.* 1955, 1956, 1957). These data are intended to fill gaps in our knowledge of the low temperature resistance of these elements and to allow possible assessment of the importance of different electron scattering mechanisms, e.g. *s*- to *d*-band scattering of electrons by thermal vibrations and the possible influence of electron–electron interaction at very low temperatures (see, for example, Kemp *et al.* (1955) and White and Woods (1957*a*) for more detailed discussion of these aspects).

The present paper deals with results of thermal resistivity measurements from 2° to 90° K. and electrical resistivity measurements from 2° to 300° K. on the elements vanadium, niobium (or columbium), and hafnium. As far as we are aware, previous low temperature thermal measurements have been confined to experiments on one sample of vanadium from 2° to 20° K. by Rosenberg (1955), and on one niobium specimen from 2° to 90° K., also by Rosenberg (1955). Other data on the heat conductivity of niobium at temperatures below the superconducting transition ($T_c \simeq 9°$ K.) have been reported by Mendelssohn and his collaborators (see compilation by Powell and Blanpied (1954)). While being very useful from other points of view, such data below the superconducting transition do not give much information about the interaction between the conduction electrons and the thermal vibrations, in which we are interested. We have been fortunate in obtaining specimens of vanadium and niobium of rather higher purity—although by no means as pure as we would desire— than those used by Rosenberg and this has enabled

[1]Manuscript received April 3, 1957.
Contribution from the Division of Pure Physics, National Research Council, Ottawa, Canada.
Issued as N.R.C. No. 4415.

us to separate the two electron scattering processes, due to impurities and thermal vibrations, in a rather more reliable manner.

There also appears to be a similar dearth of experimental information on electrical resistance of these elements at low temperatures. Many years ago Meissner and Voigt (1930) determined some resistance values on a rather impure vanadium specimen, and de Haas and Voogd (1928) measured the electrical resistance of hafnium at temperatures from 1° to 90° K.

EXPERIMENTAL DETAILS AND SPECIMENS

The specimens, generally in the form of rods about 6 to 7 cm. long, were mounted in a cryostat (White and Woods 1955) in which the thermal resistivity was determined with the aid of helium-filled gas thermometers attached to a butyl phthalate oil manometer and the electrical resistivity by a galvanometer–amplifier.

Some details of the source and purity of the specimens are given in Table I, together with their approximate diameters and physical condition.

TABLE I

DETAILS OF SPECIMENS

Specimen	Source	Specimen diameter (mm.)	Physical condition	ρ_0 ($\mu\Omega$-cm.)	$10^3\rho_0/\rho_{295}$	W_0T (cm. deg.^{2}w.$^{-1}$)	10^9L_0 (w-Ω deg.$^{-2}$)
V 1	A. D. Mackay Inc. (N.Y.) 99.7% pure 0.0005 in. foil	*	As received	2.97	129	—	—
V 2	Electrometallurgical Company ~99.9% pure rod	3.55	As received	3.10	135	120.5	2.57
V 4	As for V 2	3.55	Annealed 1300° C. *in vacuo*	4.83	196	169	2.85
Nb 1	A. D. Mackay Inc. (N.Y.)	3×1.5	As received	2.16$_5$	156	—	—
Nb 2	Johnson-Matthey & Mallory Ltd. 0.3% Ta	4.7	As received	~8.0	~350	—	—
Nb	Fansteel Metallurgical Corp. (ductile) >99.9%	0.5	Drawn and annealed†	0.45	30	—	—
Nb 5	As Nb 3	1.59	Drawn	0.47$_5$	31.7	19.0$_5$	2.49
Hf 1	Foote Mineral Co. 0.5–1% Zr	5×1.5$_2$	As received	4.23	116.5	122	3.47

*V 1 was formed by rolling some 0.0005 in. thick foil into a cylindrical coil, of which the effective cross-sectional area was determined by weighing to be 0.0037 cm.^{2}

†Nb 3 was annealed by supporting the wire in a high vacuum and passing an electrical current through it, first outgassing the wire and later raising it almost to the melting temperature.

The methods of mounting the specimens, i.e. attaching current and potential leads (thermal and electrical), varied.

V 1, made by rolling thin foil into a "rod" about 1½ inches long, had copper leads spot-welded to it and only its electrical resistance was determined.

V 2 and an annealed rod, V 3 (for which measurements were not completed owing to faulty connection of the leads), were copper plated near their ends and copper leads were soldered with Woods' alloy to the plated surface. This method of mounting seemed to cause rather unreproducible results because

the plating did not bond adequately to the vanadium. Hence for V 4 four small copper sleeves were placed on the rod and tightened by means of screws, good contact being ensured by a thin layer of silver-conducting paste ("Silver-Print" from General Cement Manufacturing Co.) between each sleeve and the rod; copper leads had previously been soldered to the sleeves.

On three of the niobium specimens, Nb 1, Nb 2, and Nb 3, electrical resistance measurements only were made. The first two of these were mounted as received, by copper plating areas near the ends and then soldering copper leads to the plating with Woods' metal. Nb 3 was drawn from a rod of ductile niobium (Fansteel Corporation) and annealed and then mounted in an alumina tube with four small brass screws in pressure contact with points near the extremities. Nb 5, on which thermal conductivity measurements also were made, was platinized over a small region at each end and copper leads were soldered to the platinum coating.

We were able to copper plate the ends of the hafnium specimen* by first electropolishing the surface to remove the oxide layer; copper leads were then attached with a non-superconducting Zn–Cd solder.

RESULTS

In Figs. 1 and 2 are shown the results of thermal conductivity measurements together with data from Rosenberg (1955) on vanadium and niobium. Our results on V 3 are not given as they are similar in pattern to those on V 4, but showed some lack of reproducibility owing to a faulty thermal contact between the leads and the specimen.

As might be expected for metals in which heat is transported predominantly by the conduction electrons the thermal conductivity, λ, is proportional to T at low temperatures (except in the superconducting state where λ decreases markedly below $T = T_c$), where impurity scattering of the electrons is dominant. If we define $W_0 = 1/\lambda_0$ to be the thermal resistivity due to scattering of the conduction electrons by impurities or static imperfections and ρ_0 to be the "residual" electrical resistivity produced by the same mechanism, then at these very low temperatures, where the resistivity due to scattering of the electrons by thermal vibrations is much less than the impurity resistivity, that is $W_t \ll W_0$ and $\rho_t \ll \rho_0$, it is expected that the Weidemann–Franz–Lorenz law should be valid, i.e.

$$\rho_0\lambda_0/T = \rho_0/W_0T = L_0,$$

where L_0 has a theoretical value of 2.45×10^{-8} w-Ω deg.$^{-2}$. The experimental values of W_0T, ρ_0, and L_0 given in Table I indicate that this is true for the niobium specimen. For V 4, L_0 is somewhat greater suggesting that impurities reduce the conductivity due to the free electrons to such an extent that lattice thermal conductivity becomes significant. In the case of hafnium, for which experimentally we find $L_0 \simeq 3.47\times10^{-8}$, it appears probable that lattice conductivity is quite appreciable.

*This hafnium specimen was cut from a hafnium "starter wire" supplied by Foote Mineral Company, through the kindness of the United States Atomic Energy Commission. We are very grateful to the Pittsburgh Area Office of U.S.A.E.C. for facilitating this gift.

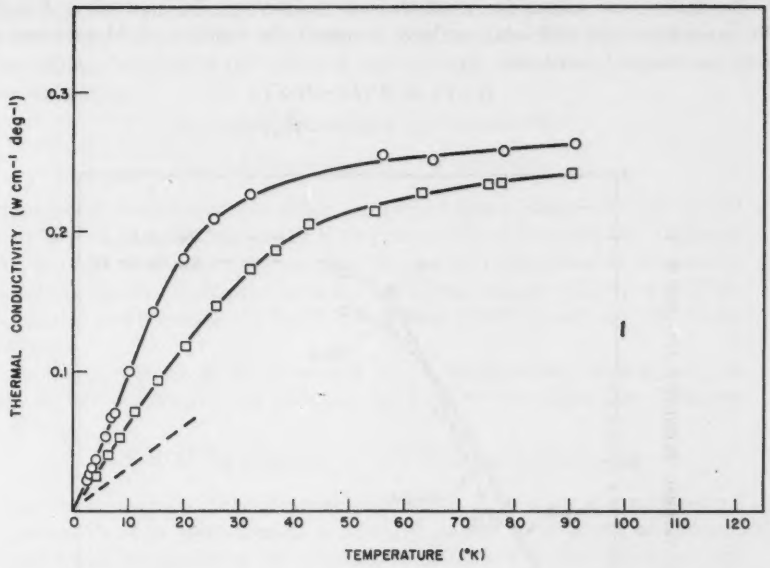

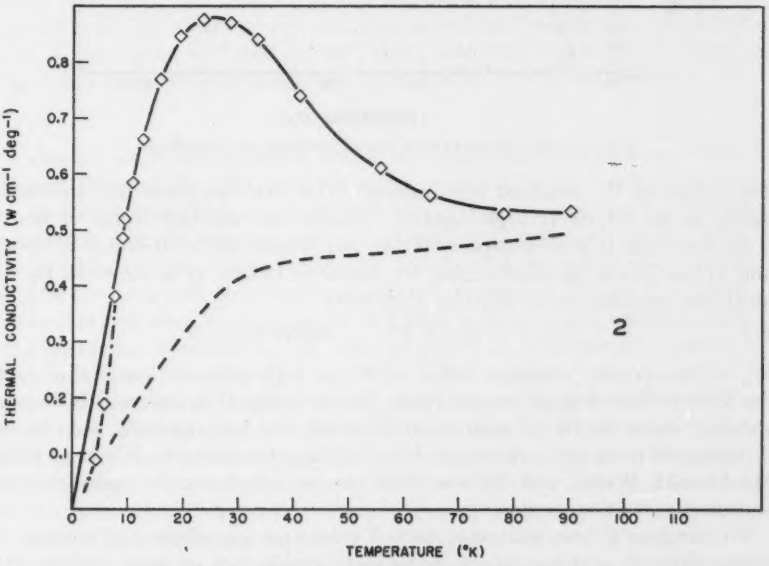

FIG. 1. Thermal conductivity of vanadium and hafnium.
—— ○ —— Hf 1 —— □ —— V 4 — — — Vanadium (Rosenberg 1955)

FIG. 2. Thermal conductivity of niobium.
——◇—— Nb 5 (normal) —·—◇—·— Nb 5 (superconducting)
— — — — Rosenberg (1955)

To deduce the values for ideal thermal resistivity, W_i, plotted in Fig. 3 for vanadium and niobium, we have assumed the validity of Matthiessen's rule for thermal resistivity, i.e.

$$W_i(T) = W(T) - W_0(T)$$
$$= 1/\lambda(T) - \overline{W_0 T}/T.$$

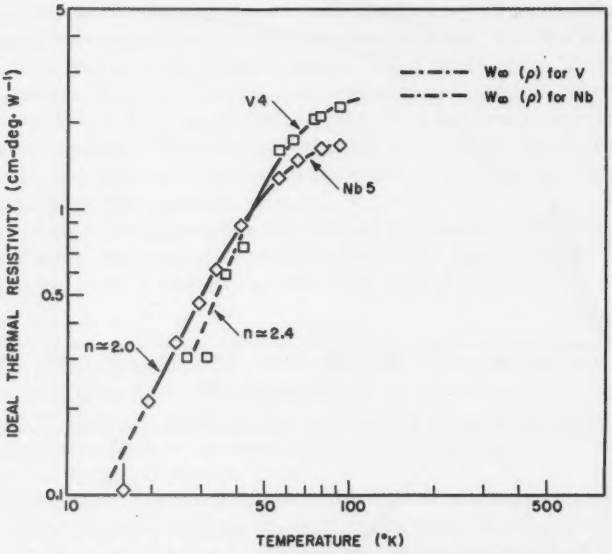

FIG. 3. Ideal thermal resistivity of niobium and vanadium.

The values of W_i obtained below about 30° K. for vanadium are unreliable owing to the relatively high impurity content, i.e. the high value of W_0.

As discussed in earlier papers (White and Woods 1957*a*; Kemp *et al.* 1955) and in the recent detailed review by Klemens (1956), it is expected for an ideal free electron metal that for $T \leqslant \theta/10$

$$W_i = C.W_\infty(T/\theta)^n, \qquad \text{where } n = 2.0; \tag{1}$$

W_∞ is the sensibly constant value of W_i at high temperatures, i.e. $T \geqslant \theta$, the Debye characteristic temperature. Theoretically C is expected to have a value of about 60–70 for such an ideal metal, but has generally been found experimentally to be in the range 10 to 20 (see, for example, Klemens 1956; MacDonald, White, and Woods 1956) for the alkali metals, noble metals, and most transition metals.

To compute C from the experimental values for vanadium and niobium is rather difficult, as there appears to be no available data on heat conductivity near room temperature from which W_∞ might be calculated. However a good estimate of W_∞ may be obtained by applying the Wiedemann–Franz–Lorenz law in the form

$$\rho_i/W_i T = 2.45 \times 10^{-8} \text{ w-}\Omega \text{ deg.}^{-2}$$

to the data for the electrical resistivity at room temperature. Our electrical resistance data indicate that ρ_i at 295° K. has the value 19.9×10^{-6} ohm-cm. for vanadium, and 14.5×10^{-6} ohm-cm. for niobium; thus using the equation above we deduce

$$W_\infty = 2.75 \text{ cm-deg. w.}^{-1} \text{ for vanadium}$$

and

$$W_\infty = 2.00 \text{ cm-deg. w.}^{-1} \text{ for niobium.}$$

In the case of vanadium, this value appears at least consistent with values for λ at 100° C. and 500° C. quoted in the "Rare Metals Handbook" (Hampel 1956). In order to deduce C in equation (1) we must also know θ; the specific heat data of Brown, Zemansky, and Boorse (1952) suggest that $\theta_D \simeq 250°$ K. for niobium, and the data of Clusius and Buhler (1955) give $\theta_D \simeq 390°$ K. for vanadium.

Now taking values of W_i from Fig. 3, at temperatures $T \simeq \theta_D/10$, we obtain $W_i/T^2 = 5.5\times10^{-4}$ for niobium and 4.7×10^{-4} for vanadium. Thus we find finally:

$$C \simeq 17 \text{ for niobium,} \qquad C \simeq 25 \text{ for vanadium.}$$

From the measurements of electrical resistivity, ρ, we have also endeavored to separate the two components: a constant ρ_0 due to impurity scattering, and $\rho_i(T)$ due to scattering by thermal vibrations. For the vanadium and hafnium specimens the experimentally measured ρ is apparently constant below about 8° K.; values of the impurity or residual resistivity, $\rho_0 = \rho$ for $T \leqslant 8°$ K., are given in Table I. The "ideal" electrical resistivity, ρ_i, shown in Fig. 4 has been obtained assuming Matthiessen's rule to be valid, i.e.

$$\rho_i = \rho - \rho_0.$$

For a simple monovalent metal in which the conduction electrons are "free" we expect theoretically that $\rho_i \propto T^m$ where $m \simeq 5.0$ for $T < \theta/10$; this has been generally confirmed experimentally for copper, silver, gold, and the alkali metals. For the transition metals investigated previously m has been found to have various values between 3 and 5, with an indication in some very pure elements (where ρ_i can be accurately studied as low as $T \sim \theta/50$) that the index m may decrease again to about 2 at very low temperatures; such a quadratic dependence has been proposed as evidence of electron–electron interaction.

In the three elements discussed in this paper, the purity has not been such as to allow a detailed study of the ideal resistivity at temperatures below $\theta/20$. In fact for hafnium and vanadium, ρ_0 is already becoming the dominant part of the resistance at temperatures as high as $\theta/5$ so that if small departures from Matthiessen's rule do occur, we cannot expect to obtain truly representative values of ρ_i in the range near say $\theta/10$. With niobium, in particular Nb 3 and Nb 5, the purity is much better but the high temperature of the superconducting transition—we find $T_c \simeq 9.25\pm0.03°$ K.—makes it impossible to obtain directly a value of ρ_0. From a detailed series of measurements of electrical resistance of Nb 3 between 9° and 17° K., it was apparent that the resistance was still decreasing quite markedly with decreasing temperature

as the temperature was reduced below 10° K. To obtain a value for ρ_0, various algebraic polynomials were fitted to the values of $\rho(T)$. It was found that expressions of both the types $A+BT^2+CT^5$ and $A+BT^3$ represented the experimental values quite well, the values required for A in the alternative expressions being not very different. However the form of the $\rho_i(T)$ curve at temperatures below 12° or 15° K. does depend quite markedly on the particular value of A that is adopted. Therefore no definite conclusion can be drawn regarding the temperature dependence of ρ_i below about 12° K. without more certain knowledge of ρ_0. Nor can this knowledge be achieved with sufficient certainty by applying a magnetic field to restore niobium to the non-superconducting state at 2° or 3° K., as any extrapolation of magneto-resistance data to zero magnetic field is bound to give questionable values of ρ_0.

No more detailed analysis of the thermal conductivity of hafnium has been made, as it is apparent that assumptions of dubious validity would have to be made concerning the temperature dependence of the lattice thermal conductivity, or of the ideal electronic thermal resistivity, before a separation of conductivity or resistivity into various components could be made.

DISCUSSION

It is apparent from the rather low value found for the index m (Fig. 4) in

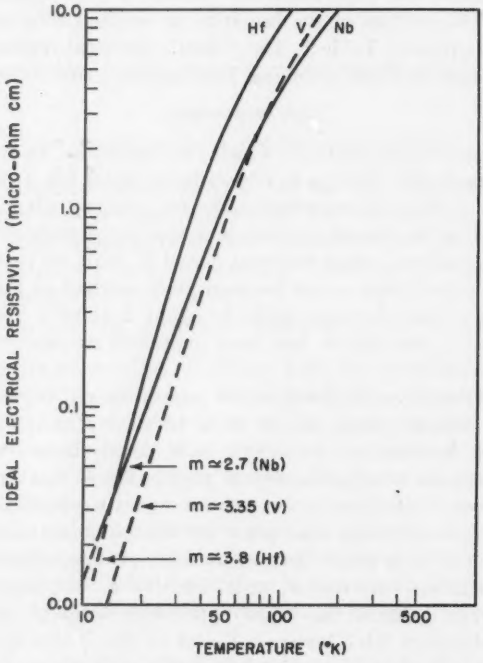

FIG. 4. Ideal electrical resistivity of vanadium, niobium, and hafnium.

the expression $\rho_i \propto T^m$ at temperatures $T < \theta/10$ that scattering of electrons from the *s*- to the *d*-band by the lattice vibrations may be important in the transition elements vanadium, niobium, and hafnium. If *s–d* transitions are still the dominant cause of the ideal electrical resistance at low temperatures, as Mott (1935, 1936) suggested is the case at room temperature, then we might expect (Wilson 1938) $\rho_i \propto T^3$. On the other hand it might be expected that at sufficiently low temperatures *s–d* transitions should become very infrequent because of the small wave number of the phonons with which the electrons interact; if this is so, normal *s–s* transitions would produce an electrical resistance varying as T^5, with the possible addition of a quadratic term representing electron–electron interactions. The elements discussed in this paper do not seem to be of sufficiently high purity to allow detailed conclusions to be drawn regarding $\rho_i(T)$ at temperatures $T < \theta/10$.

Nevertheless a set of values for ρ_i for each of the three elements has been compiled from the experimental data and is given in Table II. Although these

TABLE II

VALUES OF "IDEAL" ELECTRICAL RESISTIVITY IN MICRO-OHM-CM.

T, ° K.	V	Nb	Hf
θ	26.6* (390° K.)	12.3 (250° K.)	21.6 (210° K.)
295	19.9	14.5	32.1
273	18.3	13.5	29.4
250	16.6_5	12.3	26.5
200	12.9_5	9.8	20.4
150	8.7	7.0	14.3
100	4.2_5	3.9_0	8.2
75	2.3	2.3_6	5.2
50	0.7_4	0.9_7	2.3
40	0.38	0.5_6	1.3
30	0.1_4	0.2_5	0.5_6
20	0.03_8	0.08_4	0.13
15	0.01_4	0.03_8	0.04
10	—	—	—
Index m for $T<\theta/10$	3.3_5	2.7	3.8

*Extrapolated using data of Potter (1941).

may be regarded as somewhat tentative below 30° K., Matthiessen's rule not being strictly valid, they may represent a useful addition to our knowledge of the behavior of electrical resistance. The room temperature values of electrical resistivity seem reasonably consistent with those quoted by Adenstedt (1952) for hafnium and Potter (1951) for vanadium, although the value of about 13.1×10^{-6} ohm-cm. quoted for niobium in many physical tables seems rather low compared with our value of 14.5×10^{-6} for the "ideal" resistivity.

We wish to draw attention to the superconducting transition temperature of niobium for which our resistive measurements give 9.25° K. Our belief that this value of T_c is perhaps more representative for pure niobium than a value of 8.70° K. (see review by Eisenstein 1954) seems confirmed by Preston-Thomas (private communication, unpublished), who has found $T_c \simeq 9.2°$ K. for ductile annealed niobium by both magnetic and resistive measurements. The agreement between magnetic and resistive values for T_c obtained by

Preston-Thomas, and a considerably lower value of the critical field slope, dH_c/dT, contrast with earlier results (Jackson and Preston-Thomas 1950) on unannealed specimens.

It is hoped that in the not too distant future much purer samples of elements such as vanadium and hafnium may be available for further investigation of their transport properties at low temperatures.

We wish to express our thanks to Messrs. J. Broome and F. Richardson for their technical assistance, to Mr. F. Anglin for helping with much of the experimental work, and to Drs. D. K. C. MacDonald and Z. S. Basinski for helpful discussions at various times.

REFERENCES

ADENSTEDT, H. K. 1952. Trans. Am. Soc. Metals, **44**, 949.
BROWN, A., ZEMANSKY, N. W., and BOORSE, H. A. 1952. Phys. Rev. **86**, 134.
CLUSIUS, K. and BUHLER, H. H. 1955. Z. Naturforsch. **10a**, 930.
EISENSTEIN, J. 1954. Revs. Mod. Phys. **26**, 277.
DE HAAS, W. J. and VOOGD, J. 1928. Leiden Comm. 194c.
HAMPEL, C. A. 1956. Rare metals handbook (Reinhold Publishing Corporation, New York).
JACKSON, L. C. and PRESTON-THOMAS, H. 1950. Phil. Mag. **41**, 1284.
KEMP, W. R. G., KLEMENS, P. G., SREEDHAR, A. K., and WHITE, G. K. 1955. Phil. Mag. **46**, 811.
KEMP, W. R. G., KLEMENS, P. G., TAINSH, R. J., and WHITE, G. K. 1957. Acta Met. **5**, 303.
KEMP, W. R. G., KLEMENS, P. G., and WHITE, G. K. 1956. Australian J. Phys. **9**, 180.
KLEMENS, P. G. 1956. Handb. der Physik, **14**, 198.
MACDONALD, D. K. C., WHITE, G. K., and WOODS, S. B. 1956. Proc. Roy. Soc. A, **235**, 358.
MEISSNER, W. and VOIGT, B. 1930. Ann. Physik, **7**, 892.
MOTT, N. F. 1935. Proc. Phys. Soc. **47**, 571.
——— 1936. Proc. Roy. Soc. A, **153**, 699.
POTTER, M. H. 1941. Proc. Phys. Soc. **53**, 695.
POWELL, R. L. and BLANPIED, W. A. 1954. N.B.S. Circular 556 (U.S. Govt. Printing Office, Washington, D.C.).
ROSENBERG, H. M. 1955. Trans. Roy. Soc. A, **247**, 441.
WHITE, G. K. and WOODS, S. B. 1955. Can. J. Phys. **33**, 58.
——— 1957*a*. Can. J. Phys. **35**, 248.
——— 1957*b*. Can. J. Phys. **35**, 346.
——— 1957*c*. Can. J. Phys. **35**, 656.
WILSON, A. H. 1938. Proc. Roy. Soc. A, **167**, 580.

THE EMISSION SPECTRUM OF THE PH^+ MOLECULE[1]

N. A. NARASIMHAM[2]

ABSTRACT

A system of three red degraded bands at 3854, 4228, and 3567 Å has been obtained in emission from a hollow cathode discharge through helium containing a little phosphorus vapor and hydrogen. Rotational analyses of the bands show that they are the 0–0, 0–1, and 1–0 bands of a $^2\Delta$—$^2\Pi$ transition of the PH^+ molecule. The $^2\Delta$ state is regular with small spin splitting (case *b*) while the $^2\Pi$ state is regular with large spin splitting (case *a*). For $v = 0$, the F_1 levels of the $^2\Delta$ state with $N \geqslant 13$ and the F_2 levels with $N \geqslant 15$ are predissociated. Also the lines arising from the F_1 levels of the $^2\Delta$ state with $v = 1$ are found to be extremely weak compared to those arising from the F_2 levels. Vibrational and rotational constants have been determined and the dissociation energy has been found to be 3.06 ± 0.25 ev.

I. INTRODUCTION

Prior to the present investigation, no spectrum of the PH^+ molecule was known. PH^+ is isoelectronic with SiH, i.e., has an electronic structure similar to that of the hydrides of the carbon group. It may therefore be expected to have a strong band system around 4000 Å corresponding to the $^2\Delta$—$^2\Pi$ transitions in the CH-type molecules (Mulliken 1932). In an investigation of the spectrum of P_2^+ (Narasimham 1956), a band was observed at 3854 Å which had the appearance of a hydride band. A systematic search produced two more bands belonging to the same system. Vibrational and rotational analyses of these bands showed that they were the 0–0, 0–1, and 1–0 bands of the expected $^2\Delta$—$^2\Pi$ transition of the PH^+ molecule. The method of excitation and the results of the rotational analysis of the bands are presented in the following.

II. EXPERIMENTAL

The spectrum was excited in a hollow cathode discharge through helium containing a little phosphorus vapor and hydrogen. The discharge tube and a side bulb containing phosphorus were enclosed in a water bath at a temperature of about 50° C. A continuous flow of helium at 2–3 mm. of mercury was maintained through the discharge tube. The current through the discharge was about 400 ma. The spectrum was photographed on a 35 ft. concave grating spectrograph in the second order at a dispersion of 0.35 Å/mm. Besides the new bands of PH^+, the stronger band systems of PH, AlH, and AlH^+ were emitted with considerable intensity in the spectrum. The rotational structure of the 4228 Å band was partly overlapped by the 0–0 band of the $^1\Pi$—$^1\Sigma$ transition of AlH. A search for other new systems of PH and PH^+ in the spectral region 2000–8000 Å, using the same source, proved unsuccessful.

[1]Manuscript received May 6, 1957.
Contribution from the Division of Pure Physics, National Research Council, Ottawa, Canada.
Issued as N.R.C. No. 4417.
[2]National Research Laboratories Postdoctorate Fellow.

III. ANALYSIS OF THE BANDS

The rotational analysis of the PH^+ band system is essentially similar to that of the $^2\Delta$—$^2\Pi$ system of the SiH molecule given in detail by Rochester (1936). The 0–0 band is reproduced in Fig. 2. An energy level diagram for a $^2\Delta$—$^2\Pi$ transition is given in Fig. 1. It is assumed that the $^2\Delta$ state belongs to case *b* and the $^2\Pi$ state to case *a*. The validity of these assumptions will be evident in the following analysis of the bands. As can be seen from Fig. 1, there are 24 branches which form close pairs of Λ-doublets. The expected first lines of the branches are indicated in the figure. The observed wave numbers of the lines of the 0–0, 0–1, and 1–0 bands are given in Tables I, II, and III.

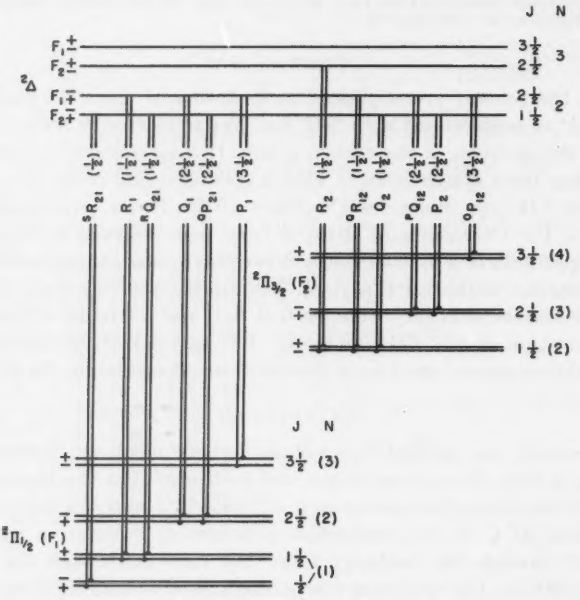

FIG. 1. The energy level diagram of a $^2\Delta$ (case *b*)—$^2\Pi$ (case *a*) transition. The first lines of the 24 branches are indicated in the diagram.

1. $^2\Delta$ *State*

(*a*) *Determination of* B_v *and* D_v

The rotational terms of a doublet state are given by the modified Hill–Van Vleck expression (Mulliken and Christy 1931)

$$F(J) = B_v[(J+\tfrac{1}{2})^2-\Lambda^2\pm\{(J+\tfrac{1}{2})^2- Y(Y-4)\Lambda^2\}^{\frac{1}{2}}] - D_vJ^2(J+1)^2+\tfrac{1}{2}\gamma[J(J+1)-N(N+1)-\tfrac{3}{4}] \quad (1)$$

where the + sign in ± refers to the F_2 levels and the − refers to the F_1 levels and $Y = A/B_v$, A being the coupling constant between S and Λ.

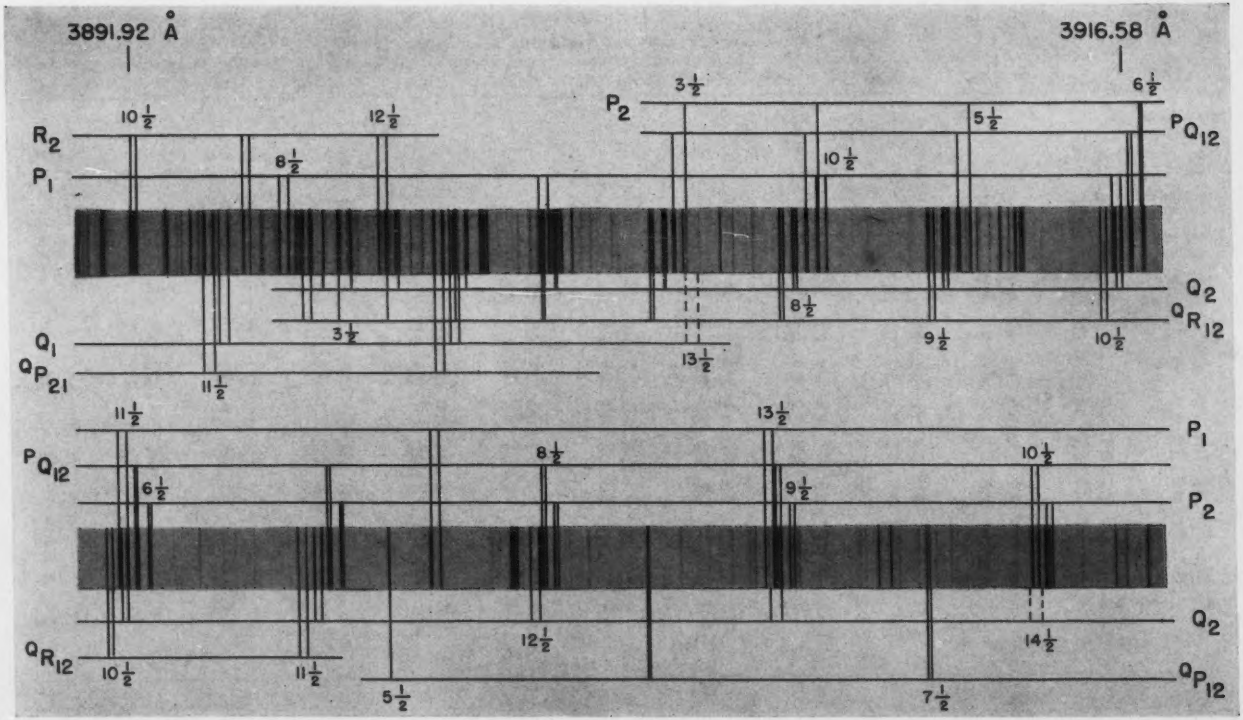

FIG. 2. The 0–0 band of the $^2\Delta$—$^2\Pi$ system of the PH^+ molecule. The predissociations in the Q_1 and Q_2 branches are indicated by broken leading lines.

TABLE I

WAVE NUMBERS OF THE LINES OF THE PH^+ BANDS, 0–0 BAND

J	$P_1(J)$	$Q_1(J)$	$R_1(J)$	$P_2(J)$	$Q_2(J)$	$R_2(J)$	${}^{O}P_{12}(J)$	${}^{P}Q_{12}(J)$	${}^{Q}R_{12}(J)$	${}^{Q}P_{21}(J)$	${}^{R}Q_{21}(J)$	${}^{S}R_{21}(J)$
½												25961.83
												61.61
1½											25937.53	79.78
											37.07	79.33
2½		25899.69	25941.36		25655.69	25711.53				25807.04	39.23	95.09
		99.01	40.67							96.33	38.55	94.43
3½	25842.96	84.60	40.23	25595.31	51.15	20.75		25597.47	25653.12	82.47	38.30	26007.88
	42.02	83.73	39.37							81.59	37.42	07.00
4½	11.56$_5$	67.27	36.76	73.64	43.20	26.48	25519.93	75.60$_5$	45.10	65.30	34.83	18.12
	10.50$_5$	66.21	35.70							64.24	33.78	17.06
5½	778.00	47.53	30.78	48.71	31.93	28.83	481.08$_5$	50.63	33.87	45.61	28.84	25.74
	76.78	46.32$_5$	29.58	48.53	31.75	28.64$_5$	80.91	50.43	33.69	44.39	27.65	24.54
6½	42.06*	25.37	22.30	20.41	17.27	27.69	39.06	22.36	19.29	23.43	20.28	30.71
	40.74	24.03	20.95	20.12$_5$	16.98$_5$	27.41	38.78$_5$	22.07	18.99	22.08	18.96	29.35
7½	†	00.71	11.19	488.82	599.24	23.05$_5$	393.90$_5$	490.84	01.35	798.69	09.09	32.88
	†	799.27	09.75	88.42	98.83	22.65$_5$	93.49	90.44	00.94	97.26	07.66	31.46
8½	662.96	73.47	897.39	54.04	77.86	14.91	45.65	56.14	580.07	71.36	895.18	32.22
	61.47	71.96	95.89	53.47	77.30	†	45.08	55.56$_5$	79.51	69.86	93.68	30.71
9½	19.67	43.60	80.79	16.00	53.08	03.35*	294.29	18.20	55.41	41.39	78.46	28.60
	18.14	42.06*	79.25	15.24$_5$	52.31	02.50	93.52	17.49	54.65	39.86	76.93	27.05
10½	573.81	†	61.30	374.65	24.87	687.95	39.80	376.98	27.32	†	58.85	21.92
	72.29	†	59.76	73.67	23.85	86.98	38.81$_5$	76.00	26.34$_5$	†	57.31	20.40
11½	25.28	675.58	38.83	30.05	493.17	69.03	182.21	32.49$_5$	495.78	673.13	36.23	12.07
	23.85*	74.05$_5$	37.30	28.83	91.95	67.81	81.03	31.27	94.54	71.60	34.73	10.54
12½	474.05	37.24		282.17	58.04$_5$	46.44	21.52	284.79			10.50$_5$	
	72.58$_5$	35.78		80.67	56.52	45.12*	20.03	83.25			09.06$_5$	
13½	20.00				19.35							
	18.62				17.50*							

*Overlapped lines.
†Overlapped but not measured.

TABLE II

WAVE NUMBERS OF THE LINES OF THE PH^+ BANDS, 0–1 BAND

J	$P_1(J)$	$Q_1(J)$	$R_1(J)$	$P_2(J)$	$Q_2(J)$	$R_2(J)$	${}^{O}P_{12}(J)$	${}^{P}Q_{12}(J)$	${}^{Q}R_{12}(J)$	${}^{Q}P_{21}(J)$	${}^{R}Q_{21}(J)$	${}^{S}R_{21}(J)$
½												23663.04$_5$
												62.84
1½												81.66
												81.21$_5$
2½		23602.74	23644.46							23599.99	23642.33	98.12
		02.07	43.80							†	41.66$_5$	97.46
3½	23547.50$_5$	589.21	44.92							87.07	42.97	712.50
	†	88.34	44.05							86.22	42.11	11.64
4½	18.17	73.90$_5$	43.48	23280.19	23349.78					71.94	41.56$_5$	24.78
	17.21	72.86	42.40							70.90$_5$	40.51	23.74
5½	487.15	56.67	40.01	58.07	41.33	23438.23			23343.31	54.78	38.07	34.81*
	85.94	55.49	38.81		41.17	38.04			43.12	53.55	36.86	33.71
6½	54.09	37.46	34.46		29.98	40.40			31.97	35.54	32.46	42.82
	52.87	36.15	33.14		29.70	40.13			31.71	34.11*	31.13	41.50
7½	†	16.21	26.78		15.71$_5$	39.57			17.83	14.26	24.67	48.43
	17.84	14.80	25.34		15.33	39.18			17.44	12.80	23.24	47.02
8½	382.30	492.88	16.84		298.60	35.71			00.80	490.77	14.63	51.67
	80.84	91.37	15.34		98.06	35.17			00.40*	89.27	13.12	50.16
9½	43.31	67.43*	04.56		78.59	28.86			280.77*	65.10*	02.24	52.42
	41.85	65.81	03.02		77.86	28.11			80.19	63.57	00.70	50.95*
10½	†	39.57	590.00		56.09	19.64*					†	†
	00.80	38.04*	88.34		55.43	18.78					585.89	48.97
11½		09.65*	72.68									
		07.90	71.16									
12½		377.53										
		75.68										

*Overlapped lines.
†Overlapped but not measured.

TABLE III

WAVE NUMBERS OF THE LINES OF THE PH^+ BANDS, 1–0 BAND

J	$P_1(J)$	$Q_1(J)$	$R_1(J)$	$P_2(J)$	$Q_2(J)$	$R_2(J)$	${}^{O}P_{12}(J)$	${}^{P}Q_{12}(J)$	${}^{Q}R_{12}(J)$	${}^{Q}P_{21}(J)$	${}^{R}Q_{21}(J)$	${}^{S}R_{21}(J)$
½												27356.81
												56.60
1½			27334.37								27332.54	72.03
			33.90								32.12	71.57
2½		27293.82	33.04								31.52	83.90
		93.14	32.40								30.86	83.21
3½	27237.08	76.27	28.63		27039.61	27105.26		26989.13	27041.54*	27274.75	27.13	92.40
	36.12*	75.44$_5$	27.74							73.87	26.26	91.53
4½	03.17	55.59	20.93		27.77	05.92		63.96	29.32	†	19.44$_5$	97.47*
	02.29*	54.54	19.87							53.05	18.35	96.47
5½	166.33	31.65$_5$	09.93$_5$	26933.25	11.40	02.31		34.75	12.98	30.13	08.32	99.22
	65.11	30.44	08.71	33.05	11.21	02.14		34.59	12.83	28.96	07.11	98.01
6½	26.24	04.48	295.50	899.84	26990.75	094.36		01.44	26992.45	02.86	293.82	97.47*
	24.87	03.17	94.32*	99.58	90.48	94.09		01.16	92.19	01.56	92.45	96.05
7½	†	173.91	77.64	62.33	65 93	82.28	26773.04	864.01	67.77	172.18	75.78	91.91
	†	72.45	76.27*	61.94	65.53	81.88	72.61	63.65	67.41	†	74.38	90.52
8½	036.23	39.93	56.18	20.79	36.92	65.65		23.07*		38.07	54.17	82.59
	†	38.41*	†	20.17	36.35	65.08		22.05		36.57	52.76	81.02
9½		02.31	31.13	775.06	03.83	44.58					28.96	
		00.86		74.31$_5$	03.01	43.82*					27.48	
10½					866.14	18.99*						
					65.16	18.07						
11½					24.28	26989.13						
					23.07	87.92						
12½					778.17							
					76.64							
13½					27.56							
					25.75							

*Overlapped lines.
†Overlapped but not measured.

Equation (1) gives for the rotational term differences of the $^2\Delta$ state

$$\Delta_1F_1(J+\tfrac{1}{2})+\Delta_1F_2(J+\tfrac{1}{2}) = 4B_v(J+1)-8D_v(J+1)^3. \tag{2}$$

The $\Delta_1F_1(J+\frac{1}{2})$ values were obtained from the differences

$$R_1(J)-Q_1(J) = Q_1(J+1)-P_1(J+1) = {}^QR_{12}(J)-{}^PQ_{12}(J) = {}^PQ_{12}(J+1)-{}^OP_{12}(J+1)$$

and the $\Delta_1F_2(J+\frac{1}{2})$ values from similar differences of lines arising from the F_2 levels of the $^2\Delta$ state. Averages of these differences were used for the $\Delta_1F_1(J+\frac{1}{2})$ and the $\Delta_1F_2(J+\frac{1}{2})$ values in equation (2). B_v and D_v were determined from the graph of $[\Delta_1F_1(J+\frac{1}{2})+\Delta_1F_2(J+\frac{1}{2})]/(J+1)$ against $(J+1)^2$ and the resulting values are given in Table IV.

TABLE IV

ROTATIONAL CONSTANTS OF PH^+ (cm^{-1})

	$^2\Pi$ state	
$B_e'' = 8.505_1$	$\alpha_e = 0.240_1$	$r_e = 1.425_1$ Å
$B_0'' = 8.385_1$		$B_1'' = 8.145_0$
$D_0'' = 4.16\times10^{-4}$		$D_1'' = 4.0\times10^{-4}$
$A_0'' = 295.94$		$A_1'' = 296.2$
$p = 0.23$ and $q = 0.011$ for $v'' = 0$		
	$^2\Delta$ state	
$B_e' = 7.195_5$	$\alpha_e = 0.424_5$	$r_e = 1.548_3$ Å
$B_0' = 6.983_2$		$B_1' = 6.558_8$
$D_0' = 6.28\times10^{-4}$		$D_1' = 6.2\times10^{-4}$
$A_0' = 1.38$		$A_1' = 0.82$
$\gamma_0' = 0.175$		$\gamma_1' = 0.175$

(*b*) *Determination of* γ *and* A

Expression (1), on substitution of $J = N+\frac{1}{2}$ for F_1 levels and $J = N-\frac{1}{2}$ for F_2 levels, gives for the spin splitting, $\Delta\nu_{12}$, of a $^2\Delta$ state approaching to case *b*,

$$\Delta\nu_{12} = F_1(N)-F_2(N) = \frac{B_v(4-Y)\,Y(N+\frac{1}{2})}{N(N+1)} + \gamma(N+\tfrac{1}{2}). \tag{3}$$

The spin splittings of the $^2\Delta$ state were obtained from the following differences:

$$\Delta\nu_{12} = R_1(J)-{}^RQ_{21}(J) = Q_1(J+1)-{}^QP_{21}(J+1) = {}^QR_{12}(J)-Q_2(J) = {}^PQ_{12}(J+1)-P_2(J+1)$$

and averages of their values were used in equation (3). γ and Y were determined from a graph of $\Delta\nu_{12}/(N+\frac{1}{2})$ against $1/[N(N+1)]$. Two positive values of Y were obtained for each vibrational level of the $^2\Delta$ state. Therefore the $^2\Delta$ state is regular.

The two values of Y for the $v = 0$ level of the $^2\Delta$ state are 3.8 and 0.2 and those of $v = 1$ are 3.875 and 0.125. In each case, the value of $Y < 2$ is the correct one since it was found that the lowest rotational levels, $F_1(2\frac{1}{2})$ and $F_2(1\frac{1}{2})$, of the $^2\Delta$ state form a close pair with the $F_2(1\frac{1}{2})$ lying lower (Mulliken 1932). These Y values lead to the spin coupling constants A given in Table IV.

(*c*) *Λ-Doubling*

If the Λ-doubling in the $^2\Delta$ state were appreciable, it could be noted by the fact that the Λ-splitting in the Q_1 branches would not be the same as in the corresponding R_1 branches, and similarly for other pairs. However, these doublet separations agree well within the accuracy of the measurements. It is, therefore, to be concluded that the Λ-doubling in the $^2\Delta$ state is negligible.

2. $^2\Pi$ *State*

(*a*) *Determination of* B_v *and* D_v

The rotational terms for the $^2\Pi$ state are given by equation (1) if Λ is set equal to 1. B_v and D_v were again determined from equation (2) using the appropriate differences for the $\Delta_1F_1(J+\frac{1}{2})$ and the $\Delta_1F_2(J+\frac{1}{2})$ values of the $^2\Pi$ state. The resulting values of B_v and D_v are given in Table IV.

(*b*) *Determination of the Spin Coupling Constant A*

Taking the appropriate terms for $F_1(J)$ and $F_2(J)$ from equation (1) and solving for $Y(Y-4)$, we get

$$Y(Y-4) = \left[\frac{F_1(J)-F_2(J)}{B_v}\right]^2 - 4(J+\tfrac{1}{2})^2. \tag{4}$$

Small terms involving D have been omitted from equation (4). $F_1(J)-F_2(J)$ is equal to the following differences:

$$Q_1(J) - {}^PQ_{12}(J) = R_1(J) - {}^QR_{12}(J) = P_1(J) - {}^OP_{12}(J)$$
$$= {}^RQ_{21}(J) - Q_2(J) = {}^SR_{21}(J) - R_2(J) = {}^QP_{21}(J) - P_2(J).$$

An average value of these differences was taken for $F_1(J)-F_2(J)$ in the right-hand side of equation (4) and $Y(Y-4)$ was determined for each J value. The values of Y obtained were not constant but were found to decrease slightly with increasing J. The value of Y obtained from an extrapolation of equation (4) to $(J+\frac{1}{2})^2 = 0$ was used for the determination of A. The values of A so obtained for the vibrational levels $v = 0$ and 1 of the $^2\Pi$ state are given in Table IV.

(*c*) *Determination of the Λ-Doubling*

Theoretical expressions for the separations, $\Delta\nu_{ab}$, of the Λ-doublets for regular $^2\Pi$ states approaching case *a* were given by Mulliken and Christy (1931) as

$$^2\Pi_{1/2}: \quad \Delta\nu_{ab} = -p(J+\tfrac{1}{2}) \tag{5}$$

and

$$^2\Pi_{3/2}: \quad \Delta\nu_{ab} = +(p/Y^2+2q/Y)(J-\tfrac{1}{2})(J+\tfrac{1}{2})(J+3/2), \tag{6}$$

where p and q are the Λ-type doubling coefficients. Experimental values of the separations of the Λ-doublets are given directly by the observed splitting of the lines of the P_1, Q_1, R_1, ${}^QP_{21}$, ${}^RQ_{21}$, and ${}^SR_{21}$ branches of the $^2\Delta$—$^2\Pi_{1/2}$ subbands and of the P_2, Q_2, R_2, ${}^OP_{12}$, ${}^PQ_{12}$, and ${}^QR_{12}$ branches of the $^2\Delta$—$^2\Pi_{3/2}$ subbands. From a graph of $\Delta\nu_{ab}$ of $^2\Pi_{1/2}$ against $J+\frac{1}{2}$, p was determined. Substituting this value of p in equation (6), q was determined. The resulting values of p and q are included in Table IV.

3. Origins of the Bands

From equation (1), it follows that the band origins can be calculated from Q_1 and Q_2 branches by the expression

$$(7) \qquad \nu_0 = \tfrac{1}{2}(Q_1+Q_2)+(4B'-B'')-(B'-B'')(J+\tfrac{1}{2})^2+(D'-D'')J^2(J+1)^2.$$

The band origins so determined for the 0–0, 0–1, and 1–0 bands are given in Table V in a Deslandres scheme.

TABLE V

DESLANDRES SCHEME OF BAND ORIGINS

v' \ v''	0		1
0	25770.59	2299.60	23470.99
	1398.76		
1	27169.35		

IV. PREDISSOCIATION OF THE $^2\Delta$ STATE

Predissociations are observed in the rotational levels of $v = 0$ and 1 of the $^2\Delta$ state. The 0–1 band at 4228 Å was badly overlapped by the rotational structure of the 4241 Å band of AlH and the expected predissociation could not be observed. Therefore, the predissociations observed in the 0–0 and 1–0 bands only are given below. The predissociations observed in the Q_1 and Q_2 branches of the 0–0 band are indicated in Fig. 2.

0–0 Band

The lines of all the branches of the 0–0 band arising from the F_1 and F_2 levels of the $^2\Delta$ state with $N \geqslant 13$ were either missing or extremely weak. In the $^2\Delta$—$^2\Pi_{\frac{1}{2}}$ subband, $P_1(13\frac{1}{2})$, $Q_1(12\frac{1}{2})$, and $R_1(11\frac{1}{2})$ were the last lines observed. Further lines of the P_1, Q_1, and R_1 branches with higher rotational quantum numbers were not observed. In the $^2\Delta$—$^2\Pi_{3/2}$ subband, the last strong lines of the Q_2 and R_2 branches were those from the F_2 levels of the $^2\Delta$ state with $N = 12$, namely the $Q_2(11\frac{1}{2})$ and $R_2(10\frac{1}{2})$ lines. However, the lines $Q_2(12\frac{1}{2})$, $Q_2(13\frac{1}{2})$, $R_2(11\frac{1}{2})$, and $R_2(12\frac{1}{2})$ were also observed, though very weakly. No further Q_2 and R_2 lines were observed. In $^PQ_{12}$, $^QR_{12}$, and $^SR_{21}$ branches the last lines to be observed were those with J equal to $12\frac{1}{2}$, $11\frac{1}{2}$, and $12\frac{1}{2}$ respectively. The intensities of the remaining branches of the $^2\Delta$—$^2\Pi$ transition were comparatively weaker and they were not observed beyond $P_2(12\frac{1}{2})$, $^OP_{12}(12\frac{1}{2})$, $^OP_{21}(11\frac{1}{2})$, and $^RQ_{12}(12\frac{1}{2})$.

1–0 Band

In the 1–0 band, all the lines arising from the F_1 levels of the $^2\Delta$ state were much weaker than those arising from the F_2 levels.

It appears that the sudden breaking off of the branches in the 0–0 band must be due to predissociation of all the F_1 rotational levels with $N \geqslant 13$ and all the F_2 rotational levels with $N \geqslant 15$ in the $v = 0$ state of the $^2\Delta$

electronic state. In the case of the $v = 1$ state, one must conclude that the F_1 levels are also predissociated even though no sharp breaking off of the branches is observed.

It is not at all evident what electronic states cause this predissociation. Since the breaking off is not a complete one (i.e., the $v = 1$ level which is above the predissociation limit is observed) the predissociation is probably a forbidden one. In both the $v = 0$ and the $v = 1$ levels, there is a difference in the behavior of the F_1 and F_2 levels. Since the coupling in the $^2\Delta$ state is close to case *b*, it appears that the only significant difference between the two types of levels lies in the fact that for F_1 levels $N = J - \frac{1}{2}$ and for F_2 levels $N = J + \frac{1}{2}$. Thus it appears that the quantum number N has some significance in the predissociation process. Also in the predissociation both Λ-components of the rotational levels are affected. Thus rotational levels of even and odd parity are equally affected by the predissociation. The problem is to determine which of the possible states of PH^+ is capable of producing a predissociation having these characteristics.

The electronic states of PH^+ arising from the lowest lying atomic states are listed below:

$$P^+ {}^3P + H\,{}^2S \rightarrow {}^4\Sigma^-,\ {}^4\Pi,\ {}^2\Sigma^-,\ {}^2\Pi$$

$$P^+ {}^1D + H\,{}^2S \rightarrow {}^2\Sigma^+,\ {}^2\Pi,\ {}^2\Delta$$

$$P^+ {}^1S + H\,{}^2S \rightarrow {}^2\Sigma^+$$

States arising from $H^+ + P$ are at considerably higher energy. The $^2\Pi$ state arising from the ground states of atoms must be the ground state of the molecule and the $^2\Delta$ state from $P^+ {}^1D + H\,{}^2S$ must be identified with the observed one. The only states which, from energy considerations alone, can predissociate the $v = 0$ and $v = 1$ levels of the $^2\Delta$ state are the $^4\Sigma^-$, $^4\Pi$, $^2\Sigma^-$, and $^2\Pi$ states. From the rigorous selection rules for predissociation, i.e., $\Delta J = 0$ and $+ \leftrightarrow -$, it follows that the $^2\Sigma^-$ state cannot predissociate both components of the Λ-doublets and therefore the $^2\Sigma^-$ state is not responsible for the observed predissociation. Both from a consideration of the relative positions of the potential curves and from the fact that N is a significant quantum number in the predissociation process, but not for the $^2\Pi$ state which has a good case *a* coupling, it follows that it is most unlikely that the $^2\Pi$ state is responsible for the predissociation. Of the two remaining states, $^4\Sigma^-$ and $^4\Pi$, each is capable of predissociating a $^2\Delta$ state even though the predissociation is a forbidden one. It seems most improbable that the $^4\Sigma^-$ state could predissociate both Λ-components of the F_1 levels of the $^2\Delta$ state for $N \geqslant 13$ and still leave the F_2 levels of $N = 14$ relatively unaffected. Thus it seems most probable that the $^4\Pi$ state is responsible for the predissociation. It is not at all evident, however, that the $^4\Pi$ state can give the observed type of predissociation, particularly the observed difference between the intensities of the lines arising from the F_1 and F_2 levels of the $^2\Delta$ state with $v = 1$.

V. DISCUSSION

It has been assumed up to this point that the emitter of the $^2\Delta$—$^2\Pi$ band system is the PH^+ molecule. This can be substantiated mainly by the following considerations:

(*a*) The observed spectrum bears close resemblance to the $^2\Delta$—$^2\Pi$ band system of the SiH molecule which is isoelectronic with the PH^+ molecule.

(*b*) The vibrational and rotational constants obtained for the $^2\Delta$ and $^2\Pi$ states of the $^2\Delta$—$^2\Pi$ transition are in good agreement with those expected of a PH^+ molecule.

(*c*) The fact that the band system is excited in a hollow cathode discharge through phosphorus vapor and hydrogen gas provides further evidence that the emitter of the $^2\Delta$—$^2\Pi$ band system is the PH^+ molecule.

The electron configurations of the PH^+ molecule will be similar to those of the CH-type molecules. The probable low lying electron configurations and the resulting electronic terms of PH^+, therefore, are as follows:

$$KL\ (3s\sigma)^2\,(3p\sigma)^2\,3p\pi\ ^2\Pi\text{reg.}$$

$$KL\ (3s\sigma)^2\,3p\sigma\,(3p\pi)^2\ ^4\Sigma^-,\ ^2\Delta,\ ^2\Sigma^+,\ ^2\Sigma^-$$

It follows from the above electron configurations that the ground state of PH^+ should be a $^2\Pi$reg. state. The lower state of the observed $^2\Delta$—$^2\Pi$ band system is almost certainly the predicted ground state.

Because the $^2\Delta$ state is certainly a very shallow one, it is possible to get an estimate of the dissociation energy of PH^+. According to the correlation of the molecular states with the states of the separated atoms, the $^2\Delta$ state dissociates into the $^1D+^2S$ states of the separated atoms while the ground state, $^2\Pi$, dissociates into $^3P+^2S$ atomic states. The dissociation energy of the $^2\Pi$ state will then be given by

$$\nu_{00}(^2\Delta\text{—}^2\Pi\text{ system})+D_0(^2\Delta\text{ state})-E(^1D-^3P),$$

where $E(^1D-^3P)$ is the energy difference between the ^1D and ^3P terms of P^+. Douglas (1957) has obtained a fair estimate of the dissociation energy of SiH adopting a similar procedure. In the present case of PH^+, however, lack of vibrational levels of the $^2\Delta$ state with $v > 1$ makes the extrapolation of the dissociation limit of the $^2\Delta$ state uncertain. From the relationship between α_e, B_e, ω_e, and $\omega_e x_e$ (see Herzberg 1950) a value of $\omega_e x_e$ has been determined. With the $\omega_e x_e$ so determined, the dissociation energy of the $^2\Delta$ state has been calculated to be 7800 cm^{-1}. The error in such a determination could be large, perhaps as much as ± 2000 cm^{-1}. The dissociation energy of the $^2\Pi$ state of PH^+, corresponding to this value for the $^2\Delta$ state, is 24690 ± 2000 cm^{-1} (3.06 ± 0.25 ev.). This may be compared with the dissociation energies of SiH (3.19 ± 0.25 ev.) and CH (3.47 ev.).

The predissociation observed in the $^2\Delta$ state (discussed in an earlier paragraph) gives a definite upper limit for the energy of the dissociation. The predissociation in the $v' = 0$ level of the $^2\Delta$ state occurs at the $K = 13$ level, which gives an upper limit of 27060 cm^{-1} (3.35 ev.) for the energy of dissociation of the $^2\Pi$ state.

ACKNOWLEDGMENTS

I am indebted to Dr. A. E. Douglas for his ready help and advice during the course of this investigation. My thanks are also due to Dr. G. Herzberg, F.R.S., for his interest and many helpful discussions.

REFERENCES

DOUGLAS, A. E. 1957. Can. J. Phys. **35**, 71.
HERZBERG, G. 1950. Molecular spectra and molecular structure, Vol. I, Spectra of diatomic molecules, 2nd ed. (D. Van Nostrand Co., Inc., New York).
MULLIKEN, R. S. 1932. Revs. Mod. Phys. **4**, 1.
MULLIKEN, R. S. and CHRISTY, A. 1931. Phys. Rev. **38**, 87.
NARASIMHAM, N. A. 1956. Symposium on Molecular Structure and Spectroscopy, Columbus, Ohio, U.S.A.
ROCHESTER, G. D. 1936. Z. Physik, **101**, 769.

THE EMISSION SPECTRUM OF ALUMINUM MONOCHLORIDE IN THE VACUUM ULTRAVIOLET[1]

S. Paddi Reddy and P. Tiruvenganna Rao

ABSTRACT

The spectrum of aluminum monochloride as excited in a high frequency discharge is photographed in the Schumann region using a 1 meter normal incidence grating spectrograph in the first order. Six brief new systems of bands were obtained in the region λλ2075–1820, in addition to three characteristic continua on the longer wavelength side of the discrete systems. The analyses of five of these systems indicate a common lower level which is identified as the ground state of the AlCl molecule. For the remaining system, only the upper state vibrational frequency ω_e' is derived. All these systems involve six new, hitherto unknown, excited electronic states of the AlCl molecule. The spectrum, when excited in a condensed discharge from a high voltage transformer through steaming $AlCl_3$ vapor, is found to consist of numerous discrete emission bands in the region λλ2365–2020. These bands are different from those occurring in the high frequency discharge. Because of overcrowding of these bands, owing possibly to lack of adequate dispersion, no analysis is presented.

I. INTRODUCTION

The study of diatomic fluorides of the related group III elements boron and aluminum has been the subject of numerous investigations in recent years. The work of Chrétien (1950) on the emission spectrum of boron monofluoride has revealed the existence of numerous singlet electronic states in the Schumann region. The term scheme of this molecule, presented by him, has shown a striking analogy with that of the isoelectronic CO molecule. Recent studies on the band spectrum of aluminum monofluoride (Rowlinson and Barrow 1953; Barrow and Rowlinson 1954; Dodsworth and Barrow 1955; Naudé and Hugo 1953, 1954, 1955, 1957) both in emission and in absorption cover an extensive wavelength region from λλ8800 to 1250. This work has led to the identification of a large number of singlet and triplet excited electronic states of the AlF molecule.

The well-known ultraviolet bands of AlCl lying between λλ2810 and 2550 were investigated by Bhaduri and Fowler (1934), Mahanti (1934), and Holst (1934) in emission and by Miescher (1936) in absorption as arising from the transition $A\ ^1\Pi—X\ ^1\Sigma^+$. Apart from this early work, recent work on the emission spectrum of AlCl has been done by Sharma (1951). This author has studied the excitation of the AlCl emission spectrum in an uncondensed discharge in the presence of helium and obtained two new band systems in the regions λλ4154–3970 and λλ5612–5265. From the structural appearance of these systems as photographed under the high dispersion of the first order of a 21-ft. grating, he interpreted the systems in the violet and green regions as corresponding to the transitions $a\ ^3\Pi \rightarrow X\ ^1\Sigma^+$ and $b\ ^3\Sigma \rightarrow a\ ^3\Pi$ respectively.

The present investigations were started with a view to obtaining analogous band systems in the remaining diatomic halides of aluminum, particularly in the Schumann region. The results of the work described in this paper have

[1]Manuscript received April 17, 1957.
Contribution from the Physics Department, Andhra University, Waltair, India.

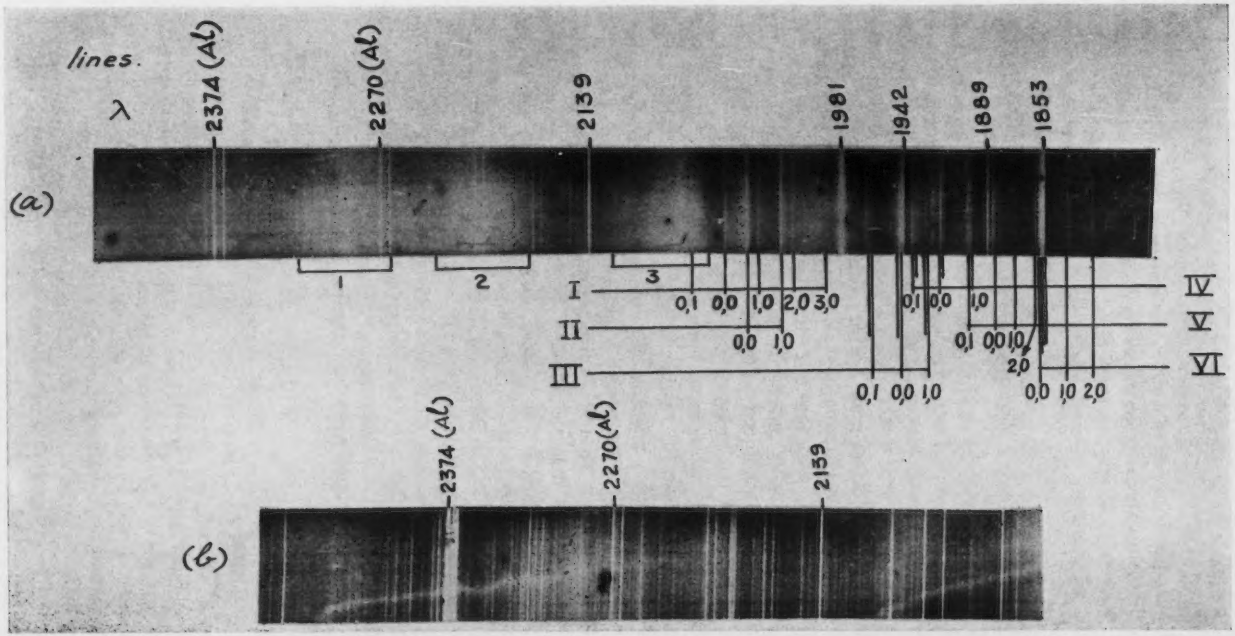

FIG. 1. The emission spectrum of AlCl. (*a*) H.F. discharge picture; 1, 2, 3—continua, I to VI—band systems. (*b*) Bands in the condensed discharge from a transformer.

shown the existence of six new discrete band systems of the AlCl molecule, which are here provisionally designated as systems I, II, III, IV, V, and VI, in the region λλ2075–1820. A preliminary report of the approximate vibrational frequencies of these band systems has been recently communicated to *Current Science*. In addition to the above band systems, discrete emission bands in the region λλ2365–2020 and three characteristic continua in the region λλ2320–2065 were also reported.

II. EXPERIMENTAL

The new band systems were excited in a high frequency discharge through $AlCl_3$ vapor using a 50 watt oscillator. The discharge tube was an ordinary pyrex tube 35 cm. long and 22 mm. in diameter, drawn into an adapter at one end and sealed at the open end by a fluorite window. The adapter end of the discharge tube was connected to a Cenco High-Vac pump through a series of absorbing towers. A pure sample of anhydrous aluminum trichloride, supplied by B.D.H., was used to excite the spectrum. The spectrum was also excited in an ordinary conventional discharge tube having two tungsten electrodes fused to the two side limbs. The terminals of the electrodes were connected to the secondary of a 20 kv. transformer. A glass condenser was connected across the secondary of the transformer. A spark gap was also provided in series in the secondary circuit of the transformer. The spectra were photographed in the Schumann region using a 1 meter normal incidence vacuum grating spectrograph* having a dispersion of 17.3 Å/mm. in the first order. The discharge tube, cemented with a fluorite window, was attached to the slit cone of the spectrograph in obtaining the spectrum on the instrument. The spectra were photographed on Special Ilford Q II plates and exposures of 2 to 3 hours' duration were found sufficient to obtain good photographs of the spectrum. Aluminum lines which appeared in the spectrum of AlCl were employed as wavelength standards. The wavelengths of these lines were taken from the M.I.T. tables and converted into vacuum wavelengths. The order of accuracy involved in the measurement of the band heads is believed to be up to 5 cm^{-1}. In the visible and ultraviolet regions, a Hilger three-prism glass littrow and medium quartz spectrographs were employed.

III. RESULTS

The spectrum as obtained in a high frequency discharge in the vacuum ultraviolet region is shown in Fig. 1(*a*). It is seen to consist of the three characteristic continua referred to above and six discrete band systems designated provisionally as systems I, II, III, IV, V, and VI. The well-known ultraviolet bands λλ2810–2550 and the bands in the green region (Sharma 1951) were also obtained when the spectrum was excited in the same source and are not reproduced here. The spectrum excited in a condensed discharge from a transformer, shown in Fig. 1(*b*), reveals a number of discrete bands in the region λλ2365–2020. These bands are different from those reproduced

*The grating employed in the spectrograph was kindly supplied by Professor Siegbahn to Professor K. R. Rao.

in Fig. 1(*a*) and occur on the longer wavelength side of the discrete band systems. Some of these bands occur in the wavelength region covered by the three emission continua shown in Fig. 1(*a*) while the remaining bands extend towards longer wavelengths up to λ2365. The well-known band system in the region λλ2810–2550 is also observed in the condensed discharge from a transformer while in the visible region none of the band systems corresponding to the transitions to the triplet levels are observed.

In all, six new band systems were identified and attributed to the AlCl molecule from an examination of the spectrum shown in Fig. 1(*a*). The wavelength, wavenumber, intensity, and classification data of the bands belonging to these systems are shown in Table I.

TABLE I

BAND SYSTEMS OF AlCl (λλ2075–1820)

Wavelength	Wavenumber	Intensity	System	Assignment
2075.4	48183	4	I	0,1
2054.9	48664	6	I	0,0
2041.0	48996	8	II	0,0
2033.8	49169	5	I	1,0
2019.8	49510	7	II	1,0
2012.2	49697	4	I	2,0
1990.8	50231	3	I	3,0
1964.6	50901	4	III	1,2
1962.0	50968	3	III	0,1
1946.2	51382	5	III	1,1
1943.6	51451	7	III	0,0
1937.2	51621	6	IV	0,1
1934.4	51696	3	IV	1,2
1930.7	51795	2	III	2,1
1928.2	51863	4	III	1,0
1924.4	51964	5		
1919.3	52102	6	IV	0,0
1917.1	52162	3	IV	1,1
1902.4	52564	4	V	0,1
1899.9	52634	4	IV	1,0
1885.2	53045	6	V	0,0
1871.9	53422	3	V	1,0
1859.3	53784	3	V	2,0
1857.0	53851	4	VI	0,0
1856.1	53876	3	VI	1,1
1855.0	53909	3	VI	2,2
1854.0	53938	3	VI	3,3
1839.5	54364	2	VI	1,0
1822.6	54867	2	VI	2,0

System I.—This system consists of five bands clearly degraded to shorter wavelengths. The wavenumber difference between the first two bands at $\nu = 48183\ \text{cm}^{-1}$ and $48664\ \text{cm}^{-1}$ is found to be $481\ \text{cm}^{-1}$. This being approximately equal to the ground state vibrational frequency of the AlCl molecule, the band at $\nu = 48664\ \text{cm}^{-1}$ is taken as the 0,0 band. The bands on the shorter wavelength side are assigned as the 1,0, 2,0, and 3,0 bands. The $\Delta G'(v')$ differences suggest an upper state vibrational frequency of about $505\ \text{cm}^{-1}$.

System II.—System II consists of only two bands, slightly degraded to the shorter wavelength side. The stronger of the two is assigned as 0,0 and the other as 1,0. The approximate ω_e' value is $514\ \text{cm}^{-1}$.

System III.—This system consists of bands degraded to longer wavelengths and occurs in three groups which are interpreted as sequences. The strongest group at about $\nu = 51450\ \text{cm}^{-1}$ is taken as the $\Delta v = 0$ sequence. The vibrational assignments of the bands are given in Table I and shown in Fig. 1(*a*). The approximate ω_e' and ω_e'' values are $413\ \text{cm}^{-1}$ and $482\ \text{cm}^{-1}$.

System IV.—This also occurs in three groups, the strongest of them at $\nu = 52102\ \text{cm}^{-1}$ being assigned as the 0,0 band. In all, five bands belong to this system. The approximate ω_e' and ω_e'' values are $537\ \text{cm}^{-1}$ and $477\ \text{cm}^{-1}$ respectively.

System V.—This system consists of four bands, the strongest of them at $\nu = 53045\ \text{cm}^{-1}$ being identified as the 0,0 band. The approximate ω_e' and ω_e'' values are $377\ \text{cm}^{-1}$ and $481\ \text{cm}^{-1}$ respectively.

System VI.—The most intense group in this system is seen to consist of four closely spaced bands which belong to the 0–0 sequence. The sequence degradation of the bands is towards the shorter wavelengths. The 1,0 and 2,0 bands are also shown in Fig. 1(*a*). The approximate ω_e' and ω_e'' values are respectively $513\ \text{cm}^{-1}$ and $481\ \text{cm}^{-1}$.

All the above brief systems with the exception of system II have for their final level the ground state of the AlCl molecule, the upper states involved corresponding to various excited upper electronic levels. Although in system II the 0,1 band is not observed, it is likely that the lower state, in common with all the other systems, is the ground state.

The three continua in the wavelength regions λλ2320–2260, λλ2240–2170, and λλ2110–2060 appear in the spectrum of AlCl as excited in the high frequency discharge. In this region and towards the longer wavelengths up to λ2365, the spectrum of AlCl as excited in a condensed discharge from a transformer consists of numerous bands (about 100 in number). All these bands occur on the short wavelength side of the well-known ultraviolet bands arising from the transition $^1\Pi$—$^1\Sigma^+$. As can be seen from Fig. 1(*b*), the bands seem to be slightly degraded towards the red on the longer wavelength side while some of the bands on the shorter wavelength end appear to be clearly degraded towards the violet. The overcrowding of the bands in the low dispersion employed in the present work makes the analysis of these bands difficult. As such, measurements of wavelengths, etc., are given in Table II. A study of the absorption spectrum of AlCl in this region may be helpful in throwing light on the analysis of these bands. It is worth while to take up the discussion of the nature of the electronic states of the AlCl molecule at a later stage.

ACKNOWLEDGMENTS

In conclusion, the authors would like to express their grateful thanks to Prof. G. Herzberg for his interest in this work and to Prof. K. R. Rao for his encouragement in the course of these investigations. One of the authors (S. P. Reddy) is grateful to the Government of India for the award of a Senior Research Scholarship.

TABLE II. MEASUREMENTS OF BAND HEADS (λλ2365–2020)

Wave-length	Wave-number	Inten-sity	Degrada-tion	Wave-length	Wave-number	Inten-sity	Degrada-tion
2365.3	42278	2	R	2198.7	45481	4	R
2359.8	42476	3	R	2196.1	45535		Line
2354.1	42479	1	R	2194.8	45562		Line
2351.4	42528	1	R	2193.2	45595		Line
2349.0	42571	5	R	2190.1	45660	2	R
2347.2	42604	4	R	2186.3	45739	2	R
2344.0	42662	7	R	2183.9	45790	2	R
2342.0	42699	1	R	2181.9	45832	5	V
2340.1	42733	5	*	2179.8	45876	2	V
2338.7	42759	2	R	2178.0	45914	4	V
2336.9	42792	5	R	2174.5	45987		Line
2333.0	42863	7	R	2172.0	46041	2	V
2329.2	42933	7	R	2169.2	46100		Line
2326.8	42977	5	R	2166.5	46157	5	V
2325.7	42997	5	R	2161.3	46268	1	V
2324.7	43016	5	R	2159.9	46298	1	V
2322.2	43063		Line	2157.2	46356	1	V
2319.8	43107		Line	2154.4	46416	1	V
2318.1	43139		Line	2151.0	46490		Line
2315.4	43189	3	R	2150.7	46496	1	V
2314.1	43213	4	Line?	2146.9	46579	4	V
2313.2	43230	4	Line?	2143.6	46650	2	V
2312.1	43251	5	V	2139.3	46743		Line
2310.1	43288	1	*	2136.6	46803	3	V
2306.4	43358	4	R	2135.3	46832	3	V
2304.5	43393	6	R	2133.3	46942	4	V
2302.6	43429	4	R	2127.4	47006	4	V
2301.0	43459	4	R	2125.0	47059	1	V
2300.1	43476	4	V	2123.7	47088	5	V
2297.4	43527	4	V	2118.9	47194	2	V
2295.3	43567	4	V	2115.8	47263	4	V
2293.3	43605	4	V	2111.9	47350	3	V
2291.0	43649	8	V	2108.7	47423	4	V
2288.8	43691	8	V	2105.5	47495	4	V
2286.7	43731	5	V	2100.8	47601	4	V
2283.6	43790	5	V	2098.0	47664	2	V
2280.3	43854	5	V	2095.2	47728		Line
2277.9	43900	5	V	2092.3	47794	2	V
2275.2	43952	3	V	2088.9	47872	2	V
2273.5	43985	3	V	2087.7	47900	4	V
2269.8	44057		Line	2084.8	47966	1	V
2267.6	44099	4	V	2082.3	48024	4	V
2264.0	44170		Line	2079.8	48082	3	V
2261.5	44218	3	V	2074.7	48200		Line
2258.4	44279	4	R	2069.6	48319	1	V
2256.3	44320	3	V	2066.3	48396	1	V
2253.9	44368	4	V	2062.7	48480		Line
2252.0	44405		Line	2060.5	48532	1	V
2249.6	44452	2	R	2058.8	48572	1	V
2247.7	44490	4	R	2057.1	48612	2	V
2245.1	44541	2	R	2054.1	48683	4	V
2243.0	44583	4	R	2050.6	48766	3	V
2241.2	44619	7	V	2046.4	48866	5	V
2236.8	44707	4	V	2044.7	48907	5	V
2226.2	44920	4	R	2042.9	48950	4	V
2221.7	45011	3	R	2041.5	48984	1	V
2218.9	45067	5	R	2039.9	49022	1	V
2215.4	45139	3	R	2037.6	49077	4	R
2212.4	45200	4	*	2036.6	49101	2	V
2210.6	45237		Line	2034.3	49157	2	V
2207.8	45294	3	*	2032.0	49213	2	V
2205.4	45343		Line	2029.4	49276	2	V
2202.0	45413	1	R	2026.1	49356		Line

*Degradation for the bands marked * is not clear.

REFERENCES

BARROW, R. F. and ROWLINSON, H. C. 1954. Proc. Roy. Soc. A, **224**, 134.
BHADURI, B. N. and FOWLER, A. 1934. Proc. Roy. Soc. A, **145**, 321.
CHRÉTIEN, M. 1950. Helv. Phys. Acta, **23**, 259.
DODSWORTH, P. G. and BARROW, R. F. 1955. Proc. Phys. Soc. A, **68**, 824.
HARRISON, G. R. 1939. M.I.T. wavelength tables (John Wiley & Sons, Inc., New York).
HOLST, W. 1934. Z. Physik, **93**, 55.
MAHANTI, P. C. 1934. Z. Physik, **88**, 550.
MIESCHER, E. 1936. Helv. Phys. Acta, **9**, 693.
NAUDÉ, S. M. and HUGO, T. J. 1953. Can. J. Phys. **31**, 1106.
——— 1954. Can. J. Phys. **32**, 246.
——— 1955. Can. J. Phys. **33**, 573.
——— 1957. Can. J. Phys. **35**, 64.
PADDI REDDY, S. and TIRUVENGANNA RAO, P. 1957. Current Sci. (India) (In press).
ROWLINSON, H. C. and BARROW, R. F. 1953. Proc. Phys. Soc. A, **66**, 437.
SHARMA, D. 1951. Astrophys. J. **113**, 210.

ABSORPTION OF SUNLIGHT BY ATMOSPHERIC SODIUM[1]

J. A. SCRIMGER[2] AND D. M. HUNTEN

ABSTRACT

A photometer has been built which is sensitive to light only in a very narrow spectral region near the sodium D-lines. The light is scattered by sodium vapor at low density and the scattered light recorded by a photoelectric spectrometer. The latter resolves the two lines and allows the effect of stray light to be eliminated. With sunlight as the source, the radiation detected is at the bottom of the Fraunhofer lines and the residual intensity there may be measured. It is found that this intensity decreases slightly (relative to the continuum) as the sun approaches the horizon. This effect is attributed to atmospheric sodium; the amount found by this method agrees well with that deduced from twilight measurements. The thickness of the sodium layer in atoms/cm.^{2} varies between 3 and 9×10^9 in winter and is about 1×10^9 in April. The measurements also give the residual intensities of the Fraunhofer lines in the incident sunlight, averaged over the whole of the sun's disk. These are $(5.90\pm0.46)\%$ for D1 and $(5.06\pm0.24)\%$ for D2.

1. INTRODUCTION

Measurements of the brightness of the sodium lines in twilight have often been used to deduce the "thickness" of the layer of free sodium atoms in the upper atmosphere. (By "thickness" we mean the number of atoms in a vertical column whose cross section is 1 cm.^{2}) There are two serious uncertainties in this procedure: a correction must be made for self-absorption, and the flux of incident sunlight is not known accurately. Self-absorption is produced by the sodium itself, and has the effect of reducing the apparent brightness; several attempts have been made to calculate the correction, but some doubt remains (Donahue, Resnick, and Stull 1956; Hunten 1956*b*; Chamberlain 1956). The uncertainty in the incident flux arises mostly in the measurement of the residual intensity at the bottom of the Fraunhofer D lines; the terrestrial lines are so much narrower than the solar that only the centers of the latter are effective in exciting the atmospheric sodium. One attempt to verify the residual intensities found by solar physicists has already been reported (Scrimger and Hunten 1955); considerably better values are found in the present paper as a by-product. The principal result is that the absorption by the atmospheric sodium has been observed directly; the thicknesses found by this method are almost entirely independent of those found in twilight and are not subject to either of the uncertainties already mentioned.

The only previous attempt to do this was made by Sanford (1950). In order to avoid the difficulty caused by absorption lines in the light source, he studied some stellar spectrograms in which the sodium lines were shifted by the Doppler effect. Of those available, he concluded that the most suitable was that of α Virginis, taken on May 27, 1940; but it showed no line that

[1]Manuscript received April 25, 1957.
Contribution from the Department of Physics, University of Saskatchewan, Saskatoon, Saskatchewan. Sponsored by the Geophysics Research Directorate of the Air Force Cambridge Research Center, Air Research and Development Command, under Contracts AF19(122)–152 and AF19(604)–1831.

[2]Now at Pacific Naval Laboratory, Defence Research Board, Esquimalt, B.C.

could definitely be attributed to telluric sodium. The upper limit deduced for the layer thickness was 10^{10} atoms/cm.^{2} Now that more is known about the seasonal variation of thickness (Fig. 4), we can see that May is far from the best month for such a measurement, and that January, February, or March is much better. This knowledge was partly responsible for our success, along with the use of an apparatus able to detect a thickness of 10^9 atoms/cm.^{2}

In order to limit the sensitivity to the region of the D lines, the sunlight was scattered by sodium vapor into a photoelectric spectrometer which separated the lines from each other and from the parasitic scattered continuum. Their intensity was found to decrease slightly, relative to the continuum, as the sun moved towards the horizon. A logarithmic plot against path length through the sodium layer gave the thickness from its slope, and the residual intensity of the Fraunhofer line from its intercept. The results have already been reported briefly (Scrimger and Hunten 1956). The residual intensities are a little larger than we found earlier and thus in slightly better agreement with the values found by Priester (1953). The thicknesses are little larger than those deduced from twilight without allowance for self-absorption, showing that the latter reduces the intensity by no more than a factor of two even in winter.

2. EXPERIMENTAL METHOD

The apparatus sketched in Fig. 1 was mounted on the front of the auroral spectrometer which has been described by Hunten (1953). The spectral slit-widths were about 1 Å and the scan covered 30 Å in the second order once

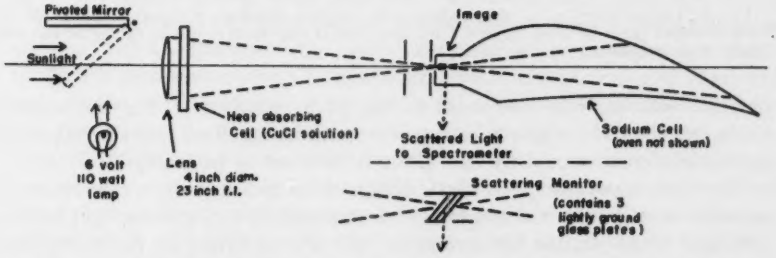

FIG. 1. Experimental arrangement (shown schematically and not to scale). When the scattering monitor is in use it replaces the sodium cell.

per minute. An image of the sun about 0.2 inch in diameter was formed in front of the entrance slit, so that scattered light came from all parts of the disk. The sodium-vapor tube was maintained within 0.1° at a temperature between 145° and 150° C. by a thermostat, with the window a few degrees higher to avoid condensation of sodium. The tube could be quickly slid back and replaced by a scattering monitor designed to duplicate the resonant scattering phenomenon as closely as possible except that it was achromatic; this allowed a measurement of the intensity of the light to be made. It consisted of three slips of glass with a few scratches on each surface produced by very

light grinding; they were mounted so that any reflection would be away from the spectrometer. The whole arrangement could be calibrated against light from a tungsten lamp by turning a mirror. Samples of the four kinds of spectrum are shown in Fig. 2. In order to avoid a possible heating of the sodium tube by the sunlight, an infrared absorption cell of $3\frac{1}{2}\%$ cuprous

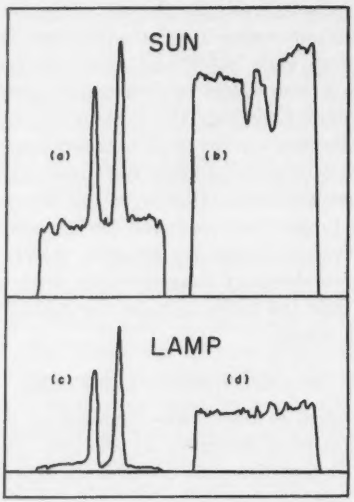

FIG. 2. Typical spectra: (*a*) sun, sodium cell; (*b*) sun, monitor; (*c*) lamp, sodium cell; (*d*) lamp, monitor (gain 10 times larger). Each spectrum is the result of a scan taking 50 seconds; longer wavelengths are on the left.

chloride solution was interposed in the path. Without it, the temperature controller showed a slight heating effect; with it, no effect could be observed. Systematic error caused by this effect is believed to be negligible.

The most important point in the design of the sodium tube was to minimize parasitic scattering of white light. This is particularly bad with sunlight because the light which excites the sodium is only 5% as bright as the continuum; notice the difference between the two sources in Fig. 2. The tube was designed with a small diameter near the windows so that the path length of the light in the vapor would be small. (If the scattered light must traverse a considerable amount of vapor most of it will be scattered and lost; for a similar reason, the solar image must be formed very near the front window.) The diameter farther back was increased so that the light diverging from the sun's image would not strike the wall until it was well out of the view of the spectrometer, and the end was given the conventional horn-shape. All the walls were painted black except for the two windows, and baffles were placed in several places. At the temperatures used the glass is not attacked by sodium vapor; ordinary Pyrex was used, but the entrance window was of flat polished material. The sodium was introduced from a small ampoule (kindly provided by Mr. R. W.

Schmies of the General Electric Company) after the tube had been baked at a temperature of 300° C. and a pressure of 5×10^{-6} mm. The pressure just before sealing off was 2×10^{-6} mm., as measured by an ionization gauge. A three-stage glass diffusion pump was used.

A single measurement consisted of the following steps:

1. Several scans were made with the monitor to be sure that the intensity of the sunlight was not varying.
2. Five scans were made on sunlight with the resonance tube.
3. One more scan with the monitor gave a check that the intensity had remained constant during Step 2.
4. Five scans were made with the monitor and the tungsten source.
5. Five scans on this source with the sodium tube completed the process.

It was possible to exchange the scatterers in the 10-second interval between scans of the spectrometer; one complete measurement thus took 20 minutes of actual observation. A typical sample of each type of spectrum is shown in Fig. 2; all but one were recorded at the same gain. The exception is the monitor scan on the lamp, for which the gain is 10 times larger. A day's run consisted of 8 to 12 such measurements distributed between noon and either sunrise or sunset; it will be appreciated that this required unusually fine weather and this accounts for the rather small number of runs to be reported. While it would be desirable to have runs covering a whole year, this was not felt to be worth the very considerable labor required, as well as the tying up of the spectrometer, which has many demands made upon it.

It may be useful to report another method which was seriously considered and for which apparatus was nearly completed. The sunlight first passed through a monochromator which selected one of the D lines and eliminated most of the continuum except for a band of about 3 Å. The beam was split into two parts, one of which traversed a sodium-vapor cell; they were then reunited at the cathode of a photomultiplier tube. A chopper was arranged to pass first one beam, then the other, and an attenuator in the reference beam allowed the two intensities to be made equal so that there was no a-c. component in the output with the sodium tube cold. When it was hot it would eliminate a narrow region of wavelength from its beam; the result would be an a-c. signal proportional to the residual intensity of the Fraunhofer line. The intensity of the continuum would be given by the d-c. component of the output. The chief defect of this method is that it depends critically on exact balance of the two beams, and the balance must be maintained for several hours. Even if this requirement could be met mechanically, it would be very difficult to guard against the possibility of sodium condensing on the windows of the tube, which could not be distinguished from a decrease in the residual intensity of the Fraunhofer line. The method which was actually used is just as sensitive to the presence of the atmospheric sodium but far less uncertain. However, it does require the use of an unusually sensitive spectrometer incorporating refrigeration of the photomultiplier with dry ice.

3. RESULTS

The apparent intensity of the D lines from the tube is affected by the presence of the Fraunhofer lines in the parasitic light when observing the sun. The correction of this effect amounts to measuring the line intensity from the bottom of the Fraunhofer line observed in the white light under the same conditions; in other words, adding a fraction of the white intensity to the line intensity as measured above the continuum. The fraction may be derived from the monitor traces of which Fig. 2(*a*) is an example. This procedure is discussed by Hunten and Shepherd (1954) and more fully by Harrison and Vallance Jones (1956). Let the corrected intensity for a given line be called D_s and the intensity of the monitor trace I_s; the corresponding intensities for the lamp may be called D_t and I_t. Then the residual intensity of the Fraunhofer line is given by

$$p = D_s I_t / D_t I_s;$$

this includes telluric as well as solar absorption and will decrease as the sun moves toward the horizon if the former is appreciable. Since the telluric absorption was found to be small, it is possible to define an effective absorption coefficient for the whole resonance line; this is further discussed in Section 4. Therefore a plot of the logarithm of p against relative slant path length through the sodium layer should give a straight line; the slope gives the thickness of sodium and the intercept extrapolated to zero path gives p_0, the residual intensity of the solar line alone. In fact 9 of the 11 runs did give straight lines within the error of measurement; the other two will be considered separately. The path length was calculated using a height of 85 km. for the sodium (Hunten and Shepherd 1954); even a 10 km. change in this height would have little effect. The abscissa used was sec α, where α is the angle between the layer and the line of observation.

In practice the accuracy with which D_t and I_t could be measured was not as high as desired, because the intensities were small and the shot noise in the photocurrent was appreciable. The ratio of these quantities should vary but slowly during the day, however, and so a plot of the ratios (one for each line) was made against time. The ratios used were taken from a curve drawn smoothly through the mass of points. This procedure resulted in a considerable reduction in the scatter of the final measurements. Straight lines were fitted to each of the final plots by the method of least squares; all the slopes, intercepts, and errors given were taken from this analysis except as noted later.

Three examples of complete runs are shown in Fig. 3; the scatter of the points in them is perhaps a little smaller than the average. Fig. 3(*a*) illustrates the majority of the runs, which gave a substantial slope, and Fig. 3(*b*) the last two, which gave a small slope. Fig. 3(*c*) shows one of the two which gave a line far from straight, suggesting non-uniform distribution of sodium in different parts of the layer. The point at which the sunlight traverses the layer moves several hundred kilometers during a run, of course. Table I gives the results of each run with their estimated probable errors. The first columns show the optical depths for each line; the calibration of these in

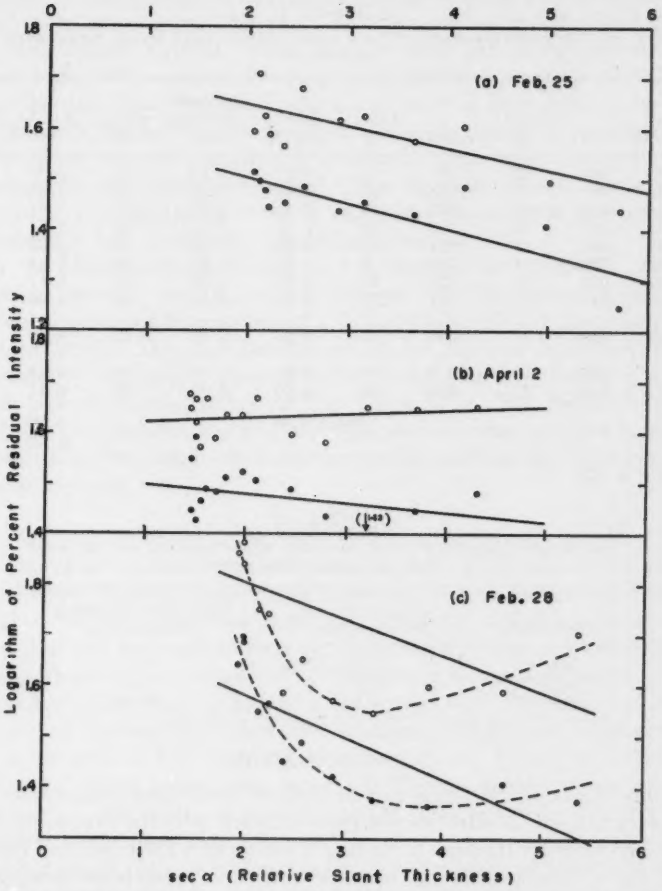

FIG. 3. Examples of complete runs: (*a*) Feb. 25 (good run); (*b*) April 2 (very little absorption); (*c*) Feb. 28 (evidence of sodium "clouds").

terms of layer thickness is discussed in the next section. The result given was derived by giving the D2 line twice the weight of the D1, since it gives twice as strong an absorption. The optical depths and thicknesses are referred to the vertical direction.

On three occasions it was possible to remove the attachment from the spectrometer and move the latter outside in time to get a twilight run. Unfortunately, this was done in such a hurry that there is some uncertainty whether the grating was set in the first or second order, and this affects the intensity calibration by a factor of 0.6. The likeliest results are given in Table II in terms of the thickness derived with no allowance for self-absorption. Along with them are the corresponding thicknesses taken from Table I.

TABLE I

SUMMARY OF EXPERIMENTAL RESULTS (ALL RUNS EXCEPT THAT NOTED WERE MADE IN THE AFTERNOON)

Date (1955–56)	τ_e(D1)	Error, %	τ_e(D2)	Error, %	Ratio D1/D2	Thickness, 10^9 atoms /cm.^{2}	Error, %	p_0(D1), %	p_0(D2), %
Dec. 29	.063	12	.067	17	0.91	7.57	15	6.99	5.26
Dec. 30	.00	*	.033	47	0.00	2.65	20	4.35	4.43
Jan. 10	.049	49	.092	15	0.523	8.89	17	5.81	5.47
Jan. 31	.035	13	.020	31	1.75	3.41	20	6.34	4.88
Feb. 25	.042	12	.051	9	0.82	5.86	10	5.66	5.00
Feb. 26	.052	12	.045	9	1.15	6.05	15	6.38	5.00
Feb. 27	.009	137	.035	45	0.26	2.84	48	5.64	4.86
Feb. 28 (a.m.)	.018	91	.041	25	0.44	3.76	31	5.96	5.10
Feb. 28 (p.m.)	.058	34	.084	19	0.69	9.37	13	6.49	5.74
Apr. 2	−.007	110	.019	46	0.00	1.14	40	5.15	4.61
Apr. 14	−.014	77	.016	39	0.00	0.95	30	6.17	5.33
					Mean 0.59			5.90 ±.46	5.06 ±.24

*Error ±.026.

TABLE II

THICKNESSES DEDUCED FROM TWILIGHT MEASUREMENTS ON THE SAME DAY AS ABSORPTION RUNS

Date (1956)	Twilight thickness, 10^9 atoms/cm.^{2}	Absorption thickness, 10^9 atoms/cm.^{2}
Jan. 9	4.2 or (2.5)	8.9
Feb. 28	3.1	6.6
Apr. 14	1.5	0.95

4. CALIBRATION

Before the layer thickness can be derived from these measurements it is necessary to know the effective absorption coefficient for the Doppler-broadened lines. The value for the peak of the line is well known (Mitchell and Zemansky 1934) but it must be averaged over the whole line. It has been shown recently (Hunten 1956*c*) that in some cases the effective optical depth τ_e is $\tau_0/\sqrt{2}$, where τ_0 is the optical depth at the center of the line; the approximation is good if $\tau_0 < 1$, and this is certainly true here. (The presence of hyperfine structure does not alter this conclusion, since it is based essentially on the area of the absorption line, which is independent of any kind of structure.) However, if the scattering tube had considerable self-absorption so that it accentuated the edges of the lines this result might not be accurate. Therefore it was thought desirable to carry out a calibration in the laboratory.

This was done using the light from the tungsten source after letting it traverse a sodium-vapor absorption cell. The vapor density was varied by varying the temperature in the region between 70° and 100° C. The length of the cell was 10 cm. and it was filled in the same way as the scattering cell. Two separate runs were made in which the measurements were as similar

as possible to those made on the sun; 10 to 20 scans of the spectrum were made at each temperature. The vapor densities were taken from Volume III of the International Critical Tables, and the mean life of the excited state used was 1.60×10^{-8} seconds corresponding to oscillator strengths of 0.33 and 0.65 for the two lines. The logarithms of the relative intensities of the scattered lines were plotted against the thickness of the vapor in the absorption cell; the points showed considerable scatter but they were consistent with the theoretical line already discussed. This result is reasonable since the temperature of the scattering cell was kept fairly low and the effects of self-absorption and line broadening should have been small.

With the theoretical relationship and a temperature of 250° K. for the atmospheric sodium, the relationship between effective optical depth and layer thickness follows from standard relations (Mitchell and Zemansky 1934 or Hunten 1956*b*). The experimental results for the two lines were added and divided by 3, giving a mean effective optical depth τ_1 referred to D1; then the layer thickness (atoms/cm.^{2}) $= 1.78 \times 10^{11}\ \tau_1$. The results are given in Table I. The probable errors given were derived from the errors for the individual lines, but where the two results disagreed greatly the error was sometimes increased.

5. DISCUSSION

It is first of all necessary to show proof that the effect observed is indeed due to sodium. There is little doubt that some atmospheric constituent is responsible; the only other one likely is water vapor, which has many lines in the yellow and particularly near D2. It is possible that the wings of one or more of these might overlap the wavelengths observed sufficiently to give a measurable absorption, as has been suggested in a different connection by Bricard and Kastler (1944). However, it is most unlikely that the absorption at the wavelength of D2 would be twice that at D1, as is true of sodium. While the individual results vary widely, as Table I shows, on the average D1 is absorbed 0.59 times as strongly as D2. This is satisfactory evidence that sodium is the absorbing agent.

A much stronger piece of evidence is found in the seasonal variation, which is just opposite for sodium and water vapor. The twilight results reported by Hunten (1956*a*) are shown in Fig. 4. The layer thickness remains large from December to March, but drops to less than half in April. On the other hand, the amount of water vapor in the atmosphere probably increased by a factor of 25 for the two April runs when compared with the others. This is based on the fact that the winter runs were made on days whose temperatures were in the range from $-35°$ to $-12°$ C., while the temperature for the April runs was above freezing. It can be seen from Table I and Fig. 4 that the absorption follows the sodium thickness very well, and behaves in a manner incompatible with the idea that water vapor is the absorber.

A detailed comparison of the absorption results with twilight ones can be made with the aid of Fig. 4. The twilight intensities have been converted to thicknesses without allowing for self-absorption, using the factor given by

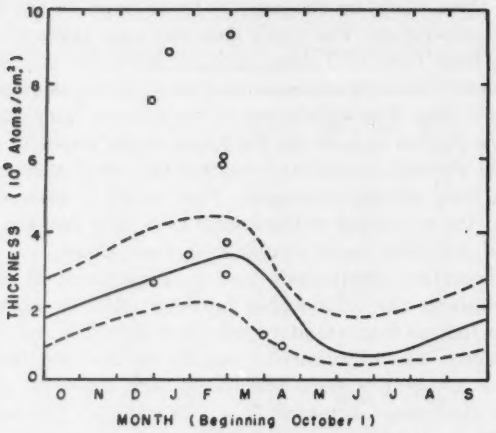

FIG. 4. Present results compared with those from twilight. No allowance for self-absorption has been made in the latter. The dashed lines give the limits between which all the twilight points fall, and the solid line gives the average.

Hunten (1956*a*); the results themselves are from the same paper. About half the winter results agree well with twilight, but the other half are higher by nearly a factor 2, showing the effect of self-absorption on the twilight. However, the effect is much less than is predicted* (references in Section 1). The two results for April agree well with the twilight; they are a bit lower but no more than is expected from the errors of measurement. It can be concluded that self-absorption has a negligible effect on twilight measurements except in winter when the sodium layer is thickest. Even then the correction does not exceed a factor of 2. The three occasions when twilight runs were obtained on the same day give similar results (Table II). Again, there is indication of self-absorption by a factor less than 2 in winter and fair agreement in April.

The average values of p_0, the residual intensity of the Fraunhofer line, are given in Table III along with others previously found for the whole sun.

TABLE III

RESIDUAL INTENSITIES OF THE TWO FRAUNHOFER LINES (PER CENT)

Line	Present result	Priester (1953)	Old result (1955)
D1	5.90±.46	6.6	5.0 ±0.6
D2	5.06±.24	5.8	4.8 ±0.6
Ratio	0.86±.085	0.88	0.96±.18

The method of averaging Priester's results (1953) is briefly described by

*Since this statement was written, J. E. Mack has pointed out that the hyperfine structure of the D lines cannot be neglected in the calculations of self-absorption, though it has no effect on the present measurements. Preliminary estimates show that the calculated self-absorption will now agree very well with the results observed here.

Scrimger and Hunten (1955), and the other result is taken from the same paper. Our new results are a little higher than our old ones, but still well below Priester's. Since there is no apparent reason to expect systematic errors in the method, we feel that the new result is the best available for the interpretation of twilight measurements. The ratio of the two residual intensities is an important quantity also in twilight work, and the agreement here with Priester is very good. The intensity ratio of the D lines in twilight can thus not exceed $1.72 \pm .17$; self-absorption will usually lower it still further.

The two runs of which Fig. 3(*c*) is one are interesting in that they appear to show a non-uniform geographical distribution of sodium over distances of the order of a few hundred to a thousand kilometers. On the other hand, the other nine runs suggest that the distribution is more often fairly uniform over such distances. The possibility of a patchy distribution of sodium results in an inherent error in our method of finding the layer thickness, but on most days this error seems to be less than that caused by a not very large signal-to-noise ratio. The noise is largely shot noise in the photocurrent, but probably variations in the atmosphere contribute too. Non-uniform distributions of the intensity of the night airglow are usually observed and may perhaps be related to those found here; Roach has given an excellent review of the work of his group in this field (1955).

We would like to thank G. F. Lyon for help with the apparatus and measurements.

REFERENCES

BRICARD, J. and KASTLER, A. 1944. Ann. géophys. **1**, 53.
CHAMBERLAIN, J. W. 1956. J. Atm. and Terrest. Phys. **9**, 73.
DONAHUE, T. M., RESNICK, R., and STULL, V. R. 1956. Phys. Rev. **104**, 873.
HARRISON, A. W. and VALLANCE JONES, A. 1956. The airglow and the aurorae, *edited by* E. B. Armstrong and A. Dalgarno (The Pergamon Press, Ltd., London), p. 95.
HUNTEN, D. M. 1953. Can. J. Phys. **31**, 681.
——— 1956*a*. The airglow and the aurorae, *edited by* E. B. Amstrong and A. Dalgarno (The Pergamon Press, Ltd., London), p. 114.
——— 1956*b*. *Ibid.*, p. 183.
——— 1956*c*. J. Atm. and Terrest. Phys. **9**, 179.
HUNTEN, D. M. and SHEPHERD, G. G. 1954. J. Atm. and Terrest. Phys. **5**, 57.
MITCHELL, A. C. G. and ZEMANSKY, M. W. 1934. Resonance radiation and excited atoms (Cambridge University Press, London).
SANFORD, R. F. 1950. Publs. Astron. Soc. Pacific, **62**, 272.
SCRIMGER, J. A. and HUNTEN, D. M. 1955. Can. J. Phys. **33**, 780.
——— 1956. Nature, **178**, 753.
PRIESTER, W. 1953. Z. Astrophys. **32**, 200.
ROACH, F. E. 1955. Ann. géophys. **11**, 214.

IONIZATION CURRENTS IN ARGON AND HELIUM LIQUIDS[1]

R. L. WILLIAMS[2] AND F. D. STACEY[3]

ABSTRACT

Ionization currents in alpha-irradiated argon and helium I and II liquids have been measured over an electric field range of 10^5:1, and conduction pulse amplitude distributions have been measured over a 300:1 range of applied field. A critical examination of theories of ionic recombination shows that they are unable to explain the results of the present experiment, and a new approach to the problem of columnar recombination is suggested.

I. INTRODUCTION

Jaffé (1913) produced the first theory of recombination in columns of ions, and showed that it agreed with his own experimental data on ionization currents, but the value of this agreement is limited by the fact that the currents were near to saturation, having a 2:1 variation over an electric field range of 100:1. The theory described ionizable media in which the positive and negative ions had equal masses and was applied to carbon dioxide, air, and hydrogen gases and methane and hexane liquids, with which Jaffé experimented.

Gerritsen's (1948) measurements of ionization currents in alpha-irradiated liquids gave reasonable agreement with Jaffé's theory for nitrogen and hydrogen, but not for argon and helium, in which the currents were found to be much more strongly field-dependent. Somewhat better agreement for argon and helium was obtained with Kramers' (1952) modification of the Jaffé theory. Ionization current experiments on gaseous argon, helium, nitrogen, oxygen, and carbon dioxide by Haeberli, Huber, and Baldinger (1953) gave agreement with Jaffe's theory over a limited range of field.

From the pulse experiments performed by Davidson and Larsh (1950), the number of electrons, n, escaping from alpha particle tracks in liquid argon was estimated as a function of applied electric field. The range of field was only 7:1 and their questionable correction for electronic noise prevented satisfactory analysis.

A considerable improvement in signal-to-noise ratio has been obtained in the present experiments on argon and helium liquids. Pulse size distributions which are explicable in terms of the geometry of the ionization chamber have been measured, the variation of pulse size with field being in good agreement with the observed ionization currents. An extension of the field range of ionization current measurements to 10^5:1 shows that the Jaffé–Kramers model for columnar recombination is not applicable to liquid argon or liquid helium.

[1]Manuscript received March 11, 1957.
Contribution from the Department of Physics, University of British Columbia, Vancouver, B.C.
[2]Now at C.A.R.D.E., Valcartier, Quebec.
[3]Now at the Geophysics Department, Australian National University, Canberra, Australia.

2. THEORY OF COLUMNAR RECOMBINATION

Jaffé's (1913) theory applied to the dense columns of ionization formed by alpha particles in materials with electron affinities, in which the positive and negative ions were assumed to have roughly equal masses, mobilities, and diffusion coefficients and initially to have the same Gaussian density distribution of standard deviation b about the particle track.

This distribution was modified by diffusion, transport of ions due to an applied field, E, and the removal of ions by recombination. Jaffé solved the resulting differential equation by first neglecting recombination and then correcting for it, so that of n_0 ions originally present n finally escape:

$$\frac{n}{n_0} = 1 \Big/ \left[1 + \frac{\alpha n_0}{8\pi D} \left\{ \frac{i\pi}{2} \exp\left(\frac{Z}{2}\right) . H_0^1\left(\frac{iZ}{2}\right) \right\} \right] \tag{1}$$

where $$Z = \frac{b^2 \mu^2 E^2 \sin^2\theta}{2D^2}.$$

In these expressions H_0^1 is the Hankel function of the first kind, of order zero, α is the coefficient of ionic recombination, D is the diffusion coefficient for both positive and negative ions, μ their mobility, θ is the angle between the direction of the applied field and the particle track, and i is $\sqrt{-1}$. For high fields ($Z \gg 1$) and low fields ($Z \ll 1$) equation (1) reduces to:

$$Z \gg 1: \quad \frac{n}{n_0} = 1 \Big/ \left(1 + \frac{\alpha n_0}{4\sqrt{2\pi}\, b\mu E \sin\theta} \right), \tag{2}$$

$$Z \ll 1: \quad \frac{n}{n_0} = 1 \Big/ \left[1 + \frac{\alpha n_0}{8\pi D} \ln\left(\frac{2.25}{Z}\right) \right]. \tag{3}$$

Kramers' (1952) solution of Jaffé's differential equation for ionic density was obtained by including the recombination term but neglecting diffusion. For high fields it gives equation (2) and for low fields:

$$\frac{n}{n_0} = \frac{Eb}{6\sqrt{\pi}\, en_0} \left(\ln\left(\frac{16ge^2 n_0}{KT}\right) \right)^{3/2} \tag{4}$$

where g is a numerical factor near to unity.

3. EXPERIMENTATION

The electrode assembly was essentially that described by Williams (1957), except that a grounded metal ring separated the bakelite supports of the two electrodes. With a grounded ring of silver paint surrounding the signal lead on the outside of the glass envelope, this completely prevented any leakage from the high voltage element to the signal electrode (except through the liquid between the electrodes). The observation of signals smaller than those used in the mobility measurements of Williams (1957) necessitated further smoothing of the high voltage supply with screened resistance-capacity filters.

Ionization currents were measured with a vibrating reed electrometer, driving a recorder. The average number n_a of electrons escaping recombination

per alpha particle was determined from the ionization currents, I, and the source strength, N_T particles per second (measured by pulse counting experiments), since

$$I = N_T n_a e,$$

e being the electronic charge.

Conduction pulses were measured with an amplifier of selected bandwidth, followed by a discriminator and counter. The collection of n ions, due to a single alpha particle, on the input capacity, C, of the amplifier was complete in a time short compared with the input RC time constant and produced a voltage pulse with a sharp rise to an amplitude ne/C. The pulse decay was controlled by the input time constant. Thus the full pulse amplitude was observed with an amplifier of restricted bandwidth, the pulse shape being of no interest in these experiments. The advantage of this restriction of bandwidth is in the reduction of noise level, for which optimum conditions were obtained with a bandwidth of 20 kc. to 200 kc.

Estimation of noise level and calibration of the pulse amplitude measurements were made by connecting a pulse generator to the amplifier input through a resistance large compared with the input resistance. As this arrangement was the same as the conditions of operation, it allowed the effect of amplifier noise on pulse amplitude distributions to be investigated. Theory relevant to this is given in the appendix.

4. PULSE SIZE DISTRIBUTIONS

Wadey (1948) showed that alpha particles from sources deposited on silver in the manner of the present experiments suffer very little straggling in energy. It is therefore assumed that the pulse amplitude distributions observed in the present experiments were due to differences in geometry and recombination between the tracks of alpha particles at different angles to the applied field, being modified by electronic noise.

The geometrical effect arises from the difference between the positive and negative ion mobilities observed in liquid argon by Williams (1957). The positive ions were too slow to contribute materially to the pulses observed in the present experiments, so that the angle, ϕ, between the alpha particle track and the source electrode determined the average fraction of the electrode separation, d, traversed by the electrons and therefore the apparent charge collection per pulse $n_{\text{eff}}e$, for n electrons actually collected.

For the source electrode negative this is expressed by:

$$\frac{n_{\text{eff}}}{n} = 1 - \frac{3}{5}\frac{R_\alpha}{d}\sin\phi, \tag{5}$$

where R_α is the range of the alpha particles, being less than d. Equation (5) applies to an ion column whose weighted center is at $\frac{3}{5}R_\alpha$ from the source as in the Bragg law (Wilkinson 1950). The ranges of polonium (5.3 Mev.) alpha particles in liquid argon and liquid helium are calculated from the ranges in the gases to be 0.052 mm. in argon and 0.27 mm. in helium. Anianson's (1955)

measurements of alpha particle ranges in liquids confirm that the inverse proportionality of range and density extends to the liquid region.

If N_T alpha particles are emitted isotropically into a hemisphere centered at the source, then the number N emitted at ϕ or smaller angles to the electrode surface is $N_T \sin \phi$. Combined with equation (5) to eliminate ϕ, this gives the pulse amplitude distribution:

$$Q = \frac{N}{N_T} = \frac{5}{3}\frac{d}{R_\alpha}\left(1 - \frac{n_{ett}}{n}\right). \tag{6}$$

For a reversed field (source electrode positive), equations (5) and (6) become:

$$\frac{n_{ett}}{n} = \frac{3}{5}\frac{R_\alpha}{d}\sin\phi\,, \tag{5'}$$

$$Q = \frac{N}{N_T} = \frac{5}{3}\frac{d}{R_\alpha}\frac{n_{ett}}{n}. \tag{6'}$$

The superposition of noise peaks whose amplitudes are described by a Gaussian distribution on pulses having a rectangular distribution is indicated qualitatively in Fig. 1(*a*), the cumulative probability, $Q = N/N_T$, being given in Fig. 1(*b*). It is shown in the appendix that if an observed pulse amplitude distribution can be approximated to the signal-plus-noise curves of Fig. 1,

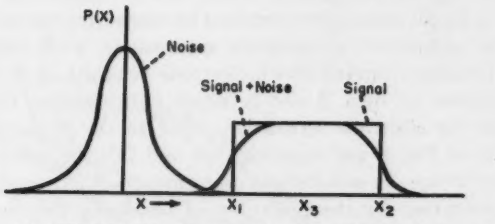

(a) PROBABILITY OF PULSES OF AMPLITUDE X vs X

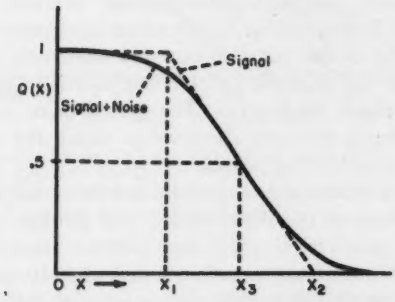

(b) PROBABILITY OF PULSES OF AMPLITUDE X OR GREATER vs X

FIG. 1. The effect of Gaussian noise on a "rectangular" pulse amplitude distribution.

then the minimum, maximum, and average values of pulse size, X_1, X_2, X_3, for the distribution in the absence of noise are readily determined. When the apparatus has been calibrated the X's correspond to minimum, maximum, and average values, n_1, n_2, n_3, of n_{ett}. From the above geometrical considerations, with the source electrode negative

$$X_1 : X_2 : X_3 = \left(1 - \frac{3}{5}\frac{R_\alpha}{d}\right) : \left(1 - \frac{3}{10}\frac{R_\alpha}{d}\right) : 1$$

and with the source electrode positive

$$X_1 : X_2 : X_3 = 0 : \frac{3}{10}\frac{R}{d} : \frac{3}{5}\frac{R}{d}.$$

Further considerations of the effect of noise on pulse amplitude distributions are given in the appendix, including a possible interpretation of results obtained by Davidson and Larsh (1950).

Deviations of the pulse amplitude distributions from the simple addition of noise to the geometrical effect indicate different degrees of recombination in particle tracks at different angles to the electrodes. Some evidence of the effect of angle upon recombination is presented in Section 5.

5. EXPERIMENTAL RESULTS

Demonstration of the geometrical effect and a measure of the range of alpha particles in liquid argon were obtained by measuring the pulse amplitude distributions for a number of electrode separations, with both field directions. The distributions obtained with electrode separations of 0.20 mm. and 0.060 mm. are given in Figs. 2 and 3, which indicate that the geometrical effect is greatest for electrode separations close to the alpha particle range. From the results of Fig. 3 and equations (6) and (6′) the value 0.049 mm. is obtained for the range, in satisfactory agreement with the calculated value 0.052 mm. Justification for the procedure of idealizing the curves of Fig. 3 to straight lines in conformity with equations (6) and (6′) and Fig. 1(*b*) is given in the appendix.

The plot of pulse amplitude distributions obtained with an electrode spacing of 0.2 mm. in argon (Fig. 2), for which the geometrical effect is small, shows that the form of the distributions was essentially independent of field and therefore that the dependence of recombination upon angle was not a function of field above 13 kv./cm. The pulses were well above the noise level, the largest being 80 times the level at which the noise pulses were as numerous as alpha particle emissions.

The ratios of the minimum to maximum pulse amplitudes, X_1/X_2, determined from the slope of the distributions and plotted in Fig. 4, have been corrected for the geometrical effect and indicate recombination differences. That this ratio has an almost constant value near to unity for fields above 20 kv./cm. indicates that recombination is not significantly dependent upon the angle between the track and the field, for fields above this value.

Confirmation is given by a comparison of pulse sizes with ionization current, as in Fig. 5, of which the dotted line represents the current calculated from the

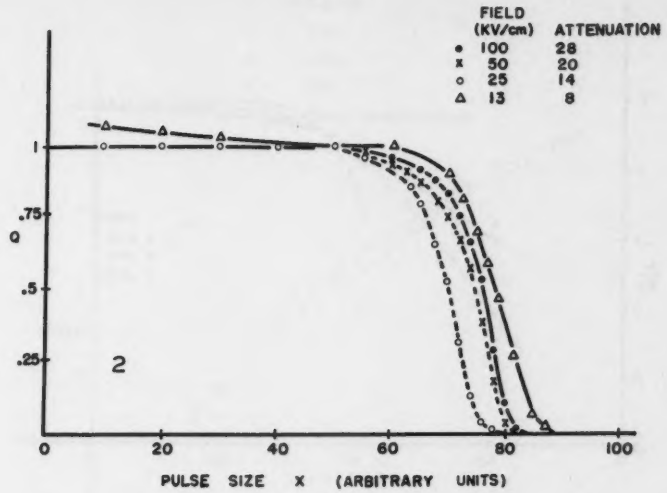

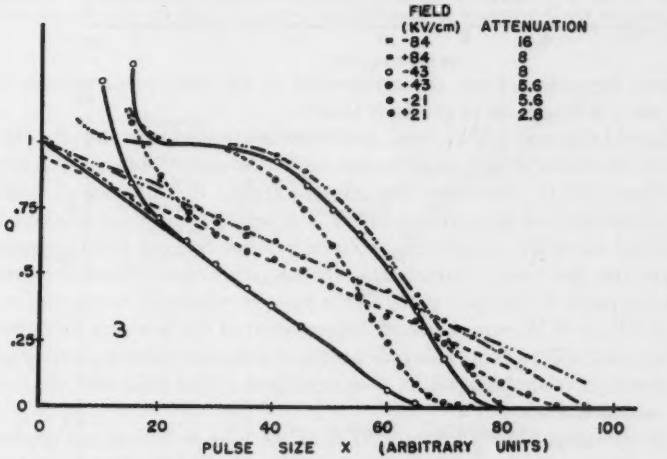

FIG. 2. Pulse amplitude distribution in argon with a small range effect. Electrode spacing = 0.20 mm. Q = fraction of pulses of amplitude X or greater.

FIG. 3. Pulse amplitude distribution in argon with a large range effect. Electrode spacing = 0.060 mm. Q = fraction of pulses of amplitude X or greater.

pulse measurements by correction for the geometrical effect but not the recombination effect. The departure of the dotted line from the direct current results at low fields is attributed to recombination differences which cause similar discrepancies between curves obtained by pulse measurements at different electrode separations. The discrepancies are consistent with ionic

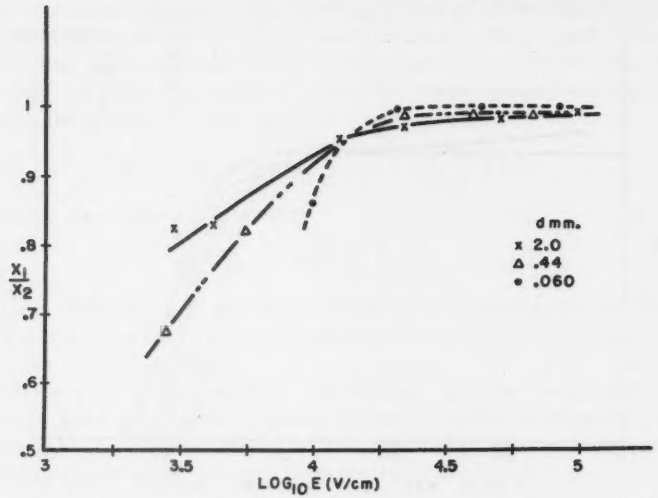

FIG. 4. Ratio of minimum to maximum pulse sizes in argon, indicating the variation with applied field of the dependence of recombination upon the angle between the particle track and the field.

collection dependent upon the component of the field perpendicular to the alpha particle tracks, as in the Jaffé theory.

In liquid helium at 4.2° K. ionic mobilities are much lower than for electrons in argon, the positive and negative ion mobilities only differing by a factor of 4 (Williams 1957). This had two effects: firstly, the absence of a distinct geometrical effect of separated positive and negative ion contributions to the pulses, and secondly, longer ionic collection time. Since it was not possible to separate the two ionic components, the amplifier was adjusted to respond equally to both. A constant value of the ratio of minimum to maximum pulse sizes, $X_1/X_2 = 0.53$, was obtained, independent of the field, for fields between 7 kv./cm. and 105 kv./cm. This indicates that although there is a strong angular dependence of recombination, it is independent of the field over the range of these measurements.

At lower temperatures the mobilities of the ions in helium are greater and more nearly equal, certainly eliminating the geometrical effect. All measurements down to 1.4° K. gave the same values of X_1/X_2 as at 4.2° K.

Fig. 6 gives the values of mean ionic collection per alpha particle for both ionization current and pulse measurements in helium. It is unlikely that the difference between the 4.2° K. curve and the 1.6° K. and 1.4° K. values is significant, so that the recombination of ions appears to be identical in helium I and II.

If the values of energy per ion pair for alpha-ionization of gaseous argon and helium, given by Bortner and Hurst (1954), are applicable to the liquids, the ionization currents were about half saturated at the highest fields used

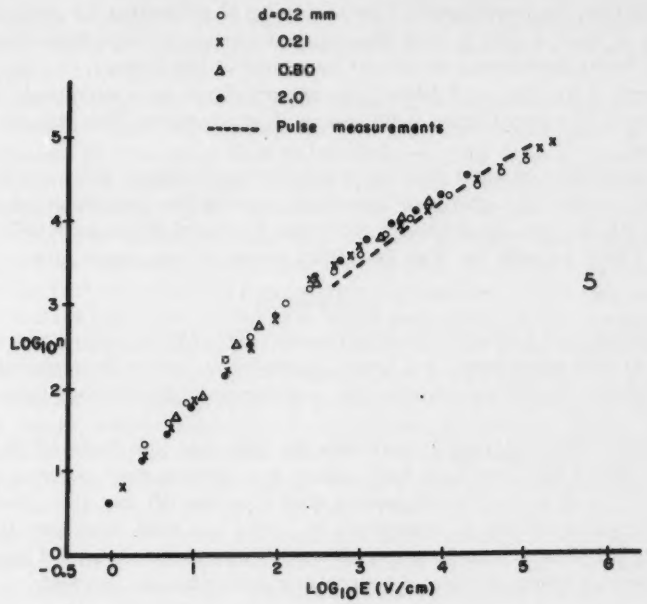

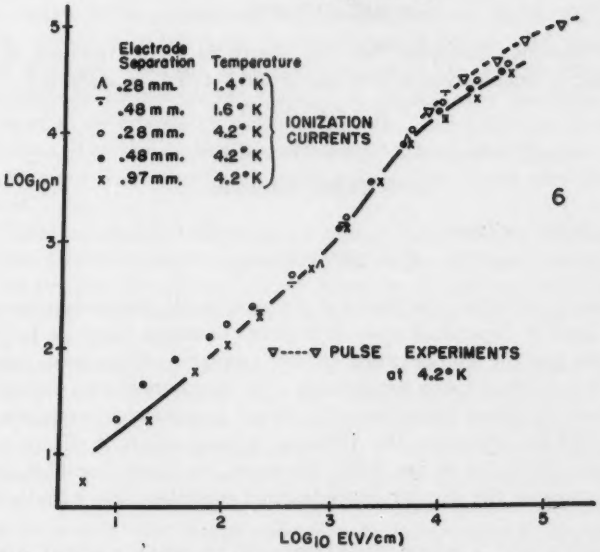

FIG. 5. The average number of ions collected per alpha particle in argon as a function of the applied field.

FIG. 6. The average number of ions collected per alpha particle in helium as a function of the applied field.

(being limited by breakdown). The beginning of saturation for both liquids appears in Figs. 5 and 6, both showing a departure at high fields from the roughly linear dependence of current upon field at low fields.

Between 1 kv./cm. and 10 kv./cm. helium shows an anomalously strong dependence of current upon field, not evident in argon. This has not been explained.

The possibility of some electron multiplication in argon must not be disregarded, as the r.m.s. energy of free electrons in liquid argon under an applied field of 100 kv./cm. is estimated from the results of Williams (1957) to be 20 ev., which exceeds the first ionization energy of the argon atom.

6. DISCUSSION

The theories of Jaffé (1913) and Kramers (1952) can be compared with the results of this experiment, but good agreement is not to be expected since these theories clearly assume that the positive and negative ions have equal masses.

An examination of Jaffé's conditions for high and low fields ($Z \gg 1$ and $Z \ll 1$) shows that the high field region was inadequately covered in the results of Fig. 4 to permit comparison with equation (2), but that the linear, low field region of Fig. 5 corresponds to Jaffé's low field condition. By substituting the Einstein relationship $\mu/D = e/kT$ into the formula for Z (equation (1)), inserting known values, and expressing E in volts/cm., we find:

$$Z = 0.83 \times 10^4 . b^2 E^2.$$

Jaffé and Kramers assumed that the length of an ion column is about $1000b$, so that in liquid argon b is of the order 5×10^{-6} cm., giving:

$$Z = 2.1 \times 10^{-7} E^2$$

from which we may take as the high field condition

$$E > 20{,}000 \text{ volts/cm.}$$

and the low field condition

$$E < 200 \text{ volts/cm.}$$

Fig. 5 shows that, within the limits of the experiment, the ionization current in argon is linearly dependent upon field over the entire range of Jaffé's low field condition, but the simplification of Jaffé's equation of low fields (equation (3)) does not indicate a linear relationship. The Kramers theory does give the required linear variation (equation (4)), which is somewhat surprising since it was obtained by neglecting the diffusion of ions, which, if effective at all, must be most noticeable at low fields. However, the Jaffé formulae give the observed decrease in the angular dependence of recombination with increasing field.

Both theories give a strong dependence of ionization current upon the ionic mobility and/or diffusion coefficient. There was no test for this in the argon experiments since there was no method of varying the mobility independently of the field, but changes of temperature in the helium experiments

gave changes of mobility by a factor of about 4. That the ionization currents were observed to be independent of temperature is therefore evidence against the validity of the theories.

The greatest objection to the Jaffé theory is in its mechanism for charge separation. In liquid argon about 10^5 ion pairs per alpha particle escape recombination in an applied field of 10^5 volts/cm. The Jaffé–Kramers model thus requires the applied field to pull apart two cylinders of charge with linear charge density 2×10^7 ions/cm. (the length of the cylinders being 5×10^{-3} cm.). The applied field can only compete favorably with the mutually attractive force between such cylinders when they are already separated by at least 4×10^{-5} cm., which is greater than the diameter which they are considered to have (10^{-5} cm.), so that the initial separation remains unexplained.

That the electrons released by the ionization of liquid argon do not combine with neutral atoms to form heavy negative ions is well established (Williams 1957). This leads to a suggestion for a new model of ionic escape from alpha particle tracks, which makes use of calculations by Erskine (1954).

Erskine showed that electrons ejected from atoms near the track of an alpha particle are given higher kinetic energies than those from atoms at the edge of the column of initial ionization. They are attracted towards the alpha particle and emerge on the other side of the track in a direction almost perpendicular to it. (δ-Rays observed by Auger (1926) and Chadwick and Emeleus (1926) are the most energetic of such electrons.) Since the same process occurs simultaneously for many electrons, an expanding cylinder of charge is formed, with the outer electrons moving fastest, and therefore being partially screened from the inward attraction of the positive charges, which for this purpose are considered stationary. In this way the faster electrons, which have more chance of escaping anyway, are held less firmly by the positive ions. The size of the initial column of ionization hardly affects this argument, since if it is only one atom across, the fastest electrons are still outermost.

The initial expansion of the negative charge cloud does not constitute escape of the fast electrons since they will suffer many collisions before becoming free of the positive ion column; it does, however, provide a possible mechanism for overcoming the potential energy which would hold together two ion columns of the Jaffé type.

Subsequent motion of the electrons is not as easily described, but kinetic theory (Williams 1957) shows that they lose their kinetic energy only after many collisions, by which time they may have moved to the side of the charge cloud which is favorable to their escape in an externally applied field.

Ionic escape is more effective in fields perpendicular to the ion column than in fields parallel to it, leading to an angular dependence as in the Jaffé theory.

The requirement that charge collection be independent of temperature or mobility is satisfied by this model.

ACKNOWLEDGMENTS

This work was financed by the Defence Research Board of Canada under

Grant No. 1680–12. We are grateful for the advice and assistance of the Low Temperature group at the University of British Columbia, which was invaluable in the helium experiments, and to Professor R. E. Burgess for discussions, particularly with regard to electronic noise.

APPENDIX. NOISE CONSIDERATIONS

The noise voltage of any electronic system has been shown by Rice (1944) to have Gaussian fluctuations. The probability of the noise voltage being between x and $(x+dx)$ at any instant is

$$P(X)\,dx = \frac{1}{\sqrt{2\pi}\sigma} \exp - \frac{X^2}{2\sigma^2}\,dx, \tag{7}$$

where σ is the standard deviation of the noise voltage. This is also the form of the probability of noise peaks having amplitudes between X and $(X+dX)$.

The superposition of random fluctuations (noise) on a series of pulses all of the same amplitude, X_3, produces a distribution with a cumulative probability of having amplitude X or greater of

$$Q(X) = \frac{1}{2}\left[1-\operatorname{erf}\left(\frac{X-X_3}{2\sigma}\right)\right], \tag{8}$$

where

$$\operatorname{erf}(t) = \frac{2}{\sqrt{\pi}}\int_0^t \exp(-u^2)du.$$

Plotted against X on cumulative probability paper, $Q(X)$ appears as a straight line, the gradient of which is determined by σ.

A check that this distribution was realized was obtained by plotting on cumulative probability paper the pulse amplitude distribution obtained by the superposition of noise on a series of uniform pulses from a signal generator. The straight line which resulted gave the standard deviation of the noise pulses.

The superposition of Gaussian noise on a "rectangular" pulse distribution:

$$P(X) = 1/D \text{ for } X_1 \leqslant X \leqslant X_2,$$
$$P(X) = 0 \text{ for } X < X_1 \text{ and } X > X_2,$$

where $D = (X_2-X_1)$, yields the distribution

$$P(X)dx = \frac{1}{2D}\left[\operatorname{erf}\left(\frac{X_2-X}{\sqrt{2}\sigma}\right) - \operatorname{erf}\left(\frac{X_1-X}{\sqrt{2}\sigma}\right)\right]dx, \tag{9}$$

which is indicated in Fig. 1(*a*) and integrates to the cumulative distribution:

$$Q(X) = \frac{1}{2} + \frac{1}{2D}\left[(X_2-X)\operatorname{erf}\frac{X_2-X}{\sqrt{2}\sigma} - (X_1-X)\operatorname{erf}\frac{X_1-X}{\sqrt{2}\sigma}\right] + \frac{1}{\sqrt{2\pi}\,D}\left[\exp\left(-\frac{(X_1-X)^2}{2\sigma^2}\right) - \exp\left(-\frac{(X_2-X)^2}{2\sigma^2}\right)\right], \tag{10}$$

which is shown in Fig. 1(*b*).

The condition $Q(X_3+\delta)+Q(X_3-\delta) = 1$ indicates symmetry about ($X = X_3$, $Q = \frac{1}{2}$), so that $(X_2-X_1) = 2X_3$ as in Fig. 1(*b*) and

$$P(X_3) = \frac{1}{D}\operatorname{erf}\frac{D}{\sqrt{8}\sigma} = \frac{d}{dX}(Q(X))\Big|_{Q=\frac{1}{2}}.$$

If the standard deviation, σ, of the noise is known, D and hence X_1 and X_2 can be determined.

A necessary condition for this analysis to apply to the pulse amplitude distributions described was their symmetry. Unsymmetrical distributions cannot be treated in this way, but if the departure from symmetry is not great, as was the case with all the measured distributions, the approximation is quite good.

For large signal-to-noise ratios the noise correction is particularly simple since the gradient of $Q(X)$ (equal to $P(X)$) at $Q(X_3) = \frac{1}{2}$ is $(1/D)\operatorname{erf}(D/\sqrt{8}\sigma)$, which for $D/\sqrt{8}\sigma \geqslant 1.5$ is equal to $1/D$ within 2%. D was thus determined graphically as indicated in Fig. 1(*b*) by extending the tangent to $Q(X)$ at ($Q = \frac{1}{2}$, $X = X_3$) to ($Q = 0$, $X = X_2$) and ($Q = 1$, $X = X_1$). This simplified correction was not applied to results which gave a small value of D/σ.

Two further effects of noise must be considered. Rice (1944) showed that the number of noise peaks per second exceeding amplitude V (greater than σ) is

$$n_p = \left[\frac{1}{3}\frac{f_2^3-f_1^3}{f_2-f_1}\right]^{\frac{1}{2}} \exp\left(-\frac{V^2}{2\sigma^2}\right) \doteq \frac{f_2}{\sqrt{3}}\exp\left(-\frac{V^2}{2\sigma^2}\right), \tag{11}$$

where f_2 and f_1 are the upper and lower frequency limits of the amplifier bandpass. The rate of emission of alpha particles from the source was 500/sec. By equation (10), noise peaks of 3.6σ or greater occur at this rate in an amplifier with a bandpass of 2×10^5 cycles/sec. (as used in these experiments), so that pulses smaller than about 4σ were lost in the noise.

In addition to their modification of pulse sizes, noise peaks appeared on the distributions on their own account, and their amplitude distribution was determined in an experiment with no alpha-induced pulses. This distribution was subtracted from each of the pulse amplitude distributions as the first process of noise correction, but only affected the smaller pulses.

As a demonstration that the noise peaks seen by the discriminator were described by equation (10), $\ln(n_p)$ was plotted against V^2 producing a straight line, of which the gradient gave a value of σ in agreement with that found from equation (7).

The last effect is that of noise peaks superimposed upon the tails of pulses, and may be regarded as a correction to the assumption that only one noise peak could affect each pulse. The bandwidth of the amplifier could not be indefinitely restricted without affecting the pulse amplitudes, so that the pulses did not completely decay within the dead-time of the discriminator. This allowed noise peaks too small to be counted alone to exceed the discrimination level by superposition on the pulse tails. Since the smaller noise peaks were much more numerous than those capable of being counted alone,

this was a significant effect in experiments with poor signal-to-noise ratios. No adequate correction has been found for it, but it was found to be negligible for signals exceeding 6 times the standard deviation of the noise peaks. Measurements were made over a 300:1 range of field without using pulses smaller than this.

In the work of Davidson and Larsh (1950) the largest signals were approximately 4 times the noise level, which appears to have been taken as the level at which noise pulses and signal pulses were equally numerous. According to the above discussion "tail note" would have become important for signal-to-noise ratios (defined in this way) of about 2:1. Davidson and Larsh noted that the distribution of pulse amplitudes became much sharper when the signal-to-noise ratio was less than 2:1, and this appears to have been a modification by "tail noise" which caused double counting of pulses. In the present experiments, the lower noise level made it possible to avoid this region.

REFERENCES

ANIANSON, G. 1955. Phys. Rev. **98**, 300.
AUGER, F. 1926. J. phys. (Ser. 6), **7**, 65.
BORTNER, J. E. and HURST, G. S. 1954. Phys. Rev. **93**, 1236.
CHADWICK, J. and EMELEUS, K. G. 1926. Phil. Mag. (Ser. 7), **1**, 1.
DAVIDSON, N. and LARSH, A. E. 1950. Phys. Rev. **77**, 706.
ERSKINE, G. A. 1954. Proc. Roy. Soc. (London), A, **66**, 224.
GERRITSEN, A. N. 1948. Physica, **14**, 381, 407.
HAEBERLI, W., HUBER, P., and BALDINGER, E. 1953. Helv. Phys. Acta, **26**, 145.
JAFFÉ, G. 1913. Ann. Physik, **42**, 303.
KRAMERS, H. A. 1952. Physica, **18**, 665.
RICE, S. O. 1944. Bell System Tech. J. **23**, 282.
WADEY, W. G. 1948. Phys. Rev. **74**, 1846.
WILKINSON, D. H. 1950. Ionization chambers and counters (Cambridge University Press), p. 71.
WILLIAMS, R. L. 1957. Can. J. Phys. **35**, 134.

THE DECAY OF THE POPULATIONS OF METASTABLE ATOMS AND IONS FROM THE SAME D-C. DISCHARGE IN NEON[1]

B. C. BLEVIS,[2] J. M. ANDERSON, AND R. W. MCKAY

ABSTRACT

Measurements of electron density and of the population of the $^3P_2$ metastable state have been made following cessation of a d-c. discharge in neon gas. Determinations of these populations were made under identical conditions at accurately determined times after termination of the discharge and decay curves were plotted for a pressure range from 0.5 to 12.0 mm. Hg. At low pressures, where diffusion is the principal factor in the decay, both curves are exponential and show the same mean life within the limits of error. Values of the diffusion constants obtained from these curves are consistent with the results of previous workers in both fields. At higher pressures the metastable decay remains exponential while the reciprocal of the electron population changes linearly with time. In general, the two decays are unrelated. Only at the highest pressure studied, and in this case for only the first half millisecond, was a measurable effect of positive ion recombination found in the metastable population curve.

INTRODUCTION

Accurate measurements of the decay of the populations of the levels of the $2p^5 3s$ configuration of neon were made at the University of Toronto by D. J. Eckl (1951, 1953) following cessation of a d-c. discharge in the gas at low pressure. The decay of the population of the $^3P_2$ state was found to be exponential in agreement with existing theory. On the other hand it was shown that the decay of the population of the $^3P_0$ state could be represented as the sum of two exponential terms. The population of the $^3P_1$ non-metastable state was found to be measurable and to behave in a similar manner to that of the $^3P_0$ state, while that of the non-metastable $^1P_1$ state was too small to be followed accurately. No form of interchange of populations between the four levels seemed to offer a satisfactory explanation for the double exponential decay curves of the $^3P_0$ and $^3P_1$ states.

It seems possible that the decay curves of the populations of these states might be affected by either the lifetime of imprisoned resonance radiation, or by the presence and recombination of positive ions and electrons. The present work was undertaken to investigate the latter of these, in particular to measure under identical conditions in the same gas the decay of the population of positive ions and of the metastable states. These measurements are made possible by the recent development of techniques for the accurate determination of free electron populations at selected times after the cessation of the discharge producing them. These methods are described by Biondi (1951) and others. The measurements on imprisoned resonance radiation require the development of special apparatus. This development is in progress but results have not yet been obtained.

[1]Manuscript received in original form September 6, 1956, and, as revised, May 13, 1957. Contribution from Department of Physics, University of Toronto, Toronto, Ontario.

[2]Holder of a National Research Council Studentship, 1954–1956.

Present address: Defence Research Telecommunications Establishment, Defence Research Board, Shirley Bay, Ottawa, Canada.

METHOD

Under suitable conditions (see, for example, Eckl 1953) metastable atoms revert to lower levels either by diffusion to the walls and electrodes or by collision with another particle in the gas. The rate of the first of these processes is inversely proportional to pressure, while that of the second is directly proportional to pressure. Three-body collisions of one metastable atom with two normal atoms would occur at a rate proportional to the square of the pressure. Such a process has not been found to occur at an appreciable rate in inert gases at room temperature (Phelps and Molnar 1953). Theory based on the two processes of reversion above, largely due to Zemansky (1929), predicts that the decay of population of a metastable state should be exponential and of the form

$$n = n_0 \exp(-t/\tau),$$

where n is the density of metastable atoms, n_0 the initial density, t the time, and τ the mean life of a particle in the metastable state. τ is given by the relation

$$\frac{1}{\tau} = \frac{D_0}{\Lambda^2} \cdot \frac{1}{p} + Bp,$$

where D_0 is the diffusion coefficient of a metastable atom in the normal gas at unit pressure, B is the frequency of destruction of metastable atoms by two-body collisions at unit pressure, and Λ is the characteristic diffusion length of the container. In the case of a cylindrical container, Λ is given by

$$\frac{1}{\Lambda^2} = \left(\frac{\pi}{h}\right)^2 + \left(\frac{2.4}{r_0}\right)^2,$$

where h and r_0 are the length and radius of the cylindrical container.

The decay of the population of a metastable level is determined by measuring the absorption, shown by lines of the neon spectrum ending in that level, at accurately determined intervals following the cessation of the exciting discharge. For such a line of incident intensity I_0 and transmitted intensity I, it can be shown from the theory above that

$$\ln \ln(I_0/I) = -(t/\tau) + \text{constant}.$$

This form is valid under certain conditions fully discussed by Eckl (1951) and adequately fulfilled in the experimental apparatus used in this work.*

When the electrical excitation in the discharge tube ceases there remains, in addition to the metastable atoms, a population of positive ions and electrons distributed throughout the unexcited gas. Because of the relatively enormous Coulomb forces these ions and electrons form a plasma of essentially zero net charge per unit volume. The diffusion of the charged entities subject to the additional condition of over-all neutrality is referred to as ambipolar diffusion.

*The validity of the above expression for all absorption levels and other conditions of the experiment has been discussed at length by Eckl (1951). Much of this discussion was removed from his published paper (1953) for lack of space. The authors do not feel that a repetition of this discussion is appropriate.

The method of measurement of electron and hence positive ion densities makes use of the alteration of the resonance frequency of a microwave cavity enclosing the plasma under investigation. Slater (1946, 1950) has shown that

$$\Delta\omega = \frac{e^2}{2m\omega_0\epsilon_0} \frac{\int_{V'} nE^2 dV'}{\int_V E^2 dV},$$

where ω_0 is the angular resonant frequency of the cavity in the absence of free electrons, $\Delta\omega$ is the change in angular resonant frequency due to the presence of free electrons, n is the number of free electrons per unit volume as a function of spatial coordinates, E is the electric field strength of the resonant mode used, ϵ_0 is the permittivity of free space, e and m are the electronic charge and mass, and V and V' are the volume of the cavity and of the discharge tube respectively. This relation is shown to be valid provided that $\Delta\omega \ll \omega_0$. The integrals may be evaluated if the spatial distribution of the electric field and electron density are known. For the TM_{010} (or E_{010}) mode in a cylindrical cavity of radius R

$$E_r = E_\theta = 0, \qquad E_z = E_0 J_0(2.405r/R).$$

Thus the field is entirely axial and uniform along the length of the cavity. Solutions for $\Delta\omega$ in terms of the electron population for such a cavity for distributions characteristic of both diffusion decay and recombination decay are indicated by Biondi (1951).

EXPERIMENTAL

The method and apparatus for the measurement of the population of atoms in metastable states has been described by Eckl (1953). Only a brief outline is included here. A simplified block diagram of the apparatus is shown in Fig. 1.

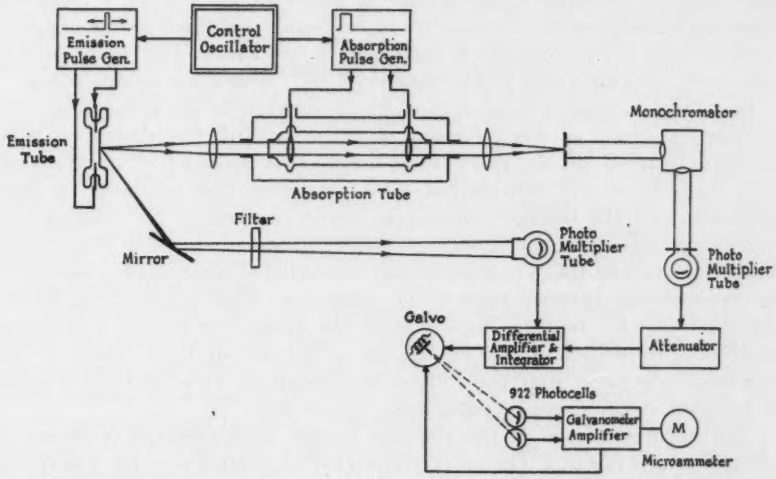

FIG. 1. Simplified block diagram of apparatus for metastable state measurements.

All triggering and timing intervals are fixed by a stable audio-oscillator operating at 2000 cycles per second. Low pressure gas in the absorption tube is excited by a sharp rectangular pulse of 500 microseconds' duration, having a repetition frequency which is a submultiple of the original oscillator frequency. At any integral multiple of 500 microseconds after excitation has ceased the emission tube may be fired with a pulse of 18 microseconds' duration. The light from the emission tube is collimated and passes through the absorption tube where some of the light is absorbed, raising metastable atoms to higher levels. The absorption tube is diaphragmed to limit the light beam to the central part of the tube. The degree of absorption is dependent on the population of the metastable level at the time of the emission tube flash.

After passing through the absorption tube, the light is focused on the slit of a monochromator which focuses a single spectrum line on a photomultiplier tube. The resulting voltage pulse is applied through a stepped calibrated attenuator to one input of a differential amplifier. To the second input of this amplifier a similar voltage pulse is applied, this pulse being produced by light from the emission tube which passes through a red filter directly to a second photomultiplier tube. The filter serves to limit the wavelength response in the reference channel to the same region as used in the absorption channel. After several stages of amplification and gating to reduce noise the two pulses are applied to the grids of two carefully matched pentode amplifiers each with a large integrating condenser in its plate circuit. Thus the output of the differential amplifier is proportional to the difference in amplitude of the two input pulses averaged over many cycles to reduce the effect of random fluctuations in the number of electrons emitted from the photomultiplier surfaces during any pulse. The d-c. output voltage, instead of being read on a galvanometer as was done by Eckl (1953), is applied to a d-c. negative feedback galvanometer amplifier whose output is indicated on a Type J Sensitive Research microammeter. This system is thoroughly stabilized by the negative feedback and can be read much more quickly and easily. The circuit used is essentially that described by Montgomery (1947) with a few modifications.

In taking readings a large attenuation is inserted in the absorption tube channel by means of the calibrated attenuator. With the absorption tube excitation turned off, the two-channel amplifier is balanced by uncalibrated gain controls to give zero output. The absorption tube excitation is then turned on and the balance restored as nearly as possible by reducing the attenuator setting in the absorption tube channel. Departure from exact balance is read on the output meter and converted to decibels of attenuation by interpolation between steps of the attenuator. Thus values of $\log_{10}(I_0/I)$ are read directly to three figures from the attenuator setting and meter deflection. Repetition of this process for a number of time delays of the emission tube pulse after the end of the absorption tube excitation yields a complete decay curve of population against time.

The apparatus used in the electron density measurements is shown in simplified form in Fig. 2. The pyrex discharge tube, referred to as the absorption tube in the metastable measurements above, is contained wholly within the

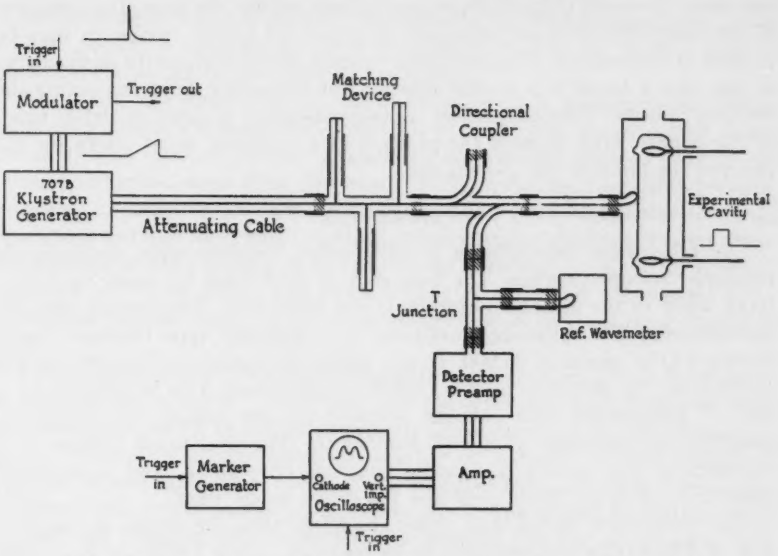

FIG. 2. Simplified diagram of apparatus for electron density measurements.

experimental microwave cavity. The gas in this tube is excited by the same 500 microsecond d-c. voltage pulse as described above. The delayed pulse, used to fire the emission tube for the metastable state measurements, triggers a saw-tooth wave which swiftly varies the frequency of a low level probing microwave signal voltage through the expected resonance frequency of the cavity. This signal is coupled into the cavity through a piece of RG-21/U attenuating cable and a matching device. The reflected wave from the cavity, acting as termination of the transmission line, is sampled by the directional coupler, and is then detected, amplified, and applied to the vertical plates of a triggered oscilloscope. Because the coupling loop to the cavity is adjusted to present a very nearly matching load at the resonance frequency of the cavity, the amplitude of the reflected wave decreases as the microwave frequency approaches resonance, reaching a minimum value when the applied frequency coincides with the resonance frequency of the cavity containing a population of electrons.

To determine the frequency at which this minimum reflection occurs, a second resonance minimum from a calibrated reference wavemeter cavity, also coupled to the system as shown in Fig. 2, is superimposed on the oscilloscope display. This second minimum is brought into coincidence with the first by tuning the wavemeter cavity while watching the oscilloscope display. The frequency of resonance is determined from the wavemeter cavity setting. A time marker generator is used to measure the small delay time between the initial trigger pulse for the saw-tooth and the occurrence of the resonance

minimum. Since the delay of the trigger pulse is known, the time after cessation of the discharge at which resonance occurs at the known frequency may be accurately determined. The resonant frequency of the cavity with no discharge in the tube is found in a similar manner, the frequency difference giving the electron density. Repeating these measurements for a series of delay times of the trigger pulse permits the plotting of a complete decay curve for the electron (or positive ion) population.

APPARATUS

The microwave generator is a 707B reflex klystron with electronically regulated voltage supplies. The frequency is modulated by applying a sawtooth wave to the reflector electrode in the usual way. The circuits used are conventional. The reference wavemeter is a reflection type resonant cavity having a Q in excess of 25,000. It was calibrated against a Marconi Crystal Calibrator. The detector uses a 1N23B crystal diode. This is followed by a 12AY7 preamplifier and cathode follower output feeding to commercial amplifiers of adequate gain and bandwidth. The directional coupler is a commercial unit having a nominal coupling of -30 db. and a minimum directivity ratio of 36 db. over the frequency range used.

The microwave cavity and pyrex discharge tube are shown in detail in Fig. 3. The cavity was designed to be resonant in the TM_{010}, or E_{010}, mode

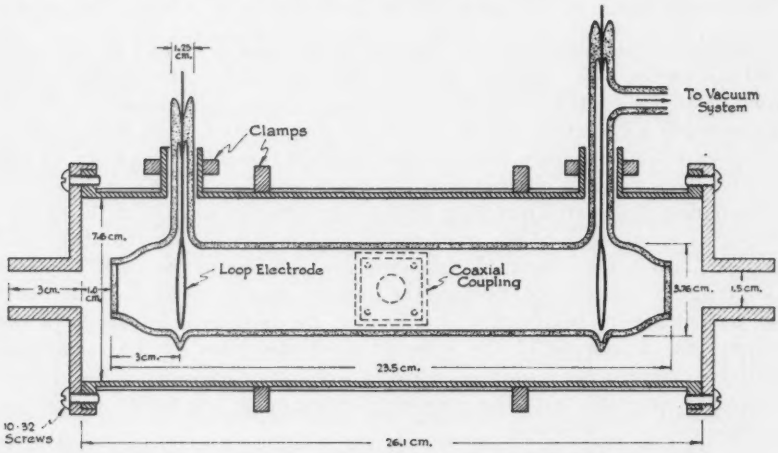

FIG. 3. Cross-sectional view of experimental cavity and pyrex discharge tube.

in the neighborhood of 3000 megacycles per second. At this frequency coaxial line can be used for short microwave connections without too much loss. Fixing the resonance frequency fixes the diameter of the cavity, if operation in this mode is assumed, but the length is still arbitrary. The length actually chosen is a compromise value permitting long absorption paths for the meta-

stable measurements while still preventing excitation of higher and undesirable modes. To aid in suppressing these undesirable modes, the feeding loop is placed at the center of the length of the cavity.

The cavity was constructed so that it could be easily dismantled to permit outgassing of the electrodes in the discharge tube. The use of a split brass cylinder with carefully fitted overlapping end flanges allowed this to be done. Two rigid clamps along the length of the cavity were added to prevent warping. To permit metastable state measurements to be made under identical conditions to those for electron density measurements, windows or ports allow the passage of light from end to end. These were made 1.5 cm. in internal diameter and 3 cm. long. The effect is that of a window surrounded by a waveguide beyond cutoff. Microwave energy loss is reduced to a negligible value.

The pumping line and one electrode are brought out through a hole centered at the split in the cavity at one end, and the other electrode through a hole symmetrically placed at the opposite end. These openings are surrounded by halved cylinders which are clamped together on assembly to give additional rigidity. Sleeves can be used to adjust the length of these cylinders to minimize the loss of microwave energy along the concentric line formed by the electrode support and cylinder. The probe signal is coupled into the cavity by a loop coupling to the magnetic field H_θ at the central plane of the cavity.

In spite of the sources of loss introduced by the necessity of using a demountable cavity, the Q was about 4000 without the discharge tube. This fell considerably with the tube mounted. A large part of the additional losses appeared to be due to the tungsten electrodes necessary for d-c. excitation of the discharge. These electrodes were circular rings of tungsten wire mounted as nearly as possible in a plane perpendicular to the axis of the cavity and the electric field of the resonant mode. Small departures from exact positioning in this plane allow a small coupling to the microwave field and permit energy to escape along the electrode connections. This escape was minimized as above.

A major difficulty arose owing to sputtering of metal from the electrodes by the exciting d-c. discharge. These sputtered metal films formed conducting paths parallel to the microwave electric field and when a certain critical thickness was reached caused the Q to fall quite suddenly to values at which the resonance minimum became so broad that its frequency could not be determined with sufficient accuracy. The discharge tube had then to be removed from the cavity for cleaning. In spite of this difficulty, it was considered advisable to retain the d-c. excitation of the gas so that the metastable state results would be strictly comparable to those of Eckl (1953) and others.

Treating the discharge tube as a cylinder of the dimensions shown in Fig. 3, the characteristic diffusion length Λ is 0.697 cm. In preparing for operation the discharge tube was pumped down and maintained at pressures registering less than 10^{-6} mm. Hg on a VG-1A ionization gauge. The electrodes were outgassed at bright red heat in an induction heater and the walls of the glass system were flamed for long periods. The neon used was spectro-

scopically pure and furnished in 1 liter pyrex flasks. Impurities remaining or introduced in the handling process were removed by exposing the gas to calcium vapor. With these procedures little trouble was experienced with contamination.

RESULTS AND DISCUSSION

Decay curves for both electron and metastable density were obtained for the pressure range from 0.5 to 12.0 mm. Hg. As previously observed and as predicted by theory, the decay of the population of the $^3P_2$ metastable state is exponential at all pressures. A slight initial departure from linearity is indicated in the lower pressure curves, as in Fig. 4, the first point showing a consistent tendency to be high. This was also observed by Eckl (1953). Since

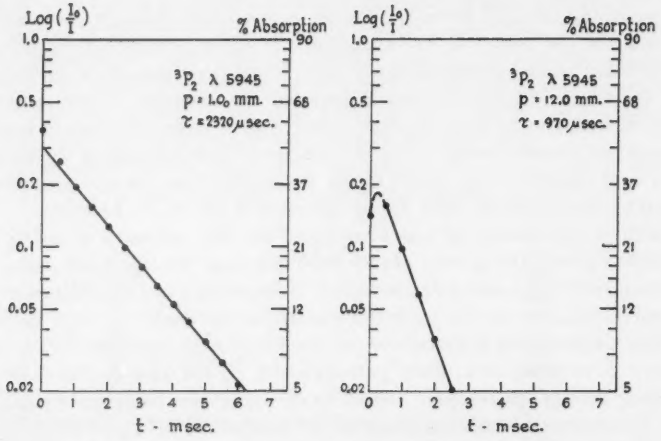

FIG. 4. Representative curves for metastable state decay.

it seemed possible to enhance the effect by using very slightly impure neon, it is believed that this may be due to the presence of a light impurity, possibly hydrogen, which is rapidly adsorbed after the discharge ceases. This small effect is of an entirely different order of magnitude from the double exponential decay shown by the $^3P_0$ level in Eckl's observations and repeatedly checked during the early part of this work. At the highest pressure, however, the first point is low as shown in Fig. 4. This effect also was observed by Eckl (1951). This increase in population of the $^3P_2$ level at high pressures in the first half millisecond after the discharge ceases is certainly real; it will be discussed below.

The decay of the $^3P_2$ metastable state was chosen for the comparison with the electron density decay because the absorption of the spectral lines ending in the $^3P_2$ state is sufficiently large that measurements are possible at much lower excitations than is the case with the $^3P_0$ state. In this work the excitation had to be kept rather low to avoid rapid sputtering of the walls of the tube

with consequent lowering of the cavity Q. Eckl (1953) has established the relationship between the decay of the populations of the metastable $^3P_2$ and $^3P_0$ states and this relationship was checked repeatedly for various excitation levels in the early part of this work. Hence it was judged sufficient to establish the relationship of the electron population decay to the decay of population of the single metastable state.

The variation of the mean life τ of the $^3P_2$ metastable state with pressure is shown in Fig. 5. The curve is described by the equation

$$\frac{1}{\tau} = \frac{280}{p} + 65p + 125,$$

where τ is in seconds and p is in mm. Hg. This may be compared with

$$\frac{1}{\tau} = \frac{D_0}{\Lambda^2} \cdot \frac{1}{p} + Bp$$

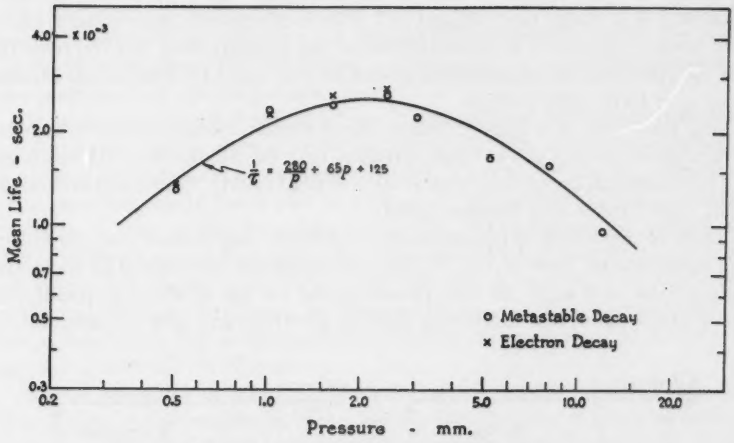

FIG. 5. Variation of mean life with pressure.

as derived by Zemansky (1929). In this expression the first term represents destruction of the metastable state by diffusion to the walls and the second represents destruction of the state by collision with a normal atom.

The constant term in the experimental expression was suggested by Eckl (1951, 1953) as one of a number of empirical attempts to represent his results for the pressure dependence of the mean life of this state. Inspection of the results of Phelps and Molnar (1953) indicates that their experimental values would fit a curve with such a constant term somewhat better than the fit shown for the theoretical form of the equation. The added constant term would seem to indicate that an appreciable amount of spontaneous reversion, independent of pressure, occurs from the metastable to the normal state. Theoretical estimates of the transition probability indicate that such a reversion should be negligibly small but these estimates are admittedly crude.

Reversion due to external illumination as found by Meissner and Graffunder (1928) is inadequate to explain the effect because of the large intensities found by these workers to be necessary to cause an appreciable effect. In the present work, the absorption tube was enclosed in the microwave cavity, reducing ambient light to a minimum. Since the results of the present work and of Eckl (1953) and Phelps and Molnar (1953) agree in representing the decay of the population of this state at any one pressure as a straight line logarithmic relation, it would seem unlikely that experimental error could take this form.

This deviation from the simple theory may also be indicated by the introduction of non-integral powers of pressure into the expression as suggested by Eckl (1953) and by Phelps (1955).

The coefficient of the term directly proportional to the pressure shows that the frequency of destruction of metastable atoms by two-body collisions at 1 mm. pressure is only 65 per second. Comparison of this value with the frequency of two-body collisions as calculated for neon at 1 mm. pressure shows that only about one collision in 7×10^4 is effective in destroying a metastable atom. The use of a squared term in the pressure does not improve the fit of the curve to the experimental points as was found by Phelps and Molnar (1953) and Eckl (1951, 1953).

Using the value of Λ quoted above, the diffusion coefficient of a $^3P_2$ metastable atom in normal gas at 1 mm. pressure may be calculated as 136 cm.^{2}/sec. This is in essential agreement with results of Eckl (1951), Grant and Krumbein (1953), and Phelps and Molnar (1953).

Curves of $\Delta\nu$, which is proportional to electron population, are plotted on a log scale against time in Fig. 6. The curves chosen correspond to the metastable curves of Fig. 4. At low pressures the curves of electron population show exponential decay, indicating that the electrons and ions are recombining

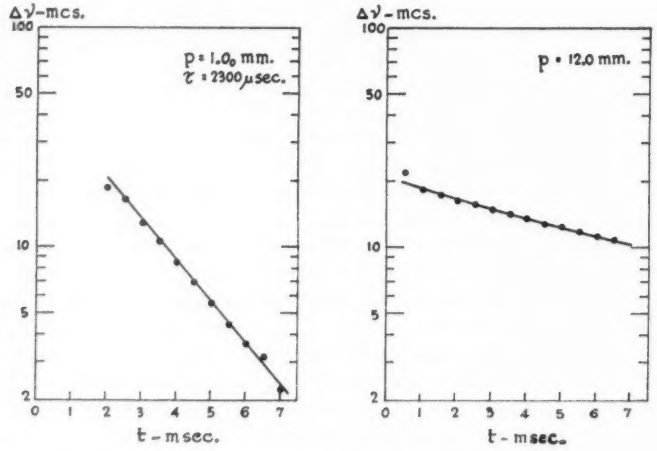

FIG. 6. Representative curves for electron density decay.

after diffusion to the walls and that volume recombination is negligible at these pressures. These low pressure results could not be extended to very short delay times because of the lowering of the Q of the cavity and change of coupling of the cavity to the transmission line due to the very high population of free electrons. The largest frequency shift used in the results was 27 megacycles per second, less than one per cent of the resonance frequency in the absence of free electrons, so that the approximation $\Delta\omega \ll \omega_0$ is amply fulfilled.

For the low pressures for which the electron population decays exponentially, the mean lives are marked in Fig. 5 along with the metastable mean lives. The close agreement of the two mean lives at these pressures indicates that the effective diffusion coefficients for the metastable atoms and positive ions and free electrons approach each other to within experimental error as the pressure becomes small. This at first seems somewhat surprising, but Biondi (1954) has shown that, given the extremely high ratio of the mass of the neon gas atoms to the mass of the electrons, the ambipolar diffusion coefficient might be expected to approach the normal diffusion coefficient of the positive ion in the normal gas. This coefficient in turn might be expected to approximate the coefficient for the metastable atom.

At pressures of 3 mm. Hg and higher the logarithmic plot of electron density against time starts to show definite curvature which becomes more pronounced for higher pressures. At the highest pressure, 12 mm. Hg, the log plot (Fig. 6) again appears nearly linear out to a time of 7 milliseconds. This appearance, however, is due to the fact that population itself changes by only a small factor in the range of measurement. At intermediate pressures, for which the curves are not shown, curvature of the log plot is very marked. Comparison of the two log plots at 12 mm. for metastable states in Fig. 4 and for electron–ion population in Fig. 6 shows that no relation between the two decays exists beyond a time of 1 millisecond.

For all pressures of 5 mm. and higher which were studied, it was found that a plot of the reciprocal of $\Delta\nu$ against time yielded a straight line. This is illustrated in Fig. 7 and is characteristic of volume recombination. For this process the appropriate differential equation is

$$dn/dt = -\alpha n^2$$

in which n is the electron (or positive ion) density and α the recombination coefficient. Solving this and evaluating the derivative gives

$$\frac{1}{n} - \frac{1}{n_0} = \alpha t \quad \text{and} \quad \frac{dn}{dt} = \frac{-n_0^2\alpha}{(1+n_0\alpha t)^2}.$$

This shows that the rate of recombination is very large when t is small and rapidly falls off as t increases. Since at least part of these recombinations in the body of the gas may be expected to result in a radiation cascade, such recombinations could act to increase the population of the metastable state. This effect should be very large at small delay times and decrease very rapidly thereafter. This effect is adequate to explain the initial increase in population

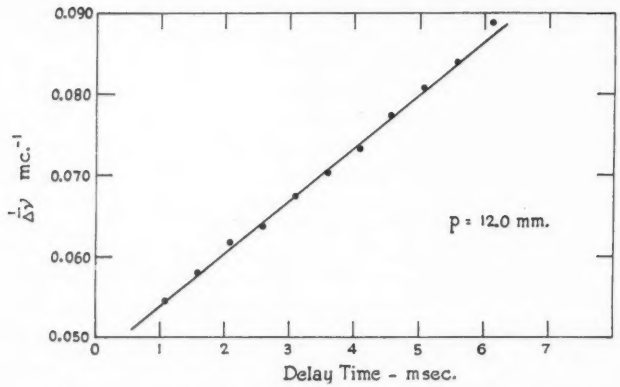

FIG. 7. Representative curve of reciprocal electron density against time at high pressure.

of the metastable state at 12 mm. Hg pressure as shown in Fig. 4. Unfortunately, as was pointed out above, it was impossible to carry the determination of electron population back to zero delay time under the same conditions because of the very large population of electrons.

The initial concentrations (i.e. at the time the exciting discharge ceases) both for electrons and positive ions, and for metastable states, may be found by extending the appropriate straight line plots back to the zero time intercepts. Expressions for these initial populations are given by Eckl (1953) and Biondi (1951) for the case of metastable states and for electrons respectively. For the discharge conditions used in this work, the two initial populations are of the same order, each being about one in 10^6 to 10^7 of the atoms present.

Recombination coefficients may also be calculated for the cases in which this process is the predominant cause of disappearance of free electrons, that is for pressures above 5 mm. Hg. From the slopes of the linear plots of the reciprocal of the electron population against time, α is found to have values of 3.0×10^{-7} cm.^{3}/ion-sec., 1.2×10^{-7} cm.^{3}/ion-sec., and 4.5×10^{-8} cm.^{3}/ion-sec. at 5.16, 8.0, and 12.0 mm. Hg pressure respectively. The values of α are of the same order as those obtained by Biondi and Brown (1949) and by Holt, Richardson, Howland, and McClure (1950). Since the pressure range in this work does not overlap that of the previous workers, exact comparison cannot be made.

CONCLUSIONS

At all pressures in the range studied the decay of the population of the $^3P_2$ metastable state of neon is exponential. At low pressures the atoms are removed from the metastable state principally by diffusion to the walls. At high pressures removal from the metastable state is due principally to collisions of the metastable atom with an unexcited atom in the body of the gas. The efficiency of such collisions is low, of the order of one in 10^5. A spontaneous

reversion term seems necessary to explain why the experimental values of mean life near its maximum for pressure variation fall consistently below the theoretical curve based on the processes above.

At low pressures the population of electrons and positive ions decays exponentially by ambipolar diffusion to give recombination at the walls of the vessel. The ambipolar diffusion coefficient for this process is, within the limits of experimental error, the same as that for the metastable atoms. At higher pressures the decay of electron population falls off so that the reciprocal of the population plotted against time gives a straight line, this being characteristic of volume electron–ion recombination. In this region of pressure no relation exists between the decay of the populations of positive ions and of metastable states, except in the first half millisecond at the highest pressure used. Here there is evidence that the population of the metastable $^3P_2$ state is increased by the recombination of positive ions and electrons. Recombination coefficients have been evaluated at the higher pressures.

There is no indication that the presence of positive ions after termination of the discharge can offer an explanation of the double exponential decay found for the $^3P_0$ metastable state.

ACKNOWLEDGMENTS

The authors are indebted to the Defence Research Board, Ottawa, Canada, for a grant to one of us (J.M.A.) with which some of the apparatus used in this work was purchased. The authors are also indebted to the National Research Council, Ottawa, Canada, for the award of a Studentship which allowed one of us (B.C.B.) to participate in this work.

REFERENCES

BIONDI, M. A. 1951. Rev. Sci. Instr. **22**, 500.
——— 1954. Phys. Rev. **93**, 1136.
BIONDI, M. A. and BROWN, S. C. 1949. Phys. Rev. **76**, 1697.
ECKL, D. J. 1951. Ph.D. Thesis, University of Toronto, Toronto, Ontario.
——— 1953. Can. J. Phys. **31**, 804.
GRANT, F. A. and KRUMBEIN, A. D. 1953. Phys. Rev. **90**, 59.
HOLT, R. B., RICHARDSON, J. M., HOWLAND, B., and MCCLURE, B. T. 1950. Phys. Rev **77**, 239.
MEISSNER, K. W. and GRAFFUNDER, W. 1928. Ann. Physik, **84**, 1009.
MONTGOMERY, C. G. 1947. Technique of microwave measurements (McGraw-Hill Book Co., Inc., New York).
PHELPS, A. V. 1955. Phys. Rev. **99**, 1657A.
PHELPS, A. V. and MOLNAR, J. P. 1953. Phys. Rev. **89**, 1202.
SLATER, J. C. 1946. Revs. Mod. Phys. **18**, 441.
——— 1950. Microwave electronics (D. Van Nostrand Co., Inc., New York).
ZEMANSKY, M. W. 1929. Phys. Rev. **34**, 213.

INFRARED INTENSITIES AND BOND MOMENTS IN SULPHUR DIOXIDE[1]

J. E. MAYHOOD[2]

ABSTRACT

New values have been obtained for the intensities of the three fundamentals of sulphur dioxide. They are $A_1 = 317 \pm 8$, $A_2 = 376 \pm 20$, $A_3 = 2560 \pm 70$, in units of 10^{10} sec.$^{-1}$ cm.$^{-1}$ at S.T.P. The normal coordinate calculation gives values for the bond moment derivatives and for the molecular dipole moment which demonstrate that the amount of charge moving in all three vibrations is greater than that inferred from the equilibrium charge distribution. The involvement of unshared electrons is suggested.

INTRODUCTION

Integrated absorption coefficients for the infrared bands of sulphur dioxide vapor have been published by Eggers, Hisatsune, and Van Alten (1955) and by Morcillo and Herranz (1956, 1957). The measurements to be reported here were made independently in the period between these two publications. They are presented to resolve the disagreement between the two previously published sets, and to revise the interpretation of these intensities in terms of dipole moments and moment derivatives for the sulphur dioxide molecule.

It has been customary to attempt to relate the observed infrared intensities to the equilibrium distribution of charge in the molecule through the assumption that the formal atomic charges of the equilibrium configuration remain fixed on their respective atoms as these atoms move in molecular vibrations. Tests of the applicability of this concept have been made difficult by the experimental problems involved in obtaining accurate intensity data and by the scarcity of data of adequate accuracy for the potential constants of even the simpler polyatomic molecules (Callomon, McKean, and Thompson 1951; Hornig and McKean 1955). Thus, despite the fact that numerous studies have already demonstrated the failure of the fixed-charge model (Hornig and McKean 1955) it is worth while to provide accurate intensity values and moment derivatives for the sulphur dioxide molecule. This is because sulphur dioxide presents an almost unique combination of convenience in measurement with the availability of accurate molecular geometry and potential constants (Crable and Smith 1951; Kivelson 1954; Polo and Wilson 1954), and should therefore be useful in the quantitative testing of more detailed theories of vibrational intensities. A further attractive feature is that all three phases of sulphur dioxide may be conveniently studied to examine the influence of intermolecular forces on the internal charge distribution; such studies will form the basis of a subsequent paper.

The paper of Eggers, Hisatsune, and Van Alten (1955) contains all the relevant procedure for the reduction of the observed intensities to dipole

[1]Manuscript received May 17, 1957.
Contribution from the Department of Physics, University of British Columbia, Vancouver, B.C.
[2]Present address: Suffield Experimental Station, Ralston, Alberta.

moment derivatives. Unfortunately a few errors were inadvertently introduced into their publication (Hisatsune 1956). The normal coordinate treatment has been repeated using their notation and symmetry coordinates, that is

$$\begin{aligned} S_1 &= 2^{-\frac{1}{2}}(\Delta r_1+\Delta r_2), \\ S_2 &= r\Delta\theta, \\ S_3 &= 2^{-\frac{1}{2}}(\Delta r_1-\Delta r_2), \end{aligned} \tag{1}$$

with the result that the transformation from the symmetry coordinates S_i to the normal coordinates Q_k takes the form

$$\begin{aligned} Q_1 &= 0.457S_1-0.00708S_2, \\ Q_2 &= 0.153S_1+0.288S_2, \\ Q_3 &= 0.390S_3, \end{aligned} \tag{2}$$

where the numerical coefficients of the S_i are in units of 10^{-11} g.$^{\frac{1}{2}}$ The definitions of the symmetry coordinates together with the assumptions of the fixed-charge model yield the relations

$$\begin{aligned} \frac{\partial\mu_{so}}{\partial r} &= \frac{2^{-\frac{1}{2}}}{\cos(\theta/2)}\frac{\partial\mu}{\partial S_1}, \\ \mu_{so} &= \frac{-r}{\sin(\theta/2)}\frac{\partial\mu}{\partial S_2}, \\ \frac{\partial\mu_{so}}{\partial r} &= \frac{2^{-\frac{1}{2}}}{\sin(\theta/2)}\frac{\partial\mu}{\partial S_3}. \end{aligned} \tag{3}$$

These relations differ from those of Eggers, Hisatsune, and Van Alten (1955) in the signs of the coefficients, and in a factor of 2 in the equation for μ. The latter error was called to our attention by S. R. Polo.

EXPERIMENTAL

Intensities were determined by the method of Wilson and Wells (1946) at total pressures of 1 and 3 atmospheres, using nitrogen as the broadening gas. Partial pressures of sulphur dioxide between 0.8 mm. and 50 mm. were used with a 10.0 cm. path length. Glass-bodied cells were used to avoid adsorption effects noted with metal cells. The effect of incomplete mixing of the two gases was investigated, and no effect was found at the pressures used. The influence of total pressure on the apparent integrated absorption coefficient was investigated for several partial pressures of SO_2, and 1 atmosphere total pressure was found to give complete broadening over most of the range of partial pressures employed.

The nitrogen used was dried by slow passage through liquid-oxygen-cooled traps followed by reheating to room temperature. This procedure avoided the loss of SO_2 observed when premium grade nitrogen was used without drying. Sulphur dioxide from the Matheson Chemical Co. (of stated purity 99.7%) was found to condense as a yellowish liquid, and to contain a few per cent of some gas not condensable at liquid oxygen temperature. It was therefore subjected to one or two vacuum fractionations prior to being evaporated

into the evacuated cell. A singly distilled sample was analyzed by mass spectrometry and shown to be not less than 99% pure, and to have no detectable sulphur-containing impurities. The amount of sulphur dioxide in the cell was determined using a differential oil manometer, and was confirmed by quantitative chemical analysis. The analysis involved complete slow passage of the cell contents through liquid air traps in series, conversion of the trapped sulphur dioxide to sulphate with ammoniacal hydrogen peroxide, and gravimetric determination of the sulphate as barium sulphate (Vogel 1951). The chemical analyses showed a scatter of ±5%, but agreed with the manometric pressure within 2%.

Spectra were recorded in the NaCl and KBr regions on a Perkin-Elmer Model 21 double-beam infrared spectrophotometer with a matched cell containing nitrogen in the reference beam. Spectral slit widths were chosen to be less than 0.65 of the half-width of one rotational wing in order to minimize the extrapolation slope (Ramsay 1952) while permitting a reduction of the noise level to 0.2% transmission with a scanning speed of 10 cm.$^{-1}$ per minute. These conditions of high performance could not be achieved in the low frequency tail of the ν_2 band which lies at the extreme of the range of the KBr prism. This tail was therefore estimated by symmetry from the high-frequency tail; the area involved was about 7% of the total band area. Band integrations were performed using Simpson's Rule with a sufficient number of intervals to keep the sums of the even and odd ordinates in agreement within 0.5% for all but the weakest bands. Background and stray light corrections were applied as required.

The integrated absorption coefficients were evaluated both from the limiting slope at the origin of a plot of band area against partial pressure and from the intercept of a plot of the apparent integrated absorption coefficients against partial pressure. The latter plots are shown in Fig. 1. It is felt that the intensities are accurate to within the uncertainty of the chemical analysis (±5%), this being the largest source of systematic error encountered. The over-all reproducibility, taken as the standard deviation of points about the least squares line in the least favorable case, was ±4.5%.

RESULTS

Table I presents a comparison of the intensities obtained in this investigation with the previously published values. The agreement between this work and that of Morcillo and Herranz is essentially within the limits of accuracy, while the results of Eggers, Hisatsune, and Van Alten are roughly 50% low. This

TABLE I

INTEGRATED ABSORPTION COEFFICIENTS FOR SULPHUR DIOXIDE

Band	Freq. (cm.$^{-1}$)	$A\times10^{-10}$ sec.$^{-1}$ cm.$^{-1}$ at S.T.P.			$\partial\mu/\partial Q_k\times10^{-10}$ e.s.u., this work
		Ref. (4)	Ref. (9)	This work	
ν_1	1151	226	350±20	317±8	± 58.1
ν_2	519	257	360±30	376±20	± 63.6
ν_3	1361	1606	2640±80	2560±70	±165.2

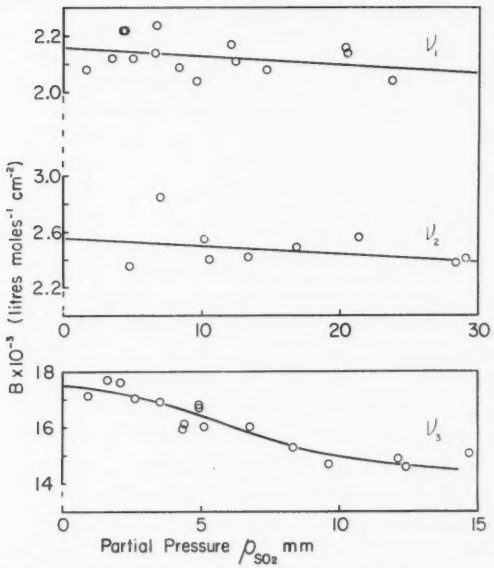

FIG. 1. Apparent integrated absorption coefficients of the sulphur dioxide fundamentals as a function of partial pressure, at 25° C. and a total pressure of 760 mm.

discrepancy has been discussed with Professor Eggers, who has conceded that some unsuspected bias, such as included nitrogen in their sulphur dioxide sample, may have prejudiced their determination of partial pressures by mass spectrometry. In any event it is felt that, in terms of the errors to which the methods are susceptible and in view of the two agreeing sets, the higher values must be considered as correct within their limits of error.

The derivatives of the total molecular dipole moment with respect to distortions in the manners specified by the symmetry coordinates S_i, $\partial\mu/\partial S_i$, are presented in Table II, together with the bond moment μ_{so} and its derivatives $\partial\mu/\partial r$ calculated from the relations (3) above.

The fact that the observed intensities are proportional to the square of the corresponding $\partial\mu/\partial Q_k$ gives rise to alternative values for $\partial\mu/\partial S_1$ and $\partial\mu/\partial S_2$ depending on whether the signs of $\partial\mu/\partial Q_1$ and $\partial\mu/\partial Q_2$ are the same or different. If these signs are the same, the predicted total molecular dipole moment for SO_2 becomes ∓ 3.00 Debyes, or ± 3.14 Debyes if they are different. These values are to be compared with the static dipole moment of 1.59 Debyes obtained from the pure rotational spectrum (Crable and Smith 1951) or from dielectric constant measurements (Brown 1956).

DISCUSSION

The disagreement between the "dipole moment" derived from the infrared intensities and the "static dipole moment" measured in the usual way is

TABLE II

MOMENTS CALCULATED FOR SULPHUR DIOXIDE
(Values of μ_{so} are Debyes; all others are e.s.u.$\times 10^{-10}$)

Moment	Relative signs of $\partial\mu/\partial Q_1$ and $\partial\mu/\partial Q_2$	Calculated value
$\partial\mu/\partial S_1$	Same	± 3.62
	Different	± 1.69
$\partial\mu/\partial S_2$	Same	± 1.80
	Different	∓ 1.88
$\partial\mu/\partial S_3$	—	± 6.44
$\partial\mu_{so}/\partial r$ (from ν_1 and ν_2)	Same	± 5.00
	Different	± 2.38
μ_{so} (from ν_1 and ν_2)	Same	∓ 2.98
	Different	± 3.12
$\partial\mu_{so}/\partial r$ (from ν_3)	—	± 5.27

much greater than any of the errors involved in measurement, so that it is quite clear that these two quantities are not the same physically.

The failure of the fixed-charge model is further emphasized by a comparison of its other predictions with the results of Table II. A molecular orbital treatment of sulphur dioxide by Moffitt (1950) assigns formal charges of $+0.48$ electrons to the sulphur atom and -0.24 electrons to each oxygen. This charge distribution is consistent with the observed static dipole moment. Thus on the assumptions of the fixed-charge model we should find not only agreement of the μ values, but we should find $\partial\mu_{so}/\partial r$ to be 0.24 electrons or about 1.0×10^{-10} e.s.u. independent of the symmetry class of the normal vibration. None of the alternatives of Table II are in good agreement with this prediction. The signs of the derivatives may also be considered. Moffitt's formal charges give the positive sign for μ in the coordinate systems used here, and predict the positive sign for $\partial\mu/\partial S_1$ and the negative sign for $\partial\mu/\partial S_2$, so that the signs of $\partial\mu/\partial Q_1$ and $\partial\mu/\partial Q_2$ should also be taken as being different. This choice, however, leads to large disagreement of the value of $\partial\mu_{so}/\partial r$ from ν_1 and ν_2 with that from ν_3. In studies on other molecules conclusions as to signs and magnitudes of derivatives have occasionally been based on the consistency argument that the magnitudes calculated from vibrations of different symmetry ought to agree. The accumulated evidence presented by Hornig and McKean (1955) calls this procedure into question; the present evidence demonstrates that the procedure is inconsistent with the hypothesis used in the calculations.

The over-all conclusion from these findings is that the amount of charge redistributed in the molecular distortions of sulphur dioxide is much greater than the formal charges of the equilibrium distribution. This suggests that the concepts of rehybridization, orbital following, and the contributions of unshared electrons which Hornig and McKean have applied successfully in NH_3 and HCN are needed for a discussion of the SO_2 intensities.

It has been shown that unshared pairs can make large contributions to the static moments (of the order of 1 Debye unit), and that they are very easily polarized (Smyth 1955). The molecular orbital calculations of Moffitt for sulphur dioxide and related compounds show that the sulphur unshared electrons occupy orbitals which are directed approximately tetrahedrally with respect to the S—O bonds, and are pulled towards the oxygen atoms. Thus the unshared pair moment in the equilibrium configuration opposes the S—O bond moment. It is found that the configuration of the sulphones, R_2SO_2, is nearly tetrahedral while the S—O bond order is almost unaltered from its value in SO_2, and the dipole moment increases from 1.59 Debyes in sulphur dioxide to more than 4 Debyes for dialkyl sulphones.

If we assume that the lone pair orbitals follow the motions of the oxygen atoms but otherwise retain the concepts of the fixed-charge model, qualitative consistency can be given to the signs and relative magnitudes of the moment derivatives in sulphur dioxide. Thus the lone pair moment, ordinarily in opposition to the bond moment but reduced in its effect by displacement of the lone pair orbitals towards the oxygens, would further decrease as the S—O bonds stretched slightly, leading to an augmented positive change in μ for distortions of type S_1. Similarly, the opposition of the lone pair moment to the bond moment would increase for increases in the bond angle, leading to an augmented negative value of $\partial\mu/\partial S_2$. Distortions according to S_3 would cause both bond and lone pair moment changes in the same direction, leading to large positive values of $\partial\mu/\partial S_3$.

Although the above discussion does not advance our understanding of infrared intensities, it does call attention to directions for further work. Moreover the provision of a well-established set of intensities and moment derivatives for a simple polyatomic molecule should be valuable in the testing of more detailed theories of molecular vibrations. The sensitivity of the infrared intensities to the details of the internal charge distribution suggests their use in the investigation of intermolecular forces, since even weak perturbations may be expected to produce observable changes in intensity.

ACKNOWLEDGMENTS

Acknowledgments and thanks are due to Prof. A. M. Crooker, who supervised the research, to the Defence Research Board of Canada for financial support, and to the British Columbia Research Council for the use of their spectrometer.

REFERENCES

BROWN, W. F., Jr. 1956. Encyclopedia of physics, Vol. XVII (Springer-Verlag, Berlin).
CALLOMON, H. J., MCKEAN, D. C., and THOMPSON, H. W. 1951. Proc. Roy. Soc. (London), A, **208**, 332, 341.
CRABLE, G. F. and SMITH, W. V. 1951. J. Chem. Phys. **19**, 502.
EGGERS, D. F., Jr., HISATSUNE, I. C., and VAN ALTEN, L. 1955. J. Phys. Chem. **59**, 1124.
HISATSUNE, I. C. 1956. Private communication.
HORNIG, D. F. and MCKEAN, D. C. 1955. J. Phys. Chem. **59**, 1133.
KIVELSON, D. 1954. J. Chem. Phys. **22**, 904.
MOFFITT, W. 1950. Proc. Roy. Soc. (London), A, **200**, 409.

MORCILLO, J. and HERRANZ, J. 1956. Anales real soc. españ. fís. y quim. (Madrid), Ser. A, **52**, 207, 217.
——— 1957. Spectroscopia Molecular, **6**, 9.
POLO, S. R. and WILSON, M. K. 1954. J. Chem. Phys. **22**, 900.
RAMSAY, D. A. 1952. J. Am. Chem. Soc. **74**, 72.
SMYTH, C. P. 1955. J. Phys. Chem. **59**, 1121.
WILSON, E. B., Jr. and WELLS, A. J. 1946. J. Chem. Phys. **14**, 578.
VOGEL, A. I. 1951. Quantitative inorganic analysis, 2nd ed. (Longmans-Green and Co. Toronto).

QUANTUM MECHANICS WITH AN INDEFINITE METRIC[1]

SURAJ N. GUPTA[2]

ABSTRACT

The formalism of quantum mechanics in a vector space with an indefinite metric is developed in a simplified way, and the properties of the indefinite vector space are discussed in detail with particular attention to vectors of negative and vanishing norms. It is shown how the present formalism simplifies the use of the indefinite metric in physical applications.

1. INTRODUCTION

Usually in quantum mechanics we use a vector space with a positive definite metric, because it is well known that an indefinite metric gives rise to the difficulty of negative probabilities (Dirac 1942; Pauli 1943). But it has been shown in recent years that a vector space with an indefinite metric can also be used in quantum mechanics without any difficulty, provided that it is ensured by means of supplementary conditions that the states of negative probabilities are unobservable. In this way it has been found possible to carry out the quantization of the electromagnetic field in a satisfactory way (Gupta 1950). An indefinite metric has also been used to carry out the quantization of the vector meson field (Gupta 1951) and the gravitational field (Gupta 1952), and to introduce auxiliary fields in quantum electrodynamics in a consistent way (Gupta 1953).

In the above applications of the indefinite metric two sets of quantities were introduced (called the Hermitian conjugates and the adjoints), which somewhat destroyed the elegance of the treatment and also made it unnecessarily complicated. Therefore, we shall here develop the formalism of quantum mechanics with an indefinite metric in a simplified way, which involves only one set of quantities. In fact, the present formalism is identical in appearance with Dirac's formalism (Dirac 1947) of the usual quantum mechanics as long as we keep our treatment in an abstract form and do not make use of the matrix representation of operators. In this paper we shall also discuss in some detail the properties of the vector space with an indefinite metric and its physical interpretation. We shall pay special attention to vectors of vanishing norms, because the role of such vectors in quantum mechanics has not been fully discussed before. Further, it will be shown how the present formalism enables us to simplify the use of the indefinite metric in physical applications.

We shall refer to a vector space with an indefinite metric as the *indefinite vector space*, while in accordance with the usual practice a vector space with a positive definite metric will be called the *Hilbert space*.

[1]Manuscript received May 3, 1957.
Contribution from the Division of Pure Physics, National Research Council, Ottawa, Ontario.
Issued as N.R.C. No. 4420.
[2]Permanent address: Department of Physics, Wayne State University, Detroit, Michigan, U.S.A.

2. THE INDEFINITE VECTOR SPACE

Let us consider a vector space of infinite dimensions, in which the components of vectors are in general complex numbers. Let us call this space the indefinite vector space, and let us denote any vector in this space by the symbol Ψ or Φ. With the indefinite vector space let us associate a dual space such that corresponding to any vector Ψ there always exists a vector Ψ^* in the dual space. Let us assume that the relationship between the two spaces is such that if Ψ and Φ are any two vectors in the indefinite vector space, then

$$(\Psi+\Phi)^* = \Psi^*+\Phi^*, \qquad (c\Psi)^* = c^*\Psi^*, \tag{1}$$

$$\Phi^*\Psi = \text{number} = (\Psi^*\Phi)^*, \tag{2}$$

where c is a number, and c^* denotes its complex conjugate. It follows from (2) that

$$\Psi^*\Psi = \text{real number}. \tag{3}$$

The only difference between the above assumptions and those of the usual treatment is that now the quantity $\Psi^*\Psi$ is not positive definite, but according to (3) it can be positive, negative, or zero.

Since the present treatment is very similar to the usual one, it will be convenient to retain the usual notation and terminology for the various quantities. Thus, the vectors Ψ and Ψ^* will be called the Hermitian conjugates of each other, and the real number $\Psi^*\Psi$ will be called the norm of the vector Ψ. But, now any vector satisfying the more general condition

$$\Psi^*\Psi = \pm 1 \text{ or } 0 \tag{4}$$

will be said to be normalized, because we cannot change the sign of the norm of a vector by multiplying it with any number. Further, if two vectors Ψ and Φ are such that their product $\Psi^*\Phi$ vanishes, they will be said to be orthogonal. If a set of vectors are normalized as well as orthogonal to each other, they will be said to form an orthonormal set.

We can also define operators in the indefinite vector space as quantities which operating on any vector change it into some other vector in the same space. Thus, if α is an operator, $\alpha\Psi$ and $\Psi^*\alpha$ are vectors in the indefinite vector space and the dual space respectively, and therefore a quantity of the form $\Psi^*\alpha\Psi$ is a number. An operator α^* will be called the Hermitian conjugate of α if for any arbitrary vector Ψ we have

$$\Psi^*\alpha^* = (\alpha\Psi)^*, \tag{5}$$

whence it follows that

$$\Psi^*\alpha^*\Phi = (\alpha\Psi)^*\Phi = (\Phi^*\alpha\Psi)^*. \tag{6}$$

It can easily be shown that the Hermitian conjugate or the complex conjugate of a product of operators and vectors is obtained by reversing the order of all the factors and then replacing each factor by its Hermitian conjugate. If an operator α is such that

(7) $$\alpha^* = \alpha,$$

it will be called a Hermitian operator.

It is important to note that the self-adjoint operators of the earlier treatments of the indefinite metric correspond to the Hermitian operators of the present treatment, while the Hermitian operators of the earlier treatments have no analogue in the present treatment.

3. BASIC POSTULATES OF QUANTUM MECHANICS WITH AN INDEFINITE METRIC

The basic postulates of quantum mechanics with an indefinite metric can be stated as follows:

(1) The dynamical state of a system at any time can be represented by a vector in an indefinite vector space.

(2) The dynamical variables for a system can be represented by suitable operators, which operate on the state vectors in the indefinite vector space.

(3) The result of a single measurement of a dynamical variable for a system cannot in general be predicted with certainty. But, if the measurement of a dynamical variable for a system in a certain state is carried out a large number of times, the average result of measurement or the so-called expectation value is always given by

(8) $$\langle\alpha\rangle = \Psi^*\alpha\Psi,$$

where the operator α represents the dynamical variable, and Ψ is a normalized vector representing the state of the system.

Now, if α represents any quantity of physical interest, its expectation value must be real, i.e. we must have

(9) $$\Psi^*\alpha\Psi = (\Psi^*\alpha\Psi)^* = \Psi^*\alpha^*\Psi.$$

Since the above relation must hold for any arbitrary vector Ψ, it follows that $\alpha^* = \alpha$. Hence, all quantities of physical interest are represented by Hermitian operators also in the present treatment.

4. PROPERTIES OF HERMITIAN OPERATORS

Although it is evident from (6) and (8) that the Hermitian operators have real expectation values even in the present treatment, some properties of the Hermitian operators are now slightly different from those in the usual treatment.

For, let Ψ be an eigenvector of a Hermitian operator α corresponding to the eigenvalue a, so that

(10) $$\Psi^*\alpha\Psi = \Psi^*a\Psi = a\Psi^*\Psi.$$

Taking the complex conjugate of the above equation, and remembering that $\alpha^* = \alpha$, we have

(11) $$\Psi^*\alpha\Psi = a^*\Psi^*\Psi.$$

From (10) and (11), we then get

(12) $$(a-a^*)\Psi^*\Psi = 0.$$

Since according to the present treatment the norm $\Psi^*\Psi$ may vanish, it does not necessarily follow from the above equation that $a^* = a$. Thus, in the present treatment all the eigenvalues of a Hermitian operator need not be real. However, we can still infer from (12) that all the eigenvalues of a Hermitian operator corresponding to eigenvectors of non-vanishing norms are real.

Similarly, we cannot now establish in general the orthogonality of all the eigenvectors of a Hermitian operator. But, we can show in the usual way that all those eigenvectors of a Hermitian operator which have non-vanishing norms form an orthogonal set of vectors in the indefinite vector space, provided that all the eigenvectors corresponding to the same eigenvalue are chosen in a suitable way.

We shall now assume that if all the eigenvectors of a Hermitian operator have non-vanishing norms, the orthogonal set of eigenvectors formed by them is a complete set, i.e. any vector in the indefinite vector space can be expressed linearly in terms of these orthogonal vectors. Thus, if the eigenvalues of a Hermitian operator α are discrete and all its eigenvectors have non-vanishing norms, we can express a normalized vector Φ as

$$\Phi = \sum_n c_n \Psi_n, \tag{13}$$

where the c_n are numbers, and the Ψ_n are orthogonal eigenvectors of α corresponding to the eigenvalues a_n. When these eigenvectors are also normalized, we have

$$\Psi_m^* \Psi_n = \pm \delta_{mn}, \tag{14}$$

where the plus and the minus signs correspond to the eigenvectors of positive and negative norms respectively. Now, let $f(\alpha)$ be any arbitrary function of α, which can be expressed in powers of α. Then,

$$f(\alpha)\Psi_n = f(a_n)\Psi_n, \tag{15}$$

and

$$\Phi^* f(\alpha)\Phi = \sum_m c_m^* \Psi_m^* f(\alpha) \sum_n c_n \Psi_n = \sum_m c_m^* \Psi_m^* \sum_n c_n f(a_n)\Psi_n, \tag{16}$$

which gives, on using (14), for the average result of measurement of $f(\alpha)$ in the state Φ

$$\langle f(\alpha) \rangle = \sum_n \pm c_n^* c_n f(a_n). \tag{17}$$

But, the average result of measurement of $f(\alpha)$ may be written as

$$\langle f(\alpha) \rangle = \sum_n P_n f(a_n) + \sum_m P_m' f(a_m'), \tag{18}$$

where a_m' is some value for α other than the eigenvalues a_n, and P_n and P_m' are the probabilities of obtaining a_n and a_m' respectively as the result of measurement of α. Since the function $f(\alpha)$ is arbitrary, we find by comparing (17) and (18)

$$P_n = \pm c_n^* c_n, \qquad P_m' = 0, \tag{19}$$

which shows that a vector with a negative norm represents a state occurring with a *negative probability.*

5. REPRESENTATION OF OPERATORS BY MATRICES

If $\Psi_1, \Psi_2, \ldots$ form a complete orthonormal set of vectors of non-vanishing norms, we can represent any operator α in the frame of reference of the vectors Ψ_n by a matrix, whose elements are given by

$$\langle m|\alpha|n\rangle = \Psi_m^*\alpha\Psi_n. \tag{20}$$

It also follows from (20) and (6) that if α is Hermitian,

$$\langle m|\alpha|n\rangle = \langle n|\alpha|m\rangle^*, \tag{21}$$

which shows that a Hermitian operator is represented by a Hermitian matrix also in the present treatment. But, we shall now obtain an important result, which is slightly different from the corresponding result in the usual treatment.

Let us define a quantity η_{lm} as

$$\eta_{lm} \equiv \Psi_l^*\Psi_m = \pm\delta_{lm}, \tag{22}$$

where, as already mentioned, the plus and the minus signs correspond to vectors of positive and negative norms respectively. Then, any arbitrary vector Φ can be expressed in terms of the Ψ_n as an expansion of the form (13), and we have

$$\sum_{l,m}\Psi_l\eta_{lm}\Psi_m^*\Phi = \sum_{l,m}\Psi_l\eta_{lm}\Psi_m^*\sum_n c_n\Psi_n = \sum_{l,m,n} c_n\Psi_l\eta_{lm}\eta_{mn}. \tag{23}$$

But, according to (22),

$$\sum_m \eta_{lm}\eta_{mn} = \delta_{ln}, \tag{24}$$

so that (23) reduces to

$$\sum_{l,m}\Psi_l\eta_{lm}\Psi_m^*\Phi = \sum_l c_l\Psi_l = \Phi. \tag{25}$$

Since the vector Φ is arbitrary, it follows that

$$\sum_{l,m}\Psi_l\eta_{lm}\Psi_m^* = 1. \tag{26}$$

Hence, we have

$$\Psi_k^*\alpha\beta\Psi_n = \sum_{l,m}\Psi_k^*\alpha\Psi_l\eta_{lm}\Psi_m^*\beta\Psi_n \tag{27}$$

or

$$\langle k|\alpha\beta|n\rangle = \sum_{l,m}\langle k|\alpha|l\rangle\,\eta_{lm}\,\langle m|\beta|n\rangle. \tag{28}$$

6. UNITARY TRANSFORMATIONS

As usual, we shall call any operator U that satisfies the relation

$$U^*U = UU^* = 1 \tag{29}$$

a unitary operator. If we carry out a transformation from a set of vectors and operators to another set according to the relations

$$\Psi' = U\Psi, \qquad \Psi'^* = \Psi^*U^*, \qquad \alpha' = U\alpha U^*, \tag{30}$$

where Ψ, Ψ^*, $\alpha, \ldots$ and Ψ', Ψ'^*, $\alpha', \ldots$ denote the corresponding quantities in the two sets, and U is a unitary operator, then the relations (30) will be said to describe a unitary transformation.

It is obvious that all the usual properties of a unitary transformation remain unchanged in the present treatment. For instance, it can easily be shown that if a pair of vectors or operators are Hermitian conjugates of each other, they preserve this property under a unitary transformation. Moreover, any algebraic relation involving vectors and operators remains unchanged under a unitary transformation, and we can pass over in the usual way from one representation of a system to another by means of such a transformation.

It is, however, interesting to note that the Hermitian operators of the present treatment correspond to non-Hermitian operators in the earlier treatments of the indefinite metric, and therefore a transformation of the form (30) corresponds to a non-unitary transformation in the earlier treatments.

7. REMARKS ON THE USE OF AN INDEFINITE METRIC

Owing to certain difficulties of physical interpretation, the formalism of quantum mechanics with an indefinite metric can be used only under special circumstances. We shall now discuss these difficulties of physical interpretation to see what limitations they impose on the use of the indefinite metric.

We have already come across a difficulty of physical interpretation in Section 4, where it was shown that a vector with a negative norm represents a state occurring with a negative probability, which is physically meaningless. Another difficulty of physical interpretation is connected with vectors of vanishing norm. For, if a vector Ψ has a vanishing norm, we can multiply Ψ by any number to obtain another vector Ψ', which also has a vanishing norm. This gives rise to the difficulty that although both Ψ and Ψ' are normalized vectors representing the same state, they lead to different expectation values for any dynamical variable α except when this expectation value vanishes.

The above difficulties of physical interpretation are connected with vectors of negative or vanishing norms. Therefore, *an indefinite metric can be used for a quantum mechanical system without any difficulty only when the states represented by vectors of negative or vanishing norms in the resulting treatment are physically unobservable.*

8. THE FIELD OSCILLATORS

In the quantization of fields of integral spin, we come across two types of "field oscillators", which may be called the normal and the abnormal field oscillators. The usual practice is to treat these field oscillators by using a vector space with a known metric, which is either a positive definite metric or a special type of indefinite metric. However, we shall show that both types of field oscillators can be treated in an analogous way by using a vector space with an unspecified metric, and then postulating the following physical condition:

Every physical system in nature has a state of lowest energy, and the vector representing this state has a positive norm.

Normal Field Oscillator

The Hamiltonian of a normal field oscillator is of the form

$$H = Ea^*a, \tag{31}$$

where E is a positive number, and the operator a and its Hermitian conjugate a^* satisfy the commutation relation

$$aa^*-a^*a = 1. \tag{32}$$

We shall determine the eigenvalues and the eigenvectors of this field oscillator by using the physical condition stated above.

If λ is any eigenvalue of H corresponding to the eigenvector Ψ, we have

$$H\Psi = \lambda\Psi. \tag{33}$$

Then, using (31) and (32), we get

$$Ha\Psi = aH\Psi-Ea\Psi = (\lambda-E)a\Psi, \tag{34}$$

$$Ha^*\Psi = a^*H\Psi+Ea^*\Psi = (\lambda+E)a^*\Psi, \tag{35}$$

which shows that $\lambda-E$ and $\lambda+E$ are also eigenvalues of H provided that $a\Psi \neq 0$ and $a^*\Psi \neq 0$. It follows that there must exist a vector Ψ_0 such that

$$a\Psi_0 = 0. \tag{36}$$

For, if it were not so, it would follow by repeated application of (34) that the eigenvalues of H have no lower limit, and this would contradict our physical condition.

The eigenvalue of H for the eigenstate Ψ_0, satisfying (36), is

$$H\Psi_0 = Ea^*a\Psi_0 = 0, \tag{37}$$

and by repeated application of (35) we find

$$0, E, 2E, \ldots, nE, \ldots \tag{38}$$

are all eigenvalues of H corresponding to the eigenvectors

$$\Psi_0, a^*\Psi_0, a^{*2}\Psi_0, \ldots, a^{*n}\Psi_0, \ldots \tag{39}$$

respectively.

Further, according to the physical condition, Ψ_0 has a positive norm, so that we can normalize it as

$$\Psi_0^*\Psi_0 = 1. \tag{40}$$

Then, we can express the normalized eigenvector Ψ_n corresponding to the eigenvalue nE and its Hermitian conjugate Ψ_n^* as

$$\Psi_n = (n!)^{-\frac{1}{2}}a^{*n}\Psi_0, \qquad \Psi_n^* = (n!)^{-\frac{1}{2}}\Psi_0^*a^n, \tag{41}$$

and the metric of the vector space of the system is given by

$$\Psi_m^*\Psi_n = \delta_{mn}, \tag{42}$$

which is positive definite.

Abnormal Field Oscillator

An abnormal field oscillator has a Hamiltonian of the form

$$H = -Ea^*a, \tag{43}$$

where E is a positive number, and the operator a and its Hermitian conjugate a^* satisfy the commutation relation

$$aa^* - a^*a = -1. \tag{44}$$

Using the physical condition, and following exactly the same procedure as in the case of the normal field oscillator, we can easily show that the eigenvalues of H are again given by

$$0,\ E,\ 2E,\ \ldots,\ nE,\ \ldots, \tag{45}$$

and the corresponding eigenvectors are

$$\Psi_0,\ a^*\Psi_0,\ a^{*2}\Psi_0,\ \ldots,\ a^{*n}\Psi_0,\ \ldots, \tag{46}$$

where Ψ_0 satisfies the relation

$$a\Psi_0 = 0. \tag{47}$$

Further, in view of the physical condition, we can normalize Ψ_0 as

$$\Psi_0^*\Psi_0 = 1, \tag{48}$$

which enables us to express the normalized eigenvector Ψ_n corresponding to the eigenvalue nE and its Hermitian conjugate Ψ_n^* as

$$\Psi_n = (n!)^{-\frac{1}{2}}a^{*n}\Psi_0, \qquad \Psi_n^* = (n!)^{-\frac{1}{2}}\Psi_0^*a^n. \tag{49}$$

But, owing to the different commutation relation (44), the metric of the vector space of the system is now given by

$$\Psi_m^*\Psi_n = (-1)^n\delta_{mn}, \tag{50}$$

which is indefinite.

We have seen how the present formalism enables us to deal with the normal and abnormal field oscillators in an analogous way. The same approach can also be used in the various physical applications of the indefinite metric, which we have mentioned in Section 1. For instance, using an indefinite vector space with an unspecified metric for the radiation field, and then applying our physical condition to all the radiation field oscillators, we easily arrive at the indefinite metric of our earlier treatment of the quantization of the radiation field. Moreover, since the physical condition is Lorentz invariant, it directly ensures the Lorentz covariance of the resulting treatment.

REFERENCES

DIRAC, P. A. M. 1942. Proc. Roy. Soc. A, **180**, 1.
——— 1947. Principles of quantum mechanics (Oxford University Press).
GUPTA, S. N. 1950. Proc. Phys. Soc. A, **63**, 681.
——— 1951. Proc. Phys. Soc. A, **64**, 695.
——— 1952. Proc. Phys. Soc. A, **65**, 161, 608.
——— 1953. Proc. Phys. Soc. A, **66**, 129.
PAULI, W. 1943. Revs. Mod. Phys. **15**, 175.

THE CUMULATIVE YIELDS OF THE KRYPTON AND XENON ISOTOPES PRODUCED IN THE FAST NEUTRON FISSION OF Th^{232} [1]

T. J. KENNETT AND H. G. THODE

ABSTRACT

The relative fission yields for mass chains ending in stable krypton and xenon isotopes have been measured for the fast neutron-induced fission of Th^{232}. Isotope dilution techniques were used to determine the krypton/xenon ratio to assist in obtaining the absolute fission yields for these mass chains. The absolute yields were determined by the use of two methods, both giving results which were in excellent agreement. The fine structure observed for the Th^{232} mass–yield curve is compared with that of heavier fissile nuclides.

INTRODUCTION

During the past few years a considerable amount of work has been done to determine the mass distribution of the products from the neutron-induced fission of U^{233}, U^{235}, and Pu^{239}. In contrast, little work has been reported on the fission yields of Th^{232}. The principal contribution to date has been the radiochemical determination of 23 fission products by Turkevich and Niday (1951). The study of neutron-induced Th^{232} fission is made difficult because of the high fission threshold of 1.10 Mev. (Haxby, Shoupp, Stephens, and Wells 1940) and the low fission cross-section, which has a maximum value of 0.7 barns at 7 Mev. (Hughes and Harvey 1955). The combination of these effects makes it necessary to irradiate the Th^{232} with a high flux of fast neutrons.

A determination of the krypton and xenon yields for the neutron fission of Th^{232} would be of considerable importance for a better understanding of the fission process. The krypton and xenon mass regions exhibit a fine structure or deviation from a smooth curve which was first observed by Thode and Graham (1947) for U^{235} fission. This effect has been qualitatively explained on the basis of shell structure by Glendenin (1949), Wiles (1950) (see also Wiles *et al.* 1953), and Pappas (1953). To test such postulates it is advantageous to obtain as many mass–yield curves as possible. The relative position of the familiar asymmetric fission yield curve depends upon the fissile nuclide. Present data indicate that the heavy mass hump remains at about the same position for all fissile nuclides. Conversely the position of the light mass hump is a function of the mass of the fissile nuclide. The relative positions of the krypton and xenon yields are such as to make the ratio xenon/krypton a good parameter for measuring this effect. To obtain such information a study of the Th^{232} fission yields was undertaken.

EXPERIMENTAL

Irradiation Conditions

The source of fission spectrum neutrons was a transformer in the N.R.X.

[1]Manuscript received May 27, 1957.

Contribution from the Departments of Physics and Chemistry, Hamilton College, McMaster University, Hamilton, Ontario.

(Chalk River) Reactor. The transformer consisted of a partially hollowed, natural uranium fuel element and occupied a lattice position where the thermal neutron density was a maximum. The cylindrical tube was 7 in. long with an outside diameter of 1.125 in. and a wall thickness of 0.125 in. The neutron distribution within the transformer consisted of the thermal and fission spectra. Three samples were irradiated for 6 weeks (irradiation A) and two samples for 3 weeks (irradiation B).

The samples were irradiated in the form of thorium metal machined to cylindrical rods of 0.125 in. diameter. The thorium was sheathed in cadmium to reduce the reactions

$$\mathrm{Th}^{232}+n \rightarrow \mathrm{Th}^{233} \xrightarrow{\beta} \mathrm{Pa}^{233} \xrightarrow{\beta} \mathrm{U}^{233},$$
$$\mathrm{U}^{233}+n \rightarrow \text{fission}$$

produced by the otherwise intense thermal neutron flux. The samples were then placed in hexagonal aluminum containers to permit air-cooling during the irradiation.

Analysis of the thorium showed the natural uranium content to be less than 0.1%. This low concentration removes the possibility of appreciable contribution from uranium fission. The thorium oxide content was about 25% and there were traces of iron possibly arising from the fabrication process.

Extraction Procedure

Two methods were employed to extract the fission product rare gases from the irradiated thorium metal. The first procedure, devised by Arrol, Chackett, and Epstein (1949) for the extraction of rare gases from irradiated uranium metal, was found to be applicable to thorium. The thorium was dissolved in a saturated solution of cupric potassium chloride and the released gases were passed through a drying train. The purification of the rare gases was achieved by the use of a calcium furnace.

The second method consisted of heating the thorium to about 1000° C. and reacting it with chlorine. When the reaction was completed the thorium chloride had all sublimed to a cool region of the vacuum system, which ensured complete release of the rare gases. After this reaction the excess chlorine was removed by a hot iron wire. The final purification was achieved by the use of a calcium furnace. Although both methods yielded the same results the chlorine reaction has the advantage of minimum handling. This reduces the likelihood of contamination with normal krypton and xenon.

Isotope Dilution Technique

Extraction of the rare gas fission products permits mass spectrometric analysis of the relative fission yields for the krypton and xenon isotopes. No information can be obtained concerning the quantity of krypton and xenon or the krypton/xenon ratio. To obtain such information it is necessary to "spike" the extracted fission gas with a known quantity of krypton and xenon that has a different isotopic composition. The most desirable condition is to spike the fission gas with rare gas isotopes which are not formed in fission as cumulative isotopes. Pure samples of Kr^{80}, Kr^{82}, and Xe^{128} were

prepared by the irradiation of potassium bromide and potassium iodide. These isotopes are formed in very low abundance as primary fission products (Kennett and Thode 1956) and so do not interfere with the cumulative fission pattern. This spiking mixture was calibrated against a standard mixture of krypton and xenon prepared by Linde Air Products.

The spiking was done by admitting a known aliquot of the prepared mixture during the chlorine reaction. Once the spike has been added and thoroughly mixed in, a 100% chemical yield is no longer necessary. Therefore, it is advantageous to add the spike to the reaction vessel as early as possible.

Mass Spectrometry

The fission product rare gases were analyzed with a 10 in. directional focusing mass spectrometer employing an electron multiplier for the detector. The output from the multiplier was integrated and amplified by a vibrating reed electrometer and then permanently displayed on a recorder. The resolving power of the instrument was 625, which permitted doublet separation of the hydrocarbon background from the rare gas isotopes. Analysis of normal krypton and xenon gave results within 0.5% of the accepted values determined by Nier (1950).

Normal contamination of the fission gases can be detected by the presence of Xe^{129} and a change in the Kr^{82}/Kr^{80} ratio found for the spiking mixture. By measurement of these quantities a correction can easily be made for the normal contribution to the observed fission pattern.

RESULTS

The observed mass spectrometric ratios for the krypton isotopes are given in Table I. The Kr^{85} values have been corrected for decay and branching and

TABLE I

THE RELATIVE FISSION YIELDS OF THE KRYPTON ISOTOPES OCCURRING IN THE FAST NEUTRON FISSION OF Th^{232}

	Mass spectrometric ratio			
Sample data	Kr^{83}	Kr^{84}	Kr^{85}*	Kr^{86}†
Irradiation A				
Sample 1	3.33±0.01	6.12±0.02	6.49±0.03	10.00
Sample 2	3.29±0.01	6.06±0.01	6.44±0.02	10.00
Sample 3	3.30±0.02	6.07±0.04	6.45±0.04	10.00
Average value	3.31±0.02	6.08±0.02	6.46±0.02	10.00
Irradiation B				
Sample 4	3.32±0.02	6.06±0.03	6.51±0.06	10.00
Sample 5	3.34±0.04	6.03±0.09	6.45±0.09	10.00
Average value	3.33±0.03	6.05±0.04	6.48±0.07	10.00

*Corrected for decay and branching.
†Normalized to 10.00.

Kr^{86} has been normalized to 10.00. The errors quoted for each sample are the standard deviations obtained from the measurement of 14 spectrograms.

The values for individual samples and the average values for the two irradiations are seen to be in good agreement.

Table II summarizes the observed relative fission yields for xenon where Xe^{134} has been normalized to 10.00. With the exception of Xe^{136} the results

TABLE II

THE RELATIVE FISSION YIELDS OF THE XENON ISOTOPES OCCURRING IN THE FAST NEUTRON FISSION OF Th^{232}

	Mass spectrometric ratio			
Sample number	Xe^{131}	Xe^{132}	Xe^{134} *	Xe^{136}
Irradiation A				
Sample 1	3.00±0.01	5.34±0.01	10.00	10.70±0.03
Sample 2	3.02±0.01	5.34±0.01	10.00	10.73±0.02
Sample 3	3.01±0.01	5.33±0.01	10.00	10.80±0.02
Average value	3.01±0.01	5.34±0.01	10.00	10.74±0.04
Irradiation B				
Sample 4	3.00±0.01	5.29±0.03	10.00	10.45±0.07
Sample 5	3.04±0.02	5.31±0.03	10.00	10.50±0.03
Average value	3.02±0.02	5.30±0.03	10.00	10.48±0.04

*Normalized to 10.00.

from both irradiations are in good agreement. Irradiation A, with twice the irradiation time of B, will exhibit a larger burn-up of Xe^{135} resulting in an increase of the Xe^{136} yield. The amount of Xe^{135} burn-up is a function of the irradiation time and also the thermal neutron flux within the sample. By combining the Xe^{136} results for both irradiations the value for the thermal neutron flux inside the thorium was found, and it proved to be less than 2×10^{12} neutrons/cm.^{2}/sec. Calculations made with this flux indicated that irradiation B had negligible burn-up and that the observed Xe^{136} yield for this sample represents the true yield for the 136 mass chain.

The irradiation conditions for both A and B are tabulated in Table III.

TABLE III

IRRADIATION CONDITIONS FOR THE FAST NEUTRON FISSION OF Th^{232}

	Irradiation A	Irradiation B
Irradiation time (days)	42	22
Integrated power (megawatt days)	1565.0	717.2
Irradiation time (days) at 40 megawatts	39.1	17.9
Thermal flux (neutrons/cm.^{2}/sec.) at transformer position for 40 megawatts	8.20×10^{13}	8.28×10^{13}

The irradiation time has been calculated on the basis of full power operation. The value for the thermal neutron flux at the transformer position has also been referred to full power operation.

Isotopic dilution was done for samples 3 and 5 of irradiations A and B respectively. The results of these experiments are summarized in Table IV. In this table Kr^{85} has been again corrected for decay and branching. The

TABLE IV

ISOTOPE DILUTION RESULTS FOR Th^{232}

Nuclide	Isotopic volume ((mm.³/g. of Th^{232})×10^3)	
	Irradiation A, sample 3	Irradiation B, sample 5
Kr^{83}	8.10±0.02	4.33±0.05
Kr^{84}	14.91±0.12	6.88±0.07
Kr^{85} *	17.04±0.18	7.65±0.06
Kr^{86}	24.47±0.18	11.79±0.10
Total Kr volume	64.52±0.42	30.65±0.28
Xe^{131}	6.78±0.02	3.17±0.04
Xe^{132}	11.98±0.06	5.54±0.05
Xe^{134}	22.49±0.08	10.42±0.04
Xe^{136}	24.23±0.12	10.92±0.05
Total Xe volume	65.48±0.42	30.05±0.18
Xenon/krypton ratio	1.007±0.008†	0.981±0.011
Average value of xenon/krypton ratio = 0.994±0.013		

*Corrected for decay and branching.
†Corrected for neutron capture by Xe^{135}.

xenon/krypton ratio is obtained by finding the ratio "total xenon volume/total krypton volume". A 3% correction was made for the Xe^{136} of sample 3 to compensate for the neutron capture by Xe^{135}. The agreement of the xenon/krypton ratio for irradiations A and B is exceptionally good considering the wide difference in irradiation conditions. By the use of the average xenon/krypton ratio in Table IV and the results given in Tables I and II, the abundance of the krypton and xenon yields for the fast fission of Th^{232} can be calculated. The results of this calculation are given in Table V.

TABLE V

THE RELATIVE FISSION YIELD ABUNDANCES OF THE RARE GAS ISOTOPES OCCURRING IN THE FAST NEUTRON FISSION OF Th^{232}

Isotope	Relative abundance (%)
Kr^{83}	6.42±0.04
Kr^{84}	11.74±0.08
Kr^{85} *	12.50±0.08
Kr^{86}	19.33±0.13
Xe^{131}	5.22±0.03
Xe^{132}	9.24±0.06
Xe^{134}	17.34±0.11
Xe^{136}	18.21±0.12
	100.00

*Corrected for decay and branching.

DISCUSSION OF RESULTS

The xenon/krypton ratio not only ties together two regions of the mass-yield curve but also represents an important parameter for determining the

displacement of the mass–yield curve as a function of the fissile nuclide. An examination of the mass–yield curves for U^{233}, U^{235}, U^{238}, and Pu^{239} (Katcoff 1957) shows that the heavy mass hump remains centered about approximately the same mass number while the light mass hump moves to lower masses as the fissile nuclide decreases in mass. The xenon yields fall near the top of the heavy mass hump while the krypton yields lie on the low mass side of the light hump. Any displacement of the light mass hump results in a marked change in the krypton yields and also in the xenon/krypton ratio. The value of the ratio changes from 4.38 ± 0.08 for U^{235} (Blades, Fleming, and Thode 1956) to 0.994 ± 0.013 for Th^{232}. Such a change indicates a 3 to 4 mass unit displacement of the light hump. For a more quantitative interpretation of this and other effects we need, of course, some knowledge of absolute fission yields.

The problem of absolute fission yields can, for this case, be approached in two ways. The first is to fit the relative krypton and xenon results to the Th^{232} mass–yield curve determined by Turkevich and Niday (1951). The second is to calculate the fission spectrum flux within the transformer and thereby to determine the number of fissions in the thorium samples. If both methods give consistent yields then reasonable weight can be associated with the calculated flux.

Absolute Fission Yields from Curve Fitting

The radiochemical technique has inherent errors of considerable magnitude so that Turkevich and Niday (1951) were only able to obtain the general nature of the Th^{232} mass–yield curve. Fig. 1 shows the fission yield curve with the

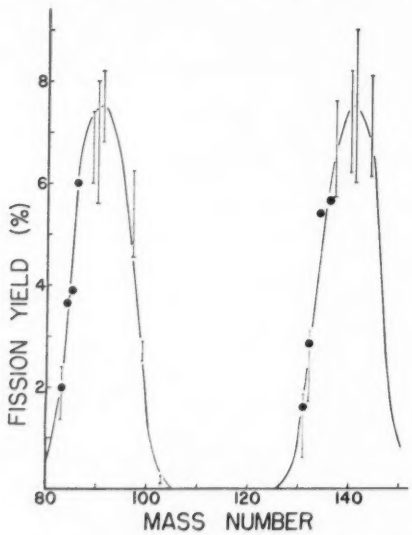

FIG. 1. The mass–yield curve for fast neutron-induced fission of Th^{232}. The mass spectrometric values are shown by ● and the radiochemical results of Turkevich and Niday (1951) by I.

mass spectrometric and radiochemical data plotted with the associated errors. The high precision of the mass spectrometer ratios is clearly shown. To obtain the absolute fission yields it is required that both the krypton and xenon results fit the curve and that all the yields for each hump add to 100%. Other than for the fine structure at Kr^{84}, Kr^{85}, and Xe^{134} the agreement with the curve is very good. The absolute fission yields used in Fig. 1 to give this excellent agreement are listed in Table VI.

TABLE VI

ABSOLUTE FISSION YIELDS OF KRYPTON AND XENON OCCURRING IN THE FAST NEUTRON FISSION OF Th^{232} *

Isotope	Fission yield (%)	Isotope	Fission yield (%)
Kr^{83}	1.99±0.01	Xe^{131}	1.62±0.01
Kr^{84}	3.65±0.02	Xe^{132}	2.87±0.02
Kr^{85}	3.88±0.02	Xe^{134}	5.38±0.03
Kr^{86}	6.00±0.03	Xe^{136}	5.65±0.03

*Normalized to the radiochemical mass-yield curve of Turkevich and Niday (1951), so as to give the best fit with all krypton and xenon values.

Neutron Multiplicity

The curve shown in Fig. 1 is symmetric about mass number 115.5 suggesting that the neutron multiplicity is approximately 2 for Th^{232}. The most probable masses are 91 and 140 as also found by Turkevich and Niday (1951).

Absolute Fission Yields from Flux Calculations

To calculate the number of fissions that have occurred in the irradiated Th^{232} it is necessary to know the fission cross section and the fission spectrum flux. The fission cross section is a function of neutron energy and so it is convenient to define

$$\bar{\sigma}_f = \frac{\int_0^{17} \sigma_f(E)N(E)dE}{\int_0^{17} N(E)dE} = \frac{\int_{1.1}^{17} \sigma_f(E)N(E)dE}{\int_0^{17} N(E)dE}, \tag{1}$$

where $N(E)$ is the number of neutrons having energy between E and $E+dE$ and $\sigma_f(E)$ is the fission cross section for neutrons of energy E. Because of the fission threshold at 1.10 Mev. (Haxby *et al.* 1940) the range of integration for the numerator is 1.10 to 17 Mev. The function $N(E)$ for fission spectrum neutrons has been determined experimentally by Watt (1952). The value of $\sigma_f(E)$ for Th^{232} has been given by Hughes and Harvey (1955). Graphical evaluation of Equation 1 gave a value of 0.075 barns for $\bar{\sigma}_f$.

Fig. 2 shows the geometric configuration of the transformer. By assuming a sphere of 1 cm.^{2} cross section at the origin it is possible to calculate the number of fission neutrons which pass through it per second. The number of fast neutrons which pass through the sphere per second from an annular uranium ring of radius r is given by

$$dN = \frac{wr \exp(-n\sigma_a\lambda)drdz}{2(r^2+z^2)}, \tag{2}$$

where w is the number of fission neutrons formed per cm.^{3} per second, n is the number of uranium atoms per cm.^{3}, and σ_a is the absorption cross section

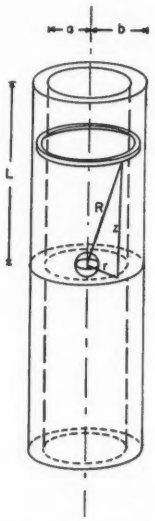

FIG. 2. The geometric configuration of the transformer.

of natural uranium. The quantity λ is the distance the fission neutrons travel through the fuel element wall and is given by

$$\lambda = \frac{r(r-a)}{(r^2+z^2)^{\frac{1}{2}}}. \tag{3}$$

The total flux is then

$$N = \int_{-L}^{L}\int_{a}^{b} \frac{wr \exp(-n\sigma_a\lambda)drdz}{2(r^2+z^2)}. \tag{4}$$

By expansion of the exponential, equation (4) can be integrated with the result for the fast flux of

$$N = 0.472w.$$

The quantity w is a slowly varying function of r but with the boundary conditions for this case it can be treated as a constant in Equation (4). To evaluate w the average thermal flux within the transformer must be known. Calculations by Case, de Hoffmann, and Placzek (1953) for self-shielding corrections indicate that the average thermal flux within the transformer, ϕ, is

$$\phi = 0.88\phi_0,$$

where ϕ_0 is the unperturbed flux at that position. At 40 megawatts power

$\phi_0 = 8.6\times10^{13}$ neutrons/cm.^{2}/sec. for the transformer lattice position. Using the above relations the fast flux is found to be

$$N = 0.208\phi_0 = \phi_f$$

or about 21% of the peak unperturbed thermal flux at the same position. The contribution to N from the solid fuel element can be shown to be negligible.

From the spiking results given in Table IV the number of fissions per gram of Th^{232} can be calculated for irradiation A and B. This has been done and the results are given in Table VII, column 1, where Y^{86} is the yield in per

TABLE VII

THE CALCULATED AND FITTED YIELD OF THE 86 MASS CHAIN FOR Th^{232} FAST FISSION

	No. of fissions/g. of Th^{232}		Yield of 86 mass chain Y^{86} (%)	
Irradiation	Experimental	Calculated	Calculated	Curve-fitted
A	$6.58\times10^{16}/Y^{86}$	1.13×10^{16}	5.82	(6.00±0.06)
B	$3.17\times10^{16}/Y^{86}$	5.19×10^{16}	6.11	(6.00±0.06)
	Average value of Y^{86} (%)		5.97±0.15	6.00±0.06

cent of the 86 mass chain. The number of fissions per gram of Th^{232} can also be determined by use of the relation

$$\text{(5)} \qquad \text{fissions/g.} = \bar{\sigma}_f \phi_f \bar{T} \text{ (no. } Th^{232} \text{ atoms/g.)},$$

where $\bar{T}$ is the irradiation time at 40 megawatts power. The value of Equation (5) for A and B is given in Table VII, column 2. Equating columns 1 and 2 a value for Y^{86} can be found. The value of Y^{86} found in this way for irradiation A and B is given in column 3. The value for Y^{86} obtained from the mass–yield curve is given in column 4.

The agreement between the two methods is remarkably good and gives support to both the normalization and the calculated fission spectrum flux.

General Characteristics of Fine Structure in the Mass–Yield Curve

Fig. 3 shows the krypton yields for Th^{232}, U^{233} (Fleming, Tomlinson, and Thode 1954), U^{235} (Blades, Fleming, and Thode 1956), and U^{238} (Wanless and Thode 1955) fission. It is apparent that the mass–yield curve in this region moves to higher yields as the mass of the fissile nuclide decreases. This indicates that the light mass hump is actually displaced. The mass displacement of these curves for a fixed fission yield is approximately equal to the mass difference between the fissile nuclides. This implies that the heavy mass hump remains at a relatively constant position. Closer examination of Fig. 3 shows the well-known fine structure of the 84 and 85 mass chains. The high 84 yield in all four cases probably arises because of a preference for this chain in the original fission process or cross-chain branching from the 85 mass chain. The behavior of the 85 yield depends on the fissile nuclide. This yield is high for U^{233}, normal for U^{235}, and low for Th^{232} and U^{238}. The deviation of the 85 yield from the smooth mass–yield curve can be correlated with the Z/A value of the fissile nuclide. This suggests that a branching (n-emission) may occur in

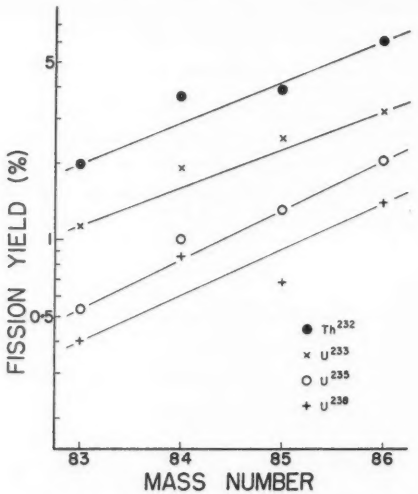

FIG. 3. The krypton yields for neutron-induced fission of Th^{232}, U^{233} (Fleming *et al.* 1954), U^{235} (Blades *et al.* 1956), and U^{238} (Wanless and Thode 1955).

the 85 chain since the primary yield of such a prompt neutron emitter would be related to the Z/A value of the fissile nuclide. The nuclide in question must have a fairly high primary yield and possess a low threshold for neutron emission. These conditions are fulfilled by $_{34}Se^{85}$. This would indicate that the fine structure of the 85 mass region can be explained by the Glendenin (1949) boil-off effect since $_{34}Se^{85}$ has 51 neutrons. Thus the Th^{232} fine structure is most similar to that of U^{238} since both have about the same Z/A value, while the magnitude of the Th^{232} krypton yields is the highest since 232 is the smallest mass number examined to date.

Fig. 4 shows the 131, 132, 134, and 136 yields for Th^{232}, U^{233} (Fleming, Tomlinson, and Thode 1954), U^{235} (Blades, Fleming, and Thode 1956), and U^{238} (Wanless and Thode 1955) fission. The Th^{232} yields are lower than for the other cases and the 136/131 ratio is larger indicating a steeper mass–yield curve. Both these facts suggest that the Th^{232} heavy mass hump may be displaced to higher masses than for the other three cases. The Th^{232} pattern, although having lower yields and, therefore, in a different region of the mass–yield curve, still shows the same general shape as the other cases. The Th^{232} mass–yield curve has a satellite on the side of the main hump. This increased fission probability appears to be a combination of structural preference for the 82 neutron shell in the initial fission process and a Glendenin boil-off effect.

ACKNOWLEDGMENTS

The authors gratefully acknowledge financial assistance from the National Research Council. They wish to thank Atomic Energy of Canada Limited for

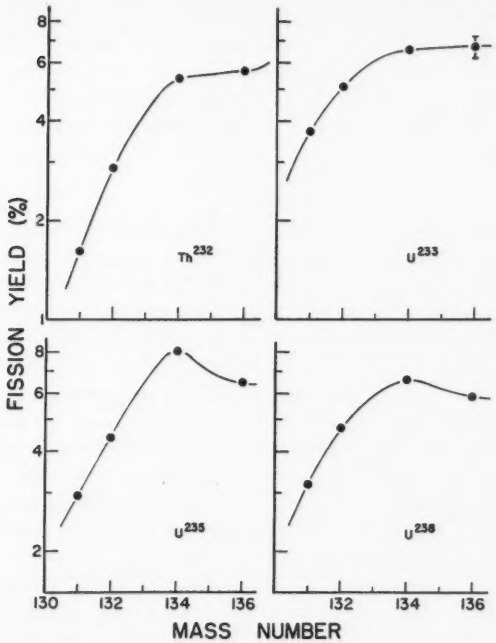

FIG. 4. The xenon yields for neutron-induced fission of Th^{232}, U^{233} (Fleming *et al.* 1954), U^{235} (Blades *et al.* 1956), and U^{238} (Wanless and Thode 1955).

providing the fissile material and arranging for the irradiations. Assistance was also provided by Dr. K. Fritze and Mr. B. G. Young in connection with some aspects of the extraction and spiking techniques.

REFERENCES

ARROL, W. J., CHACKETT, K. F., and EPSTEIN, S. 1949. Can. J. Research, B, **27**, 757.
BLADES, A. T., FLEMING, W. H., and THODE, H. G. 1956. Can. J. Chem. **34**, 233.
CASE, K. M., de HOFFMANN, F., and PLACZEK, G. 1953. Introduction to the theory of neutron diffusion, Vol. 1 (U.S. Government Printing Office, Washington, D.C.).
FLEMING, W. H., TOMLINSON, R. H., and THODE, H. G. 1954. Can. J. Phys. **32**, 522.
GLENDENIN, L. E. 1949. Laboratory for Nuclear Science, Massachusetts Institute of Technology, Technical Report No. 35.
HANBY, R. O., SHOUPP, W. E., STEPHENS, W. E., and WELLS, W. H. 1940. Phys. Rev. **57**, 1088.
HUGHES, D. J. and HARVEY, J. A. 1955. Neutron Cross Sections, Brookhaven National Laboratory Report, BNL-325.
KATCOFF, S. 1957. Handbook of nuclear engineering (Addison-Wesley Publishing Company, Inc., Cambridge, Mass., to be published).
KENNETT, T. J. and THODE, H. G. 1956. Phys. Rev. **103**, 323.
NIER, A. O. 1950. Phys. Rev. **79**, 450.
PAPPAS, A. C. 1953. Laboratory for Nuclear Science, Massachusetts Institute of Technology, Technical Report No. 63.
THODE, H. G. and GRAHAM, R. L. 1947. Can. J. Research, A, **25**, 1.
TURKEVICH, A. and NIDAY, J. B. 1951. Phys. Rev. **84**, 52.
WANLESS, R. K. and THODE, H. G. 1955. Can. J. Phys. **33**, 541.
WATT, B. E. 1952. Phys. Rev. **87**, 1037.
WILES, D. R. 1950. M.Sc. Thesis, McMaster University, Hamilton, Ontario.
WILES, D. R., SMITH, B., HORSLEY, R., and THODE, H. G. 1953. Can. J. Phys. **31**, 419.

MULTIPLE SCATTERING MEASUREMENTS OF π AND μ MESONS STOPPING IN NUCLEAR EMULSIONS*

B. JUDEK

Some previous work by the author (Judek 1957) was designed to test the accuracy of the Constant Sagitta multiple scattering method (Dilworth, Goldsack, and Hirschberg 1954) for mass determination of particles coming to rest in the emulsion. Particularly long track lengths were used, and measurements made for protons, deuterons, and tritons, indicating that the expected theoretical accuracy was attainable. Measurements have now been made on long tracks of π and μ mesons stopping in the emulsion. Tracks of π mesons were identified by their characteristic $\pi \rightarrow \mu$ decays or formation of σ stars, and of μ mesons by their $\mu \rightarrow$ electron decays. They were selected from a batch of Ilford G5 plates, 1000 μ thick, exposed to cosmic radiation in a balloon flight,† and from a stack of Ilford G5 stripped emulsions, 400 μ thick, exposed to secondary radiation from a carbon target bombarded by the 3 Bev. proton beam of the Brookhaven cosmotron.†

The scattering scheme of the Göttingen tables (Fay, Gottstein, and Hain 1954) giving the mean sagitta, $\bar{D}$, of 0.5 μ for π mesons was used, with the simplification that the cell length was varied in steps of 5 μ instead of 1 μ. (It was estimated that the error introduced by this approximation (Judek 1957, Appendix II) was less than 0.1% for the π scheme and therefore negligible.) The measured range of each track was about 1 cm., giving about 250 independent cells, and it was wholly contained in one emulsion layer. Measurements were made on a Koristka M.S.2 microscope. The noise level correction was determined for nine π meson tracks by the method of elimination using measurements at full and half cell lengths (see Judek 1957, Appendix III) and this gave a noise level of 0.13 ± 0.01 μ. On account of the rather large scattering for π and μ mesons, especially near the end of the range, it was necessary to realign the tracks frequently. The effect of imperfect alignment and also of steepness of tracks on the value of $\bar{D}$ was carefully estimated. It was found that under the experimental conditions, i.e. with the average inclination of tracks, relative to the direction of the stage movement, of 3/100 radians (a figure obtained from the mean value of the ratio: sideways displacement of the track/cell length), the error due to alignment (Judek 1957, Appendix II) was only about 0.2% when averaged over the whole length of track. The correction for steepness (taken as proportional to $\cos\theta^{0.92}$ (Dilworth, Goldsack, and Hirschberg 1954), where θ is the angle of dip), however, was found to be of the order of 5–10% for the last 1000 μ from

*Issued as N.R.C. No. 4428.

†We are indebted to the U.S. Office of Naval Research for the cosmic ray exposure in a Skyhook balloon flight, and to the Brookhaven National Laboratory for the cosmotron exposure.

the end of the range, and averaging to about 2% for the whole length of the tracks. This estimate is based on separate measurements of the angles of dip of successive small (100 μ) portions along the whole lengths of five π meson tracks selected at random.

Fig. 1 shows the distributions of the values of $\bar{D}$, the mean sagittae (corrected for the noise level only), for individual tracks of 28 π mesons and five μ

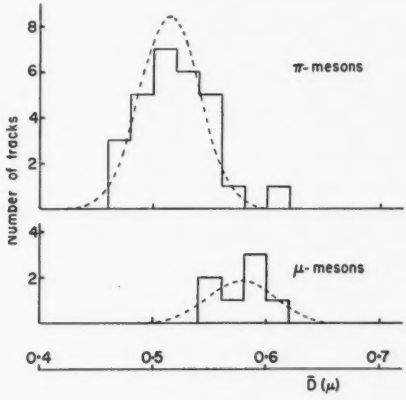

FIG. 1.

mesons. The dotted curves represent the Gaussian distributions centered at the mean values of $\bar{D}$ of 0.514 and 0.578 for the π and μ meson groups respectively and with widths corresponding to standard deviations of 5% calculated on the basis of the $75/\sqrt{N}\%$ formula (N = number of independent cells per track). The experimental values of the standard deviations, calculated from the individual values of $\bar{D}$, were found to be $5.4\pm0.7\%$ and $4.3\pm1.2\%$ for the π and μ meson groups respectively, which is in good agreement with the above theoretical value of 5%. Only a partial resolution between the π and μ mesons has been obtained on the basis of measurements of 1 cm. residual ranges, which is as expected from statistical considerations.

The mean value of $\bar{D}$ of 0.514 ± 0.008 μ for π mesons is about 3% higher than the expected value of 0.500 μ. A correction for steepness of tracks would reduce the experimental value probably by about 2% as indicated by measurements described above, thus giving a good agreement between the theoretical and experimental values. The value of the mass ratio of π to μ mesons deduced in the usual way from their respective average values of $\bar{D}$ (see Judek 1957, Appendix IV) was found to be 1.30 ± 0.07, which again is in good agreement with the expected value of $273/207 = 1.32$.

Fig. 2 shows the variation of the values of $\bar{D}$ with residual range deduced from observations on all π and μ meson tracks. In order to combine the measurements on π and μ mesons all the values of $\bar{D}$ were normalized by dividing them by the respective average values of $\bar{D}$, i.e. $\bar{D}_0$, for each group.

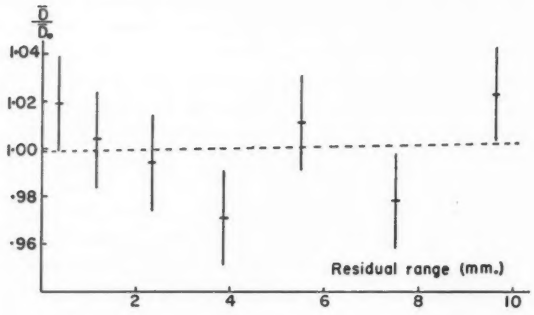

FIG. 2.

The dotted line is the best "least square" line through the points and has a slope of less than 0.5% change in $\bar{D}/\bar{D}_0$ per cm. residual range. It can be seen that there is no significant variation of $\bar{D}$ with residual range.

DILWORTH, C., GOLDSACK, S. J., and HIRSCHBERG, L. 1954. Nuovo cimento, **11**, 113.
FAY, H., GOTTSTEIN, K., and HAIN, K. 1954. Nuovo cimento, Suppl. **11**, 2.
JUDEK, B. 1957. Nuovo cimento, **5**, 886.

RECEIVED MAY 1, 1957.
DIVISION OF PURE PHYSICS,
NATIONAL RESEARCH COUNCIL,
OTTAWA, CANADA.

LETTERS TO THE EDITOR

Under this heading brief reports of important discoveries in physics may be published. These reports should not exceed 600 words and, for any issue, should be submitted not later than six weeks previous to the first day of the month of issue. No proof will be sent to the authors.

A Determination of the Hydrogen Positions in $Ca(OH)_2$ by X-Ray Diffraction

The structures of $Ca(OH)_2$ and $Mg(OH)_2$ are isomorphous and the atomic coordinates, except those of the hydrogen positions, have been known for many years (Aminoff 1919). Even for the hydrogen atoms, plausible locations had been proposed by Bernal and Megaw (1935) on the basis of symmetry and electrostatic considerations. However, the infrared absorption spectra of $Mg(OH)_2$ (Mara and Sutherland 1953) and $Ca(OH)_2$ (Petch and Megaw 1954) were found to show unexpected complexities in the region 2.3 μ to 3.5 μ. Mara and Sutherland concluded that the unit cell of $Mg(OH)_2$ must be much larger than that found from X-ray analysis and that the positions of the hydrogen atoms, as proposed by Bernal and Megaw, are incorrect. Their conclusions, if correct, should apply to $Ca(OH)_2$ as well. The unit cell dimensions and space groups of $Mg(OH)_2$ and $Ca(OH)_2$, accepted prior to the infrared work, were confirmed (Petch and Megaw 1954) by X-ray work, and strong evidence supporting the hydrogen positions proposed by Bernal and Megaw was presented in a preliminary report (Petch 1955) of a further X-ray study of $Ca(OH)_2$. The final results of this work are reported here.

The specimen, a cylinder with the dimensions 0.14 mm. by 0.8 mm. and its axis parallel to an a-axis, was ground from a crystal of $Ca(OH)_2$ prepared by the hydration of larnite by Professor C. E. Tilley, Department of Mineralogy and Petrology, Cambridge University. The relative integrated intensities of 52 (Okil) reflections were measured with a Geiger-counter X-ray diffractometer using Mo $K\alpha$ radiation. The counter readings were corrected for dead-time losses and for background counts. The balanced filter technique (Ross 1928) was used to eliminate the effect of all white radiation except that within the wave-length range 0.69–0.77 Å (the wave-lengths of the Zr K and Sr K absorption edges), which was not "balanced-out" and required a separate correction. Absorption effects were small in comparison with other possible errors and were neglected in this work. The usual corrections were made for the Lorentz and polarization effects. The observed structure factors were put on an absolute basis by scaling against the calculated values in the final stages of the analysis.

The technique of the $(F_o - F_c)$-synthesis, where the F_o's and the F_c's are the observed and the calculated structure factors respectively, was used to locate the hydrogen atoms. The $(F_o - F_c)$-synthesis was used because it greatly reduces the effect of Fourier series termination errors and shows up the contributions of hydrogen atoms very clearly when the F_c's are evaluated on the basis of a model structure not containing the hydrogen atoms. For the first syntheses the Hartree scattering factors for Ca^{++} and $O^{=}$, modified by thermal corrections, were used in the calculations of the F_c's, but in the final stages of refinement the Hartree values for the scattering factors were abandoned in favor of semiempirical values. The use of these semi-empirical scattering factors, corrected to allow for the anisotropic thermal vibrations of the calcium and oxygen ions, resulted in a much better agreement between the F_o's and the F_c's.

A projection on the $(2\bar{1}10)$ plane of the electron density in the asymmetric unit of $Ca(OH)_2$ from which the calcium and oxygen ions have been subtracted is shown in Fig. 1. This projection of the electron density, which was obtained with the final two-dimensional $(F_o - F_c)$-synthesis in which the contributions of the hydrogen atoms to the F_c's were excluded, has as its most prominent feature a large peak superposed on an undulating background. For a number of reasons, it is believed that this peak represents an electron associated with a hydrogen atom and cannot be due to an accumulation of errors. Firstly, the electron density of 0.9 e.Å^{-2} at this peak is 11 times larger than the standard deviation of the electron density. Secondly, as shown in Fig. 2, the peak disappears completely leaving the background unchanged when the hydrogen atoms are included in the model structure (on which the F_c's are based) at the positions suggested by the peak in Fig. 1. The probability of an accumulation of errors producing not only such a large peak, but also a peak with a shape identical to that of a hydrogen atom in projection, seems vanishingly small. Thirdly, the value of the reliability factor, $R \equiv \sum \big||F_o| - |F_c|\big| \div \sum |F_o|$, decreases from 0.023 to 0.011 when the hydrogen atoms are also included in the model structure at the positions suggested by this peak. Taking the position of this peak in the electron density as the hydrogen position the O—H bond is parallel to the c-axis, as originally suggested by Bernal and Megaw, with a length of 0.79±0.04 Å. The final atomic coordinates (in special positions of $P\bar{3}m1$) in $Ca(OH)_2$ obtained in this work are listed below:

Ca	$(0, 0, 0)$
O	$\pm(\frac{1}{3}, \frac{2}{3}, u)$
H	$\pm(\frac{1}{3}, \frac{2}{3}, v)$

with $u = 0.2330 \pm 0.0004$ and $v = 0.395 \pm 0.008$.

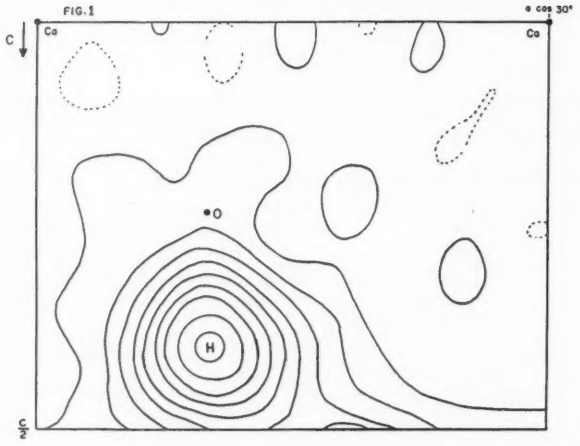

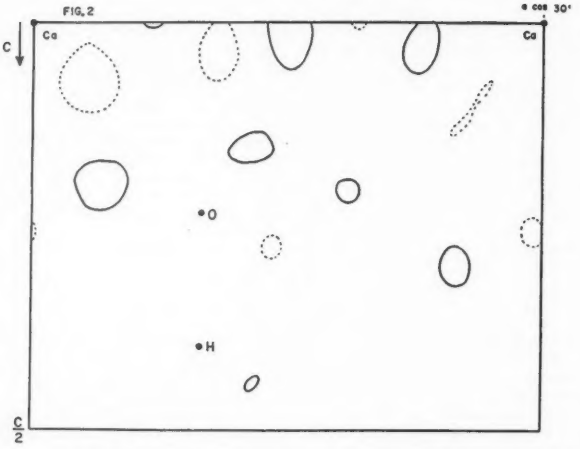

FIG. 1. A projection on the $(2\bar{1}\bar{1}0)$ plane of the electron density in the asymmetric unit of $Ca(OH)_2$ from which the calcium and oxygen ions have been subtracted. The contours are drawn at every 0.1 e. $Å^{-2}$ with the zero contour omitted and the negative contours dotted.

FIG. 2. As in Fig. 1 except that the hydrogen atom has also been subtracted.

Busing and Levy (1957) have recently located the protons in $Ca(OH)_2$ by neutron diffraction and they report that the O—H bond has the same direction as reported here but a length in projection along the *c*-axis of 0.936 ± 0.003 Å. Because of electron-bonding effects there is no reason to expect that the point of maximum density for an electron associated with a hydrogen atom in a crystal must coincide with the proton position and in this case, it is apparent that there is a considerable shift. This emphasizes the importance of stating explicitly what one means by a "hydrogen atom position" in discussions on this subject.

It should be added that Mara and Sutherland (1956), on the basis of a study of the infrared absorption spectrum of $Mg(OH)_2$ at the temperature of liquid nitrogen, have concluded that it is possible to explain the spectrum (in principle at least) without invoking a larger unit cell or changing the equilibrium positions of the hydrogen atoms from those proposed originally by Bernal and Megaw.

A complete account of this work will be published in *Acta Crystallographica*.

I am greatly indebted to Dr. H. D. Megaw for encouragement and for much helpful advice at all stages of the progress of this work. It is a pleasure to acknowledge the award of a Rutherford Memorial Fellowship by the National Research Council of Canada and the Royal Society of Canada, during the tenure of which the experimental part of this work was completed. I also wish to acknowledge the continuing financial support of my research program by the Defence Research Board.

Aminoff, G. 1919. Geol. Fören. i Stockholm Förh. **41**, 407.
Bernal, J. D. and Megaw, H. D. 1935. Proc. Roy. Soc. (London), A, **151**, 384.
Busing, W. R. and Levy, H. A. 1957. J. Chem. Phys. **26**, 563.
Mara, R. T. and Sutherland, G. B. B. M. 1953. J. Opt. Soc. Amer. **43**, 1100.
——— 1956. J. Opt. Soc. Amer. **46**, 464.
Petch, H. E. 1955. Phys. Rev. **99**, 1635.
Petch, H. E. and Megaw, H. D. 1954. J. Opt. Soc. Amer. **44**, 474.
Ross, P. A. 1928. J. Opt. Soc. Amer. **16**, 433.

Received June 6, 1957.
Howard E. Petch
Department of Physics,
Hamilton College, McMaster University,
Hamilton, Ontario.

The Effect of Incident Atomic Velocity on the Structure of Evaporated Silver Films

In a recent letter Holland (1957) has suggested certain objections to our evidence (Aziz and Scott 1956) for the effect of incident atomic velocity on the structure of evaporated silver films. The main point which Holland raises is that the latent heat of condensation of silver atoms is large compared with the kinetic energy associated with their incident velocity and when this energy is released it will mask any differences due to incident velocity. However, the structure of evaporated films depends on the mobility of the initial, individual atoms on the substrate since this mobility determines the surface concentration of nuclei on which subsequent condensation occurs. The latent heat of condensation L_{metal} applying as it does to silver atoms condensing at most favorable sites on a crystallite of bulk silver is not relevant to the question of a single silver atom moving over a glass or plastic substrate. There is what might be considered a latent heat for condensation l_1 of the vapor atoms to a two-dimensional gas on the substrate but l_1 is a small value compared with L_{metal}. Moreover, the latent heat or heat of adsorption l_1 is then shared among several of the adjacent atoms in the substrate. The adsorbed singlet atoms are in motion on the surface and collide with one another to form immobile Frenkel doublets (Frenkel 1924 and Cockroft 1928) with a release of energy l_2. These doublets act as centers of condensation for other atoms. The sum $L = l_1+l_2$, i.e., the energy required to remove one member of the metallic doublet from the surface, was found in many cases and in particular for cadmium on glass (Appleyard 1937) to be an order of magnitude smaller than L_{metal}. We are concerned, however, only with l_1, for the energy l_2 released when the atom becomes immobile will have no bearing on the concentration of nuclei and hence the degree of continuity of the film structure. l_1 then is probably only a few per cent of L_{metal} and therefore will not obscure the effect of the differences in the kinetic energy of the atoms.

Holland also mentions two unknown factors which may have influenced our results. Certainly there are unknown factors in the formation of evaporated deposits. However, the two factors referred to—substrate temperature and residual gas impurities— are not likely to be important in our experiments. From studies of the influence of substrate temperature on film structure and from direct measurements of the substrate temperature under the conditions we used, it is clear that the small temperature differences (5° to 10° C.) which may exist could not be responsible for the observed effects on film structure. The influence of the impurities in the gas is more difficult to assess but since a liquid air trap was employed in the evaporating chamber it is very unlikely that any significant quantity of water vapor would be present during the evaporations.

Appleyard, E. T. S. 1937. Proc. Phys. Soc. **49**, 118.
Aziz, R. A. and Scott, G. D. 1956. Can. J. Phys. **34**, 731.
Cockroft, J. D. 1928. Proc. Roy. Soc. A, **119**, 293.
Frenkel, W. 1924. Z. Physik, **26**, 117.
Holland, L. 1957. Can. J. Phys. **35**, 697.

Received June 17, 1957.
R. A. Aziz
G. D. Scott
Department of Physics,
University of Toronto,
Toronto, Ontario.

THE PHYSICAL SOCIETY

MEMBERSHIP of the Society is open to all who are interested in Physics.

FELLOWS pay an Entrance fee of £1 1*s*. ($3.00) and an Annual Subscription of £2 2*s*. ($6.00).

STUDENTS: A candidate for Studentship must be between the ages of 18 and 26, and pays an Annual Subscription of 5*s*. ($0.75).

MEETINGS: Fellows and Students may attend all Meetings of the Society including the annual Exhibition of Scientific Instruments and Apparatus.

PUBLICATIONS include the *Proceedings of the Physical Society*, published monthly in two sections, and *Reports on Progress in Physics*, published annually. Volume XIX, 1956, is now available (price 50*s*. ($7.15)). Members are entitled to receive any of the Publications at a reduced rate.

Further information can be obtained from:

THE PHYSICAL SOCIETY

1, LOWTHER GARDENS, PRINCE CONSORT ROAD

LONDON, S.W.7, ENGLAND

CANADIAN JOURNAL OF PHYSICS

Notes to Contributors

Manuscripts

(i) General. Manuscripts, in English or French, should be typewritten, double spaced, on paper 8½×11 in. **The original and one copy are to be submitted.** Tables and captions for the figures should be placed at the end of the manuscript. Every sheet of the manuscript should be numbered.

Style, arrangement, spelling, and abbreviations should conform to the usage of this journal. Names of all simple compounds, rather than their formulas, should be used in the text. Greek letters or unusual signs should be written plainly or explained by marginal notes. Superscripts and subscripts must be legible and carefully placed.

Manuscripts and illustrations should be carefully checked before they are submitted. Authors will be charged for unnecessary deviations from the usual format and for changes made in the proof that are considered excessive or unnecessary.

(ii) Abstract. An abstract of not more than about 200 words, indicating the scope of the work and the principal findings, is required, except in Notes.

(iii) References. References should be listed **alphabetically by authors' names,** unnumbered, and typed after the text. The form of the citations should be that used in current issues of this journal; in references to papers in periodicals, titles should not be given and only initial page numbers are required. The names of periodicals should be abbreviated in the form given in the most recent *List of Periodicals Abstracted by Chemical Abstracts.* All citations should be checked with the original articles and each one referred to in the text by the authors' names and the year.

(iv) Tables. Tables should be numbered in roman numerals and each table referred to in the text. Titles should always be given but should be brief; column headings should be brief and descriptive matter in the tables confined to a minimum. Vertical rules should be used only when they are essential. Numerous small tables should be avoided.

Illustrations

(i) General. All figures (including each figure of the plates) should be numbered consecutively from 1 up, in arabic numerals, and each figure referred to in the text. The author's name, title of the paper, and figure number should be written in the lower left corner of the sheets on which the illustrations appear. Captions should not be written on the illustrations (see Manuscripts (i)).

(ii) Line Drawings. Drawings should be carefully made with India ink on white drawing paper, blue tracing linen, or co-ordinate paper ruled in blue only; any co-ordinate lines that are to appear in the reproduction should be ruled in black ink. Paper ruled in green, yellow, or red should not be used unless it is desired to have all the co-ordinate lines show. All lines should be of sufficient thickness to reproduce well. Decimal points, periods, and stippled dots should be solid black circles large enough to be reduced if necessary. Letters and numerals should be neatly made, preferably with a stencil (**do NOT use typewriting**) and be of such size that the smallest lettering will be not less than 1 mm. high when reproduced in a cut 3 in. wide.

Many drawings are made too large; originals should not be more than 2 or 3 times the size of the desired reproduction. In large drawings or groups of drawings the ratio of height to width should conform to that of a journal page but the height should be adjusted to make allowance for the caption.

The original drawings and one set of clear copies (e.g. small photographs) are to be submitted.

(iii) Photographs. Prints should be made on glossy paper, with strong contrasts. They should be trimmed so that essential features only are shown and mounted carefully, with rubber cement, on white cardboard with no space or only a **very** small space (less than 1 mm.) between them. In mounting, full use of the space available should be made (to reduce the number of cuts required) and the ratio of height to width should correspond to that of a journal page (4¾×7½ in.); however, allowance must be made for the captions. Photographs or groups of photographs should not be more than 2 or 3 times the size of the desired reproduction.

Photographs are to be submitted in duplicate; if they are to be reproduced in groups one set should be mounted, the duplicate set unmounted.

Reprints

A total of 50 reprints of each paper, without covers, are supplied free. Additional reprints, with or without covers, may be purchased.

Charges for reprints are based on the number of printed pages, which may be calculated approximately by multiplying by 0.6 the number of manuscript pages (double-spaced typewritten sheets, 8½×11 in.) and including the space occupied by illustrations. An additional charge is made for illustrations that appear as coated inserts. The cost per page is given on the reprint requisition which accompanies the galley.

Any reprints required in addition to those requested on the author's reprint requisition form must be ordered officially as soon as the paper has been accepted for publication.

Contents

Page

A New Technique for the Study of Scatter Propagation in the Troposphere—*J. H. Chapman, W. J. Heikkila, and J. E. Hogarth* 823

Rotational Temperatures Measured in Aurorae at Churchill, Manitoba—*R. Montalbetti* - - - - - - - - - - - 831

High Resolution Raman Spectroscopy of Gases. X. Rotational Spectrum of Butatriene ($H_2C{=}C{=}C{=}CH_2$)—*B. P. Stoicheff* - 837

Ultraviolet Absorption Spectra of HCN and DCN. I. The α—X and β—X Systems—*G. Herzberg and K. K. Innes* - - - 842

Energy Levels of Slightly Asymmetric Top Molecules—*S. R. Polo* 880

Discussion of the Electrical Properties of Compounds with the Nickel Arsenide Structure—*W. B. Pearson* - - - - - - 886

Low Temperature Resistivity of Transition Elements: Vanadium, Niobium, and Hafnium—*G. K. White and S. B. Woods* - - 892

The Emission Spectrum of the PH^+ Molecule—*N. A. Narasimham* 901

The Emission Spectrum of Aluminum Monochloride in the Vacuum Ultraviolet—*S. Paddi Reddy and P. Tiruvenganna Rao* - - 912

Absorption of Sunlight by Atmospheric Sodium—*J. A. Scrimger and D. M. Hunten* - - - - - - - - - - - - - - 918

Ionization Currents in Argon and Helium Liquids—*R. L. Williams and F. D. Stacey* - - - - - - - - - - - - - - 928

The Decay of the Populations of Metastable Atoms and Ions from the Same d-c. Discharge in Neon—*B. C. Blevis, J. M. Anderson, and R. W. McKay* - - - - - - - - - - - - - - 941

Infrared Intensities and Bond Moments in Sulphur Dioxide—*J. E. Mayhood* - - - - - - - - - - - - - - - 954

Quantum Mechanics with an Indefinite Metric—*Suraj N. Gupta* 961

The Cumulative Yields of the Krypton and Xenon Isotopes Produced in the Fast Neutron Fission of Th^{232}—*T. J. Kennett and H. G. Thode* - - - - - - - - - - - - - - - 969

Notes:

Multiple Scattering Measurements of π and μ Mesons Stopping in Nuclear Emulsions—*B. Judek* - - - - - - - - 980

Letters to the Editor:

A Determination of the Hydrogen Positions in $Ca(OH)_2$ by X-Ray Diffraction—*Howard E. Petch* - - - - - - - - - - 983

The Effect of Incident Atomic Velocity on the Structure of Evaporated Silver Films—*R. A. Aziz and G. D. Scott* - - 985

Printed in Canada *by* University of Toronto Press